Exploring haptics for subsea vehicles

Haptic feedback for rate controlled vehicles in subsea environments

Kuiper, Roel

DOI
10.4233/uuid:cddcf5d0-5a9f-43f6-8903-f6d01d58b0fc

Publication date
2019

Document Version
Final published version

Citation (APA)
Kuiper, R. (2019). *Exploring haptics for subsea vehicles: Haptic feedback for rate controlled vehicles in subsea environments*. [Dissertation (TU Delft), Delft University of Technology]. https://doi.org/10.4233/uuid:cddcf5d0-5a9f-43f6-8903-f6d01d58b0fc

Important note
To cite this publication, please use the final published version (if applicable).
Please check the document version above.

EXPLORING HAPTICS FOR SUBSEA VEHICLES

HAPTIC FEEDBACK FOR RATE CONTROLLED VEHICLES IN SUBSEA ENVIRONMENTS

EXPLORING HAPTICS FOR SUBSEA VEHICLES

HAPTIC FEEDBACK FOR RATE CONTROLLED VEHICLES IN SUBSEA ENVIRONMENTS

Proefschrift

ter verkrijging van de graad van doctor
aan de Technische Universiteit Delft,
op gezag van de Rector Magnificus Prof. dr. ir. T.H.J.J. van der Hagen,
voorzitter van het College voor Promoties,
in het openbaar te verdedigen op maandag 11 februari 2019 om 15:00 uur

door

Roeland Jacobus KUIPER

Master of Science in Mechanical Engineering,
Technische Universiteit Delft, Nederland,
geboren te Rotterdam, Nederland.

Dit proefschrift is goedgekeurd door de promotoren:

Prof. dr. ir. D.A. Abbink
Prof. dr. F.C.T. van der Helm

Samenstelling promotiecommissie:

Rector Magnificus,	voorzitter
Prof. dr. ir. D.A. Abbink,	Technische Universiteit Delft
Prof. dr. F.C.T. van der Helm,	Technische Universiteit Delft
Onafhankelijke leden:	
Prof. dr. M. O' Malley,	Rice University
Prof. dr. J.B.F. van Erp,	Universiteit Twente
Prof. dr. A.M.L. Kappers,	Technische Universiteit Eindhoven
Prof. dr. H. Nijmeijer,	Technische Universiteit Eindhoven
Dr. ir. M.M. van Paassen,	Technische Universiteit Delft
Prof. dr. ir. J. Hellendoorn,	Technische Universiteit Delft, reservelid

This work is part of the research programme Perspectief with project number 12163, which is (partly) financed by the Netherlands Organisation for Scientific Research (NWO). Furthermore, the Dutch company Seatools BV. has contributed greatly in-kind supporting this research.

Keywords: Haptic feedback, Haptic shared control, Deep sea mining

Printed by: Gildeprint

Front & Back: Cover design by REM designs, Brooklyn, NY. Rob Mostransky.

ISBN 978-94-6323-524-2

An electronic version of this dissertation is available at
http://repository.tudelft.nl/.

CONTENTS

SUMMARY

Remotely controlled subsea vehicles are frequently used for oil and gas applications. A potential future application requiring remote controlled vehicles is deep-sea mining. At the envisioned water depths beyond 1500m, rare minerals are accessible without deep excavation. However, the extreme hyperbaric conditions (i.e. high pressure), limited visibility and unpredictable soil properties pose immense challenges in controlling the excavation process. Such machines are expected to be operated manually by an operator using joysticks that manipulate the machine's operational velocity (also known as 'rate control'). Large subsea vehicles are difficult to control due to their complexity and slow dynamic response. This thesis explores design choices for haptic feedback that can support the operator in controlling these machines. Offering haptic feedback (i.e. forces on the input device) can potentially improve task performance and operator awareness, by informing the operator of the naturally occurring (possibly scaled) interaction forces with the environment. Alternatively, artificial guidance forces based on a model or sensed environment can be used to guide or constrain the operator's control actions. Force reflection in a rate controlled task poses a difficulty compared to a position controlled task, because the reflected forces are no longer directly related to the operator's input position.

The goal of this thesis is to provide design guidelines for haptic feedback, by designing and evaluating several haptic feedback algorithms, for a variety of remotely controlled sub-sea vehicles. First the thesis will present an analysis of the general task environment of deep-sea mining, including a choice for the most likely options for machinery to be used in the envisioned operations. Secondly, the design of natural haptic feedback is explored for controlling a large heavy backhoe dipper excavator, operating in a shallow subsea environment. And thirdly, the implementation of haptic guidance forces is studied for rate controlled devices and its effect on steering a deep-sea mining crawler.

1) General task environment of deep-sea mining, machines and minerals

Deep-sea mining applications require large heavy machinery, to excavate mineral-rich rock materials. Excavating rock in large water depths requires more energy than on land, due to hardening of the material in hyperbaric conditions (**chapter 2**). Two possible deep-sea mining approaches are compared: using a large suspended grab with two clamshells, and track-driven drum cutters. The suspended grab is shown to reduce energy consumption, due to a reduction of hyperbaric hardening-effect caused by slow loading of the material thereby allowing water to enter the effected deformed zone (**chapter 2**).

Using a grab is a promising excavation method for deep-sea mining due to the low loading rates and only crushing parts of the material, leaving most intact. Controlling such a machine while exerting large cutting forces onto the seabed is a challenging task. Offering haptic feedback to the operator by means of natural force feedback and haptic shared control combined

potentially improves the situational awareness and control effort (**chapter 3**). Further investigation into both types of support (i.e. natural and guidance feedback) needs to be done for these type of large subsea machines.

2) Exploring natural haptic feedback for vehicles with a slow dynamic response

Subsea vehicles typically are large and heavy, thereby having a slow dynamic response. This requires predictive inputs from the operator for controlling the vehicles' position. Natural haptic feedback increases the situational awareness of the operator, enabling better understanding of the state of the machine and anticipation of the required control inputs (**chapter 4**). It is shown that scaling of the reflected forces during position control does not affect the perception of the controlled vehicle's response, thereof prediction of the required inputs.

Using rate control has an unlimited workspace, required for steering heavy machines over the seabed. Offering natural feedback in rate control is however not as obvious as it is for position control, where the measured forces can be reflected directly related to the position. Implementing stiffness feedback showed promising results for offering natural haptic feedback in rate control for operating a slow dynamic system, compared to force-based feedback and static feedback of a centering spring (**chapter 5**). This was tested for the fundamental abstract subtask of positioning in free-space, a contact transition and force level tasks.

Controlling a backhoe dipper excavator on a pontoon for excavation in harbors or offshore shallow waters is a challenging task due to the machine's complexity and slow dynamics. A high fidelity force reflecting joystick was developed to demonstrate the effect of implementing stiffness feedback for controlling an excavator, based on the measured hydraulic cylinder pressures, representing the environment interaction forces (**chapter 6**). A human factors case study showed that several operating effects can be clearly reflected by means of stiffness feedback, such as making contact with the seabed and cutting through sand layers.

3) Exploring haptic guidance feedback designs

Instead of informing the operator of what the machine is doing, haptic guidance feedback based on a model or sensed environment can assist the operator in correct task execution. This thesis explores two types of design of guidance feedback, by means of a repulsive force field around forbidden zones or attractive forces towards a suggested path. The latter requires more sensed information from the environment, but showed most improvements for steering an abstract vehicle trough a virtual maze (**chapter 7**).

Haptic shared control is an attractive guidance towards a suggested path, sharing the control with the operator on the input device. For a deep-sea crawler maneuvering over the seabed haptic guidance is compared to semi-automated control and manual control (**chapter 8**). This showed that sharing the control is beneficial due to automation during normal operating conditions, but also from manual control in unexpected events such as obstacle avoidance or slip conditions.

In conclusion, both natural haptic feedback and haptic guidance feedback were evaluated on abstract tasks as well as real-life tasks simulated in virtual reality. Combining natural haptic

feedback and guidance feedback is recommended for rate controlled tasks, to inform the operator on interaction forces as well for as assisting in task execution. The combination of feedback can be offered to the operator by means of stiffness reflection combined with guidance by haptic shared control, which shifts the neutral position of the stiffness.

SAMENVATTING

Op afstand bestuurde onderwater voertuigen worden vaak gebruikt voor olie- en gastoepassingen. Diepzee mijnbouw is een potentieel toekomstige toepassing waarvoor op afstand bestuurbare voertuigen nodig zijn. Op de beoogde waterdieptes van 1500 m of meer, zijn zeldzame mineralen zonder diepe uitgraving vrij toegankelijk. Echter door de extreme hyperbare condities (i.e. hoge druk), beperkte zichtbaarheid en onvoorspelbare bodemeigenschappen is het een uitdaging het graafproces gecontroleerd uit te voeren. Dergelijke machines zullen naar alle waarschijnlijkheid handmatig worden bediend door een bestuurder met behulp van joysticks, om de snelheid van de machine te besturen, oftewel snelheidssturing. Grote onderwatervoertuigen zijn moeilijk te bedienen vanwege hun complexiteit en langzaam dynamisch gedrag. Dit proefschrift onderzoekt ontwerp mogelijkheden van haptische terugkoppeling die de bestuurder kan ondersteunen bij het bedienen van deze machines. Het aanbieden van haptische terugkoppeling (i.e. krachten op het invoerapparaat) kan mogelijk zowel de taakprestaties als het bewustzijn van de bestuurder verbeteren, door de bestuurder te informeren van de natuurlijk voorkomende (mogelijk geschaalde) kracht interactie met de omgeving. Als alternatief kunnen kunstmatige geleidingskrachten gebaseerd op een model of op sensoren de bestuurder begeleiden of beperken in zijn stuur acties. Het terugkoppelen van krachten in een snelheidsgeregelde taak levert in vergelijking met een positie gestuurde taak een uitdaging op, omdat de gereflecteerde krachten niet langer direct gerelateerd zijn aan de invoerpositie van de bestuurder.

Het doel van dit proefschrift is om ontwerp richtlijnen aan te brengen voor haptische terugkoppeling, door het ontwerpen en evalueren van verschillende haptische terugkoppel algoritmes. Als eerste wordt in dit proefschrift een analyse gegeven van de algemene taakomgeving van diepzee mijnbouw, inclusief een keuze voor de meest waarschijnlijke machine type voor een dergelijke operatie. Ten tweede wordt het ontwerp van natuurlijke haptische terugkoppeling onderzocht voor het besturen van een grote graafmachine voor gebruik vanaf een ponton in ondiep water. En ten derde wordt de implementatie van haptische geleidingskrachten bestudeerd voor apparaten met snelheidssturing en het effect op het besturen van een diepzee mijnbouw rupsvoertuig.

1) Algemene taakomgeving van diepzee mijnbouw, machines en mineralen

Voor diepzeemijnbouw toepassingen zijn grote zware machines nodig die mineraalrijke rots afgraven. Het opgraven van gesteente in grote waterdiepten vereist meer energie dan bovenwater, vanwege verharding van het materiaal in hyperbare omstandigheden (**hoofdstuk 2**). Voor diepzee mijnbouw zijn twee methodes vergeleken: het gebruik van een grijper met twee grote schalen en een rupsvoertuig met een grote frees. Voor de grijper is aangetoond dat dit lijdt tot energie reductie vanwege een vermindering in het hyperbare verhardingseffect door

het materiaal langzaam te belasten waardoor het water de vervormde zone in kan stromen (**hoofdstuk 2**).

Het gebruik van een grijper is een veelbelovende graafmethode voor diepzeemijnbouw vanwege de lage belasting snelheden en doordat het materiaal slechts gedeeltelijk vergruisd. Een dergelijke machine besturen is een uitdagende taak door de daarbij zeer grote snijkrachten op de zeebodem. Het aanbieden van haptische terugkoppeling aan de bestuurder door middel van natuurlijke kracht terugkoppeling gecombineerd met begeleidende krachten, verbetert potentieel de situationele bewustwording en de inspanning (**hoofdstuk 3**). Verder onderzoek naar beide soorten ondersteuning (i.e. natuurlijke en begeleidende krachten) moeten voor dit type grote onderwater machines worden uitgevoerd.

2) Natuurlijke haptische terugkoppeling voor voertuigen met een langzame respons

Typisch zijn onderwater voertuigen vaak groot en zwaar, en hebben daardoor een langzame dynamische respons. Dit vereist voorspelling van de bestuurder voor het bedienen van de positie van het voertuig. Het gebruik van natuurlijke haptische terugkoppeling vergroot de situationele bewustwording van de bestuurder, waardoor beter begrip van de staat van de machine mogelijk is en anticipatie vereist voor de besturing (**hoofdstuk 4**). Er wordt aangetoond dat verschalen van de gereflecteerde krachten tijdens positieregeling geen invloed heeft op de perceptie van de voertuig respons, en daarom ook niet op de voorspelling van de vereiste besturing.

Het gebruik van snelheidssturing heeft een onbeperkte werkruimte, die nodig is om zware machines te kunnen besturen op de zeebodem. Het aanbieden van natuurlijke terugkoppeling bij snelheidssturing is alleen niet zo duidelijk als voor positie sturing, waarbij de gemeten krachten direct kunnen worden weergegeven op basis van de positie. Het implementeren van stijfheid terugkoppeling toonde veelbelovende resultaten voor het aanbieden van natuurlijke haptische terugkoppeling in snelheidssturing voor het bedienen van een langzaam dynamisch systeem, in vergelijking met terugkoppeling op basis van kracht en statische terugkoppeling van een centreer veer (**hoofdstuk 5**). Dit werd getest voor de fundamentele abstracte subtaak van positionering in vrije ruimte, een contactovergang en taken voor kracht niveau.

Het besturen van een graafmachine op een ponton voor graafwerkzaamheden in havens of in ondiepe wateren op zee is een uitdagende taak vanwege de complexiteit van de machine en de langzame dynamische respons. Een kracht teruggekoppelde joystick met hoge precisie was ontwikkeld om het effect van implementatie aan te tonen van stijfheid reflectie voor het besturen van een graafmachine, op basis van de gemeten hydraulische cilinder drukken, die de krachten van de interactie met de omgeving vertegenwoordigen (**hoofdstuk 6**). Een casus bij onderzoek naar menselijk gedrag toonde aan dat effecten zoals contact maken met de zeebodem en door zandlagen snijden duidelijk kan worden weergegeven door middel van stijfheid reflectie.

3) Onderzoek naar haptische begeleidende terugkoppeling

In plaats van de bestuurder te informeren over wat de machine aan het doen is, biedt haptische begeleidende terugkoppeling op basis van een model of waargenomen omgeving de

mogelijkheid om de bestuurder te helpen bij de juiste taak uitvoering. Dit proefschrift verkent twee soorten ontwerpen van begeleidende terugkoppeling: door middel van een afstotend krachtveld rond verboden zones of aantrekkende krachten richting een gesuggereerd pad. Dit laatste vereist meer waargenomen informatie uit de omgeving, maar vertoont de meeste verbeteringen voor het sturen van een abstract voertuig door een virtueel doolhof (**hoofdstuk 7**).

Haptische gedeelde besturing is een aantrekkend krachtveld richting een gesuggereerd pad, waarbij de bediening wordt gedeeld met de bestuurder op het invoerapparaat. Voor een diepzee rupsvoertuig die over de zeebodem manoeuvreert word haptische geleiding vergeleken met semi-automatische besturing en handmatige besturing (**hoofdstuk 8**). Dit toonde aan dat het delen van de besturing gunstig is door de automatisering tijdens normale omstandigheden, maar ook tijdens handmatige bediening bij onverwachte gebeurtenissen, zoals bij het ontwijken van obstakels of in slip omstandigheden.

Concluderend werden zowel natuurlijke haptische terugkoppeling als haptische begeleidende terugkoppeling geëvalueerd voor abstracte taken evenals realistische taken gesimuleerd in virtual reality. De combinatie van natuurlijke haptische terugkoppeling en begeleidende terugkoppeling is aanbevolen voor het gebruik bij snelheidssturing, dit om de gebruiker te informeren van de interactie krachten en daarbij ook assistentie te verlenen voor de uitvoerende taak. De gecombineerde terugkoppeling kan worden aangeboden aan de bestuurder door middel van stijfheid reflectie gecombineerd met haptische gedeelde besturing, die het nulpunt verschuift van de stijfheid.

1

INTRODUCTION

Remotely controlled subsea machines are challenging to operate, especially when interacting with the environment. This thesis explores haptic feedback supporting methods for rate controlled subsea vehicles, by reflecting natural occuring interaction forces and by means of artificial guidance forces to the operator.

This introduction explains the need for novel deep-sea mining approaches, the envisioned challenges for remotely controlling the large machines needed to harvest materials at large water depths, and the potential of haptic feedback to support operators in their task. The state-of-the art in sub-sea mining and deep-sea mining is presented, along with different options for haptic feedback to support operators, and the lack of design guidelines for operator control methods. This chapter ends with the aim and approach of this thesis, to investigate the design of effective haptic feedback in rate control for remotely controlled subsea vehicles.

1

THE use of remotely controlled vehicles (ROVs) is becoming more important over the last years in subsea environments. Current purposes for ROVs include subsea-tasks like inspection and maintenance in oil and gas applications, and for the future deep-sea mining is being investigated. The main reason for the increasing use of ROVs is that the water depth is becoming too large for human divers to operate in (e.g. for inspection, welding, opening/closing subsea oil valves). Additionally the increasing water depth also makes it difficult to operate or manipulate subsea tasks from the surface water directly, therefore requiring subsea machines (e.g., for rock dumping, trenching pipelines or excavation). For example pipelines laid in shallow waters can be protected with layers of rocks, directly dumped overboard at the side of a vessel. In larger waters rocks are dumped through a pipe of which the end is accurately positioned by a subsea machine as shown in the left of figure 1.1. Another example is trenching (i.e. burying) a pipeline into the seabed which in larger water depths requires a subsea vehicle (shown in the middle of figure 1.1). In shallow waters a trench is made by a large heavy plough tugged from the surface vessel, which is not feasible in deep waters but requires subsea machines instead. Excavation in deep-sea obviously also requires remotely controlled subsea machinery, for example a remotely controlled grab as shown in the right of figure 1.1 (Bloois and Frumau, 2009).

Subsea machines vary widely in size and function, but can be quite large in scale compared to other application domains and therefore slow in their dynamic response (Sepehri et al., 1994; Sheridan et al., 1978). However, a wide range of these machines are small free floating ROVs used for basic inspection purposes or general purpose basic manipulation (e.g. opening/closing subsea oil valves or grabbing small objects). Special purpose ROVs on the other hand are commonly large in size, installed with heavy duty equipment and complex to control due to their specific functionality. Special purpose ROVs are often used for tasks such as positioning (e.g. rock dumping), placing equipment or material on the seabed, and excavation of the seafloor (van Es et al., 2004).

Usually such machines are remotely controlled by a human operator from a surface vessel hovering over the operation. The machine is powered through a so called umbilical from the vessel, transporting power and data to and from the machine. Visual feedback is often limited due to low visibility in deep waters in combination with high turbidity due to the conducted activities. Therefore the operator must fully rely on the mounted sensors on the vehicle, monitoring its position and state of all components (e.g. pressures and temperatures) The vehicles are typically powered by thrusters or tracks on the seabed. These actuators are controlled in manual operation by human operators using joysticks, manipulating the machine's operational velocity, thereby controlling the rate of the position change instead of controlling the position directly (Kontz and Book, 2006; Sheridan, 1989). This allows an unlimited workspace to operate and most applications (e.g. position following, cutting) require a specific operation velocity, rather than a fixed target position (Kim et al., 1987). Such a control interface of manipulating the machines velocity instead of position directly can reach equal performance (McRuer and Jex, 1967; Winck et al., 2015), but often requires intensive practice for proper and efficient use.

Large special purpose ROVs are thus mostly difficult to control due to their complexity, slow

Figure 1.1: Selection of developed remotely operated vehicles by Seatools BV. On the left a rock-dump ROV Rockpiper depicted with integrated survey ROV which can undock from the main ROV. In the middle is a trencher Arthropod 600 depicted which can bury pipes up to 1.2 m in diameter. On the right is a grab excavation system GES depicted, which can collect or remove sand or clay material from the seabed. All figures above are shown with the courtesy of Seatools BV.

dynamic response and control input method, combined with unpredictable environments (Sheridan et al., 1978). Because of their slow dynamic response an operator must predict the behaviour of the controlled machine and its operating environment (Ostoja-Starzewski and Skibniewski, 1989). The distance from which the human operator is controlling normally does not cause any additional time delay due to glass fibre connections with the controlled machine. However, because of this distance, the human operator has to fully rely on the information of the sensors mounted on the machine locally. In most cases this feedback does not contain any reasonable visual camera information due to the lack of light in these depths and high turbidity due to the conducted task (e.g. rock dumping or excavation). This limits the operator's overview of the conducted task and understanding of the state of the machine (e.g. telepresence and awareness) (Endsley, 1995; Stassen and Johannsen, 1990). The sensor information (e.g. positions, pressures, temperatures) is solely offered visually to the operator (e.g. virtual representations or gauges), creating a highly visual demanding task, sometimes supplemented with auditory warnings.

A possible solution to improve the task performance and operator awareness when controlling such machines remotely could be by offering haptic feedback (i.e. forces on the input device) to the operator (Rosenberg, 1993). Haptic feedback can be offered to inform the operator of the naturally occurring interaction forces of the remote machine with its environment (Hannaford et al., 1991; Wildenbeest et al., 2013). Another solution could be to offer augmented artificial guidance forces to assist the operator in controlling such complex machines. These forces could suggest recommended control actions by an intelligent controller operating the machine in parallel to the operator (known as haptic shared control) (Abbink et al., 2012; Steele and Gillespie, 2001). More understanding and quicker response for controlling the vehicle remotely could be achieved by sensing the natural forces occurring on the remote machine. Simplifying the control in normal operating conditions could be achieved by offering guidance forces. The effect of offering haptic feedback for deep sea mining machines is still unclear, how the currently developed haptic feedback algorithms could be extended for assisting an operator

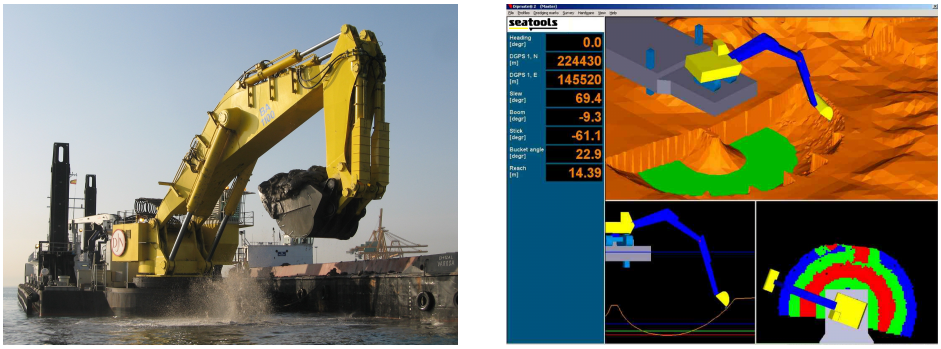

Figure 1.2: Backhoe Excavator Machine. On the left is the Backackter 1100 Vitruvius of Jan de Nul NV depicted which has Seatools BV visualization installed for subsurface operations. On the right is visualization software interface DipMateTM of Seatools BV depicted for subsurface excavation of backhoe excavators. Both figures above are shown with the courtesy of Seatools BV and Jan de Nul NV.

controlling complex slow responding machines with limited visual feedback.

1.1. FROM SUBSEA TO DEEP-SEA EXCAVATION

REMOTELY controlled subsea machines are used for a wide variety of subsea tasks, but excavation tasks are particularly interesting due to their constant interaction with the environment. Excavation requires positioning to a specific excavation location, making contact with the seafloor and cutting through the seabed to remove material (sand, clay or rock). Therefore this task normally consists of all three fundamental task types: free-space, contact transition and force-level tasks. Offering haptic feedback for a rate controlled machines for such an excavation task can be investigated for this wide range of task types. Each of these tasks types can benefit differently from haptic feedback, for example when moving through water for positioning or when making initial contact with the seabed.

Subsea excavation tasks can be executed with a variety of machines and applications. In the middle of figure 1.1 a trencher is depicted which removes the seabed under a laid oil or gas pipeline to bury it entirely. However such operation is almost a continuous fully automated process and does not require much human intervention. The depicted grab on the right of figure 1.1 can remove sand or hard clay with large boulders embedded for placing sensitive equipment in a protective ditch in waters with large icebergs scraping over the seabed (van Es et al., 2004). Such a grab can also be used for future applications such as deep-sea mining (Bloois and Frumau, 2009), as depicted in the left of figure 1.3. For mining applications the top layer containing so called SMS deposits (Seafloor Massive Sulfides) is removed, this layer has formed into a coarse volcanic terrain containing so called black smokers or chimneys (Tivey, 2007). It is also suggested to use drum cutters as depicted in the right of figure 1.3 to remove these mineral rich materials. However such machines rely on the seabed support (i.e. soil conditions) to operate on, due to their track driven propulsion. A grab on the other hand is suspended from a cable and therefore more suitable to remove the top layer of such rough terrain. Previous studies (Kuiper et al. (2016, 2013)) have also shown the advantage of a grab over

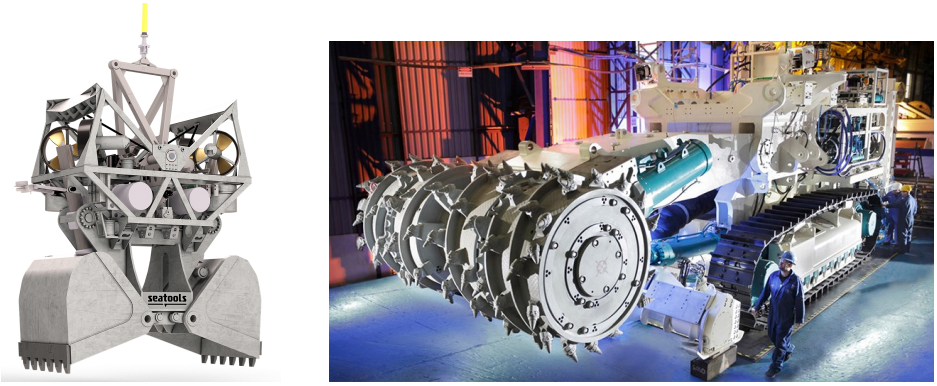

Figure 1.3: Deep-sea mining machines. On the left is a proposed deep-sea mining grab of Seatools BV depicted. On the right is a drum-cutter of Nautulus Minerals depicted, developed for deep-sea mining at the Solwara-1 project in Papua New Guinea. Both figure above are shown with the courtesy of Seatools BV and Nautulus Minerals

drum cutters based on their energy consumption due to not fully crushing the rock materials subsea. Controlling these machines would require constant intervention of a human operator due to the unpredictability of the operating environments and large financial consequences for these future applications. The remaining difficulty of deep-sea mining is the uncertainty of the entire process because it has never been done so far. Initial test runs and sampling expeditions have been conducted, but an actual mining operation has not been started yet in deep-sea. This leaves several items unclear, such as what the stability of the seabed in general is, the variability in production rates that can be achieved and what type of excavation methods will be successful.

Even though excavation in deep-sea is not yet being conducted, excavation in subsea conditions in shallow waters of several meters up to 30 meters of water depth is common. Subsea excavation typically consists of removing of sand or clay materials in harbors or near shallow offshore structures, with the use of for instance backhoe excavators as shown in figure 1.2. Even though these machines are placed on floating pontoon structures at the surface, their task remains subsea, without any visual information of the subsea conducted task due to high turbidity. Such backhoe excavators for offshore applications are heavy duty machines, with capacities up to 40 m3 of bucket volume comparable to a fully loaded dump truck. Because of the lack of visual feedback, operators have to rely entirely on the measured sensor information which can be presented as a virtual excavator to the operator as shown in the right of figure 1.2 (Kontz and Book, 2006). A difference with operating a remote subsea vehicle is the presence of vestibular and auditory feedback when operating a backhoe excavator, because the operator is placed on top of the machine itself. However the executed task itself is comparable to excavating with remotely operated machines in subsea or deep-sea. When operating a backhoe excavator, the bucket has to be placed at a specific point on the seafloor. Thereby the bucket end point first needs to transition to this place, sequentially make contact with the seabed and finally remove part of the seabed by cutting though the material. Thereby the three fundamental

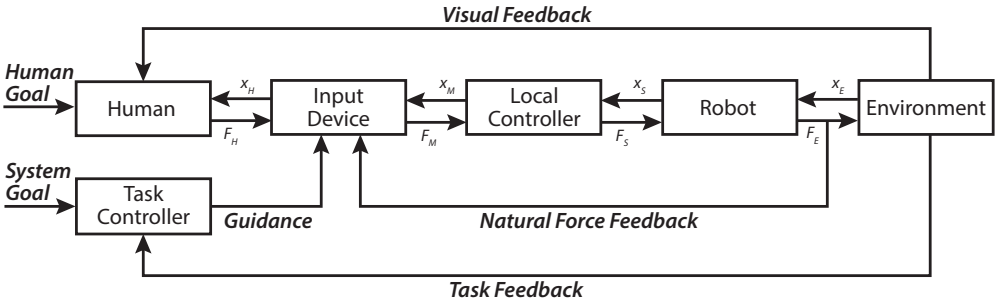

Figure 1.4: Demonstrating two haptic feedback methods: natural feedback and guidance forces.

subtasks of operating a rate controlled remote machine can be tested for this known application of which all parameters of the machine and environment are known. These tasks required the positioning of the cutting teeth through the seabed up to a specific target depth profile, removing materials in a cost effective manner. Such an excavation task is in essence similar to what can be expected in future deep-sea projects.

1.2. ASSISTING HAPTIC FEEDBACK METHODS

OFFERING haptic feedback to the operator, either by reflecting natural force feedback or by haptic guidance forces is indicated schematically in figure 1.4. It shows the reflection of the environment interaction forces and the forces from the controller, where the controller has comparable task and feedback as the human and working as a shared controller on the input device. Both feedback types can potentially be combined on the input device for assisting the operator in controlling complex deep sea mining machines, when designed such to not interfere each other.

NATURAL HAPTIC FEEDBACK

Reflecting natural occurring interaction forces to the human operator has been researched extensively for position controlled interface architectures (e.g. Lawrence (1993); Yokokohji and Yoshikawa (1994)). In this case the remote machine copies the (scaled) behavior of the human operator and reflects the interaction forces to the input device. The measured forces due to inertia and interaction on the remote machine are directly scaled if appropriate and fed back to the human operator (Hannaford, 1989; Wildenbeest et al., 2014). In subsea applications controlling large special purpose ROVs, down scaling of the reflected forces is required due to their magnitude. However it remains unclear what the effect on the perception of the force is when scaled and up to what level this can be done and how this affects task execution.

For rate controlled machines reflecting natural forces is more complex, because the machine does not copy the input directly, the measured forces can also not be reflected directly as well (Zhu and Salcudean, 1995). In this case the position of the operator is integrated to the machines

position, thereby the derivative of measured force should be reflected as force to the human operator (Salcudean et al., 1998, 2000). Another method is to reflect the interaction forces of the machine as stiffness modulation to the human operator (Lawrence et al., 1997; Parker et al., 1993). This has the benefits of remaining stability around zero, where the stiffness and therefore feedback force remain directly coupled to the interaction forces and therefore more tangible to the operator. The usability for the operator of both types of feedback is still unclear of how this would effect the understanding of the machine and conducted task.

Excavation tasks of subsea machines are largely dependent on the interaction of the machine with the environment and could potentially benefit from haptic feedback (Ostoja-Starzewski and Skibniewski, 1989). The effectiveness and usability of haptic feedback needs to be investigated for parts of the task when moving in water (i.e. free-space tasks), during a contact transition with the seabed or when in contact with the seabed exerting a specific force (e.g. during cutting).

HAPTIC GUIDANCE FEEDBACK

Reflecting augmented guidance forces to human operators has proven increasing task performance and reduced control effort in automotive, aerospace and maintenance in nuclear applications (e.g. Abbink and Mulder (2009); Abbott and Okamura (2003); Boessenkool et al. (2013)). The designed guidance forces can be categorized into two types: repulsive guidance forces to prevent collision with an obstacle and attractive guidance forces towards a suggested path (Prada and Payandeh, 2009).

Repulsive guidance forces have been applied in research for aerospace applications when remotely controlling UAVs (Unmanned Aerial Vehicles), to avoid buildings and obstacles based on local sensor information (Lam et al., 2009). Repulsive guidance can be offered as passive guidance forces in the form of potential fields around objects, also known as virtual fixtures, e.g. a virtual wall to support operators in task execution (Rosenberg, 1993). Attractive guidance forces actively calculates suggested steering inputs to steer the controlled vehicle towards a suggested path, acting as a second controller by means of forces, known as haptic shared control (Abbink et al., 2012; Steele and Gillespie, 2001). In automotive applications attractive guidance forces are commonly applied to support lane keeping on highways for instance (Griffiths and Gillespie, 2005). This lane assist can be based on local sensors but can also consist of global task information and strategy. However, both methods of repulsive and attractive guidance have never been compared for their effectiveness, based on the information content entailed in these methods.

Both repulsive and attractive guidance forces have not been applied for controlling any subsea machines so far. Potentially attractive guidance (i.e. haptic shared control) can be applied for controlling a subsea tracked vehicle over a suggested path driving on the seafloor. Haptic shared control has shown to be capable of smoothly switching between automation and manual control by the operator, by agreeing to the suggested inputs or actively overwriting these forces (Abbink et al., 2012). It needs to be investigated how this compares to full automation (by means of supervisory control) for normal operation and the impact during unexpected events

when takeover is required (by means of manual control).

1.3. PROBLEM OF EXISTING CONTROL INPUT METHODS

REMOTELY operated subsea vehicles such as a deep-sea grab or a backhoe excavator are difficult to operate due to their large size and therefore often slow dynamic response. These machines are controlled using limited visual feedback of the measured system parameters of the vehicle, operated by joysticks controlling the velocity of the vehicle. Rate control enables an infinite workspace but requires a high visual demand of controlling position and forces in the environment. Therefore the problem of the existing control input methods for these machines is the lack of haptic feedback for understanding the state of the vehicle. Additionally using complex partial automation of the subtasks improves task performance during normal operation, but increases the complexity of the machine and its dynamic response.

Natural force feedback based on the natural occurring interaction forces with the remote environment could improve the understanding of the state of the machine and its environment. However for rate controlled input devices it is unknown how to give effective and useful natural force feedback for a task including all three fundamental task types of such machines (free-space, contact transition and force level tasks). Additionally supporting the operator with artificial guidance forces from an intelligent controller calculating the optimal control input could simplify and improve the task execution. However for such large machines with a slow dynamic response it is unclear if repulsive guidance forces to avoid obstacles are more useful or attractive forces towards a suggested path and target. Also guidance forces can be comparable to automatic control in normal operation, but possibly deteriorate the performance when manual take over is required in unforeseen situations.

1.4. THESIS AIM AND METHOD

THE aim of this thesis is to investigate the design of effective haptic feedback in rate control for remotely controlled subsea vehicles, including both natural force feedback and guidance forces. This is investigated in three parts, as visualized in figure 1.5. First the general task environment of deep-sea mining is analyzed, secondly the design and effect of natural haptic feedback is explored, and thirdly the implementation of haptic guidance forces is studied.

The last two parts of natural and guidance feedback are first investigated for their fundamental design in detail on an abstract task level. For this purpose comparisons are made for both types of feedback between several existing design methods and designs originating from other domains. This is tested on abstract task experiments including free-space environments combined with virtual abstract objects (e.g. blocks and circles) to avoid or made contact with.

Furthermore the outcome of the abstract task level is used for studying the effect on an applied task level. For natural feedback this is investigated for controlling a backhoe excavator as shown in figure 1.2, an existing application of a rate controlled machine including free-space and in-contact parts of the task. Haptic guidance feedback is investigated for controlling deep-sea mining equipment as depicted in figure 1.3, driving a tracked vehicle over the seabed.

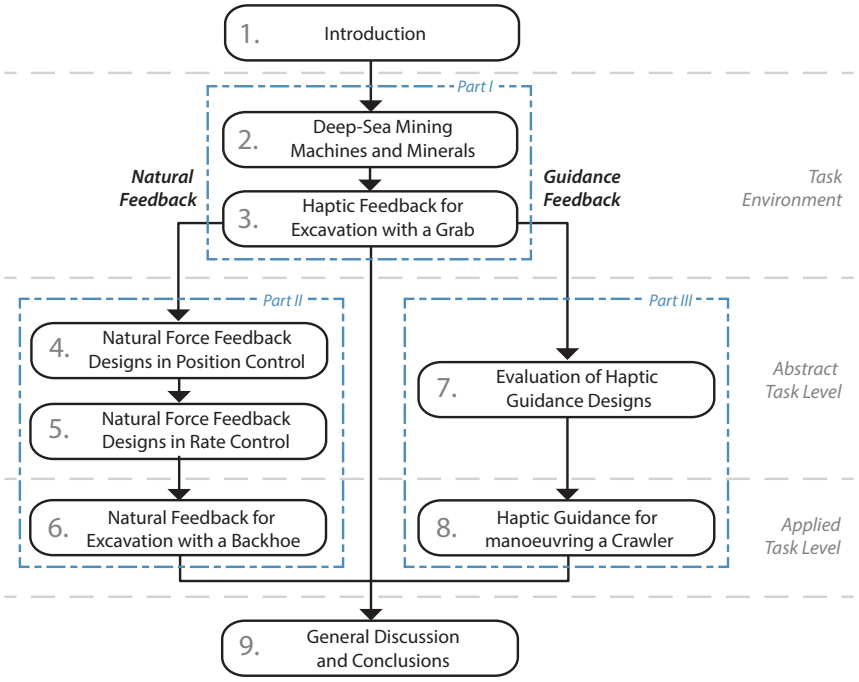

Figure 1.5: Dissertation overview and structure of linking chapters. The chapters are split in three parts: 1) general task environment, 2) exploring natural haptic feedback and 3) exploring haptic guidance feedback. Part 2 and 3 can also be subdivided based on their task level, abstract or applied.

1.5. THESIS OUTLINE

THE chapters of this thesis are based on articles which have been published prior to this thesis or currently under review, at the time of this thesis. Some of the chapters have been modified and/or contain overlap to some degree. The structure of the chapters and relating links are shown in figure 1.5.

PART I: GENERAL TASK ENVIRONMENT

A most challenging application for controlling subsea vehicles is deep-sea mining, with large uncertainty in sea floor properties for excavation and traction. In **chapter 2** a novel theory is given on the hardening of rock material in deep sea, currently the main underlying uncertainty of the sea floor properties. The theory of marginal hardening effect for high pressured rock is validated with material tests for low loading rates. Additionally, the implications for excavation energy are given on these findings by comparing the energy consumption of two excavation methods to be used in deep-sea mining. Conventionally track driven drum cutters are applied with high loading rates, now compared to a suspended grab with low strain rates for reduced excavation energy subsea.

Using a grab for deep-sea mining showed promising results in chapter 2. Controlling

such complex machinery however is challenging for human operators. It remains impossible to fully automate such a machine in these harsh environments with unforeseen events and unpredictable detailed material properties. The possibility for haptic shared control and natural force feedback is therefore investigated in **chapter 3** for controlling a suspended hydraulic grab. Both concepts of haptic feedback are investigated for their potential on improving situational awareness and control effort of controlling such heavy machinery remotely.

Controlling a vehicle for deepsea mining is challenging due to its scale and operating environment. Two possibilities for offering support to the human operator are natural haptic feedback and haptic shared control, which both needs to be investigated further for these type of machines.

PART II: EXPLORING NATURAL HAPTIC FEEDBACK

Offering natural haptic feedback potentially increases the situational awareness, but needs to be investigated in detail how this can be applied and effects controlling large heavy machines with a slow dynamic response.

Large heavy machines as described in chapter 2 and chapter 3 are challenging to control due to their slow dynamic response, requiring anticipation for the control inputs. **Chapter 4** investigates the effect of varying dynamic response of the controlled machine on the effectiveness of (scaled) haptic feedback when controlling such machines. This was investigated for an abstracted 1 DoF virtual task, for which the control input position is slowly mimicked by the controlled machine. No, scaled, or full haptic feedback was given of the inertial effects of the remote machine (i.e. (de)accelerations). A cybernetic model was used to identify the control behaviour of the operator and explain the effect of offering haptic feedback when operating slow dynamic systems.

Remotely operated subsea vehicles typically are operated by controlling their velocity instead of position directly due to the operational workspace and dynamic response. Based on the findings of chapter 4 for position control, **chapter 5** compares the effectiveness of offering natural feedback designs in rate controlled tasks. The fundamental design of natural feedback in rate control is compared for two approaches (force-based feedback and stiffness feedback) These designs are compared when conducting three fundamental tasks types; free-space, contact transition and force level tasks.

The developed stiffness feedback design of chapter 5 is applied to a realistic task of controlling a backhoe dipper excavator in **chapter 6**. This typical application is a rate controlled large heavy machine consisting of all subtask types; moving in water, making contact with the seafloor and cutting through sand. An excavator simulator with haptic feedback is developed to enable the operator to feel the interaction forces the excavator exerts on the environment. This includes the design and fabrication of a high quality force reflecting joystick and design and implementation of a haptic feedback algorithm for such a task. A human factors case study demonstrates the proof of principle of the combined simulator in a closed control loop.

PART III: EXPLORING HAPTIC GUIDANCE FEEDBACK

Offering haptic guidance forces potentially improves task performance and reduces control effort, but can be offered in various ways for such unstructured tasks.

A different approach to improve the remote control of a machine is to offer guidance forces to the operator, compared to offering natural feedback as described in chapters 4,5 and 6. The basic design of two guidance methods (repulsive and attractive guidance) are evaluated in **chapter 7** for task performance and control effort. This comparison is done based on the nature of conveyed information, either only including local environment information or global task information. The evaluation of reflected information content is tested on two modalities (by haptic or visual cues) and on task complexity.

Based on the outcome of chapter 7, haptic shared control (i.e. attractive haptic guidance) is applied in **chapter 8** for controlling a subsea tracked vehicle over a suggested path on the seafloor. This chapter investigates the guidance method for a more realistic task. Offering haptic shared control is compared to full automation (by means of supervisory control) and manual control. This experiment investigates the benefits of full automation for normal operational conditions and the benefits of manual control in unexpected events. This was tested for controlling a deep-sea mining crawler in rate control for a path following experiment.

In the general discussion in **chapter 9** conclusions are drawn for offering haptic feedback to improve task performance with remotely controlled subsea vehicles with a rate controlled interface, and discusses the limits and recommendations based on the found results.

REFERENCES

Abbink, D., Mulder, M., and Boer, E. (2012). Haptic shared control: smoothly shifting control authority? *Cogn. Technol. Work*, pages 19–28.

Abbink, D. A. and Mulder, M. (2009). Exploring the Dimensions of Haptic Feedback Support in Manual Control. *J. Comput. Inf. Sci. Eng. Spec. Haptics Ed.*, 9(March):1–9.

Abbott, J. and Okamura, A. (2003). Virtual fixture architectures for telemanipulation. *IEEE Int. Conf. Robot. Autom.*, pages 2798–2805.

Bloois, J. W. V. and Frumau, J. C. L. (2009). Deep Sea Mining , The New Horizon for Dredging Technology. In *Proc. Offshore Technol. Conf.*, number May, page 8.

Boessenkool, H., Abbink, D. A., Heemskerk, C. J. M., van der Helm, F. C. T., and Wildenbeest, J. G. W. (2013). A task-specific analysis of the benefit of haptic shared control during telemanipulation. *IEEE Trans. Haptics*, 6(1):2–12.

Endsley, M. R. (1995). Measurement of Situation Awareness in Dynamic Systems. *Hum. Factors J. Hum. Factors Ergon. Soc.*, 37(1):65–84.

Griffiths, P. and Gillespie, R. B. (2005). Sharing Control Between Human and Automation Using Haptic Interface : Primary and Secondary Task Performance Benefits. *Hum. Factors*, 47(3):574–590.

Hannaford, B. (1989). A design framework for teleoperators with kinesthetic feedback. *IEEE Trans. Robot. Autom.*, 5(4):426–434.

Hannaford, B., Wood, L., McAffee, D. A., and Zak, H. (1991). Performance evaluation of a six-axis generalized force-reflecting teleoperator. *IEEE Trans. Syst. Man Cybern.*, 21(3):620–633.

Kim, W. S., Tendick, F., and Stark, L. W. (1987). Visual Enhancements in Pick-and-Place Tasks: Human Operators Controlling a Simulated Cylindrical Manipulator. *J. Robot. Autom.*, 3(5):418–425.

Kontz, M. E. and Book, W. J. (2006). *Kinematic analysis of backhoes/excavators for closed-loop coordinated control*, volume 8. IFAC.

Kuiper, R. J., Chen, X., and Frumau, J. C. L. (2016). Reduction of Energy Consumption When Using a Grab for Deep-Sea. In *Offshore Technol. Conf. 2016*, page 13, Houston. OnePetro.

Kuiper, R. J., Frumau, J. C., and Miedema, S. A. (2013). Influence of the Hyperbaric Effect on Apparent Material Strength of Fully Saturated Porous Rock for Low Strain Rates. In *Offshore Technol. Conf. 2013*, pages 1–13.

Lam, T., Boschloo, H., Mulder, M., and van Paassen, M. (2009). Artificial Force Field for Haptic Feedback in UAV Teleoperation. *IEEE Trans. Syst. Man, Cybern. - Part A*, 39(6):1316–1330.

Lawrence, D. A. (1993). Stability and Transparency in Bilateral Teleoperation. *IEEE Trans. Robot. Autom.*, 9(5):624–637.

Lawrence, P., Salcudean, S., and Sepehri, N. (1997). Coordinated and force-feedback control of hydraulic excavators. In *Exp. Robot. IV*, pages 181–194.

McRuer, D. and Jex, H. (1967). A Review of Quasi-Linear Pilot Models. *IEEE Trans. Hum. Factors Electron.*, HFE-8(3):231–249.

Ostoja-Starzewski, M. and Skibniewski, M. (1989). A master-slave manipulator for excavation and construction tasks. *Rob. Auton. Syst.*, 4(4):333–337.

Parker, N., Salcudean, S., and Lawrence, P. (1993). Application of force feedback to heavy duty hydraulic machines. *[1993] Proc. IEEE Int. Conf. Robot. Autom.*, pages 375–381.

Prada, R. and Payandeh, S. (2009). On study of design and implementation of virtual fixtures. *Virtual Real.*, pages 117–129.

Rosenberg, L. (1993). Virtual fixtures: Perceptual tools for telerobotic manipulation. *IEEE Virtual Real. Int. Symp.*, pages 76–82.

Salcudean, S., Tafazoli, S., Hashtrudi-Zaad, K., Lawrence, P., and Reboulet, C. (1998). Evaluation of impedance and teleoperation control of a hydraulic mini-excavator. *Exp. Robot. V*.

Salcudean, S. E., Zhu, M., Zhu, W.-H., and Hashtrudi-Zaad, K. (2000). Transparent Bilateral Teleoperation under Position and Rate Control. *Int. J. Rob. Res.*, 19(12):1185–1202.

Sepehri, N., Lawrence, P. D., Sassani, F., and Frenette, R. (1994). Resolved-Mode Teleoperated Control of Heavy-Duty Hydraulic Machines. *J. Dyn. Syst. Meas. Control*, 116(2):232.

Sheridan, T. (1989). Telerobotics. *Automatica*, 25(4):487–507.

Sheridan, T. B., Verplank, W. L., and Brooks, T. L. (1978). Human/computer control of undersea teleoperators. Technical report, Tokyo.

Stassen, H. G. and Johannsen, G. (1990). Internal Representation , Internal Model , Human Performance Model and Mental Workload. 26(4):811–820.

Steele, M. and Gillespie, R. B. (2001). Shared control between human and machine: Using a haptic steering wheel to aid in land vehicle guidance. *Proc. Hum. Factors Ergon. Soc. 45th Annu. Meet.*, pages 1671–1675.

Tivey, M. K. (2007). Generation of Seafloor Hydrothermal Vent Fluids and associated Mineral Deposits. *Oceanography*, 20(1):50–65.

van Es, B., de Vlaming, R., and de Vries, J. (2004). Construction of Wellhead Protection Glory Holes for White Rose Project, Canada. *Terra Aqua*, (95):22–32.

Wildenbeest, J. G., Kuiper, R. J., van der Helm, F. C., and Abbink, D. A. (2014). Position control for slow dynamic systems: Haptic feedback makes system constraints tangible. *2014 IEEE Int. Conf. Syst. Man, Cybern.*, pages 3990–3995.

Wildenbeest, J. G. W., Abbink, D. A., Heemskerk, C. J. M., Helm, F. C. T., and Boessenkool, H. (2013). The Impact of Haptic Feedback Quality on the Performance of Teleoperated Assembly Tasks. *IEEE Trans. Haptics*, 6(2):242–252.

Winck, R. C., Elton, M., and Book, W. J. (2015). A practical interface for coordinated position control of an excavator arm. *Automation in Construction*, 51(C):46–58.

Yokokohji, Y. and Yoshikawa, T. (1994). Bilateral Control of Master-Slave Manipulators for Ideal Kinesthetic Coupling - Formulation and Experiment. *IEEE Trans. Robot. Autom.*, 10(5):605–620.

Zhu, M. and Salcudean, S. E. (1995). Achieving Transparency for Teleoperator Systems under Position and Rate Control. *IEEE Int. Con. Intell. Robot.*, pages 1–6.

PART I

GENERAL TASK ENVIRONMENT

2

DEEP-SEA MINING MACHINES AND MINERALS

Roel J. Kuiper, Xiuhan Chen, Jan C.L. Frumau and Sape A. Miedema

published in OTC proceedings, 2013 & 2016

Deep-sea mining is a challenging application for controlling vehicles subsea, with large heavy complex machines to control and large uncertainties in seafloor properties. In this chapter the hardening effect of rock material in high pressurized environments is investigated, by means of material tests and its implications for excavation energy. A novel rock failing mechanism in high pressured ambient conditions is described and validated with rock crushing tests. Results show increasing hardening as expected but substantial less for low loading rates (<50%). Additionally this chapter extrapolates these findings by comparing the energy consumption of two excavation methods to be used in deep-sea mining, using a suspended grab or drum cutter. It is shown that using a grab requires substantially less excavation energy (21%) due to the low loading rates and therefore lower effective rock strength.

The content of this chapter is divided into two parts. Section 2.1 describes the novel theory of marginal hardening effect for high pressured rock with low loading rates and the validating material test results[1]. Section 2.2 describes the implications for excavation energy for the found difference of low loading rates, by comparing the energy consumption of two excavation methods to be used in deep-sea mining (drum cutter and suspended grab)[2].

[1] R.J. Kuiper, J.C.L. Frumau, S.A. Miedema; Influence of the Hyperbaric Effect on Apparent Material Strength; Offshore Technology Conference proceedings 2013, 23956-MS

[2] R.J. Kuiper, X. Chen, J.C.L. Frumau, S.A. Miedema; Reduction of Energy Consumption when using a Grab; Offshore Technology Conference proceedings 2016, 27080-MS

2.1. Influence of the Hyperbaric Effect on Apparent Material Strength

Published in Offshore Technology Conference proceedings, 2013[3]

Abstract

Excavation of rock materials such as Seafloor Massive Sulfide deposits at great depths is greatly influenced by ambient water pressure, but little is known about the processes involved. Dry rock specimens are known to exhibit a large increase of apparent material properties in high-pressure environments. However, in deep-sea mining processes rock material is fully saturated and it is unknown how the hyperbaric effect changes apparent material strengths and involved physical processes under these conditions. This paper discusses the influence of hyperbaric effect on fully saturated brittle rock specimens during deep-sea excavation using a grab, and the resulting changes in apparent material properties. Computations are described which are used to predict the outcome of this effect, and the validating experiments that were carried out. A new theorem is stated based on elastic deformation of the grain matrix, which causes a pressure difference in the matrix and reinforces the material. This is based on the low cutting speed of a grab, allowing the material to deform elastically and enabling water ingress into the deformed material, resulting in less cutting energy. Moreover the cutting mechanism of a grab has a very low ratio of cutting energy over excavated rock volume. The theoretical model was developed in collaboration with Delft University of Technology and experiments were carried out with Seatools BV. Experiments were conducted to investigate the phenomenon and to validate the stated theorem for saturated rock material. An experimental setup was developed in collaboration with Seatools BV, to test rock material properties at different hyperbaric conditions with a low rate of loading. The experiments were designed to carry out standard material tests of the American Society for Testing and Materials to determine the compressive and tensile strength, by crushing the material specimens up to their breaking point in different hyperbaric conditions. The experiments were used to validate the theoretical computations that predicted differences in tensile strength between saturated and dried specimen, due to ingress of water during deformation causing not the full increase of the apparent material strength. The results were consistent and a correlation between the environment pressure and the added apparent material strength was found.

2.1.1. Introduction

Active volcanic areas in the deep-sea create metal-rich mineral deposits that are a promising solution to cope with the fast increasing metal demand and decreasing supplies from conventional mines (Rona, 2003; Scott, 2001; Yang and Scott, 1996). Initially after the discovery of widespread abundance of manganese nodules in the deep-sea in the 1980s, the main focus for deep-sea mining was to collect these nodules in deep waters exceeding 4500m (Glasby,

[3] R.J. Kuiper, J.C.L. Frumau, S.A. Miedema; Influence of the Hyperbaric Effect on Apparent Material Strength; Offshore Technology Conference proceedings 2013, 23956-MS

2000). However this turned out to be a technical challenge and metal prices decreased shortly after that time. In the last ten years the metal prices have continued to rise again, leading to an increased interest in deep-sea mining near hydrothermal vents, which form locally metal-rich mineral deposits in water depths of 1000m to 2000m (Rona, 2003). High concentrations of common and rare-earth metals are found in these mineral deposits in rock material named seafloor massive sulphides (SMS) deposits (Tivey, 2007). Because these minerals are formed due to a condensation process on the seafloor from superheated water vapour with dissolved minerals from the so called 'black smoker' chimneys, the material is shown to be very porous saturated rock (Tivey, 2007). The behavior of the material properties at great water depth of such a material is unknown and has great influence on the excavation method of these minerals. The reaction forces of the porous material in high pressure hyperbaric conditions are unknown and could be largely increased compared to traditional on-land rock excavation. Therefore this paper focusses on the influence of the hyperbaric effect on the apparent material properties of fully saturated porous rock, to be able to determine the cutting forces required to excavate SMS deposits at great water depths.

A promising alternative method to excavate these deposits at such water depths is to use a large suspended grab (Bloois and Frumau, 2009). The grab would cut the submerged rock material using two opposite clamshells hydraulically actuated as shown in the left of Figure 1 for a design study of Seatools BV. To make a deep-sea mining process economically viable production calculations have shown that the size of the clamshells should be approximately 40m3, roughly the size of a large dump truck. An example of such an existing, but smaller (16m3) comparable machine developed by Seatools BV is shown in the right of figure 2.1, for removing soil in arctic conditions (van Es et al., 2004). Using a grab has advantages over a conventional crown or drum cutter for rock excavation due to the low ratio of cutting energy over excavated rock volume (Kuiper, 2012a), by not fully crushing the rock material. When

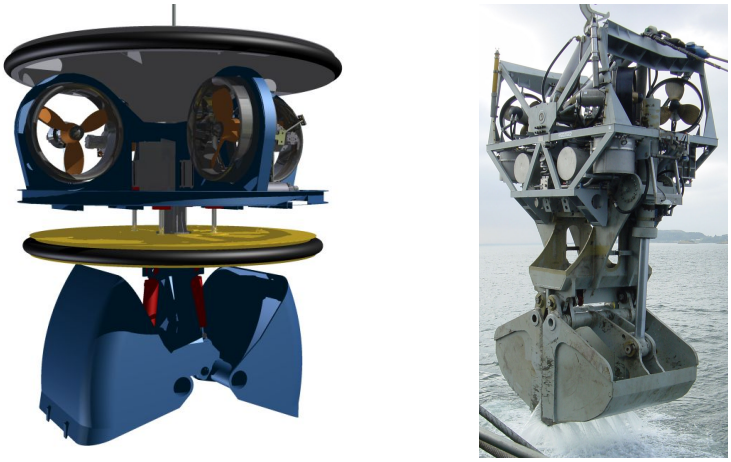

Figure 2.1: Example of two grabs. Left – Designed grab by Seatools BV proposed for deep-sea mining, from Bloois and Frumau (2009). Right – Fabricated grab by Seatools BV for dredging in Arctic conditions, from van Es et al. (2004).

closing the clamshells of the grab most of the rock material will stay intact, therefore only a small amount of material needs to be cut by the grab in relation to the excavated rock volume. A deep-sea mining task using a suspended grab would mainly only consist of excavating the rock material and placing it nearby on the seabed. Therefore the excavated rock materials are not intended to be vertically transported to the surface using the grab. There are multiple solutions investigated for the vertical transportation, one is to crush the materials subsea and pumping it to the ship through a vertical pipeline. An optimal method has to be determined in a later stage to transport the large pieces of rock material from the seabed to the surface.

Controlling a grab as shown in the left of figure 2.1 for a mining task can most likely not be fully automated due to the uncertainties of the remote environment and requires therefore a human operator to control part of the operation. A human operator is also required due to the financial risks involving the entire mining process dependent on the excavation at great depths, causing long operational downtime after automation failure. The control of the process can be done remotely from the operating ship by teleoperation. Important aspects of a teleoperation of such a large machine at great depth are the operators' performance and situation awareness. Operator error and/or suboptimal performance could reduce operational efficiency and might even lead to failure when not undertaking appropriate responses in critical situations. Applying haptic support to the human operator has shown promising results for controlling such a machine during a deep-sea mining process (Kuiper, 2012b). That type of support combines the available information of the continuous attentive automatic controller and the insight of the human operator for controlling the operation, causing an increase of the entire excavation performance and decrease periods of operational downtime due to incorrect execution of the operator.

Using a grab for excavating mineral deposits is beneficial due to the suspension of the grab and therefore not having to be supported by the unstable and rough terrain. Especially in the early stage of field development it can be beneficial to use a grab for excavation, due to the rough terrain which could be cleared by the grab. Excavating rock material using a grab is an extremely slow cutting process due to the limited closing velocity of the clamshells. The research in this paper will focus on this slow cutting process of fully saturated porous rock material and the influence of hyperbaric pressure on such a cutting process. When the clamshells of the grab cut the material it creates a pure tensile stress in the rock material between the clamshells, combined with some compressive crushing locally around the clamshell teeth themselves. However due to the low cutting velocities it is hypothesized that the hyperbaric effect will have little influence on the tensile stress in fully saturated porous rock compared to theory for dry rock under confining pressures. In section 2.1.2 the theoretical approach is described for dry rock under confining pressure and the developed theorem for saturated rock in hyperbaric conditions. Validating experiments are conducted to verify the developed theorem as described in section 2.1.3 and the experimental results are given in section 2.1.4.

2.1.2. ROCK FAILURE MECHANISM THEORY

ROCK FAILURE CRITERION

Several cutting models for rock cutting are described in literature to predict the behavior of an excavation process. However none of these models were developed to describe a rock cutting process in deep-sea. A two dimensional cutting model for cutting elastic-plastic material mainly based on shear failure is described by the model of Merchant (Merchant, 1945). However this model is not intended for brittle rock and is therefore not suitable for the type of excavation method such as a grab in deep sea. Evans developed a two dimensional cutting model for cutting coal based on tensile breakage (Evans, 1965). The theorem of Evans is very suitable because rock cutting using a grab is mainly based on a tensile stress between both clamshells. Bieniawski also developed a cutting model for brittle rock, based on a brittle fracture mechanism (Bieniawski, 1967). However this model is mainly based on failure due to compressive forces causing a shear failure based on the relation of normal and shear stress of Griffith (1921). Similar to the theorem of Merchant a two dimensional cutting model is developed by Nishimatsu mainly for shear failure of rock including, a compressive crushed zone at the tool tip (Nishimatsu, 1972). A two dimensional cutting theory for cutting water saturated sand is developed by Miedema, intended for excavating elements such as cutterheads and dragheads (Miedema, 1987). This model describes the process of cutting underwater and is therefore very suitable for modeling the influence of water in the pore volume of submerged rock. In more recent work by Miedema

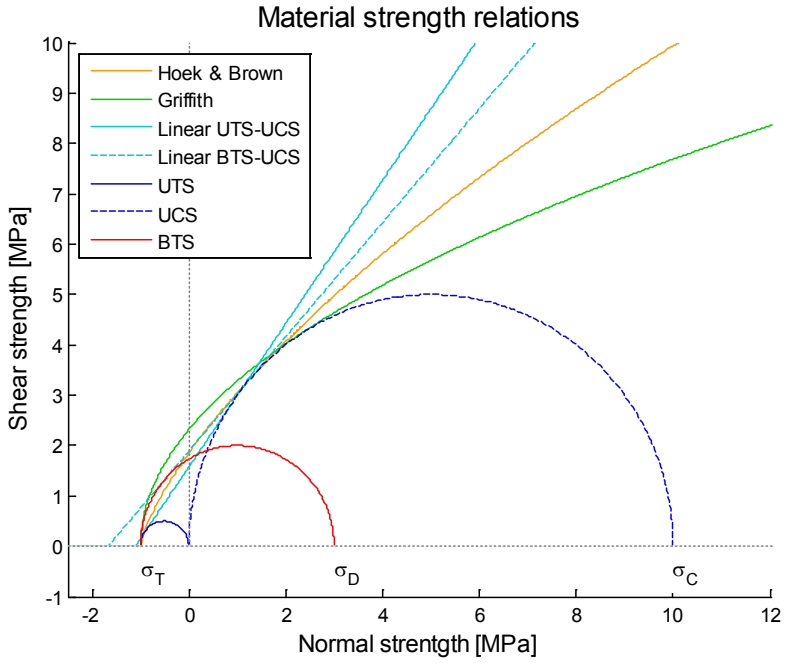

Figure 2.2: Rock material strengths shown in UCS, UTS and BTS Mohr circles with different equations for shear strength, based on (Fairhurst, 1964; Griffith, 1921; Hoek, 1964; Hoek and Brown, 1997; Nishimatsu, 1972).

a simplified model is developed to estimate the cutting force in water saturated sand for deep waters (Miedema, 2011) The model of Basheyev describes a model for breaking rock using a wedge shaped impact tool (Basheyev et al., 1999). This model gives a good insight for crack forming and stress distribution from a wedge shaped tool tip such as a clamshell teeth loading rock.

None of the above mentioned cutting models are directly suitable for describing a rock cutting process in deep sea. One of the key things these models do not describe is the confining pressure acting on the rock material. From other literature is known that confining pressure result in higher apparent material properties (Lockner, 1995), which is mainly based on the theorem of Mohr as described by Hoek (1964). Nonetheless the theorem of Evans describes a clear tensile failing method for brittle rock and the model of Miedema includes pressure differences in pore fluids, which both are essential parts to describe a rock cutting process in deep-sea (Miedema, 1987).

Essentially a rock cutting model for excavating deep-sea minerals using a grab would be based on loading the material slowly with high stresses up to the material strength failing point. It is therefore required to describe the material strength appropriately for developing a theorem of deep-sea rock cutting, which can be done using several methods. In figure 2.2 several of these methods are shown, describing the normal strength and the relation to shear strength of the material in different ways. The most widely known method is to use Mohr circles for showing the normal strength of materials and their maximum shear strength at that point of normal stress (Hoek, 1964). The normal strength can be shown by the unconfined compressive strength (UCS) and unconfined tensile strength (UTS) as shown in blue in figure 2.2. A linear method is developed to determine the shear strength based on these UTS and UCS Mohr circles as shown in light-blue solid line in figure 2.2. However the unconfined tensile strength is difficult to test for rock and soil specimens. A more common method for determining the tensile strength is to use the method of the Brazilian tensile strength (BTS) as shown in red in figure 2.2 (Fairhurst, 1964). This method uses compressive loading on usually a circular specimen, creating tensile stress at the centerline of the specimen. A linear expression is also developed for shear strength based on the UCS and BTS Mohr circles as shown with the dashed light blue line in figure 2.2 (Nishimatsu, 1972). However both linear relations have an overshoot of shear strength at large normal stresses and therefore nonlinear relations describe the shear strength relations more appropriately. The most commonly used nonlinear shear strength relation is developed by Griffith as shown in green in figure 2.2 (Griffith, 1921). However a more recently developed method by Hoek and Brown is shown with the orange line in figure 2.2 (Hoek and Brown, 1997).

MATERIAL STRENGTH IN HYPERBARIC CONDITIONS

Mineral excavation in deep sea is mainly different from previous work due to the hyperbaric conditions the material is submerged in. This ambient pressure would result in a confining pressure for rock material which would not be fully saturated and would result in higher apparent material properties (Lockner, 1995). However the rock material in deep-sea is fully saturated because the formation of these minerals occurred in equal conditions. Therefore the ambient pressure does not cause a confining pressure in static conditions. However during

excavation the structure of the material is altered and could cause pressure differences acting on the apparent material properties.

A possible theorem for changing apparent material properties due to the ambient pressure could be the reinforcement of crack forming. During rock cutting the material is opened at the tool tip and a tensile crack will form from there on, as described by Evans for brittle material (Evans, 1965). This opening of the tensile crack could be reinforced by the ambient pressure acting on the pressure drop in the opening of the crack due to the local volume increase. This reinforcement would be dependent on the permeability of the material, based on the research of van Kesteren on drained and undrained material conditions (van Kesteren, 1995) and described in the book of Winterwerp and van Kesteren (2004).

Nonetheless this theorem of crack reinforcement is dependent on the penetration velocity of the tool tip in relation to the crack formation velocity. For excavating using a grab the tool penetration is much slower than the reinforcement could slow down the formation of the crack. However it is hypothesized when using a grab the apparent material will be marginally influenced by the hyperbaric conditions. Therefore an alternative theorem is developed in the MSc thesis of Kuiper for excavating using a grab in hyperbaric conditions for saturated rock (Kuiper, 2012a). This theorem is based on the elastic deformation of the grain matrix when slowly loaded up to the failure of the matrix. A tensile stress is created between both clamshells of a grab when the matrix is deformed and the pore volume is locally increased at the tensile stress plane. This is schematically shown in figure 2.3, where on the left the theoretical matrix is loaded with F at initial pressure conditions p_0 and deformed on the right. This deformation causes a local volume increase and pressure drop P_{core} due to the bulk modulus of water when no water has penetrated the deformed zone. The penetration of water however will occur at a rate Q_{water} dependent on the permeability of the material. The influence of the hyperbaric conditions on the apparent tensile strength will depend on the ratio of the rate of inflow of water and the rate if loading of the specimen.

The apparent material strength changes during the deformation of the material as shown in

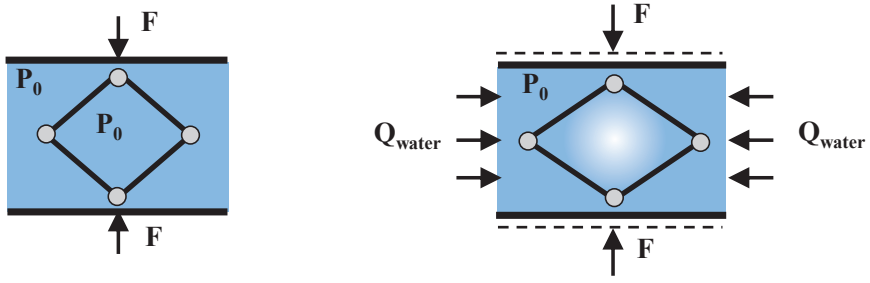

Figure 2.3: Schematic drawing of pore pressure decrease due to deformation of the grain matrix, adapted from (Kuiper, 2012a). Left – Initial condition of the grain matrix with pore and ambient pressure equalized and loading force applied creating a tensile stress on the matrix. Right – Elastic deformation of the grain matrix due to loading forces with pore volume increased causing a pressure drop at the core and an inflow of water into the matrix from the surrounding water.

figure 2.3, due to the pressure difference in the core compared to the ambient pressure. The two changing states of the grain matrix can be described with material strength relations applied to cylindrical specimens as used in the experiment as described in section 2.1.3. At the initial condition where the core pressure is equal to the ambient pressure, the normal compressive material strength $S_{compression}$ can be described with Eq. (2.1) relating the loading force F and the diameter D_s of a cylindrical specimen as described by Hoek and many other literature (Hoek, 1964). This relation to determine compressive strength from loading forces is also used in the ASTM guidelines for unconfined compressive strength experiments (ASTM C 39/C 39M, 2005).

$$\sigma_{compression} = \frac{F}{\frac{1}{4} \cdot \pi \cdot D_S^2} \tag{2.1}$$

For the deformed condition as shown in the right of figure 2.3 the compressive strength can be adjusted with the factor of influence λ_C of water pressure p_W as given in (2.2). Previous research of Brace and Martin observed a dilatancy hardening effect due to trapped water in the pore volumes for high strain rates (Brace and Martin, 1968). The previous and more recent work of Miedema includes the dilatancy phenomenon into the cutting theory for water saturated sand (Miedema, 1987, 2011). However it is hypothesized the influence of water pressure on apparent compressive strength will not be present at low strain rates, enabling the excessive water to flow out of the matrix and not noticeably increase the apparent compressive strength.

$$\sigma_{compression} = \frac{F}{\frac{1}{4} \cdot \pi \cdot D_S^2} - \lambda_C \cdot p_w \tag{2.2}$$

The relation for tensile strength $\sigma_{tensile}$ can be described by Eq. (2.3) dependent on the loading force, diameter of the cylindrical specimen and length L_s for the Brazilian tensile strength experimental method as described by Fairhurst (1964). This relation for the tensile strength from the compressive loading forces is also used in the ASTM guidelines for Brazilian tensile strength experiments (ASTM C 469/C 496M, 2004).

$$\sigma_{tensile} = \frac{2 \cdot F}{\pi \cdot L_S \cdot D_S} \tag{2.3}$$

The tensile strength relation can also be adjusted with the factor of influence λ_T of water pressure as given in Eq. (2.4) comparable to the compressive strength relation adjustment. For the tensile strength it is hypothesized the influence of ambient pressure on apparent tensile strength is relative low for fully saturated material, dependent on the permeability of the material.

$$\sigma_{tensile} = \frac{2 \cdot F}{\pi \cdot L_S \cdot D_S} - \lambda_T \cdot p_w \tag{2.4}$$

From the two normal stresses the shear strength can be determined using one of the theorems as described in section 2.1.2. The linear methods are not very accurate and therefore the most commonly used method of Griffith is used in this paper (Griffith, 1921). The relation of

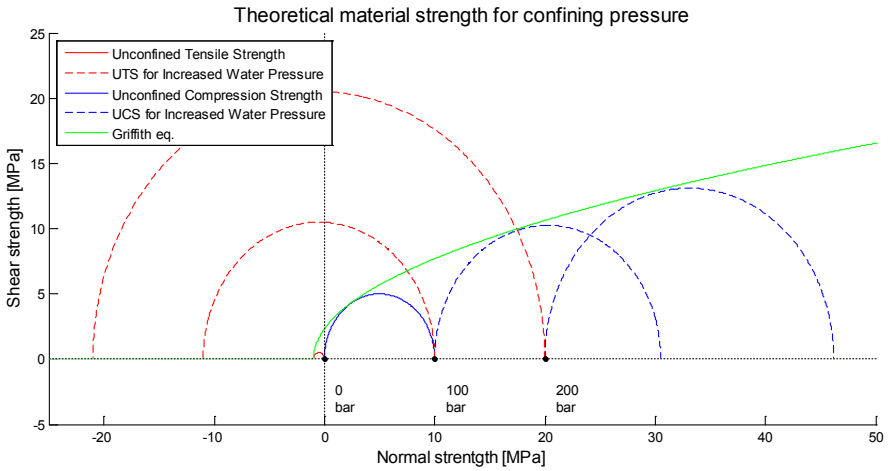

Figure 2.4: Fictive theoretical Mohr circles for confining pressure on dry samples indicating the increase of apparent material properties for the full hyperbaric effect.

shear strength τ dependent on confining normal stress σ is given in Eq. (2.5) where m is the ratio of unconfined compressive strength over unconfined tensile strength σ_T.

$$\tau^2 = \sigma_T \cdot \left(\sqrt{m+1}-1\right)^2 \cdot (\sigma + \sigma_T) \tag{2.5}$$

The relation of Griffith for shear strength and normal stress could be adjusted for the influence of ambient water pressure as done for the compressive and tensile strength relations. However this adjustment is not that trivial as before and is only adjusted for the tensile strength as hypothesized. The adjusted relation is given in Eq. (2.6), where the entire relation is shifted due to the changing apparent tensile strength as shown in the right of the equation and scaled in the left of the equation to correct for the unchanging apparent compressive strength.

$$\tau^2 = \left(\sigma_T \cdot \frac{\lambda_T \cdot p_w}{5}\right) \cdot \left(\sqrt{m+1}-1\right)^2 \cdot \left(\sigma + \sigma_T - \lambda_T \cdot p_w\right) \tag{2.6}$$

A summarizing graph of the material strength relations for compressive, tensile and shear strength is given in figure 2.4 for the unchanged relations as described in Eq. (2.1), Eq. (2.3) and Eq. (2.5) with Mohr circles and the Griffith equation. The figure shows with solid lines the initial condition as shown in the left of figure 2.3. The dashed lines show the increase of apparent material properties for confining pressures when using dry samples as described by many literature for triaxial confining experiments (Lockner, 1995). The adjusted relations for the influence of ambient water pressure as described in Eq. (2.2), Eq. (2.4) and Eq. (2.6) are shown for the experimental results figure 2.9 in section 2.1.4.

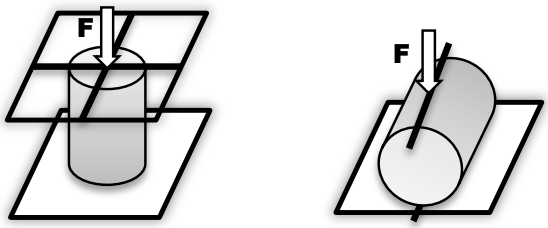

Figure 2.5: Schematic drawing of experimental method for both experiment types, adapted from (Kuiper, 2012a). Left - Unconfined compressive strength test by loading the axial surfaces of the cylindrical specimen. Right - Brazilian tensile strength test by loading the two contact lines on the radial surface of the cylindrical surface.

2.1.3. EXPERIMENTAL METHODS FOR ROCK CRUSHING TESTS

EXPERIMENTAL DESCRIPTION

The theorem in section 2.1.2 describes the theoretical approach for dry rock under confining pressure and the developed theorem for saturated rock in hyperbaric conditions. An experiment is designed to determine the influence of the hyperbaric condition on the apparent material properties in fully saturated porous rock. The experiment consists of two parts; unconfined compressive strength and Brazilian tensile strength experiment. For both parts of the experiment cylindrical rock specimens are required of the same size, only the orientation of the specimen during the experiment changes. The materials were formed using a concrete mix to create equally strong fully saturated specimens. The specimens were stored fully submerged and hardened over 70 days to remove the hardening effect of concrete during experiments. The specimens during the experiment were loaded up to breaking point at a fixed loading rate of 0.30MPa/s as described in the guidelines of the American Society for Testing and Materials (ASTM) for testing the material strength of rock specimens.

The unconfined compressive strength experiment is schematically shown on the left of figure 2.5 and is based on the ASTM guidelines (ASTM C 39/C 39M, 2005). The experiment is partly designed such to prove the full saturation of the porous rock during the compressive experiments at hyperbaric conditions. At very low cutting velocities when fully saturated the compressive strength experiment is unconfined, however when not fully saturated the trapped air results in a confining pressure.

The Brazilian tensile strength experiment as shown schematically on the right of figure 2.5 is based on the ASTM guidelines as well (ASTM C 469/C 496M, 2004). The experiment is used to validate the partial influence of the hyperbaric effect for fully saturated porous rock at very low cutting velocities.

EXPERIMENTAL CONDITIONS

The experiment as described in section 2.1.3 is designed to determine the apparent material properties at hyperbaric conditions. To determine the influence of the hyperbaric conditions both experiments also have to be conducted at atmospheric conditions as a baseline. The atmospheric condition is applied in air as a baseline and in water to determine solely the effect

of a different medium on the apparent material strength. For the hyperbaric conditions two different conditions are applied, 100 and 200 bar in water to determine the relation between ambient pressure and apparent material strength. This gives in total four different conditions as shown in table 2.1 with three experimental conditions and one baseline condition.

When specimens were tested at hyperbaric conditions, all specimens were pressurized for 24 hours at their specific hyperbaric condition prior to the experiment.

APPARATUS

An experimental setup is developed in collaboration with Seatools BV to conduct the experiments as described in section 2.1.3. Basically a portable hydraulic press is developed as shown schematically in the left of figure 2.6 to load either the compressive or tensile experiment as shown in figure 2.5. A large hydraulic cylinder, capable of pressing sufficient force is mounted in a rigid steel frame. An electrical motor is mounted on the frame which is designed to be submerged in water and is powering a hydraulic pump to control the cylinder. The entire setup is designed such to just fit in the hyperbaric chamber available at Seatools BV as shown in the right of figure 2.6. Both the electrical power connection and the sensor signals are fed through the cover of the hyperbaric chamber and the setup is controlled using a frequency drive with real-time control system also for data collection. The experimental setup is described in more details in the MSc thesis of Kuiper (Kuiper, 2012a).

DATA ANALYSIS

To analyze the conducted experiments several measured variables are recorded as listed in table 2.2. The main variable used in this paper is the cylinder hydraulic pressure which can easily be converted to applied force by multiplying by the surface area of the hydraulic cylinder. The measured variables were recorded at 1000Hz to measure even the smallest fracturing in the specimen and to be able to filter the data without removing the details of the data.

The maximum loading force is used from the recorded data to calculate the material strength for each specimen. For the unconfined compressive strength experiment Eq. (2.1) is used to calculate the compressive strength from the maximum loading force along with the dimensions of the specimen. For the Brazilian tensile strength experiment Eq. (2.3) is used to calculate the tensile strength of the specimen. The results of both experiments are given normalized to atmospheric conditions along with the mean and their 95% confidence interval (CI) of the mean (Drummond and Vowler, 2011).

A one-way analysis of variance (ANOVA) is used to determine if there is a difference between

Table 2.1: Experimental conditions for both unconfined compressive strength experiment and Brazilian tensile strength experiment

	Baseline	EC1	EC2	EC3
Experimental Condition	0 dry	0 wet	100 wet	200 wet
Ambient Pressure	Atmospheric	Atmospheric	100 bar	200 bar
Ambient Medium	Air	Water	Water	Water

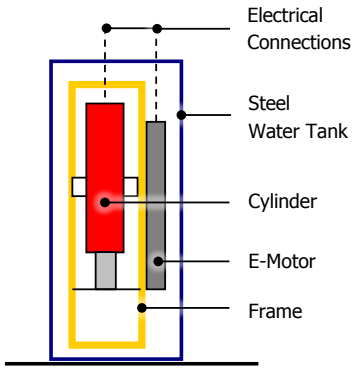

a)

b)

Figure 2.6: a) Schematic representation of experimental setup, adapted from (Kuiper, 2012a). b) Photograph of setup lowered in hyperbaric chamber

all conditions for each experiment (Drummond and Vowler, 2012). A significance level of 5% ($\alpha = 0.05$) is used and each condition for each experiment consisted of three specimens (N=3). When a difference is found for the entire experiment a post-hoc analysis is conducted to determine if there is a difference for each experimental condition compared to the baseline condition, also using a one-way ANOVA. No corrections are applied for the post-hoc analysis due to the low number of data points.

2.1.4. EXPERIMENTAL RESULTS OF ROCK IN VARIOUS AMBIENT PRESSURES

Two types of experiments are conducted as described in section 2.1.3 using three experimental conditions and a baseline condition as described in section 2.1.3. The results of the unconfined compression strength experiments are presented in this paper with a normalization correction factor as given in Eq. (2.7). This factor is applied to make the results independent from the used

Table 2.2: Recorded measured variables during each experiment

Measured variables
Cylinder hydraulic pressure
Water pressure hyperbaric chamber
Cylinder stroke
Experiment time
Desired hydraulic pressure
Motor control signal
Motor number of revolutions
Motor direction

material and comparable to other materials in the future, with compressive stress $\sigma_{compression}$, individual measurement point $\sigma(i)$ and mean baseline condition $\sigma_{Compression,material}$.

$$N_i(\sigma_{Compression}) = \frac{\sigma(i)}{\sigma_{Compression,material}} \tag{2.7}$$

The results of the Brazilian tensile strength experiment are presented in this paper with a different normalization factor as the compressive strength results as given in Eq. (2.8) with the mean baseline condition $\sigma_{Tensile,material}$. This factor is applied to scale the increase in material strength to one, where tensile stress $\sigma_{tensile}$ and $\sigma_{t,max}$ is the mean of the condition with the maximal strength increase, in this case the 200 wet condition.

$$N_i(\sigma_{Tensile}) = 1 + \frac{\sigma(i) - \sigma_{Tensile,material}}{\sigma_{t,max} - \sigma_{Tensile,material}} \tag{2.8}$$

The compression strength results are shown in the left of figure 2.7 and the tensile strength results in the right of figure 2.7 for all four conditions of ambient pressure and medium.

The compressive strength results in the left of figure 2.7 show a small spread of data compared to the tensile strength results in the right of figure 2.7 due to the difference in material strength which was about a factor of ten higher for compression. A one-way ANOVA of the compression strength results showed no significant difference for all four conditions (p=0.73, F=0.44). The tensile strength results showed a significant difference between the conditions of the experiment (p<0.01, F=10.53). Therefore a post-hoc analysis is performed to show where the difference between which conditions compared to the baseline condition are using a one-way ANOVA, as listed in listed in table 2.3.

The tensile stress results in the right of figure 2.7 show a linear increase when ambient pressure is increased. A linear regression analysis roughly through the mean of all three experimental conditions has a high significance ($p < 0.001$, F=35.60). This indicates a linear relation between ambient pressure and apparent tensile strength as hypothesized and described in the methodology in section 2.1.2.

The linear relation with a factor λ_t between ambient pressure and apparent tensile strength is given in eq. (2.4). This theorem is shown in the left of figure 2.8 combined with the experimental results for an arbitrary fictive value. This means when the value would be set to one, the full hyperbaric effect acts on the apparent material strength which the theorem for dry samples with confining pressure states as shown in figure 2.4. The right of figure 2.8 shows the same

Table 2.3: ANOVA results of post-hoc analysis of tensile strength results compared to the baseline condition (0 dry)

	Tensile strength	
Condition	p-value	F-value
0 dry (baseline)	-	-
0 wet	0.921	0.01
100 wet	0.091	4.89
200 wet	0.016	16.34

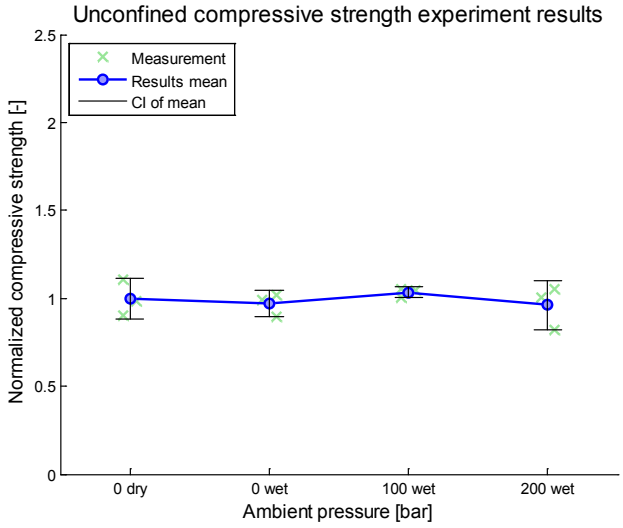

a)

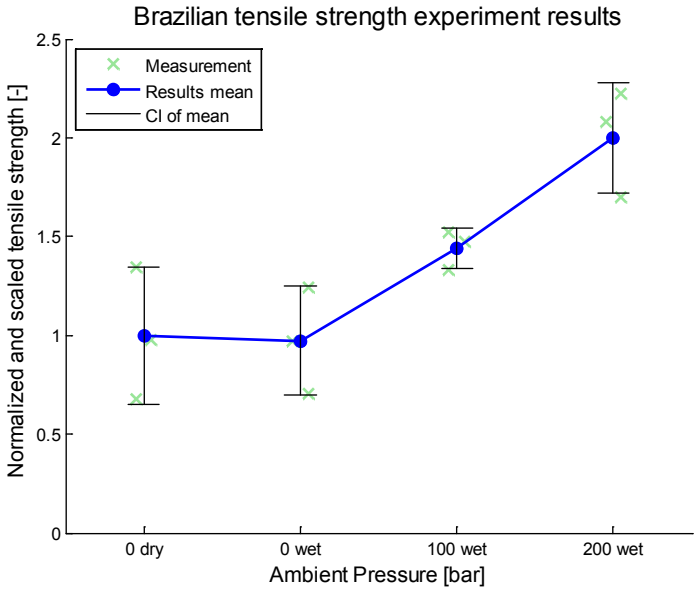

b)

Figure 2.7: Experimental results of material strength of all specimens (N=3) for each condition with the mean and 95% confidence interval per condition. Left - Normalized results of calculated compressive strength from measured results of unconfined compression strength experiment. Right - Normalized and scaled results for calculated tensile strength from measured results of Brazilian tensile strength experiment

information, only relative to the fictive theoretical values. This figure shows the relative amount of influence of the ambient pressure on the apparent tensile strength, and shows therefore factor λ_t. However these graphs are for fictive theoretical values (λ_t is not set to one for the theorem, which would represent full hyperbaric effect) and therefore these graphs only give an indication of the influence and not the actual influence of the hyperbaric effect.

The theoretical method of section 2.1.2 describes a linear relation between ambient pressure and tensile strength for fully saturated rock and the application for the adjusted theorem of Griffith as given in Eq. (2.6). This theorem is in figure 2.9 applied for the experimental results for the compressive and tensile strength. Where the material strengths are represented with the scaled Mohr circles with the compressive strength ten times the tensile strength and the increase for ambient pressure of the tensile strength as in the previous scaled figure. This graph shows the summary of the influence of the hyperbaric effect on the apparent material strength. It shows the unchanged compressive strength due to no confining pressure, the small change of tensile strength and the fit of the developed adjusted theorem of Griffith for the relationship of normal and shear stress.

2.1.5. DISCUSSION

The theoretical model as described in section 2.1.2 for rock cutting in hyperbaric conditions is developed for excavation methods using low strain rates such as a grab. When using a conventional excavation method with high strain rates such as a crown or drum cutter, this developed method will not be correct. The method is also solely developed for saturated porous rock and different type of rock will have different behavior. Therefore this theorem has to be extended for different types of material and to include parameters such as permeability, density, porosity and perhaps connected porosity. The factor λ_T of water pressure influence on the apparent tensile strength will be dependent on these mentioned material parameters. However the overall factor will most likely be a linear or quadratic function of the cutting velocity. Additional experiments have to be conducted to be able to develop this extended model for determining the effect of each of these values to the apparent material strength.

However besides additional factors influencing the apparent material properties, also the method of stiffening of the grain matrix is not directly validated by the conducted experiments. A direct measurement of the elastic deformation of the grain matrix in relation to the increased apparent tensile strength or a direct measurement of the pressure drop would suffice to validate the method itself. The latter method however would be very difficult to actually achieve in practice, but an elongation measurement could be realized in additional experiments.

The theoretical method for shear strength is based on the model of Griffith. However no experiments were conducted to actually validate this part directly. The conducted experiments however do validate the initial part of the theorem for apparent tensile strength and do seem to comply with the compressive strength circle. But additional experiment could also validate the influence of ambient pressure on direct shear strength for unconfined conditions. Also the end of the curve as shown in figure 2.9 is most likely altered from the displayed graph and shear strength will eventually come to zero at high compressive strength by grain failure as described

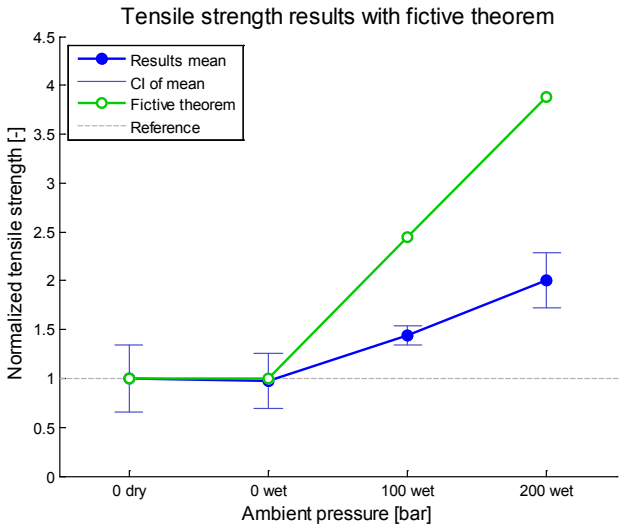

a)

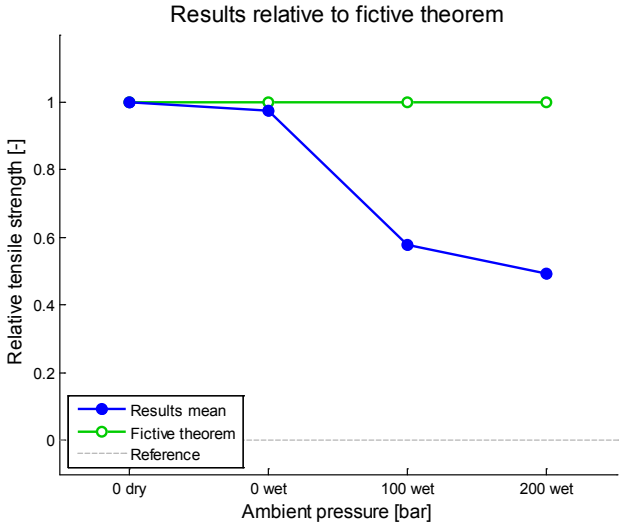

b)

Figure 2.8: Tensile strength experiment results shown with fictive theorem for full-hyperbaric effect. Left - Scaled normalized tensile experiment results with fictive theoretical full hyperbaric effect. Right - Relative tensile experiment results to fictive theoretical full hyperbaric effect values

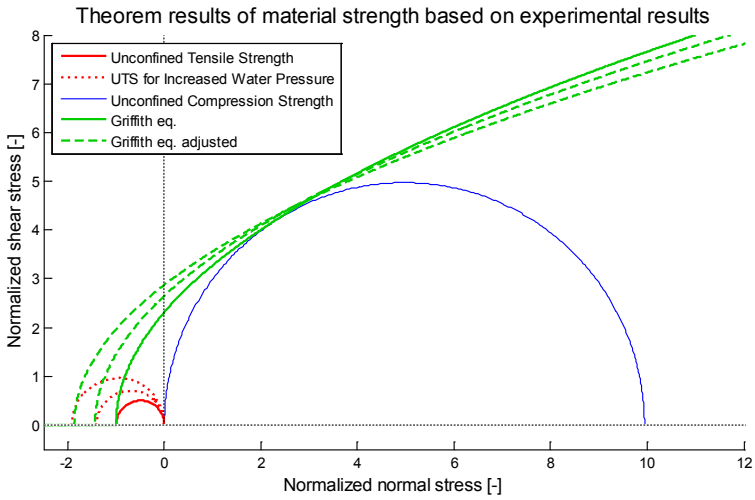

Figure 2.9: Scaled normalized experiment results of material stresses for different hyperbaric conditions. The graph shows the scaled measured compressive and tensile stresses with Mohr circles and the fit of the developed adjusted Griffith relationship for normal stress and shear stress

in literature for high strain rates (Verhoef, 1997).

The experiment results for compressive strength show a small spread of data caused by the normalization of the material strength in dry atmospheric conditions. This effect however does not change the outcome of the statistical analysis of detecting a difference in mean over the four conditions, because the relative differences do not change. In other words no difference in mean is found for the absolute data. Therefore it can be concluded that all specimens were fully saturated with pressurized water during each experiment. If however the loading rate would be greatly increased for conducting the compressive experiment, the ambient pressure would presumably also increase the apparent compressive strength results. This dilatancy hardening effect is already observed in previous research, due to the trapped water in the pore volumes for high strain rates (Brace and Martin, 1968; Miedema, 1987, 2011). Therefore the compressive experiment results as shown in this paper clearly show the applied strain rates during the conducted experiment were not in this high strain rate range while still experiencing an increase in apparent tensile strength.

The tensile strength experimental results show a linear relation for increasing ambient water pressure and no difference for both atmospheric conditions. This shows the different ambient medium have no effect on the apparent material strength, only the ambient pressure is affecting the apparent tensile strength, even when the pore fluid is in equilibrium with the surrounding water at the start of the experiment. This validates the hypothesis of the developed methodology for the linear relationship of apparent tensile strength with ambient water pressure. However the low number of specimens did not gave a highly significant result and additional experiments should include a larger number of specimens. The results are found at a fixed loading rate of 0.30MPa/s as stated in the ASTM guidelines. Due to this low rate of loading the found results

hold for low cutting velocities such as a grab uses when closing its clamshells at approximately 10mm/s and do not hold for high cutting velocities such as a conventional crown or drum cutter with velocities up to 4000mm/s.

The theoretical full hyperbaric effect acting on dry specimen in confining pressure is solely based on literature and is calculated for the used specimen material. Results for the theoretical full hyperbaric effect as shown in figure 2.8 are given with scaling for a fictive calculation not representing the actual values. Therefore the relative values of the experimental results to the theorem are scaled and fictive as well. Nonetheless the given graph does indicate the found results of substantially less influence of the ambient pressure on the apparent tensile strength for fully saturated rock material at low strain rates. Adding validating experiments of dry specimens in confining pressure could substantiate the drawn conclusions on the reduced influence of ambient pressure on tensile strength for saturated rock. In figure 2.4 are shown comparable summarizing results of full hyperbaric effect acting on dry specimen in confining pressure. By also having experimental results of this effect, the results could be combined to the experimental results as shown in figure 2.9.

Unfortunately no material properties were recorded for the used specimen such as porosity, permeability and density. Future work on this topic will include these properties in the experimental protocol and based on these properties along with the material strength three or more materials will be selected to repeat the experiments in a more extensive way. By doing so, also a relation can be distinguished between these material properties and there influence on the apparent material strength as stated for the theorem development. Furthermore the cutting velocity can be varied in for instance three to five different steps to distinguish a relation between the cutting velocity and apparent material properties.

Another interesting effect would be to do an experiment based on the principle of the theorem of elastic deformation validating the effect of the inflow of water. The theorem states the full hyperbaric effect is not noticeable due to the inflow and dispersion of water into the deformed zone of the specimen. When an experiment is conducted that will load at hyperbaric conditions a specimen up to a certain loading force which is higher than the breaking point at atmospheric conditions and lower than the previous results show at equal low rate of loading. If this loading force is kept constant the specimen will not fail initially at this point, however due to the inflow of water into the deformed zone the specimen will eventually fail at a certain time. This will occur when equilibrium at the deformed zone is reached and the pressure drop in the core will be eliminated. This could verify the mechanism of the developed theorem of elastic deformation of the grain matrix, causing a pressure drop at the core of the specimen. Another way of doing so would be to measure the pressure at the core of the specimen while conducting the experiment, however this measurement is hard to achieve.

The found results imply a low cutting force is required for excavation at low cutting velocities compared to cutting at cavitation. This results in low cutting energy and implies using a grab with low cutting velocities is more energy efficient compared with conventional rock cutting techniques like a crown or drum cutter.

2.1.6. CONCLUSION

This paper has described a theorem developed to define the relation between ambient pressure and apparent material strength of fully saturated rock under low strain rates and a verifying experiment.

- The developed theorem is based on the elastic deformation of the grain matrix for slow strain rates instead of crack reinforcement. This theorem is applied for describing the linear relation between ambient pressure and apparent tensile strength, the absence for a relation of apparent compressive strength and the adjusted relationship of Griffith for normal and shear strength.
- The experimental results showed no difference in compressive strength in changing hyperbaric conditions, as was hypothesized for compressive strength due to the low strain rate where dilatancy hardening will not occur The absence of change of compressive strength verifies for slow strain rates the full saturation of the used specimen, by not showing any confining pressure on the specimen which would increase the apparent compressive strength.
- The experimental results show an increase and linear relation for the apparent tensile strength at increasing hyperbaric conditions, the linear increase of tensile strength is in accordance with the proposed theorem. This increase of tensile strength is substantially less compared to the full hyperbaric theoretical effect as described in literature. The developed theorem for elastic deformation of the grain matrix is based on this phenomenon of not the full increase of tensile strength due to the ingress and distribution of water in the deformed rock at slow strain rates.
- The developed adjusted relationship of Griffith for normal and shear stress that incorporates the linear relation of ambient pressure and apparent tensile strength fits the experimental results for low strain rates.

Therefore this experiment shows that substantially less cutting forces is required for saturated porous rock with low strain rates compared to the full hyperbaric theoretical effect acting on the material. At great depths this results in substantially less required cutting energy of the excavation process and this implies using a grab which excavates with slow strain rates is therefore more energy efficient compared to conventional excavation methods. This would add up to the energy efficiency of excavating using a grab due to the low ratio of cutting energy over excavated rock volume, compared with a conventional crown or drum cutter for rock excavation. Therefore excavating SMS deposits using a grab is a promising method for porous rock and uneven rough terrain.

Future work on this topic will focus investigating this theorem for different materials and several different cutting velocities to cover the entire area of the influence of the hyperbaric effect on the apparent material properties for porous saturated rock.

2.2. REDUCTION OF ENERGY CONSUMPTION USING A GRAB

Published in Offshore Technology Conference proceedings, 2016[4]

ABSTRACT

Recent developments for deep-sea mining have shown multiple scenarios of gaining mineral deposits of Seafloor Massive Sulfides (SMS). One of the problems for these scenarios is the overall large energy consumption of processing rock material which are a technological challenge and are increasing production costs. This paper compares two methods for deep-sea rock excavation on their energy consumption, based on rudimentary calculations. The best known scenario for gaining mineral deposits from the seabed is to excavate rock materials with a crown or drum cutter and pump the fluidized crushed materials to the vessel at the surface. This process requires high cutting forces deep-sea due to the hyperbaric effect at large water depths, when cutting with full cavitation. This high energy consuming process therefore requires a considerable amount of subsea installed power. An alternative scenario is to use a hydraulic grab for excavating mineral deposits and not crush all the materials entirely subsea. Using a grab would be very beneficial in rough terrains and unstable seafloor conditions, compared to track-driven vehicles typically used for crown or drum cutters. Also specific cutting forces are much lower when using a grab, because it is not cutting at full cavitation in hyperbaric conditions. However the main advantage is to keep most of the rock intact which allows the material to be crushed at the surface. Mechanically uplifting large pieces of rock therefore could have the advantage that most of the required power can be installed at the surface, rather than subsea for the traditionally proposed hydraulic pumping systems. The rock can then be further crushed under atmospheric pressure at the surface, avoiding the hyperbaric effect. The combination of using a grab and further crushing at atmospheric conditions is more energy efficient and therefore requires substantially less installed subsea power. Using rudimentary calculations, a great reduction of energy consumption is found for using a grab compared to typically used crown or drum cutters. Substantially less subsea installed power is required for excavating the mineral deposits with a grab. Although additional crushing needs to be done at the surface, the overall required installed power for using a grab still can be much less than fully subsea excavating and crushing.

2.2.1. INTRODUCTION

METAL-rich mineral deposits created in the deep-sea are of main interest as a new mining perspective to cope with the fast increasing metal demand and decreasing supplies from conventional mines (Rona, 2003; Scott, 2001; Yang and Scott, 1996). High concentrations of common and rare-earth metals are found in these mineral deposits in rock material named seafloor massive sulfides (SMS) deposits (Tivey, 2007) in water depths of 1000m to 2000m (Rona, 2003). These mineral deposits are formed over a long period of condensation from superheated water vapor with dissolved minerals from the so called 'black smoker' chimneys

[4]R.J. Kuiper, X. Chen, J.C.L. Frumau, S.A. Miedema; Reduction of Energy Consumption when using a Grab; Offshore Technology Conference proceedings 2016, 27080-MS

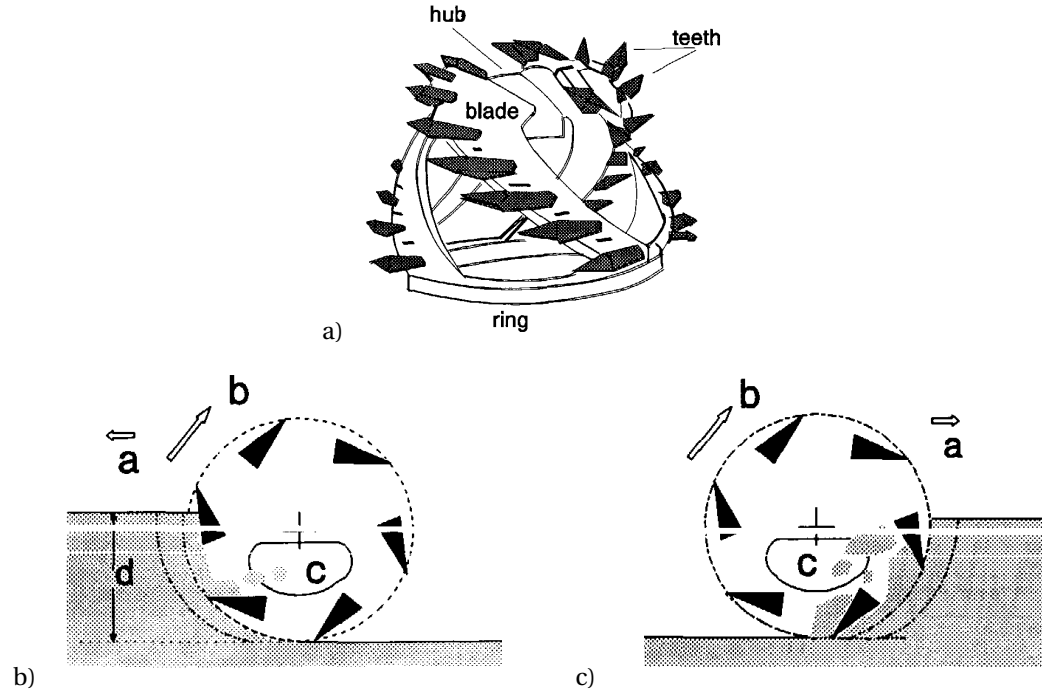

Figure 2.10: a) Crown cutter-head mounted with teeth (pick points). b) Cutter-head cutting motion of undercutting. c) Overcutting only for soft materials. All three figures adapted from (Verhoef, 1997)

and therefore is a very porous but fully saturated rock material (Tivey, 2007). The behavior of the material properties at great water depth of such a material is unknown and has great influence on the excavation method of these minerals (Kuiper et al., 2013). A key aspect in the material behavior due to the ambient water pressure will be the change of pore volume during excavation, affecting the pore pressure of the material and therefore creating a dilatancy hardening effect (Chen, 2011; Kuiper et al., 2013). Therefore this paper focusses on the influence of great water depth on the energy consumption of commonly proposed cutter excavation method and a promising alternative method of using a grab.

Currently no deep-sea mining project is developed until now, however several proposals have been developed over the last ten years. Most of these proposals are based on large production rates of nearly 2 Mt/yr for the economic feasibility of such a large scale project, having high operational costs. One of the driving factors for the economic feasibility is the energy consumption of such a project besides obviously the metal prices. The developed proposals all incorporate comparable excavation methods mainly based on dredging and on-land mining methods, using drum or crown cutters. The excavation methods mainly compose of several rotating teeth cutting through a thin layer of rock and a pump will then transport a mixture of rock and water as schematically shown in figure 2.10. However these methods are based on techniques where no high-pressure water is acting on the rock material and the flow rates of the extracted rock material is not comparable to the required rates for deep-sea mining.

a) 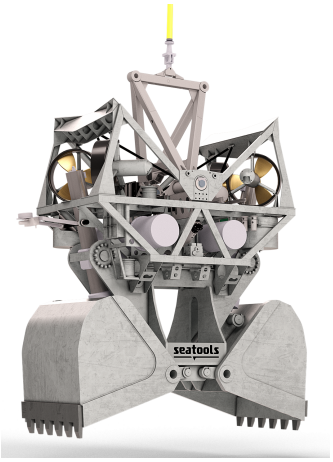

b) 

Figure 2.11: Example of two hydraulically actuated suspended grabs. a) Designed grab by Seatools BV. proposed for deep-sea mining, from Bloois and Frumau (2009). b) Fabricated grab by Seatools BV. for dredging in arctic conditions, from van Es et al. (2004).

An alternative method for excavating mineral deposits is to use a hydraulically actuated suspended grab as shown in figure 2.11. Using a grab could be very beneficial in rough terrain where the seafloor is highly uneven and the soil properties have large variations. Because SMS deposits are generated during a condensation process they have produced a highly uneven terrain with large chimneys and large slopes of the seafloor. Also the condensation process created a mixture of sand and rock mixture layers causing a very unstable seafloor. Therefore a suspended grab has an advantage over a track-driven vehicle depending on contact with the seafloor. The positioning of a suspended grab at large water depths would be done by using thrusters for the horizontal motion.

High energy consumption during a deep-sea mining process causes high running costs and decreases the economic feasibility. Therefore the energy consumption of the excavation process determine a large part of the economic feasibility of the entire process. This paper focuses on the influence of the water depth on this energy consumption of the process for using conventional methods such as a cutter-head and alternative methods using a grab. It is hypothesized that the energy consumption and installed subsea power, when using a grab is greatly reduced compared to conventional methods.

Therefore in section 2.2.2 the conventional methods of excavating using a cutter-head is calculated for a typical case. In section 2.2.3 the same case is used to calculate the energy consumption for using a grab. Both type of systems are compared on their required installed power and specific energy in section 2.2.4.

2.2.2. EXCAVATION ENERGY WHEN FULLY CRUSHING THE MATERIAL

Rock material is fully crushed when using a common excavation method such as a crown cutter-head for cutting the material. The crushing of the material is achieved by compressive and shear failure of small rock cuttings. The required energy for such a cutting method is estimated using

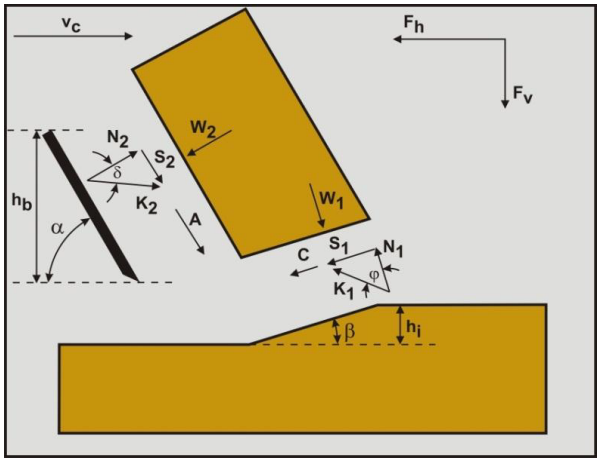

Figure 2.12: Definitions of the cutting process of the forces and angles on the layer cut in rock in hyperbaric conditions, adapted from (Miedema and Zijsling, 2012)

a basic calculation method of Miedema developed for dredging applications (Miedema, 1987). Recently Miedema added ambient hyperbaric conditions to the method for rock cutting and validated this with experimental results (Miedema and Zijsling, 2012). Based on this renewed method an estimation of the required cutting energy is calculated in this section.

It is conventional to use a cutter head in underwater excavation process in dredging engineering, especially for hard materials like rock. However, the water pore pressure has created a major difference between rock cutting in atmospheric condition and in deep water condition. Due to the high hydrostatic pressure in deep sea, a ductile rock cutting process will occur where the rock tends to fail in shear more than in tensile crack. Recently Miedema has derived an analytical model to calculate the forces in the hyperbaric rock cutting process (Miedema and Zijsling, 2012). Here below figure 2.12 gives out the illustrations of the forces and angles in the model.

In Figure 2.12, N_1 is the normal force acting on the shear zone; S_1 is the shear force generated by internal friction; K_1 is the resultant force by the combination of N_1 and S_1; C is the cohesion force due the cohesive stress c inside the rock; W_1 is the force generated by the water under pressure on the shear zone; N_2 is the normal force acting on the shear layer from the blade; S_2 is the shear force due the external friction between the blade and rock; K_2 is the resultant force by the combination of the N_2 and S_2; A is the adhesion force due to the adhesive stress a between the blade and the rock; W_2 is the force due to the water under pressure on the blade; F_h is the overall horizontal cutting force; F_v is the overall vertical cutting force; h_i is the cutting depth; h_b is the blade height; v_c is the cutting speed; α is the cutting angle of the blade; β is the shear angle of the shear layer; φ is the internal friction angle of the rock and δ is the external friction angle between the blade and the rock.

It should be stated that no matter in atmospheric condition or hyperbaric condition, the rock itself is always a brittle material, it is just in hyperbaric condition the high confining pressure

has induced such a macroscopically ductile behavior in the cutting process, but microscopically the break between the particles inside the rock will always be brittle failure.

Corresponding to figure 2.12, Miedema has also derived the equations to calculate the forces in macro scale, and the ones which are relevant to the energy calculation are shown below in eq. (2.9)-eq. (2.14) (Miedema and Zijsling, 2012).

$$W_1 = \frac{\lambda_{c1} \cdot \rho_w \cdot g \cdot (z + z_{atm}) \cdot h_i \cdot w}{sin(\beta)} \tag{2.9}$$

$$W_2 = \frac{\lambda_{c2} \cdot \rho_w \cdot g \cdot (z + z_{atm}) \cdot h_b \cdot w}{sin(\alpha)} \tag{2.10}$$

$$C = \frac{c \cdot h_i \cdot w}{sin(\beta)} \tag{2.11}$$

$$A = \frac{a \cdot h_b \cdot w}{sin(\alpha)} \tag{2.12}$$

$$K_2 = \frac{W_2 \cdot sin(\alpha + \beta + \varphi) + W_1 \cdot sin(\varphi) + C \cdot cos(\varphi) - A \cdot cos(\alpha + \beta + \varphi)}{sin(\alpha + \beta + \varphi + \delta)} \tag{2.13}$$

$$F_{h,conf} = -W_2 \cdot sin(\alpha) + K_2 \cdot sin(\alpha + \delta) \tag{2.14}$$

In eq. (2.9) and eq. (2.10), the density of seawater ρ_w is 1025 kg/m3, the gravitational acceleration g is 9.81 m/s2, z is the water depth and w is the width of the blade. It is a deep sea excavation process, so z is set to 2000 m. Moreover, it is known that with high cutting speed, cavitation will happen in the cutting zone. In the situation of full cavitation, the water under pressure equals to the local hydrostatic pressure, thus the cavitation coefficients λ_1 and λ_2 are used to express the influence of the cavitation on the water under pressure. Basically in very fast cutting, full cavitation will occur, so $\lambda_{c1} = \lambda_{c2} = 1$. While on the contrary, if the cutting speed is very low, then the water can flow freely through the cutting area, so $\lambda_{c1} = \lambda_{c2} = 0$. In the calculation of this paper due to the used high cutting speed, it is assumed that $\lambda_{c1} = \lambda_{c2} = \lambda_c = 0$.

The unconfined horizontal force is equal to eq. (2.14) without the addition of water pressure W_2, but also without the addition in K_2 of water pressure and adhesion forces. This results therefore in eq. (2.15) written directly for horizontal forces.

$$F_{h,unc} = \frac{2 \cdot c \cdot h_i \cdot w \cdot cos(\varphi) \cdot sin(\alpha + \delta)}{1 + cos(\alpha + \delta + \varphi)} \tag{2.15}$$

The cohesive stress c in eq. (2.11) can be obtained by using Mohr's circle, the calculation is shown below in eq. (2.16) where σ_c is the unconfined compressive strength (UCS) of the rock. Besides, for most rocks, the adhesion force A and the adhesive stress a can be neglected, so in this paper these two items are taken to be zero.

$$c = \frac{\sigma_c \cdot (1 - sin(\phi))}{2 \cdot cos(\phi)} \tag{2.16}$$

In the calculation of energy consumption, the material properties and the parameters of the cutting process are adjusted to the values in normal dredging practice. The internal friction

angle φ is set to 300, which is quite common in rock materials. According to the empirical relation that the external friction angle is usually close to two thirds of the internal friction angle, so δ is set to 200. Besides, the cutting angle α is 450, which is widely applied in dredging and mining practice. Finally, through eq. (2.17) (Miedema and Zijsling, 2012), the shear angle β is calculated to be 42.50.

$$\beta = \frac{\pi - \alpha - \phi - \delta}{2} \tag{2.17}$$

Furthermore, the cutting speed is set to 1.0 m/s, the cutting depth is 0.2 m and the blade height is set to 0.5m, which are all quite common in dredging engineering. The expected production rate of a large scale deep sea mining project of about 2 Mt/y would be roughly 7000 t/d with some downtime for bad weather, therefore 700 t/d would be a small scale project, or only removing the top rough layer of a larger project. Thus the local production flow of pure rock Q should reach 3.40 L/s including an efficiency of 22 hours per day average. According to eq. (2.18), the blade with w is obtained to be 0.170 m.

$$Q = h_i \cdot w \cdot v_c \cdot \eta_{day} \tag{2.18}$$

The rock used in the calculation has a UCS of 20 MPa. Since it is a brittle material, so the ductility number m should be bigger than 9 (Verhoef, 1997). In this paper m is taken to be 10, so the tensile strength σ_t of the rock is then 2 MPa. According to all the equations above, the overall horizontal cutting force $F_{h,conf}$ is obtained of 17.57 t, and then the cutting power $P_{c,conf}$ and the specific energy $E_{SP,conf}$ can be calculated by eq. (2.19) and eq. (2.20) (Miedema and Zijsling, 2012).

$$P_{c,conf} = F_{h,conf} \cdot v_c \tag{2.19}$$

$$E_{SP,conf} = \frac{P_c}{Q} = \frac{F_{h,conf} \cdot v_c}{h_i \cdot w \cdot v_c} = \frac{F_{h,conf}}{h_i \cdot w} \tag{2.20}$$

Therefore based on eq. (2.19) and (2.20) the required cutting power $P_{c,conf}$ is 172.3 kW for production of 700 t/day in 2000 m confining water pressure and the specific energy $E_{SP,conf}$ is 50.70 MPa. In addition, if the forces (W_1, W_2) generated by water under pressure are neglected, then it is possible to calculate the energy consumption in unconfined condition. Therefore it is

Table 2.4: Cutting energy when fully crushing the material

Environmental parameters			Production process			Required energy		
ρ_w	1025	kg/m^3	α	45	deg	Q	3.40	L/s
z_{atm}	10	m	β	42.5	deg	$F_{h,conf}$	17.57	t
g	9.81	m/s^2	δ	20	deg	$F_{h,unc}$	3.44	t
m	10	-	ϕ	30	deg	P_{conf}	172.3	kW
σ_c	20	MPa	w	0.016	m	$E_{SP,conf}$	50.70	MPa
σ_t	2	MPa	h_i	0.2	m	P_{unc}	33.8	kW
z	2000	m	h_b	0.3	m	$E_{SP,unc}$	9.93	kW
λ_c	0	-	v_c	1.0	m/s			
ρ_r	2600	kg/m^3	n_{day}	92	%			

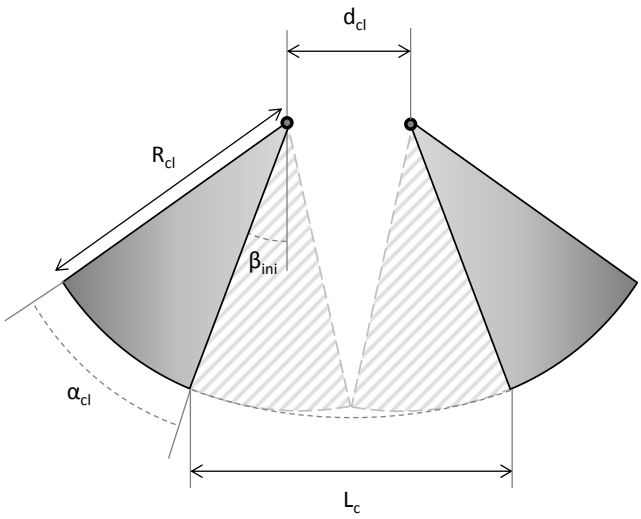

Figure 2.13: Production using a grab

computed that the unconfined required cutting force $F_{h,unc}$ is only 3.44 t, required power P_{unc} only 33.8 kW, and the unconfined specific energy $E_{SP,unc}$ is 9.93 MPa. From this it is clear that compared to the surface situation, at 2000 m water depth more than five times the power and energy are needed to excavate the seabed rock.

2.2.3. EXCAVATION ENERGY USING A GRAB

Excavating mineral deposits using a large suspended grab is accomplished by cutting the rock material with teeth mounted on two opposite clamshells as shown in figure 2.13. The clamshells are hydraulically actuated and therefore can produce high cutting forces, although limited at initial position by the weight of the entire grab.

The excavated rock volume V_{grab} to be produced by a single cycle of the grab is calculated using eq. (2.21), with the length of the tensile crack L_c as defined in eq. (2.22), width w_c, initial clamshell angle β_{ini} and triangular height of rock above starting point h_{pr}. This results in the production volume as listed in table 2.5 using a grab volume of 1.5 m3 with the filling efficiency η_{fill}.

$$V_{grab} = \eta_{fill} \cdot w_{cl} \cdot \left[\left(\frac{d_{cl}/2}{sin(\beta_i)} + R_{cl} \right)^2 - \left(\frac{(d_{cl}/2)^2}{tan(\beta_i)} \right) \right] \tag{2.21}$$

$$L_c = 2 \cdot R \cdot sin(\beta_i) + d_{cl} \tag{2.22}$$

The production rate can be calculated using the excavated volume of the grab per cycle as given in eq. (2.24), combined with the cycle time of the gab T_{cycle} as given in eq. (2.23). This results in the required production of approximately 700 t/day as listed in the right of table 2.5, where the daily efficiency η_{day} is based on 22 hour production efficiency per day. The dimensions of the grab are chosen such that the required production rate is achieved and

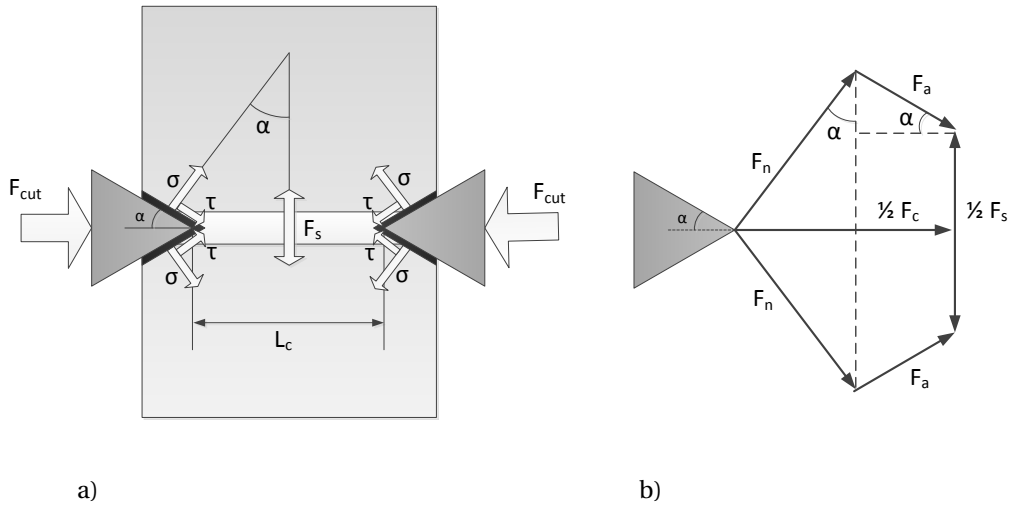

Figure 2.14: Cutting theorem for pure horizontal tensile forces, adapted from (Kuiper, 2012a).

optimized such that the cutting force is minimized, based on the quadratic relation of the grab volume for L_c and linear for w_c and the force being linear for both dimensions.

$$T_{cycle} = T_{cut} + T_{lift} + T_{transport} + T_{dump} + T_{transport} + T_{lift} \tag{2.23}$$

$$\Phi_{prod} = \frac{T_{day}}{T_{cycle}} \cdot V_{grab} \cdot \rho_r \cdot \eta_{day} \tag{2.24}$$

Based on these given dimensions to obtain the required production rate, the required cutting energy for using a grab is calculated in this section in a basic way for pure horizontal loading of the rock.

An estimation of the cutting energy is calculated in a basic way for pure horizontal cutting, creating a pure tensile crack due to the wedge shaped teeth as shown in figure 2.14a. This specific approach of horizontal cutting could be the case for excavating hydrothermal vents. However for excavating rough surfaces as shown in figure 2.13a slightly more complex method should be used. Nonetheless this paper will use solely use the basic approach to prove in general the differences between both excavation methods and gives a rough comparison.

Table 2.5: Dimensions grab with the resulting production volume and cycle time with mineral production per day.

Grab dimensions			Production process		
R_{cl}	2.4	m	η_{day}	92	%
d_{cl}	0.7	m	T_{cut}	26	s
w_c	0.7	m	T_{dump}	10	s
L_c	1.53	m	$T_{transport}$	180	s
β_{ini}	10	deg	T_{lift}	20	s
V_{grab}	1.42	m^3	Φ_{prod}	687	t/day

The given calculation method is based on cutting rock under tensile failure between both clamshells. This failure mechanism will be enforced by the large ambient hyperbaric pressure. However excavating using a grab is a slow cutting process as given in table 2.5 and therefore will presumably not occur under full cavitation (Kuiper et al., 2013).

In figure 2.14b the decomposition is shown of the cutting force when cutting pure horizontally. Due to the wedge shape of the blade the horizontal cutting force F_c is decomposed into two compressive forces F_n normal to the blade edge. Combined with the two adhesive forces F_a due to the friction between the blade and the rock material depending on the normal force, both normal forces create a single splitting force which is only half the total tensile splitting force F_s. The splitting force depends on the vertical component of the normal force $F_{n,ver}$ and adhesive force $F_{a,ver}$ as is given in eq. (2.25). The cutting force F_c is pure horizontal and determines the horizontal component of the normal $F_{n,hor}$ and adhesive force $F_{a,hor}$ as is shown in eq. (2.26).

$$F_s/2 = 2 \cdot F_{n,ver} - F_{a,ver} = 2 \cdot F_n \cdot cos(\alpha_{blade}) - 2 \cdot F_a \cdot sin(\alpha_{blade}) \tag{2.25}$$

$$F_c = 2 \cdot F_{n,hor} + F_{a,hor} = 2 \cdot F_n \cdot sin(\alpha_{blade}) + 2 \cdot F_a \cdot cos(\alpha_{blade}) \tag{2.26}$$

The friction angle δ determines the adhesive friction force F_a from the normal force F_n as is given in eq. (2.27). Therefore eq. (2.27) can be substituted into eq. (2.25) and eq. (2.26) as is shown in eq. (2.28) and eq. (2.29) respectively.

$$F_a = F_n \cdot tan(\delta) \tag{2.27}$$

$$F_s/2 = 2 \cdot F_n \cdot [cos(\alpha_{blade}) - tan(\delta) \cdot sin(\alpha_{blade})] \tag{2.28}$$

$$F_c = 2 \cdot F_n \cdot [sin(\alpha_{blade}) + tan(\delta) \cdot cos(\alpha_{blade})] \tag{2.29}$$

The normal force in eq. (2.28) can be extracted from the formula as is shown in eq. (2.30) and substituted in eq. (2.29) as is given in eq. (2.31).

$$F_n = \frac{F_s}{4 \cdot [cos(\alpha_{blade}) - tan(\delta) \cdot sin(\alpha_{blade})]} \tag{2.30}$$

$$F_c = \frac{F_s}{2} \cdot \frac{sin(\alpha_{blade}) + tan(\delta) \cdot cos(\alpha_{blade})}{cos(\alpha_{blade}) - tan(\delta) \cdot sin(\alpha_{blade})} \tag{2.31}$$

The splitting force creates a tensile stress on the tensile plane between both clamshells as shown in figure 2.14a. However due to the ambient hyperbaric pressure the tensile strength has an apparent partial addition of water pressure defined by the cavitation coefficient for tensile strength λ_t as given in eq. (2.32). The cavitation coefficient for tensile strength is based on the findings of an initial study of material strength experiments at hyperbaric conditions (Kuiper et al., 2013). The cavitation coefficient for tensile strength at low loading rates is shown to be substantially less than full cavitation, but in this paper we will assume λ_t=0.5 to be generic but could be much less. The splitting force as expressed in eq. (2.32) is substituted in eq. (2.33) giving cutting force for a single clamshell as shown in figure 2.14a.

$$F_s = w_c \cdot L_c \left(\sigma_t + \lambda_t \cdot p_t\right) \tag{2.32}$$

$$F_c = \frac{1}{2} \cdot w_c \cdot L_c \left(\sigma_t + \lambda_t \cdot p_t\right) \cdot \frac{sin(\alpha_{blade}) + tan(\delta) \cdot cos(\alpha_{blade})}{cos(\alpha_{blade}) - tan(\delta) \cdot sin(\alpha_{blade})} \tag{2.33}$$

$$F_{vert} = F_c \cdot sin(\beta_i) \tag{2.34}$$

From the cutting force in eq. (2.33) for a single clamshell the total maximum cutting power consumption can be calculated using the average cutting velocity v_{cut} as shown in eq. (2.35). The specific cutting energy based on the maximum cutting force used along the entire cycle of the grab is shown in eq. (2.36). The results of the required cutting force, power and specific energy for the given case are shown in table 2.6.

$$P_{cut,max} = 2 \cdot F_c \cdot v_{cut,avg} \qquad \text{with,} \quad v_{cut,avg} = \frac{L_c/2}{T_{cut}} \tag{2.35}$$

$$E_{SP,cut,max} = \frac{P_{cut,max}}{V_{grab}/T_{cut}} \tag{2.36}$$

However the cutting process when using a grab will not consist of the maximal cutting power along the entire cycle. In this case only the first part of the cutting length κ_l the maximal cutting force and available cutting power $P_{installed}$ is required. Where for the rest of the cutting length only partial cutting force κ_f and partial available power κ_p is required to overcome some frictional losses. The time and velocity is given in eq. (2.37) when requiring the maximal cutting force and for the partial force in eq. (2.38).

$$T_{cut,HF} = \frac{\kappa_l \cdot L_c/2}{v_{cut,HF}} \qquad \text{with,} \quad v_{cut,HF} = \frac{P_{available}}{2 \cdot F_{cut}} \tag{2.37}$$

$$T_{cut,LF} = \frac{(1-\kappa_l) \cdot L_c/2}{v_{cut,LF}} \qquad \text{with,} \quad v_{cut,LF} = \frac{P_{available}}{2 \cdot \kappa_f \cdot F_{cut}} \tag{2.38}$$

Table 2.6: Rock cutting force and specific cutting energy for using a grab

Production process			Required energy		
σ_t	2.0	MPa	F_{cut}	459.7	t
p_w	20	MPa	F_{vert}	79.8	t
λ_t	0.5	-	$v_{cut,avg}$	29.49	mm/s
α_{blade}	15	deg	$P_{cut,max}$	266.0	kW
			$E_{SP,cut,max}$	4.86	MPa

Table 2.7: Cutting time, velocity and specific energy with limiting available power for using a grab with maximum cutting force only required partially

Production process			Required energy		
$P_{available}$	50.0	kW	$v_{cut,HF}$	5.54	mm/s
κ_l	10	%	$T_{cut,HF}$	13.83	s
κ_f	10	%	$v_{cut,LF}$	55.43	mm/s
			$T_{cut,LF}$	12.45	s
			$E_{SP,cut,avg}$	0.92	MPa

In table 2.7 are the results of the required cutting time and velocity given along with the specific energy as given is eq. (2.39). The total cutting cycle time is approximately 50 s, as is also used in previous production calculations as shown in table 2.5.

$$E_{SP,cut,avg} = \frac{2 \cdot F_{cut} \cdot v_{cut,HF} \cdot T_{cut,HF} + 2 \cdot \kappa_f \cdot F_{cut} \cdot v_{cut,LF} \cdot T_{cut,LF}}{V_{grab}} \tag{2.39}$$

The specific cutting energy as given in eq. (2.39) for using a grab is shown graphically in figure 2.15 for different material properties. The graph shows the specific cutting energy depending on the material compressive strength with the ductility number m, the ratio of compressive strength over tensile strength. The specific cutting energies are given several combinations of m and λ. For comparison the specific cutting energy when fully crushing the material using a cutter-head as described in section 2.2.2 in eq. (2.20) is also shown in figure 2.15 for the used material $m = 10$.

In figure 2.15 several materials and cavitation coefficients are shown to demonstrate the influence on these parameters on the specific energy for cutting. However in this paper a single average material is used with the compressive of 20 MPa and a ductility number m=10. The results for this material are numerically given in table 2.8 and are also indicated in figure 2.15, where the grab cuts with a cavitation coefficient of λ=0.5 and the cutter-head under full cavitation so λ=1.0.

2.2.4. DISCUSSION

The computations used to determine the energy consumption of both excavation methods using a cutter-head or grab are largely simplified, including their cutting blade designs to cut the rock material. Improvements can be made to compare both cutting processes in more detail, however this would not change the main difference between both methods.

In table 2.9 a summary is given of the required power and specific energy of both grab or cutter-head based excavation method. For the alternative method of using a grab, fully crushing the rock material at the surface is added to the required power and energy for comparison, to end up with equal end-products of rock material. These values are based on the computations of section 2.2.2 for unconfined conditions, as also listed in table 2.9. With this addition both methods end up with the same rock material although require a different amount of energy.

Table 2.8: Average specific cutting energy for using a grab and cutter

Cutting type		Specific energy	
$E_{SP,cut,avg}(\lambda = 0.0, m = 10)$		0.15	MPa
$E_{SP,cut,avg}(\lambda = 0.5, m = 10)$	[•]	0.92	MPa
$E_{SP,cut,avg}(\lambda = 1.0, m = 10)$		1.69	MPa
$E_{SP,conf}(\lambda = 0.0, m = 10)$		9.93	MPa
$E_{SP,conf}(\lambda = 0.5, m = 10)$		30.36	MPa
$E_{SP,conf}(\lambda = 1.0, m = 10)$	[•]	50.70	MPa

Using rock material compressive strength of 20 MPa with a ductility number m of 10, resulting in a tensile strength of 2 MPa.

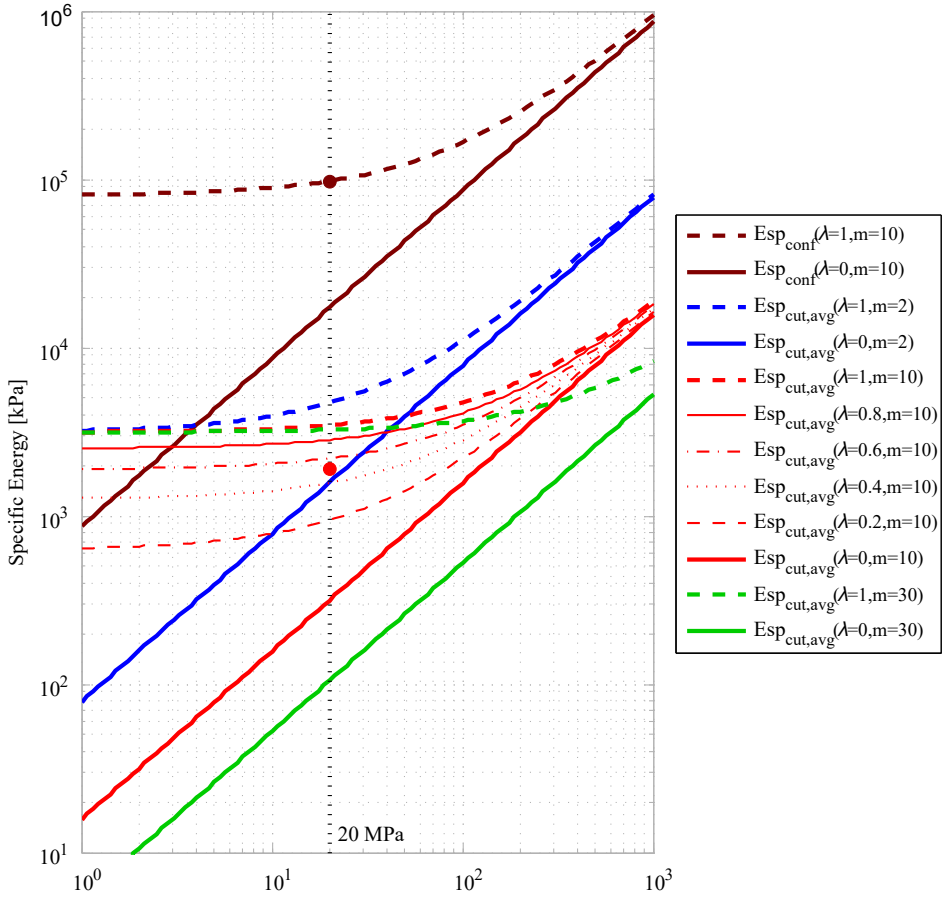

Figure 2.15: Average specific cutting energy for materials with different ductility numbers (m), affecting water pressure (λ) and cutting mechanism.

The computation of the cutting theory for using a grab in section 2.2.3 result in high cutting forces required for a relative small amount of time during the cycle, therefore not requiring large energy consumption. In addition the required power is also not exceptionally large, due to the low cutting velocity when requiring this peak force. Nonetheless the cutting forces are exceptionally large for using a grab. To cope with these high forces the cutting method can be redesigned to start cutting with a pure horizontal force and therefore not having to compensate

Table 2.9: Total overview of required powers and specific energy for both systems

Required Power			Specific Energy		
$P_{cut,conf}$	172	kW	$E_{SP,cut,conf}$	50.70	MPa
$P_{cut,grab}$	50.0	kW	$E_{SP,cut,avg}$	0.92	MPa
$P_{crush,dry}$	33.8	kW	$E_{SP,crush}$	9.93	MPa

any vertical component of this force with the weight of the grab. Another option would be to use multiple grabs to produce the stated production rate. This would not be beneficial for the energy consumption because half the grab volume requires more than half the cutting force. However the main advantage of a grab is the large reduction of subsea installed power and energy reduction, therefore reduction of CAPEX and OPEX. Therefore due to the lower costs the required production rate for economic feasibility can be lower too, requiring a smaller vessel and therefore smaller costs as well. The use of a grab therefore can be beneficial in small projects and the initial phase of projects.

However to maintain the advantage of using a grab, by not having to crush all the rock material subsea, an innovative vertical transportation system has to be developed. This system has to cope with the larger pieces of rock a grab produces, therefore a mechanical lift system seems most plausible. By using either a type of baskets or smaller grabs for transportation only, the advantage also remains that the required power for such a system would be placed on deck rather than subsea.

This paper compares two excavation methods solely on the basis of energy consumption, however the applicability of both methods is in principle rather different. The applicability of a grab lies for rough uneven and unstable terrain, while the cutter-head is suitable for excavating flat surfaces as well.

2.2.5. CONCLUSION

Based on several rudimentary calculations, the required excavation energy for using a grab is substantially less compared to common excavation methods.

- Only 20% of power and specific energy is required to crush rock fully in atmospheric conditions compared to confined conditions at 2000 m water depth.
- Only 29% of subsea installed power is required to excavate the rock material when using a grab compared to conventional excavation of using a crown or drum cutter.
- Taking into account the additional power for a crusher on deck, to arrive at the same end product, a grab only requires 49% of the power needed for a subsea cutter.
- The specific energy of excavating rock material using a grab only requires 1.8% compared to a cutter subsea and 21% in total for crushing the rock material when using a grab. The required specific energy subsea is so low because most of the rock material is kept intact subsea when using a grab.

This implies the use of a grab to be very beneficial on the bases of required power and energy consumption. However a vertical transportation system has to be developed, possibly mechanical instead of traditionally proposed hydraulic pumping, which keeps the advantages of using a grab and not crushing the rock materials subsea. This makes a grab a viable option for small scaled production operations or removing the initial rough top layer.

REFERENCES

ASTM C 39/C 39M (2005). Standard Test Method for Compressive Strength of Cylindrical Concrete Specimens. Technical report.

ASTM C 469/C 496M (2004). Standard Test Method for Splitting Tensile Strength of Cylindrical Concrete Specimens. Technical report.

Basheyev, G., Yefimov, V., and Martynyuk, P. (1999). Calculation model for roch breaking with a wedge-shaped impact tool. *Journal of Mining Science*, 35(5):494–501.

Bieniawski, Z. T. (1967). Mechanism of Brittle fracture of rock; Part 2 - experimental studies. *International Journal of Rock Mechanics and Mining Sciences*, 4(c):407–423.

Bloois, J. W. V. and Frumau, J. C. L. (2009). Deep Sea Mining , The New Horizon for Dredging Technology. In *Proc. of Offshore and Technology Conf.*, number May, page 8.

Brace, W. and Martin, R. (1968). A test of the law of effective stress for crystalline rocks of low porosity. *International Journal of Rock Mechanics and Mining Sciences*, 5:415–426.

Chen, X. (2011). *Discrete element modeling of underwater sand/rock cutting process*. Msc. thesis, MSc thesis at Delft, University of Technology.

Drummond, G. B. and Vowler, S. L. (2011). Show the data, don't conceal them. *The Journal of physiology*, 589(8):1861–1863.

Drummond, G. B. and Vowler, S. L. (2012). Analysis of variance: variably complex. *The Journal of Physiology*, 590(6):1303–1306.

Evans, I. (1965). The force required to cut coal with blunt wedges. *International Journal of Rock Mechanics and Mining Sciences*, 2(1):1–12.

Fairhurst, C. (1964). On the validity of the 'Brazilian' test for brittle materials. *International Journal of Rock Mechanics and Mining Sciences*, 1(4):535–546.

Glasby, G. P. (2000). Economic Geology: Lessons Learned from Deep-Sea Mining. *Science Magazine*, 289(5479):551–553.

Griffith, A. (1921). The phenomena of Rupture and Flow in Solids. *Philisophical Transactions of the Royal Society of London*, 221:163–198.

Hoek, E. (1964). Fracture of Anisotropic Rock. *Journal of the South African Institute of Mining and Metallurgy*, 64(10):501–518.

Hoek, E. and Brown, E. (1997). Practical estimates of rock mass strength. *International Journal of Rock Mechanics and Mining Sciences*, 34(8):1165–1186.

Kuiper, R. J. (2012a). *Influence of the Hyperbaric Effect on Apparent Material Strength of Fully Saturated Porous Rock*. Msc thesis, MSc thesis at Delft, University of Technology.

Kuiper, R. J. (2012b). *The effect of offering Natural Force Feedback and Haptic Shared Control on Rate and Force Control of a Deep Sea Mining Grab.* Msc. thesis, MSc thesis at Delft, University of Technology.

Kuiper, R. J., Frumau, J. C., and Miedema, S. A. (2013). Influence of the Hyperbaric Effect on Apparent Material Strength of Fully Saturated Porous Rock for Low Strain Rates. In *Offshore Technology Conference 2013*, pages 1–13.

Lockner, D. A. (1995). Rock Failure. *Rock physics and phase relations: A handbook of physical constants*, 3:127—-147.

Merchant, M. E. (1945). Mechanics of the Metal Cutting Process. I. Orthogonal Cutting and a Type 2 Chip. *Journal of Applied Physics*, 16(5):267.

Miedema, S. A. (1987). *Calculation of the Cutting Forces when Cutting Water Saturated Sand.* Distertation, PhD Thesis, Delft University of Technology.

Miedema, S. A. (2011). Soil Cutting Processes: The Cutting of Water Saturated Sand. In *ASME 2011 International Conference on Ocean, Offshore and Arctic Engineering*, pages 841–853. ASME.

Miedema, S. A. and Zijsling, D. (2012). Hyperbaric Rock Cutting. In *Proc. of ASME Int. Conf. on Ocean, Offshore and Artic Engineering*, pages 1–14.

Nishimatsu, Y. (1972). The mechanics of rock cutting. *International Journal of Rock Mechanics and Mining Sciences*, 9(February 1971):261—-270.

Rona, P. A. (2003). Resources of the sea floor. *Science Magazine*, 299(5607):673–674.

Scott, S. (2001). Deep ocean mining. *Geoscience Canada*, 28(2):87–96.

Tivey, M. K. (2007). Generation of Seafloor Hydrothermal Vent Fluids and associated Mineral Deposits. *Oceanography*, 20(1):50–65.

van Es, B., de Vlaming, R., and de Vries, J. (2004). Construction of Wellhead Protection Glory Holes for White Rose Project, Canada. *Terra et Aqua*, (95):22–32.

van Kesteren, W. (1995). Numerical simulations of crack bifurcation in the chip forming cutting process in rock. *Fracture of Brittle Disordered Materials: Concrete, Rock and Ceramics*, pages 505–524.

Verhoef, P. N. W. (1997). *Wear of rock cutting tools: Implications for the site investigation of rock dredging projects.* Dissertation, PhD thesis, Delft University of Technology.

Winterwerp, J. and van Kesteren, W. (2004). *Introduction to the physics of cohesive sediment in the marine environment.* Elsevier B.V.

Yang, K. and Scott, S. (1996). Possible contribution of a metal-rich magmatic fluid to a sea-floor hydrothermal system. *Letters to Nature*, 383(October):420–423.

3

HAPTIC FEEDBACK FOR A GRAB

Roel J. Kuiper, Jan C.L. Frumau, David A. Abbink and Frans C.T. van der Helm

Published in IEEE SMC conference proceedings, 2013

Excavation in deep-sea using low strain rates such as a suspended hydraulic grab showed promising results in chapter 2. However environmental uncertainties such as unpredictable seabed properties prohibit autonomous control, and requires human operator to remotely control the grab. This chapter compares two design options to assist the operator with forces on the joystick: natural haptic feedback of the interaction forces of the grab with the seabed, and haptic shared control to guide the operator in controlling the suspension cable of the grab.

A grab simulator was developed for remotely controlling a virtual grab in deep-sea including a force reflecting input device, briefly described in section 3.2. Both concepts of haptic feedback are designed for controlling a grab as also described in section 3.2. A human factors experiment was conducted (section 3.3) to investigate the effect of both methods and their potential on improving situational awareness and control effort of controlling such heavy machinery remotely. Results show that natural force feedback increases the situational awareness by reflecting the information of the exerted forces on the environment, while haptic shared control reduces control effort for the human operator.

R.J. Kuiper, J.C.L. Frumau, D.A. Abbink and F.C.T. van der Helm; Haptic Support for Bi-Manual Control of a Suspended Grab for Deep-Sea Excavation; IEEE proceedings of SMC, 2013

ABSTRACT

Deep-sea mining is an envisioned solution to cope with the fast increasing demand for rare-earth metals and decreasing supplies from conventional mines. It could involve a hydraulically actuated suspended grab to excavate metal-rich minerals from the seabed. Due to environmental uncertainties such an operation cannot be automated and should therefore be controlled by teleoperation, which traditionally suffers from suboptimal performance and limited situation awareness. The current study proposes two methods of haptic feedback, natural force feedback and haptic shared control, to improve the control of a grab in deep-sea mining. Natural force feedback is offered to improve the transparency of the system, which is hypothesized to improve situation awareness of the operation. Secondly it is hypothesized to reduce control effort by guiding the operator when offering haptic shared control. Besides the individual effect, combining both haptic feedback methods should also improve the overall task performance of the operation. A deep-sea mining simulation experiment is conducted to investigate the effect of these two haptic feedback methods and their combination on operator control behaviour. The results show improvement of situation awareness (i.e. control errors) when offering natural force feedback and a reduction of control effort (i.e. control inputs) when offering haptic shared control. However the results do not show an increase of task performance (i.e. excavated rock production) for either method. Although reduction of control error and effort will result eventually in long-term performance benefits. Combining both methods is therefore the best haptic feedback method for improving a deep-sea mining teleoperation using a grab.

3.1. INTRODUCTION

HIGH concentrations of common and rare-earth metals are found on the seafloor in rock material named seafloor massive sulphides deposits, at depths up to 2000 meters (Rona, 2003). The deep-sea mineral deposits could be the solution for the rising demand for metals and decreasing supplies on land. A promising method to excavate these deposits at such great water depths is to use a large suspended grab (van Bloois and Frumau, 2009), controlled remotely. The grab would cut the submerged rock material using two opposite clamshells hydraulically actuated as shown in the left of figure 3.1. To make a deep-sea mining process economically viable the size of the clamshells should be approximately $40m^3$, roughly the size of a large dump truck. An example of such an existing, but smaller ($16m^3$) machine is shown in the right of figure 3.1, for removing soil in Arctic conditions (Es et al., 2004). Using a grab has advantages over a conventional crown or drum cutter for rock excavation due to the low cutting energy over excavated rock volume, by not fully crushing the rock material (Kuiper, 2012b). A deep-sea mining task using a suspended grab would mainly consist of excavating the rock material and placing it nearby on the seabed. Excavated rock materials are not intended to be transported vertically to the surface using the grab. There are multiple solutions investigated for the vertical transportation; one is to crush the materials subsea and pumping it to the ship through a vertical pipeline (Espinasse, 2010). The task for controlling a grab near the seabed consists of several intermediate steps. First the grab should be positioned in the horizontal plane at the correct position for excavating minerals. Secondly the grab should be lowered on the seabed,

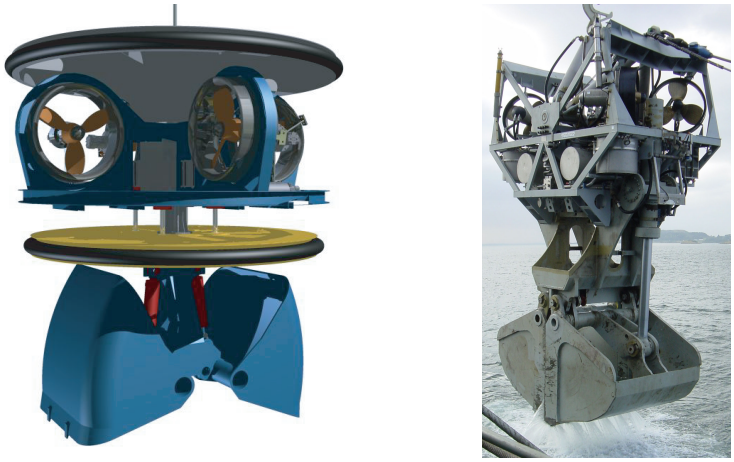

Figure 3.1: Examples of hydraulically actuated suspended grabs. *Left* — Designed grab by Seatools B.V. proposed for deep-sea mining (from van Bloois and Frumau (2009)). *Right* — Fabricated grab by Seatools B.V. for dredging in Arctic conditions (from Es et al. (2004)).

using appropriate impact to crush the rock material and not let the machine topple over at the same time. After placed on the seabed the grab can start closing the clamshells and cut the rock material. During this process the rock material can behave unexpectedly (Kuiper et al., 2013), causing the grab to fall when inappropriate hoisting cable forces are used. At the same time enough downward force onto the seabed has to be maintained to be able to cut the rock materials. After the clamshells are closed the grab can be uplifted to dump the materials at the dump location.

A deep-sea mining operation has the goal to excavate the maximal amount of minerals at the minimal amount of time. Environmental uncertainties (e.g. bathymetry and rock material properties) combined with subsea positioning uncertainties prohibit the use of full automation (Rona, 2003; Whitcomb, 2000). Deep-sea mineral excavation additionally requires planning and adaptation of the process, inducing the need of an operator controlling the process remotely by teleoperation. General problems that are expected to occur with a teleoperation of a large machine on great depths are the operator's performance resulting in reduction of excavated rock production and the operator's reduced situation awareness (Abbink and Mulder, 2012; Endsey, 1995; Wildenbeest et al., 2013). The latter can reduce operational efficiency and might even lead to failure when not undertaking appropriate responses in critical situations, for instance causing the machine to topple over. Therefore optimization of the grasping teleoperation is needed to increase the entire excavation performance and decrease periods of operational downtime due to incorrect execution of the operator. So far no haptic support has been developed for operating a deep-sea mining machine. Research has been done for subsea manipulator control by Sayers and Paul (1994), applying synthetic fixtures, comparable to the virtual fixtures of Rosenberg (1993). Offering natural force feedback partially restores transparency of a teleoperation (Yokokohji and Yoshikawa, 1992; Zhu and Salcudean, 1995),

enabling the operator to feel the environment. Another possibility is offering artificial guiding forces, such as has been proposed for driving (Abbink and Mulder, 2012; Griffiths and Gillespie, 2005), teleoperated surgery (Marayong and Okamura, 2004) and assembly (Boessenkool et al., 2013). Since both options have been shown to be beneficial for other tasks, this study explores to what extent deep-sea mining operators might benefit from either of two, or a combination of both types of support.

Offering natural force feedback (NFF) should improve the situation awareness of the operation because he can feel the forces acting on the machine. Therefore the operator is expected to make less mistakes, for instance in controlling the heeling angle of the machine. Offering guidance by haptic shared control (HSC) should decrease the effort for controlling the machine because the intelligent controller is helping to control the machine. Reduction of control effort results in more attentional resources available of the operator to monitor the many screens needed for good operation. Combining both haptic feedback methods should both increase the efficiency of the operation and therefore increase the production. An experiment is designed to validate the effects of offering natural force feedback and haptic shared control to improve a deep-sea mining operation. Because no mining in deep-sea currently exist, the experiment consists of controlling a virtual grab excavating rock minerals on the ocean floor using a haptic interface.

3.2. METHODS

3.2.1. APPARATUS

The experimental setup consists of a haptic interface for controlling two parameters, the vertical hoisting cable force of the grab and the cutting force of the clamshells as shown in figure 3.2. A virtual model of the process is developed for a fictive mining process (due to non-existing mining in deep-sea currently) to investigate the effect of haptic feedback for possibly any future deep-sea mining projects. The behaviour of the ship and grab are simulated in a dynamic model based on rudimentary calculations with a grab of 50 tons and with maximally 350 tons of clamshell cutting forces.

The stick for controlling the hoisting cable force is dual-directional one degree of freedom (DOF) with force feedback. The stick for controlling the clamshell cutting force is single-directional 1-DOF stick with a static stick as a hand rest for controlling the cutting force with a gripping motion, as shown in figure 3.2. Both sticks have identical force feedback mechanisms, using geared electric motors with a series-elastic actuation to the sticks, therefore also enabling force sensing (Veneman et al., 2005). The force was controlled by a local real-time controller at 1000 Hz controlling the force based on values from the simulation to be used as set-points at 10 Hz. Both sticks have a lever arm ranging from 50 to 150 mm at the hand rest. The maximal applied force of both sticks at 100 mm was limited to 30 N.

The operator is controlling the task using visual feedback, displayed on the monitor in front of the haptic interface as shown in figure 3.2. The visualization shown to the operator is based on parameters gained from the virtual model, containing the behaviour of the grab and several

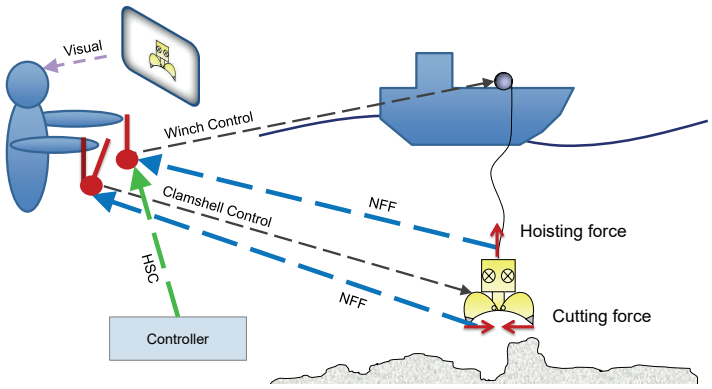

Figure 3.2: Schematic overview of experiment with two control inputs (Winch and Clamshell control) and two haptic feedback methods; Haptic Shared Control (HSC) and Natural Force Feedback (NFF).

control parameters along the optimal hoisting force. The design of the experimental setup is described more detailed in the thesis of Kuiper (2012a).

3.2.2. TASK DESCRIPTION

The task to conduct by the operator was not a complete deep-sea mining operation, but only focused on the excavation part of the process using a suspended grab. The task consisted of lowering the grab on the seabed, cutting the rock material and lifting up the grab with a full load from the seabed. This entire cycle would take roughly 60 seconds, of which 30 seconds were needed to cut the rock material and close the clamshells. The operator was instructed to operate the excavation process with a grab as fast as possible, when operating safely. A virtual starting and stopping line were made visible to the operator at a fixed height of 12m above the seabed, shown in the top-right of figure 3.3. This starting and stopping line enabled a comparison of the conducted task time to completion. Two types of tasks were conducted during this experiment, normal and critical excavation situation.

- *Normal excavation situation:* three tasks at every condition, where the ground profile and properties were changed slightly. Identical tasks for each condition but in a semi-random order.
- *Critical excavation situation:* one task at every condition, identical for each condition

The subjects conducted all task consecutively for each condition, where the tasks were semi-random given for each condition. The presented order of conditions were semi-random given between subjects to minimize the impact of learning effects and fatigue. Therefore each subject had to conduct four tasks during each condition, sixteen tasks in total.

Excavating rock material during tasks in the normal excavation situation was achieved by closing the clamshells and with sufficient vertical force by the weight of the grab, the clamshells would penetrate the seafloor. The critical excavation situation consisted of a situation in which the clamshells were not penetrating the seafloor and would only scrape of the top layer of

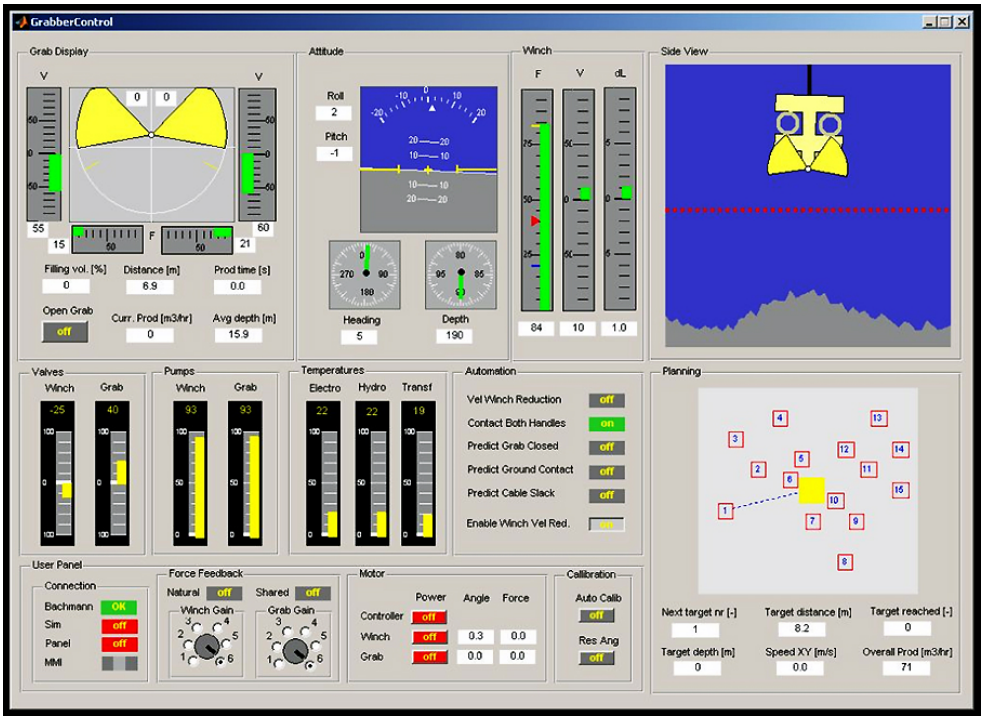

Figure 3.3: Developed visual interface for operating the virtual grab.

the seafloor. This causes sudden movements of the grab by rapidly changing forces on the clamshells, because the grab is not fixed to the seafloor. These sudden movements could cause large inclination angles and even tumbling over of the grab.

3.2.3. EXPERIMENTAL CONDITIONS

Two haptic feedback methods are offered during these experiments to validate the effect of these methods on controlling a deep-sea mining process using a suspended grab. Natural force feedback and haptic shared control are the two offered haptic feedback methods. These two methods are compared to a baseline condition without haptic feedback to compare the effect of either method. Both haptic feedback methods are also combined to determine if these methods would interfere with each other and confuse the operator. This results therefore in four experimental conditions to determine the effect of these two haptic feedback methods.

- Manual Control (MC; baseline conditions)
- Haptic Shared Control (HSC)
- Natural Force Feedback (NFF)
- Combining both feedback methods (NFF-HSC)

3.2.4. HAPTIC FEEDBACK DESIGN

Natural Force Feedback (NFF) is offered to inform the operator of the two controlled forces acting on the virtual grab, clamshell cutting and cable hoisting forces. However both forces are controlled with a joystick, which is a rate-controlled input mechanism. NFF is most often offered as a contact force for a position controlled task (Yokokohji and Yoshikawa, 1992). Nonetheless due to the continuous force to be controlled, stiffness feedback gives the operator more transparency of the hydraulic actuator stiffness and allows the operator to probe the environment. This is based on the findings of Abbink et al. (2008) who applied this method on feedback of a gas pedal to support car following, based on the impedance control of Hogan (1984). Impedance control is applied on a joystick by making the applied natural feedback force F_{NFF} dependent on the steering angle θ_{steer} of the joystick.

$$F_{NFF} = \max\left\{\frac{F_{hydr}}{\theta_{stroke}}, F_{min}\right\} \cdot \theta_{steer} \tag{3.1}$$

The change in stiffness dK of the natural feedback force is based on the hydraulic actuator forces F_{hydr} of the virtual grab and the maximal stroke θ_{stroke} of the joysticks. The feedback forces of the winch F_w and clamshell F_c dependent on their control input angle for the winch θ_w and clamshell θ_c for all four conditions, as schematically shown in figure 3.4. The feedback force also has a minimum feedback force F_{min} for returning to the initial zero point of the joystick. This is shown for clamshell control in figure 3.4, although it also applies for winch control.

Haptic Shared Control (HSC) is offered to guide the operator controlling the virtual grab during excavation tasks. The method is based on the method by Abbink and Mulder (2009) for assisting lane keeping while steering a car. This method is applied on a joystick by altering the equilibrium point of the joystick, shifting the initial zero point of the joystick. The operator is exerted with a guiding force F_{HSC} by shifting the equilibrium point with the angular difference $d\theta$ between the calculated optimal θ_{opt} and actual steering angle θ_{steer}. This is only applied for the winch control as shown in figure 3.4, because clamshell control is a one directional 1-DOF joystick. Additional guiding forces are applied on both joysticks to limit the control input F_{lim} when maximal velocity of the actuators is reached, to reduce the control effort.

$$F_{HSC} = \max\left\{F_{min} \cdot \left(\theta_{steer} - \theta_{opt}\right), F_{lim}\right\} \tag{3.2}$$

Guiding forces for the HSC method are controlled by the intelligent controller, which calculates the optimal control input θ_{opt} based on its sensory inputs, such as operational forces and states of the virtual machine. Guiding forces to the operator are only applied on the joystick for controlling the hoisting cable force. The optimal input for this parameter can be predicted based on the grab making contact with the sea-floor, the inclination angle of the grab and the angle of the clamshells indicating the progress of the excavation process. Therefore the intelligent controller can predict the correct cable hoisting force to optimally control the grab during the process and prevent the grab from falling. The calculated optimal hoisting force,

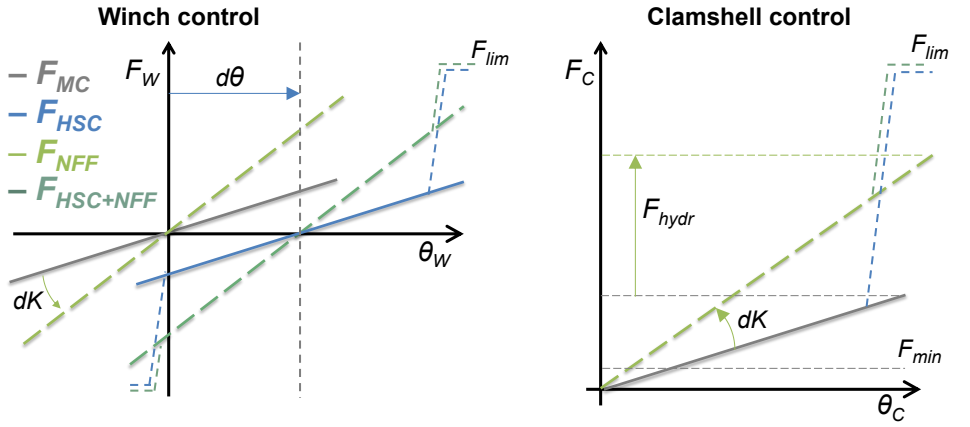

Figure 3.4: Offered haptic feedback for each control input for all four conditions. *Left* —- winch control, where all conditions fully apply. *Right* — clamshell control where the HSC forces only consists of the limiting force.

from which the steering input is calculated, is also shown visually to the operator as can be seen in figure 3.3 with a red triangle in the winch force indicator.

Combining both feedback mechanisms is simply done by substituting the stiffness feedback into the guiding feedback forces.

$$F_{HSC} = \max\left\{\max\left\{\frac{F_{hydr}}{\theta_{stroke}}, F_{min}\right\} \cdot \left(\theta_{steer} - \theta_{opt}\right), F_{lim}\right\} \tag{3.3}$$

3.2.5. SUBJECTS

The experiment to determine the effect of the two haptic feedback methods was conducted by 10 subjects, nine male and one female. All subjects were right handed with a mean age of 25.2 years old and 1.3 years standard deviation. They were not compensated financially for their participation. The participants had no prior experience in handling teleoperations. All subjects were given a written instruction on the task and apparatus combined with at least 10 training tasks, including all conditions. Each task took approximately 60 seconds to complete, 16 tasks in total to complete per subject combined with breaks in between took approximately 2 hours per subject.

3.2.6. EVALUATION METRICS

To analyse the effect of both haptic feedback methods, a vast amount of variables were recorded during the experiment, sampled at different rates ($\leq 50Hz$). From these recorded variables six metrics were calculated to determine the difference between the four given conditions. In addition two subjective measures were tracked for all four conditions.

- *Production* $[m^3/hr]$: Total excavated rock volume divided by task completion time of a single task.

- *Total Control Input [deg]*: Mean absolute of both control input angles of the joysticks during a single task.
- *HF Control Input [deg]*: Mean absolute of both high-pass frequency (>0.1Hz) control input angles of the joysticks during a single task.
- *Applied Force [N]*: Mean absolute of applied control input force on both joysticks by the operator during a single task.
- *Grab Angle [deg]*: Maximum inclination angle of the grab on the seabed during a task. The angle has a warning level at 15 degrees and failure level at 30 degrees of inclination.
- *Cognitive Workload [%]*: Self-reported cognitive workload, adapted from NASA-TLX questionnaire (Hart and Staveland, 1988). Using a 20 point scale ranging from 0 to 100 to report their workload, based on mental demand, physical demand, temporal demand, performance, effort and frustration level.
- *Overall Rating [%]*: Self-reported overall rating of the haptic support measured per experimental condition on a 20 point scale ranging from 0 meaning hindering to 100 meaning very helpful.

Task performance is based on the production metric of the conducted task, which determines the effectiveness of the task. Control effort of the subject is based on the total control input, High Frequency (HF) control input, applied force and cognitive workload metric. The grab angle is influenced by control errors and therefore is a measure for situation awareness (Endsey, 1995), by understanding operating situation and acting correct.

3.2.7. DATA ANALYSIS

The comparison of experimental conditions was made on basis of populations, assuming a normal distribution, using a repeated measures design. The experimental results are shown with the mean data for each subject per condition and the group mean per condition along with the 95% Confidence Interval (CI) (Drummond and Vowler, 2011). Statistical differences are analysed using the two-way repeated measures analysis of variance (Drummond and Vowler, 2012) with the mean of repetitions for each subject per condition, with conditions as a factor (F1) and subject inter-variance (F2). A post-hoc analysis was executed to compare the haptic feedback methods. Only the post-hoc results will be presented in the results section. Results were regarded as statistical significant when $p \leq 0.05$.

3.3. RESULTS

The average results for each subject of all three tasks in the normal excavation situation and the group mean with their 95% CI of each condition are shown in the top-left of figure 3.5. The results of the total control inputs are shown in the top-right of figure 3.5, the bottom-left part shows the results of the HF control inputs of both joysticks. The bottom-right of figure 3.5 shows the results of the applied force on the control inputs of both joysticks for controlling the virtual grab. The results in normal excavation situation do not show statistical difference in production results for the different experimental conditions ($p \geq 0.1$). The total control input

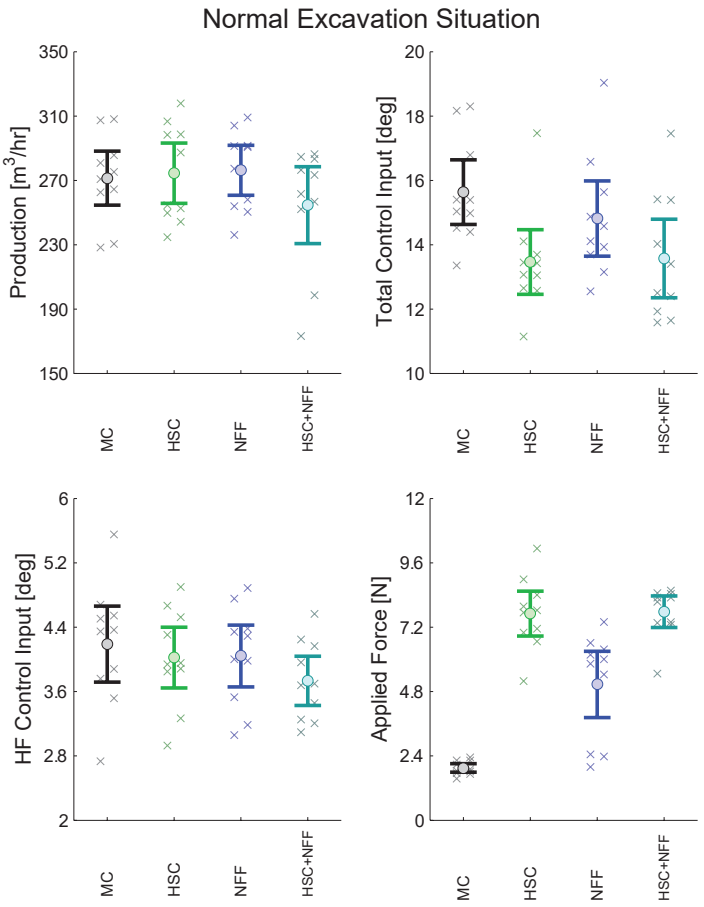

Figure 3.5: Experimental results of trials in normal excavation situation, showing individual mean results of each subject (N=10) for each condition and the mean and 95% CI for each condition of all subjects. *Top-left* — production results. *Top-right* —- total control input. *Bottom-left* —- high frequency control input. *Bottom-right* — applied force.

shows a difference for all three haptic conditions HSC, NFF, HSC-NFF compared to the manual condition ($p < 0.01, F \geq 12$). The HF control input however only shows a slight difference for the HSC-NFF condition ($p = 0.032, F = 6.4$). The applied force on the control input shows a large significant difference for all three haptic conditions HSC, NFF, HSC-NFF ($p < 0.01, F \geq 22$) compared to the manual control condition where no feedback force is applied, besides the returning spring force F_{min}.

Performance results during the critical excavation situation of the production for each subjects is shown in the top-left of figure 3.6, along with the group mean and its 95% CI. The total control input is shown in the top-right of figure 3.6 and the HF control input is shown in the bottom-left of figure 3.6. The maximal inclination angle of the virtual grab during the task of each subject is shown in the bottom-right of figure 3.6. This graph also shows the critical inclination angle ($30deg$) and the warning inclination angle ($15deg$) with dashed lines.

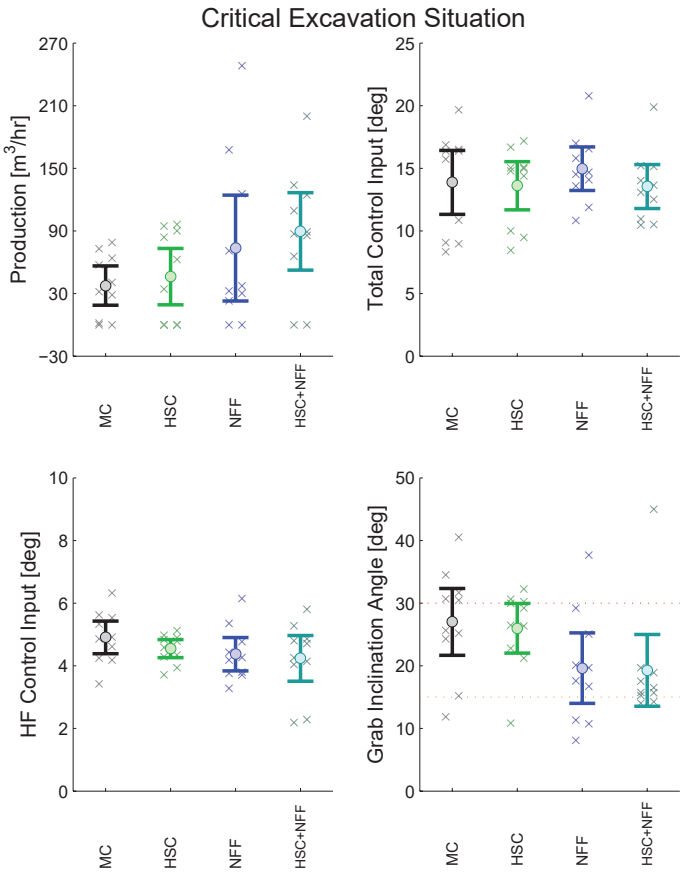

Figure 3.6: Experimental results of trials in critical excavation situation of each subject ($N = 10$) for each condition. *Top-left* — production results. *Top-right* —- total control input. *Bottom-left* — high frequency control input. *Bottom-right* — maximal inclination angle of virtual grab.

The production results do not show any statistical difference compared with manual control, for HSC, NFF ($p \geq 0.3$) and for HSC-NFF ($p = 0.052, F = 5.0$). The total control input shows no difference ($p \geq 0.4$), neither does the high frequency component ($p \geq 0.1$). The maximal inclination angle of the virtual grab does show a decrease for both the NFF and HSC-NFF conditions ($p < 0.05, F > 5$). This decrease causes the maximal inclination to decrease below the critical level of 30 degrees, which therefore reduced the control error.

The self-reported cognitive workload results of the conducted tasks in normal excavation situation showed no significant difference ($p > 0.1$), with a mean cognitive workload of 35.8% (standard deviation of 12.5%). The subjective results for the critical excavation situation however did show differences as shown in figure 3.7, on the left the self-reported cognitive workload and on the right the self-reported overall rating of each condition. The reduction of cognitive workload during the HSC condition is not significantly different compared to the manual

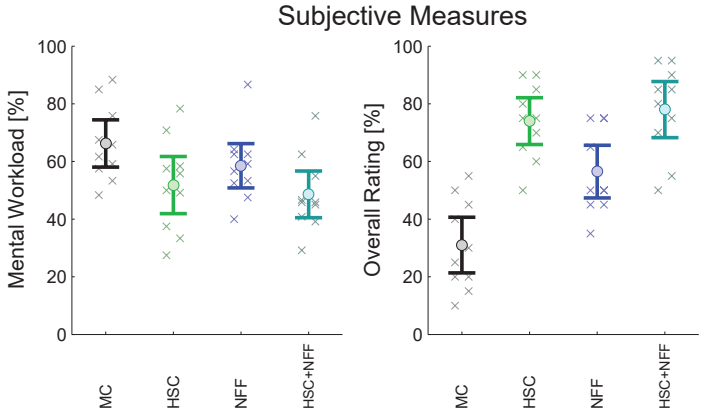

Figure 3.7: Results of subjective measures. *Left* — self-reported cognitive workload from NASA-TLX questionnaire during critical excavation situation. *Right* —- self-reported overall rating of each experimental conditions.

condition ($p = 0.066, F = 4.4$), but for the NFF condition a difference is found ($p = 0.023, F = 7.5$) and for the HSC-NFF condition too ($p = 0.004, F = 14.3$). All experimental conditions HSC, NFF, HSC-NFF show a significant difference for the overall rating ($p < 0.01, F > 11$).

3.4. DISCUSSION

The experimental results in normal excavation situation do not show any difference for excavated rock production. This could be because the normal situation is less critical on inputs affecting the production. The control effort however did significantly reduce for both total control input and HF control input when offering any type of feedback. However when guiding the operator it greatly reduces the control effort during the HSC and HSC-NFF conditions, which is consistent with the research of Boessenkool et al. (2013) and Abbink and Mulder (2009). Even though the optimal hoisting force was also visually shown to the operator in all four conditions. The main reason for the reduced control inputs when offering guidance can be explained because guidance informs the operator when maximum system velocity is reached, therefore the operator reduces the unnecessary control inputs more.

The tasks in critical excavation situation were designed such that incorrect control of the grab would result in large inclination angles of the grab and even tumbling over of the grab. Incorrect control in this type of task would mean an incorrect balance between the cutting progress and the hoisting force of the grab. Different control inputs would also affect the performance more during the critical task. Larger variations in production results can be seen for the critical task, some of the subjects did not even succeed in any production at all. The experimental results for the critical tasks seem to have production improvement when offering natural force feedback during NFF and HSC-NFF. However because only one repetition per subject is used during this situation this trend is not significantly different. More repetitions per subject would most likely remove the zero production outcomes and thereby lower the variations largely. Inclination angles of the grab reduced significantly when offering NFF and

HSC-NFF in critical situations. This indicates that natural force feedback improves the situation awareness of such critical tasks, therefore eventually improving the performance of the task. This is similar to what Abbink states in his survey on haptic shared control literature (Abbink and Mulder, 2012).

Subjective results show a reduction of cognitive workload when natural force feedback is offered during both NFF and HSC-NFF conditions. This suggest that additional information feedback of the virtual machine creates more insight for controlling the machine and therefore requires less attention of the operator, which is similar to what Wildenbeest found (Wildenbeest et al., 2013). The increase of physical effort when offering any type of haptic feedback is also consistent with the results of Wildenbeest et al. (2013), which is obviously caused due to the interaction forces applied. The self-reported overall rating of each experimental condition showed an increasing result for offering any haptic feedback and mainly for offering haptic shared control. This confirms the feedback was designed properly and found helpful. Especially when combining the two methods it also shows that they do not interfere and help the operator in conducting the task.

No change in production is found between the conditions during the conducted tasks. However the reduction of control effort in normal excavation situations when offering haptic shared control reduces the strain of the operator which eventually improves performance and therefore production. The reduction of control errors by reduced inclination angles in critical excavation situations when offering natural force feedback also could attribute to long-term performance benefits. Therefore offering both haptic feedback methods could eventually increase the production of such a task.

3.5. CONCLUSION

The current pilot study shows that two types of haptic feedback are promising to support operators with a bi-manually controlled teleoperated excavation process. Two feedback methods were investigated: natural force feedback to make hoisting forces and grabbing forces tangible; and haptic shared control to guide operators towards the correct hoisting command input.

- Natural force feedback showed an increase in situation awareness, causing a reduction of grab inclination angle in critical situations and a decrease in cognitive workload. However no increase in performance was found.
- Haptic shared control also showed no increase in performance, but did show a reduction of control effort at normal excavation situations due to less control inputs and reduced cognitive workload. Offering guidance was also rated highly positive.
- The advantages of both methods remained present when combining haptic shared control and natural force feedback.

Therefore this experiment showed when controlling a deep-sea mining teleoperation using rate and force control, natural force feedback mainly improves the situation awareness and haptic shared control mainly reduces the control effort. However improvements of excavated rock production were not found for either haptic feedback mechanisms. Nonetheless the

results during short-term operation studied here imply that during long-term operation less production loss is likely to occur due to incorrect control and damage of the system when combining the haptic feedback mechanisms for a deep sea mining teleoperation.

REFERENCES

Abbink, D. A., Boer, E. R., and Mulder, M. (2008). Motivation for continuous haptic gas pedal feedback to support car following. In *IEEE Conf. of Intelligent Vehicles Symposium*, pages 283–290.

Abbink, D. A. and Mulder, M. (2009). Exploring the dimensions of haptic feedback support in manual control. *J. of Computing and Information Science in Engineering, Special Haptics Edition*, 9:1–9.

Abbink, D. A. and Mulder, M. (2012). Haptic shared control: smoothly shifting control authority? *Cognition, Technology and Work*, 14(1):19–28.

Boessenkool, H., Abbink, D. A., Heemskerk, C. J. M., van der Helm, F. C. T., and Wildenbeest, J. G. W. (2013). A task-specific analysis of the benefit of haptic shared control during telemanipulation. *IEEE Tran. on Haptics*.

Drummond, G. B. and Vowler, S. L. (2011). Show the data, don't conceal them. *Journal of physiology*, 589(8):1861–1863.

Drummond, G. B. and Vowler, S. L. (2012). Analysis of variance: variably complex. *Journal of physiology*, 590(6):1303–1306.

Endsey, M. R. (1995). Measurement of situation awareness in dynamic systems. *Human Factors*, 37(1):65–84.

Es, B., de Vlaming, R., and de Vries, J. (2004). Construction of wellhead protection glory holes for white rose project, canada. *Terra et Aqua*, (95).

Espinasse, P. (2010). Understanding sms behavior to define the subsea mining operating system. In *Proc. of Offshore Tech. Conf.*

Griffiths, P. G. and Gillespie, R. B. (2005). Sharing control between humans and automation using haptic interface: Primary and secondary task performance benefits. *Human Factors*, 47(3):574–590.

Hart, S. G. and Staveland, L. E. (1988). Development of nasa-tlx (task load index): Results of empirical and theoretical research. *Human Mental Workload*, 589:139–183.

Hogan, N. (1984). Impedance control: An approach to manipulation. *American Control Conference*, pages 304–313.

Kuiper, R. J. (2012a). The effect of offering natural force feedback and haptic shared control on rate and force control of a deep sea mining grab. Master's thesis, Delft University of Technology.

Kuiper, R. J. (2012b). Influence of the hyperbaric effect on apparent material strength of fully saturated porous rock. Master's thesis, Delft University of Technology.

Kuiper, R. J., Frumau, J. C. L., and Miedema, S. A. (2013). Influence of the hyperbaric effect on apparent material strength of fully saturated porous rock for low strain rates. In *Proc. of Offshore Tech. Conf.*

Marayong, P. and Okamura, A. M. (2004). Speed-accuracy characteristics of human-machine cooperative manipulation using virtual fixtures with variable admittance. *Human Factors*, 46(3):518–532.

Rona, P. A. (2003). Resources of the sea floor. *Science Magazine*, 299(5607):673–674.

Rosenberg, L. B. (1993). Virtual fixtures: Perceptual tools for telerobotic manipulation. *IEEE Int. Conf. on Robotics and Automation*, pages 76–82.

Sayers, C. P. and Paul, R. P. (1994). An operator interface for teleprogramming employing synthetic fixtures. *Presence*, 3(4):309–320.

van Bloois, J. W. and Frumau, J. C. L. (2009). Deep sea mining, the new horizon for dredging technology. In *Proc. of Offshore Tech. Conf.*

Veneman, J. F., Ekkelenkamp, R., and van der Helm, F. C. T. (2005). Design of a series elastic actuation system for use as torque-actuator in exoskeleton training. In *IEEE Conf. Rehabilitation Robotics*, pages 496–499.

Whitcomb, L. L. (2000). Underwater robotics: Out of the research laboratory and into the field. In *IEEE Int. Conf. on Robotics and Automation*, pages 1–8.

Wildenbeest, J. G. W., Abbink, D. A., Heemskerk, C. J. M., van der Helm, F. C. T., and Boessenkool, H. (2013). The impact of haptic feedback quality on the performance of teleoperated assembly tasks. *IEEE Tran. on Haptics*, 6(2):242–252.

Yokokohji, Y. and Yoshikawa, T. (1992). Bilateral control of master-slave manipulators for ideal kinesthetic coupling. In *IEEE Int. Conf. on Robotics and Automation*, pages 849–858.

Zhu, M. and Salcudean, S. E. (1995). Achieving transparency for teleoperator systems under position and rate control. In *IEEE Int. Conf. on Intelligent Robots*, volume 2, pages 7–12.

PART II

EXPLORING NATURAL HAPTIC FEEDBACK

4

NATURAL FORCE FEEDBACK IN POSITION CONTROL

Jeroen G.W. Wildenbeest & Roel J. Kuiper*, Kasper van der El, Frans C.T. van der Helm and David A. Abbink*

to be submitted to IEEE Transactions on Haptics, 2019

Remotely controlling large machines required for sub-sea mining is difficult for a variety of reasons, one of them being the slow dynamic response. Slow dynamic systems do not respond immediately to control inputs, requiring the operator to anticipate on the effects of control inputs. This chapter investigates the impact of (scaled) haptic feedback on operator control behavior for slow dynamic systems, as compared to fast dynamic systems. A 1 DoF virtual task is proposed in section 4.2, that allows cybernetic modeling to identify the control behavior of the operator and explains the effect of offering haptic feedback when operating slow dynamic systems.

The study contains two main contributions: an experiment to quantify the effect of haptic feedback on operators controlling either a fast or a slow dynamic system, and a cybernetic model to identify the control behavior. The experimental results in section 4.3 shows substantial improvements for slow dynamic system with feedback, but no effect for scaling or for the fast dynamic system. The cybernetic modeling analysis in section 4.3 indicates that haptic feedback enabled the operators to generate lead, thereby compensating for the system response and enabling more accurate control with a higher bandwidth.

J.G.W. Wildenbeest & R.J. Kuiper, K. van der El, F.C.T. van der Helm and D.A. Abbink; A Cybernetic Approach to Quantify the Effect of Haptic Feedback on Operator Control Behavior in Free-Space Telemanipulation; to be submitted to IEEE Transactions on Haptics in 2019

*Both authors contributed equally to this study

ABSTRACT

Telemanipulation encompasses applications with a wide variety of slave dynamics, ranging from minimally-invasive surgery to large-scale nuclear maintenance. Hence, the haptic feedback from the remote site - which is considered essential to effectively perform tasks - is often scaled. The objective of this study is to quantify the effect of slave dynamics and such scaling of haptic feedback on task execution, and to identify the corresponding changes in underlying control behavior of the operator using a cybernetic model. In a human factors study, subjects (n=13) used a haptic master device to control a virtual slave in a 1 DoF pursuit task with preview. The simulated slave dynamics were either fast or slow with respect to human operator dynamics. Four levels of haptic feedback scaling were provided, namely 0%, 25%, 50% or 100%. The experimental results indicate that task execution was only marginally affected when manipulating haptic feedback for fast dynamic systems. For slow dynamic systems, full haptic feedback substantially improved task execution compared to no haptic feedback, but at the cost of increased operator physical workload. Interestingly, these effects persisted for scaled haptic feedback. Additional frequency domain analysis for the slow dynamic system revealed that, compared to no feedback, any haptic feedback level enables operators to generate phase lead, allowing for improved compensation of the slow slave system's lag. A quasi-linear cybernetic control model was fit to the data to quantify underlying control behavior; the operator's effective time delay and future viewpoint were substantially reduced for all haptic feedback conditions, compared to no haptic feedback. We conclude that the proposed model accurately describes the effect of slave dynamics and haptic feedback on operator control behavior, namely that scaled haptic feedback allows operators to adapt their feedback and feedforward responses, such that slow slave systems can be controlled more accurately in free-space, with a higher bandwidth.

4.1. INTRODUCTION

TELEMANIPULATION entails a wide variety of tasks to be performed. Operators may use the master device to control a slave directly (where movements may be scaled), with rate-control, or through set-points to a semi-autonomous system. In many real-world teleoperation applications haptic feedback is absent, especially during rate control, set-point control – and scaled direct control. This paper focusses on *bilateral* teleoperation, where the slave is under direct control from the master device, but where control and haptic feedback may be scaled. In subhuman-scale applications (e.g., micro-assembly of micro-electro-mechanical systems Bolopion and Regnier (2013) or minimally-invasive surgery De Gersem et al. (2005)), master device movements need to be scaled down and force feedback in the slave environment needs to be scaled up in order for the operator to be able to perceive and respond to it. Note that in this case the human arm dynamics are dominant over the slave manipulator dynamics. Conversely, when manipulating a superhuman-scale slave (e.g., in nuclear Boessenkool et al. (2014) or sub-sea environments Kuiper et al. (2013)), master device movements need to be scaled up, and force feedback on the master device needs to be scaled down. Note that in this case the slave dynamics dominate the human arm dynamics and unscaled coupling of the dynamics on the master device would make movement impossible.

When available, haptic feedback from the remote environment is often considered essential to effectively perform tasks with these systems, while different forms of augmented haptic feedback (e.g. Alaimo et al. (2011); Janabi-Sharifi and Hassanzadeh (2011); O'Malley et al. (2006)) are seen as promising methods to improve task execution. However, how the quality and quantity of haptic feedback affects task execution is not well understood. Similarly, the operator response to augmented forces is not fully comprehended. As a result, the design and evaluation of haptic interfaces and augmented support systems is often subjected to trial-and-error.

This study focuses on measuring and modeling operator control behavior of free-space tasks while controlling a system with substantial dynamics (e.g., cranes, large slave robots, vehicles). A formalized understanding of the effects of haptic feedback and system dynamics on operator control behavior, captured in a computational modeling framework, is expected to help with model-based design of haptic feedback and augmented support systems.

'Haptics' is often referred to as our sense of touch: tactile feedback via our skin that provides information on forces (e.g., pressure, vibrations), but also temperature, humidity and pain. However, haptics also includes kinesthetic or proprioceptive feedback via our muscles and tendons, that provides feedback on muscle stretch and tendon forces, and by integration: feedback on orientation of our body and interaction forces with the environment. A telemanipulation system reflects haptic information from the remote site to the local site, and vice versa. The quality and quantity of this haptic feedback transfer is often captured by 'transparency', commonly defined as the fidelity with which force and positional information is sent from remote (or slave) side to local (or master) side (Dudragne et al., 1989; Lawrence, 1993; Yokokohji and Yoshikawa, 1994). The haptic feedback to the operator can comprise both the reflected dynamics of the slave (i.e. the inertia and damping of the slave are partially felt by the operator), as well as the contact forces of the slave in the remote environment.

The fact that we can control many devices with only visual feedback often obscures the benefits of haptic feedback. However, the benefits of haptic feedback are substantial: when in physical contact with the remote environment, haptic feedback has shown to improve task execution in terms of task completion time (Draper et al., 1986; Hannaford et al., 1991; Massimino and Sheridan, 1994), contact forces (Draper et al., 1986) and errors (Draper et al., 1986; Hannaford et al., 1991), and reduces control effort measured in terms of reversal rate (Wildenbeest et al., 2013a), cognitive workload (Vitense, 2003) and energy consumption (Hannaford et al., 1991), compared to solely visual feedback.

But even when there is no physical contact of the slave system with the remote environment (i.e. free-space tasks), haptic feedback gives the operator a feel of the dynamics of the controlled system (e.g., the slave device and any objects held). In visuo-manual control of a system with a priori unknown dynamics (Hanneton et al., 1997) and manual excitation of a sprung mass (Huang et al., 2004), operators improved their control input when haptic feedback was available. (Dan, 2012) conclude that haptic feedback enhances the control of nonrigid objects. Also, several studies (e.g. Ito (2005); Shadmehr and Mussa-ivaldi (1994)) suggest that haptic feedback improves high-level neuromuscular planning; it enhances building the causal relation between

operator input, system dynamics and subsequent system response . To this extent we found that an operator's ability to generalize beyond a set of pre-experienced motions in an abstract curl force field increases when the quality of the fed back haptic information is (close to) natural Wildenbeest et al. (2013b).

In short, while the effects of haptic feedback during free-space task execution are widely acknowledged, it is not well understood how the feedback affects underlying operator dynamic control behavior. Computational models would help to understand and quantitatively describe the effects of, among others, slave dynamics or reflected haptic feedback. Specifically, such computational models would help to describe and predict changes in human operator control behavior, such that haptic interfaces and systems with augmented feedback can be optimized a priori. However, contrary to pilot (e.g. McRuer and Rex (1967); van der El et al. (2016)) or driver behavior (e.g Pick and Cole (2008)), operator models for telemanipulation are not readily available.

Control-theoretic models have been widely accepted in the field of neuroscience (e.g. Ito (2005); Passot and Arleo (2010); Uzawa et al. (2012)). These models describe how basic movements (i.e. reaching movements) are performed and learned, and incorporate mechanisms for feedforward control, feedback control and learning; our central nervous system learns associations between action and sensory feedback, either by reconstructing the motion from sensory feedback (inverse dynamics), or by translating desired behavior into motor commands (forward dynamics) (Uzawa et al., 2012). These neuroscience models describe the execution of the actual limb movement, but only with a-priori knowledge of the goal. The models do not describe how this goal is derived from dynamic sensory information (i.e. perception).

A more unifying approach addressing perception-action coupling is given by the theory of *successive organization of perception* Krendel and McRuer (1960). This theory is based on the premise that human operators control a device based on high-level control strategies derived from (dynamic) sensory information. The theory classifies three types of control strategies, namely compensatory, pursuit, and precognitive control. In compensatory control the operator can only use feedback control, which is often realized by solely visualizing the error between reference target and system output to the human operator. During pursuit control, the operator combines feedback with feedforward control, typically by visualizing both output and reference target, such that the operator may use past experience and knowledge of the near future. In precognitive control the human operator acts as an open-loop controller and performs purely feedforward.

Operator control behavior during compensatory tracking tasks is accurately modeled by the *crossover model* by (McRuer and Rex, 1967). This quasi-linear model characterizes the operator as a gain with a time delay, and possible lead-lag equalization, depending on the controlled dynamics For pursuit tasks, (Wasicko et al., 1966) suggested an extension to the crossover model, which used a combination of feedback control based and feedforward control to control the plant. However, Wasicko et al. did not formulate a generic model. Only recently, feedforward models were developed and validated with experimental data for pursuit tasks with predictable

reference signals (Drop et al., 2013), and for pursuit tasks with preview (van der El et al., 2016). The model by (van der El et al., 2016) extends the quasi-linear operator model for compensatory tracking tasks, with two points of the previewed reference as input to the human operator (i.e., a look-ahead controller).

In practice, telemanipulation tasks are rarely performed purely based on feedback information, or purely based on feedforward information; an operator uses an estimate of the system's dynamics to plan its movements, while any distortions are corrected using feedback control. Hence, in order to study operator control behavior in telemanipulation tasks, it is important to use a model which incorporates both feedforward and feedback: the pursuit model.

The pursuit models show that, in the human-machine system's frequency range most critical to its performance and stability, the human operator has the capability to adjust or equalize his behavior such that the closed-loop characteristics yield some desired command-response relationship, disturbances can be suppressed, variations and uncertainties can be minimized and adequate closed-loop stability margins can be attained McRuer and Rex (1967). In telemanipulation, the controlled device dynamics for, for example, space, nuclear Boessenkool et al. (2014) and sub-sea Kuiper et al. (2013) tasks, are often in the range of, or even larger than, human operator dynamics. Control of such systems is characterized by large control lag, typically caused by large inertias combined with relatively low power actuators. This means that, from a dynamics point of view, the slave system being controlled is the limiting factor in the closed-loop human-machine system Kim et al. (1987). What is the extent to which human operators can adjust or equalize their behavior such that the basic requirements of any good feedback control system are fulfilled (e.g., adequate command-response relations and closed-loop stability margins McRuer and Rex (1967))? And how does haptic feedback affect operator control parameters, given certain slave dynamics?

The objective of this study is to quantify operator control mechanisms underlying haptic feedback in visuo-motor coordination. A control-theoretic approach is adopted to measure and model operator responses, yielding quantitative insights of observed operator control behavior. As such this study expands on previous work Wildenbeest et al. (2014), in which mainly time domain metrics were analyzed. Subjects were subjected to a visuo-motor control task, in which a previewed reference trajectory was to be tracked using a (virtual) telemanipulation system, with either fast or slow dynamics. The dynamics of the controlled system were fed back fully (i.e. the slave's dynamics are directly presented to the operator), scaled (i.e. the slave's dynamics are scaled before being presented to the operator) or not at all. Besides metrics derived in the time domain, a black-box identification method was used to quantify causal relationships in operator control behavior, and a recently published cybernetic model van der El et al. (2016) was fit to the data.

We hypothesize that when either full or scaled haptic feedback is provided, operators are able to more accurately control the slave system compared to not providing haptic feedback. We expect reductions in tracking errors and mental control effort, as haptic feedback may improve

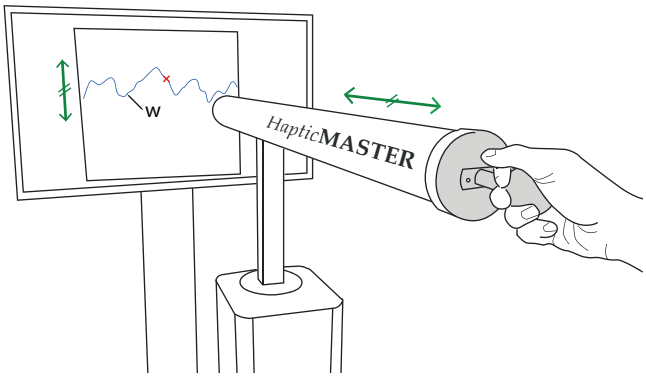

Figure 4.1: The experimental setup showing master device, virtual slave system (red cross) and reference trajectory w (blue line) in a pursuit display with preview. Subjects were standing in front of the HapticMASTER, which was aligned with the sagittal plane of the subject. Pushing the master device forward moves the slave system upwards, pulling it moves the slave system downwards. Subjects were instructed to track the reference as accurately as possible.

the operator's estimates of the system's state. The root of these effects may be found in improvements of the operator's feedback and feedforward responses; we expect that haptic feedback allows a reduction of the effective time delays, because of the generally faster sensorimotor response to haptic stimuli compared to visual stimuli.

4.2. MATERIALS & METHODS

4.2.1. SUBJECTS

Thirteen healthy, right-handed subjects aged between 24 and 35 years all affiliated with the Delft University of Technology were recruited. The participants had none or limited experience with robotic systems. All subjects gave informed consent. The study was approved by the Delft Human Research Ethics Committee.

4.2.2. APPARATUS

The experiments were performed on the 3 degree-of-freedom admittance-controlled FCS Moog HapticMASTER with a simulated slave device. The HapticMASTER was constrained to only allow movement along the forward/backward-axis of the device, which was aligned with the sagittal plane of the subject (figure 4.1). The HapticMaster has a position resolution of <12e-6 m, a stiffness of >10 kN/m and a force sensitivity of 100 mN (Linde et al., 2002). The virtual inertia and damping of the master device were respectively set at J_m = 2.5 kg and B_m = 5 Ns/m. The manipulator was controlled with a VxWorks RT operating system running at 2048 Hz. The slave system, designed in Matlab Simulink, was simulated on an additional real-time controller by Bachmann GmbH. This industrial controller runs at 1000 Hz and logs position and force at the same frequency. The visualization was updated at a rate of 30 Hz.

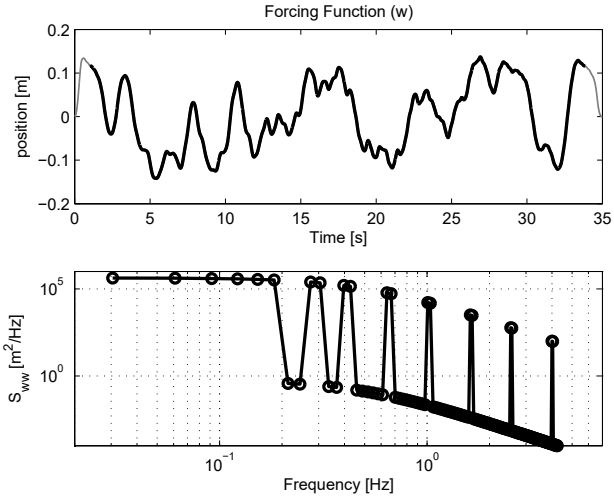

Figure 4.2: One of six realizations of the time trace and the auto spectrum of reference trajectory w. The multisine signal consists of 10 pairs of two log-spaced frequencies ranging from 0.03 to 4 Hz. The signal is filtered with a second-order Butterworth filter with a cutoff frequency of 0.5 Hz.

4.2.3. EXPERIMENTAL DESIGN

TASK DESCRIPTION

Subjects controlled a second-order virtual slave system (a mass-damper), actuated via a servo actuator, with the goal of tracking a multisine reference trajectory w as accurately as possible. A forward movement in the sagittal plane of the subject allowed control of the vertical position of the slave system (figure 4.1). The scaling between movement and visualization was approximately 1:1. Reference trajectory w was displayed as a pursuit display with two seconds of preview and history. The multisine signal consisted of 10 logarithmically distributed frequency pairs ranging from 0.03 to 4 Hz. In order to represent a realistic tracking task, the power spectrum of the reference trajectory contained a significant amount of power at the lower frequencies, with a second-order roll-off (20 dB/decade) (Damveld et al., 2009). To achieve this, the reference trajectory was filtered with a second-order Butterworth filter with a cutoff frequency of 0.5 Hz. Six different random phase time domain signals were generated all with a duration of 35 s. Two signals were solely used for training purposes and four for the measurement trials. All subjects performed the trials with the same signals, while the order in which the signals were presented was randomized. Figure 4.2 shows a time trace and the auto spectrum of w.

EXPERIMENTAL CONDITIONS

The two independent variables were slave dynamics (*fast* or *slow*) and force reflection gain (K_{fb}=0 ∨ 1 for the *fast* system and K_{fb}=0 ∨ 0.25 ∨ 0.5 ∨ 1 for the *slow* system).

The dynamics of the second-order mass-damper slave system were chosen with respect to

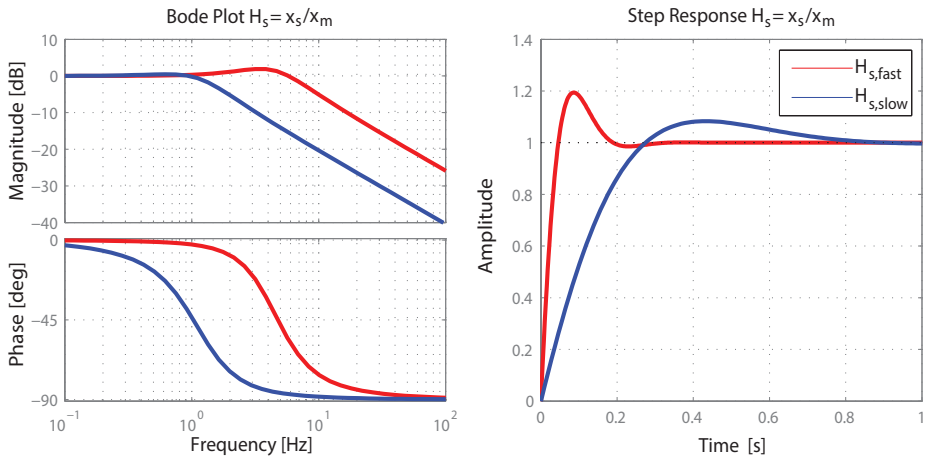

Figure 4.3: Bode plot and step response of the slave system (open-loop). The *slow* slave system ($H_{s,slow}$) has a cutoff frequency of ~1.5 Hz, whereas the *fast* slave system's ($H_{s,fast}$) cutoff frequency is ~8 Hz.

the frequency range of the operator's voluntary control inputs. The human's neuromuscular system only allows for precision movements up to approximately 1 Hz, with voluntary inputs up to several Hertz (up to 6-8 Hz for skilled professionals like pilots (Wasicko et al., 1966)). As such, the dynamics of the *fast* and *slow* dynamic systems were chosen to have a cutoff frequency - the point at which the output of the system drops -3 dB relative to the nominal value - of $f_c \simeq$ 8 Hz and $f_c \simeq$ 1.5 Hz, respectively. Hence the *fast* dynamic system predominantly appears to the human operator as a gain, whereas the *slow* dynamic system appears as a second-order system (a mass-damper) above its cut-off frequency, substantially affecting closed-loop human-machine performance. The transfer function of the second-order slave system and its position servo actuator is given by:

$$H_s(s) = \frac{x_s(s)}{x_m(s)} = \frac{k_d s + k_p}{J_s s^2 + (B_s + k_d)s + k_p} \tag{4.1}$$

Here x_m and x_s represent master and slave position, respectively. Slave inertia J_s and damping B_s were set at 2.5 kg and 10 Ns/m for the *fast* system and 50 kg and 200 Ns/m for the *slow* system. The systems were tuned to be critically damped. Limited by closed-loop stability, proportional gain k_p and derivative gain k_d were set at 2000 [-] and 80 [-], respectively, for the *fast* and 2500 [-] and 300 [-] for the *slow* dynamic system. Figure 4.3 shows a bode plot and step response for the two controlled dynamics.

The force reflection gain K_{fb} was selected to be K_{fb}=0 or 1 for the *fast* and K_{fb} = 0, 0.25, 0.5 or 1 for the *slow* dynamic system. The equation for the force feedback is given by:

$$F_{fb}(t) = K_{fb}\Big(\big(x_s(t) - x_m(t)\big)k_p + \big(\dot{x}_s(t) - \dot{x}_m(t)\big)k_d\Big) \tag{4.2}$$

Thus for K_{fb}=0, no haptic feedback is provided to the human operator, whereas for K_{fb}=1, the servo system tries to equate $x_m(t)$ with $x_s(t)$.

EXPERIMENTAL PROTOCOL

Each of the six experimental conditions were performed in blocks of four repetitions. Each block was preceded by four training trials. The two blocks with *fast* and the three blocks with *slow* system dynamics were grouped. When the switch between slave dynamics was made, subjects performed another four training trials. The order in which conditions were presented to subjects, and the order of reference trajectories within a block of four repetitions, were randomized by means of a balanced Latin square for the first twelve subjects and randomized for the thirteenth subject. Subjects rested and relaxed their arm between trials.

4.2.4. DATA PROCESSING

DATA ACQUISITION

Force and position data of the master device, as well as position data of the simulated slave were logged at 1 kHz. Figure 4.4 shows a typical example of the tracking behavior of a subject. For each trial, the first and last second were discarded. Based on the recorded signals, time domain analysis was performed for both the *fast* and *slow* dynamics system. System identification and parameter estimation was performed for the data for the *slow* dynamic system.

TIME DOMAIN ANALYSIS

For both the *fast* and *slow* dynamic system, task performance and control effort were evaluated in terms of:

e_m Mean tracking error [mm] of the slave position (x_s) with respect to reference trajectory w.

n_{rr} Number of reversals [-]. The amount of steering corrections by the operator as a measure of his mental effort (MacDonald and Hoffmann, 1980). n_{rr} was calculated by counting the number of sign changed of the filtered operator input force (second-order Butterworth with 5 Hz cutoff).

$F_{i,m}$ Mean interaction force [N] between operator and master device.

Additionally, for the *slow* dynamic system, the mean tracking error (e_m) was evaluated for frequencies < 0.5 Hz and frequencies ≥ 0.5 Hz. To do so, the data was anti-causally filtered (Abbink, 2006) according to: $X(f) = X(f_{<0.5}) + X(f_{\geq 0.5})$, where $X(f)$ is the Fast Fourier Transform of $x(t)$. Subscripts indicate frequency bands < 0.5 and ≥0.5 Hz, of which the boundaries are not absolute.

FREQUENCY DOMAIN ANALYSIS

A) Nonparametric Analysis A closed-loop identification method was adopted to estimate the Frequency-Response Functions (FRFs) from reference trajectory to control input ($\hat{H}_{wc}$) and from control input to slave position ($\hat{H}_{cx}$). As such, the recorded time data of each trial was transformed to the frequency domain using the Discrete Fourier Transform (DFT), according to $w(t) \Rightarrow W(f)$, $c(t) \Rightarrow C(f)$ and $x_s(t) \Rightarrow X(f)$. The DFTs were used to estimate cross- and

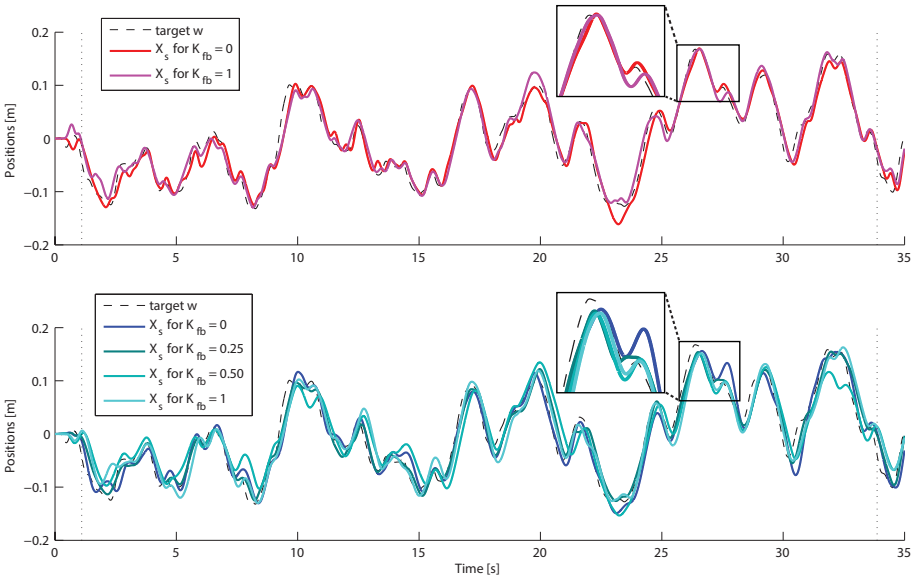

Figure 4.4: Typical example of time traces for each of the five experimental conditions. The red trajectories represent the *fast* dynamic system, whereas the *slow* dynamic system is represented in blue. It appears that in the *slow* dynamic condition operators lag the reference ω more than in the *fast* dynamic condition.

autospectral densities ($\hat{S}$), which were averaged over frequency bands and over repetitions to reduce variance due to noise. The FRFs were estimated of these spectral densities:

$$\hat{H}_{wc} = \frac{\hat{S}_{wc}}{\hat{S}_{ww}} \tag{4.3}$$

As a measure for the linearity between the signals the coherence (Γ) between input (w) and output (x_s) was estimated. A high coherence (i.e., close to 1) indicates linear behavior and justifies the use of quasi-linear operator models.

$$\Gamma_{wx} = \sqrt{\frac{|\hat{S}_{wx}(f)|^2}{\hat{S}_{ww}(f)\hat{S}_{xx}(f)}} \tag{4.4}$$

B) Model Structure The model used to quantify the operator control behavior is adapted from (van der El et al., 2016), which is an extension to of the quasi-linear operator model for compensatory tracking tasks by (McRuer and Rex, 1967). The model (van der El et al., 2016) incorporates an operator describing function ($H_{o,e}$), models for both a near ($H_{o,n}$) and a far ($H_{o,f}$) viewpoint response to a previewed reference trajectory, and an element modeling physical interaction of human operator and master device (H_{PI}). The near viewpoint response ($H_{o,n}$) is omitted, as its contribution to the operator control behavior is limited (van der El et al., 2017). Also, parameter estimations were performed up to the FRFs at 1.63 Hz (i.e., the highest

two FRF estimates at 2.55 and 4.01 Hz have been omitted). This is in line with (van der El et al., 2016), which only validated the model to describe human control behavior up to 1.84 Hz.

The operator describing function $H_{o,e}$ modulates an operators' response to a tracking error, just as in McRuer's crossover model (McRuer and Rex, 1967). The dynamics of the controlled system affect $H_{o,e}$. For the *slow* dynamics system, which appears to the human operator as a gain for the lowest frequencies and as a second order system at higher frequencies, $H_{o,e}$ is given by a lag system:

$$H_{o,e}(s) = K_e \frac{1}{T_{Ie}s+1} e^{-\tau_v s}, \tag{4.5}$$

with gain K_e, lag time constant T_{Ie} and effective time delay τ_v. The Laplace operator is given by s.

Far viewpoint response $H_{o,f}$ modulates an operators response to a future point on the reference trajectory, located τ_f seconds ahead. The future signals are weighted with gain K_f and low-pass filtered with lag time constant T_{If}, according to:

$$H_{o,f}(s) = K_f \frac{1}{T_{If}s+1} e^{\tau_f s} \tag{4.6}$$

The operator's intrinsic muscle visco-elasticity, limb mass and the interaction dynamics with the haptic master device are lumped in a physical interaction model H_{PI}. H_{PI} is parameterized using a second-order model:

$$H_{PI}(s) = \frac{\omega_{PI}^2}{s^2 + 2\zeta_{PI}\omega_{PI}s + \omega_{PI}^2} \tag{4.7}$$

As can be derived from Fig. 4.5, the transfer from visual reference trajectory w to control input c is given by:

$$H_{wc}(s) = \frac{H_{o,f}(s)H_{o,e}(s)H_{PI}(s)}{1 + H_{o,e}(s)H_{PI}(s)H_{cx}(s)}, \tag{4.8}$$

where H_{cx} is the (pre-defined) response from control input to slave output. H_{cx} thus equals the dynamics of the *slow* dynamic system as given by Eq. (4.1).

C) Parameter Estimation The operator control model (H_{wc}, Eq. (4.8)) was fitted to the FRFs of the data ($\hat{H}_{wc}$, Eq. (4.3)) in the frequency-domain, using a grid search methodology. Random initial conditions for the optimization procedure were generated within the parameter space spanned by 0-5 [-] for K_e, 0-2 s for T_{Ie}, 0-0.3 s for τ_v, 0.05-5 [-] for K_f, 0-0.5 s for T_{If}, 0.2-0.8 s for τ_f, 1-3 Hz for ω_{PI} and 0-0.4 [-] for ζ_{PI}, which is in agreement with previous work (van der El et al., 2017, 2016).

Parameter estimates were evaluated by minimizing a least-squares error criterion in the frequency domain for each of the initial condition sets (m):

$$\epsilon(m) = \sum_k f(k)(log\frac{H_{wc}(k)}{\hat{H}_{wc}(k)})^2, \tag{4.9}$$

in which $f(k)$ is the frequency vector. The best fit was selected according to $min(\epsilon(m))$.

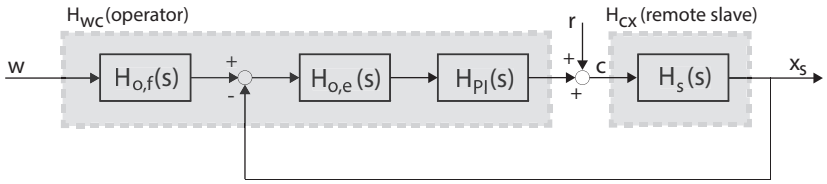

Figure 4.5: Closed-loop control diagram of the human operator (H_{wc}) controlling the remote slave system (H_{cx}), adapted from (van der El et al., 2016). The human operator is to minimize the error between slave position x_s and reference trajectory w, by controlling the master position c. $H_{o,f}$ is the transfer function of the far-viewpoint response (Eq. (4.6)), $H_{o,e}$ is the operator describing function (Eq. (4.5)), H_{PI} the physical interaction (Eq. (4.7)) and H_{cx} describes the transfer function of manipulator dynamics (Eq. (4.1)). Remnant signal r accounts for non-linearities of the human operator, and is a residual that is not modeled by the linear model.

4

D) Model Validation The variance accounted for (VAF) was calculated to obtain a validity index for the quantified parameters. A VAF of 100% indicates that the linear model fully describes the measurements. Noise, non-linearities and other unmodelled behavior reduce the VAF. Low coherence (noise or non-linearities) result in low VAFs. To calculate the VAF the model is simulated in time with the reference trajectory w as input and the simulated operator control input $\check{c}(t)$ as output for each time sample n:

$$VAF\big(c(n),\check{c}(n)\big) = \left(1 - \frac{\sum_n ||c(n)-\check{c}(n)||^2}{\sum_n ||c(n)||^2}\right) * 100\% \tag{4.10}$$

DATA ANALYSIS

Experimental conditions were compared using a repeated measures ANOVA, assuming normal distributions and variance homoscedasticity. A p-value of 0.05 or below was deemed significant ($\alpha = 0.05$). Results for the *fast* and *slow* dynamic system are presented independently.

4.3. RESULTS

4.3.1. TIME-DOMAIN RESULTS

Means (μ) and standard deviations (σ) for the time domain metrics e_{mean}, n_{rr} and $F_{i,m}$ for each of the experimental conditions are shown in table 4.1.

For the mean tracking error (e_{mean}) of a *fast* dynamic system there is no difference when providing haptic feedback compared to not having haptic feedback (K_{fb}=1 versus K_{fb}=0; p=0.82, F=0.05), as shown by figure 4.6(a). The mean tracking error for the *slow* dynamic system is affected by the force reflection gain (p=0.001, F=6.64): K_{fb}=0.25, K_{fb}=0.50 and K_{fb}=1 yield an approximately 8% lower mean error than K_{fb}=0 (p<0.035, F>5.67). The is no difference between the conditions with haptic feedback (p>0.25, F<1.92).

The number of reversals (n_{rr}, shown in figure 4.6(b)) for a *fast* dynamic system is about 9% lower when feedback is provided (p<0.001, F=28.5). Similarly, the force reflection gain affects the number of reversals (p<0.001, F=193) for the *slow* dynamic system. The post-hoc analysis

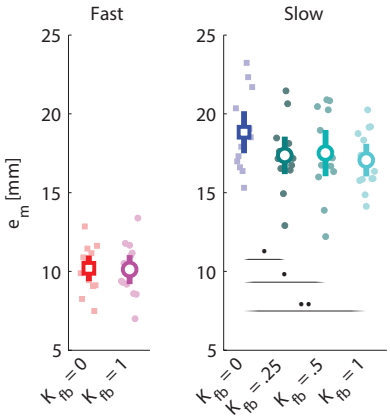

(a) Mean Tracking Error

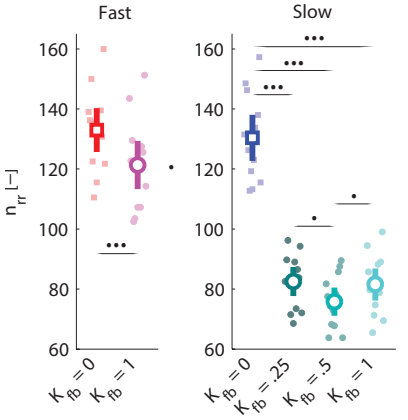

(b) Number of Reversals

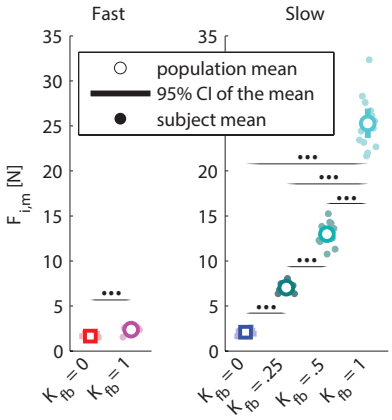

(c) Mean Interaction Force

Figure 4.6: Time domain metrics for (a) mean tracking error (e_m), (b) number of reversals (n_{rr}) and (c) mean operator interaction force ($F_{i,m}$) for each of the six experimental conditions. Open circles represent population means (n=13), with the error bars representing the 95% confidence interval of the mean. A subject mean is represented by a filled circle. Significance levels of p≤0.05, p≤0.01 and p≤0.001 are denoted by '•', '••' and '•••', respectively. Any force feedback (K_{fb}=0.25, K_{fb}=0.5 or K_{fb}=1) for the *slow* dynamic conditions improves the mean tracking error and number of reversals, at the cost of an increased operator input force.

Table 4.1: Mean (μ) and standard deviation (σ) of the metrics mean tracking error (e_{mean}), number of reversals (n_{rr}) and mean operator interaction force ($F_{i,m}$), for each of the experimental condition. The metrics are calculated from a population of 13 subjects each with 4 repetitions per condition.

		μ (σ) **for** $K_{fb}=0$	μ (σ) **for** $K_{fb}=0.25$	μ (σ) **for** $K_{fb}=0.5$	μ (σ) **for** $K_{fb}=1$
Fast	e_m [-]	10.19 (1.49)	-	-	10.11 (1.69)
	n_{rr} [s]	133 (13)	-	-	121 (15)
	$F_{I,m}$ [s]	1.65 (0.21)	-	-	2.38 (32)
Slow	e_m [-]	18.83 (2.46)	17.36 (2.19)	17.51 (2.70)	17.06 (1.90)
	n_{rr} [s]	130 (14)	83 (9)	76 (9)	82 (10)
	$F_{I,m}$ [s]	2.09 (0.31)	7.04 (0.50)	13.0 (1.2)	25.3 (3.0)

4

shows that compared to not having haptic feedback (K_{fb}=0), any feedback substantially reduces the number of reversals (p<0.001, F>264) by about 40%. Between the conditions with feedback, K_{fb}=0.5 yields a lower number of reversals than K_{fb}=0.25 and K_{fb}=1 (p<0.022, F>6.98).

Haptic feedback increases the mean operator interaction force ($F_{i,m}$, figure 4.6(c)) for both the *fast* (p<0.001, F=86) and the *slow* dynamic system (p<0.001, F=675). For the *slow* dynamic system, the mean interaction force proportionally increases as the force reflection gain increases (p<0.001, F>419); K_{fb}=0.5 yields almost double the interaction forces as K_{fb}=0.25. Similarly, K_{fb}=1 almost doubles the forces compared to K_{fb}=0.5.

Anti-causal filtering of the signals shows that for perturbations below 0.5 Hz, there are no differences in the mean tracking error (e_m) between haptic feedback conditions for both the *fast* and *slow* dynamic system (p=0.34, F=0.97 and p=0.25, F=1.41 respectively).

Also above 0.5 Hz, there is no difference between K_{fb}=0 and K_{fb}=1 for the *fast* dynamic system (p=0.66, F=0.21). For the *slow* dynamic system however, haptic feedback affects the mean tracking error (p=0.012, F=4.20); compared to K_{fb}=0, haptic feedback reduces the error for K_{fb}=0.25, K_{fb}=0.5 and K_{fb}=1 (p<0.030, F>6.1) by about 9-13%. Between conditions with feedback, there is no difference (p>0.20, F<1.9).

4.3.2. FREQUENCY-DOMAIN RESULTS

The identified operators' FRFs are taken from reference trajectory w to operator control input c. Figure 4.8 shows these FRFs for the *slow* dynamic system, averaged over all operators. Squares indicate the estimated magnitude and phase for the condition without feedback ($K_{fb}=0$). Similarly, circles denote the estimated magnitude and phase for conditions with feedback (K_{fb}=0.25, K_{fb}=0.5 and K_{fb}=1). The errorbars (in black) represent the 95% confidence interval of the population mean. For the condition without feedback ($K_{fb}=0$), the phase for the highest two frequencies in the reference trajectory at approx. 1.0 and 1.6 Hz is 22 and 5 degrees, respectively, whereas for the conditions with feedback the phase for these two frequency points is about 30 and 25 degrees, respectively.

Coherences of the FRFs were calculated of the power spectral densities, based on averages over two adjacent frequencies. Coherence is >0.9 for the lowest seven frequency points and

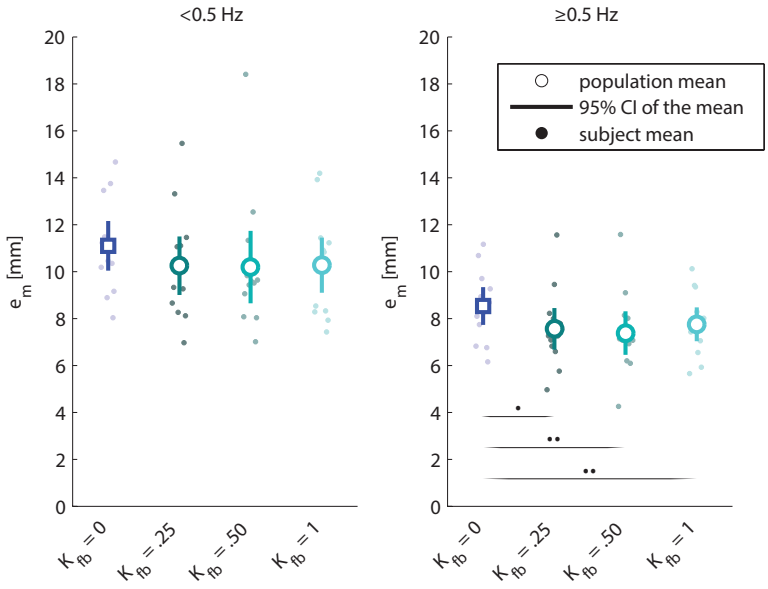

Figure 4.7: Mean tracking error (e_m) calculated for anti-causal filtered signals <0.5 Hz and ≥0.5 Hz, for the *slow* dynamic system. For perturbations below 0.5 Hz, there are no differences between haptic feedback conditions (p=0.25, F=1.41). Above or equal to 0.5 Hz, feedback decreases the tracking error (p<0.030, F>6.1), while haptic feedback conditions K_{fb}=0.25, K_{fb}=0.5 and K_{fb}=1 do not differ from each other (p>0.20, F<1.9).

>0.8 for the highest frequency (see figure 4.12), indicating linear operator control behavior.

The parameters of the operator's control model were fitted to the identified response functions per subject. Parameters estimations for the population of 13 subjects are shown in table 4.2 and displayed in figure 4.9

For the parameters of the operator error response model $H_{o,e}$, no differences are found for K_e and T_{Ie} (p=0.79, F=0.34 and p=0.42, F=0.95, respectively). τ_v is affected by haptic feedback (p<0.001, F=7.71). A post-hoc analysis reveals that compared to K_{fb}=0, τ_v decreases from 0.087 to 0.032, 0.026 and 0.029 for K_{fb}=0.25 (p=0.008, F=7.7), K_{fb}=0.5 (p=0.008, F=9.9), and K_{fb}=1 (p=0.014, F=8.3), respectively. Between conditions with feedback, there is no difference (p>0.39, F<0.77).

For the far-viewpoint response $H_{o,f}$, no differences are found for K_f and T_{If} (p=0.41, F=0.98 and p=0.81, F=0.32, respectively). The mean of τ_f is reduced from 0.527 s for K_{fb} = 0 to 0.461, 0.473 and 0.475 s for K_{fb} = 0.25 (p=0.008, F=10.11), K_{fb} = 0.5 (p=0.005, F=11.5) and K_{fb} = 1 (p=0.047, F=4.9), respectively. Again, between conditions with haptic feedback no differences are found (p>0.31, F<1.2).

The neuromuscular model $H_{o,PI}$, the mean of ω_{PI} increases by approx. 8% from 1.59 to 1.70-1.74 Hz when feedback is provided (p<0.028, F>6.24). ζ_{PI} shows no differences between conditions (p=0.18, F=1.7).

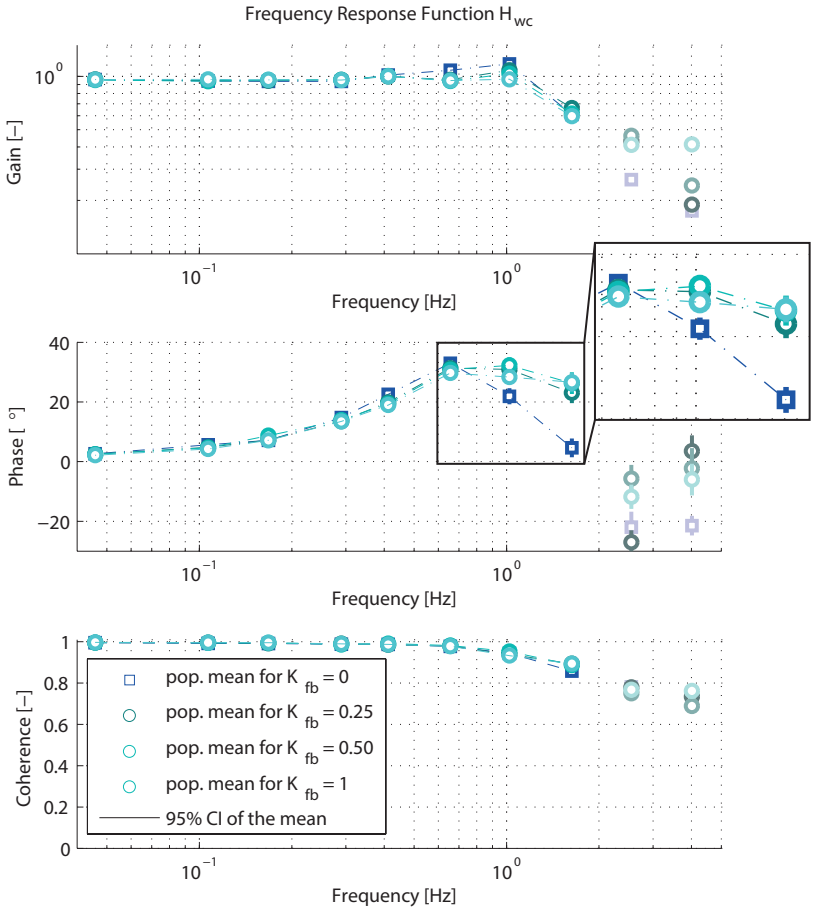

Figure 4.8: Population means of the identified operators' FRFs (H_{wc}). For $K_{fb} = 0$, the phase for the responses at approx. 1.0 and 1.6 Hz is 22 and 5 degrees, respectively. For the conditions with feedback the phase for these two frequency points is about 30 and 25 degrees, respectively. The operator model is fit on the first eight FRFs up to 2 Hz, such that the fitted frequency spectrum is in line with (van der El et al., 2016).

Table 4.2: Mean (μ) and standard deviation (σ) of the parameter estimations of the operator control model (n=13).

	μ (σ) for $K_{fb} = 0$	μ (σ) for $K_{fb} = 0.25$	μ (σ) for $K_{fb} = 0.5$	μ (σ) for $K_{fb} = 1$
K_e [-]	1.696 (1.342)	1.662 (1.259)	1.603 (0.945)	1.969 (1.126)
T_{Ie} [s]	0.604 (0.438)	0.604 (0.431)	0.594 (0.371)	0.787 (0.455)
τ_v [s]	0.087 (0.066)	0.032 (0.019)	0.026 (0.025)	0.029 (0.023)
K_f [-]	2.22 (1.05)	2.05 (0.82)	2.09 (1.04)	1.70 (0.57)
T_{If} [s]	0.240 (0.052)	0.220 (0.083)	0.235 (0.034)	0.220 (0.094)
τ_f [s]	0.527 (0.074)	0.461 (0.061)	0.473 (0.037)	0.475 (0.057)
ω_{PI} [Hz]	1.59 (0.11)	1.74 (0.19)	1.70 (0.09)	1.70 (0.14)
ζ_{PI} [-]	0.105 (0.051)	0.160 (0.087)	0.159 (0.081)	0.137 (0.050)

Figure 4.10 shows the mean VAFs per subject per condition. VAFs are calculated per repetition, hence each bar graph is an average of four repetitions. Over all repetitions the mean VAF is 95%, with a standard deviation of 1.9%, whereas the minimum VAF for a single repetition is 85%. Such high VAFs indicate that the model accurately describes operator control behavior in both conditions with and without haptic feedback.

The frequency response of the parameterized models of two typical subjects, subject 1 and 9 are shown in figure 4.11a and figure 4.11b, respectively. Figure 4.12 shows the measured (dashed line) and modeled (solid line) operator control input of a single repetition of two conditions for subject 1. The high similarity between measured and modeled control input illustrate the VAFs of typically >90%.

4.4. DISCUSSION

Haptic feedback of reflected dynamics in free-space pursuit tasks only marginally affects task execution for *fast* dynamic systems: performance measured in terms of tracking accuracy is unaffected, while the effects on control effort are limited (~9% reduction for the number of reversals, and a ~0.8 N increase in operator input force). Supposedly, for fast dynamic systems in which the operator's limb dynamics dominate overall system behavior, additional haptic feedback of system dynamics is superfluous.

For *slow* dynamic systems on the other hand, full haptic feedback substantially improves task execution compared to no haptic feedback; the mean tracking error and number of reversals decrease (by ~10% and ~39%, respectively), while the operator's input force increases proportionally with force feedback gain. Interestingly, the same improvements for tracking error and number of reversals occurred for scaled force feedback (i.e., $K_{fb} = 0.25$ and $K_{fb} = 0.5$) as for full haptic feedback, with a substantial reduction of operator input forces. In other words, any of the tested scaled haptic feedback yields the full benefit of unscaled haptic feedback, but with a beneficial decrease in physical control effort. Apparently, feedback of the dynamics of the relatively slow slave device allows operators to adjust their behavior accordingly, such that the closed-loop human-machine characteristics better match the task requirements.

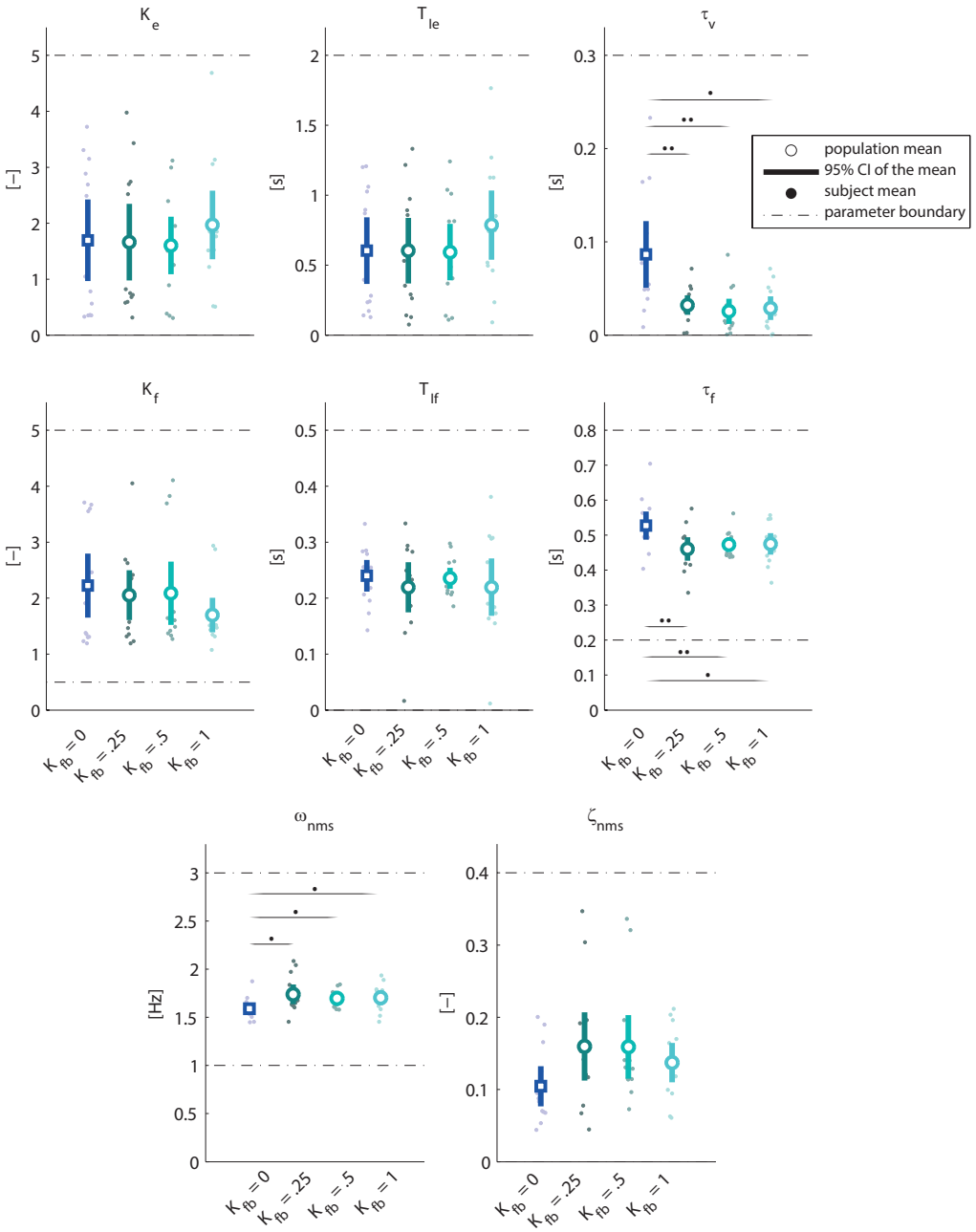

Figure 4.9: Estimated parameters of the operator control model, for for each of the six experimental conditions. Open circles represent population means (n=13), with the error bars representing the 95% confidence interval of the mean. A subject mean is represented by a filled circle. Any force feedback (K_{fb}=0.25, K_{fb}=0.5 and K_{fb}=1) reduces the operator's effective time delay τ_v, whereas scaled force feedback (K_{fb}=0.25 and K_{fb}=0.5) reduces look-a-head time τ_f.

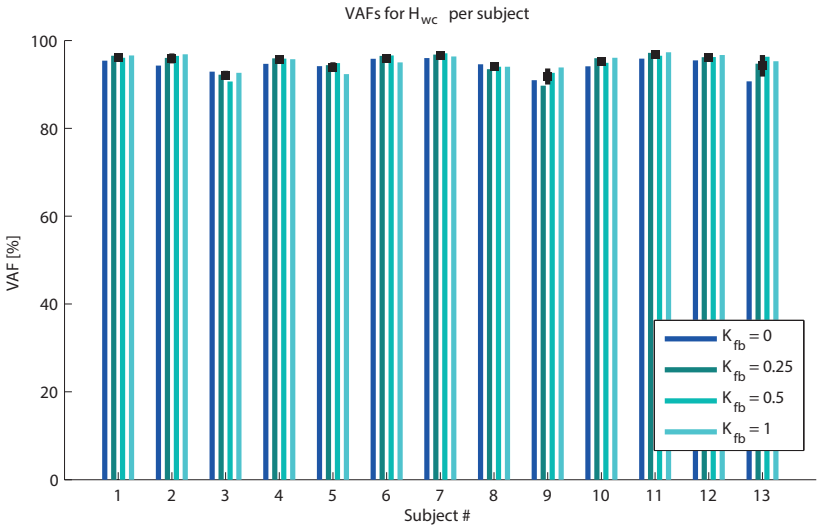

Figure 4.10: Mean VAFs per subject per condition. Each bar graph represents an average of four repetitions. The minimum VAF for a single repetition is 85%. The mean VAF over all repetitions is 95%, with a standard deviation of 1.9%. Such high VAFs indicate that the model accurately describes the data in the time domain.

To attain accurate tracking behavior, the operator needs to equalize the *slow* dynamics of the remote slave. These dynamics appear to the human operator as a gain up to the cutoff frequency (~1.5 Hz), and as a critically damped second-order system above this frequency. Thus, the slow dynamic system introduces lag into the human-machine system (approximately 45 degrees at 1 Hz). In previous work (Wildenbeest et al., 2014) we have shown that haptic feedback improves matching of operator control activity to the frequencies of the reference trajectory, especially at higher frequencies (>1 Hz). Putatively, the observed control activity at higher frequencies generates lead to compensate for the lag introduced by the slow dynamic system. Indeed, Frequency-Response Functions (FRFs) of the operators control actions (H_{wc}, see figure 4.8) show that any of the tested feedback levels enables operators to generate an increased phase lead, compared to no feedback. This suggests a correlation between increasing phase lead and decreasing tracking error, when haptic feedback is available. By quantifying underlying operator control equalizations, the cybernetic model enables identification of the causal relation between its parameters and the phase lead.

The parameters of the operator's control model were fitted to the identified FRFs on a per subject basis. The model consists of an operator describing function that modulates the response to a tracking error $H_{o,e}(K_e, T_{Ie}, \tau_v)$, a response to a far viewpoint $H_{o,f}(K_f, T_{If}, \tau_f)$ and a model for the passive physical interaction of human and master device $H_{o,PI}(\omega_{PI}, \zeta_{PI})$. Haptic feedback was observed to affect each of these three transfer functions, specifically the parameters representing the operator's effective time delay τ_v, future viewpoint τ_f and natural frequency ω_{PI}.

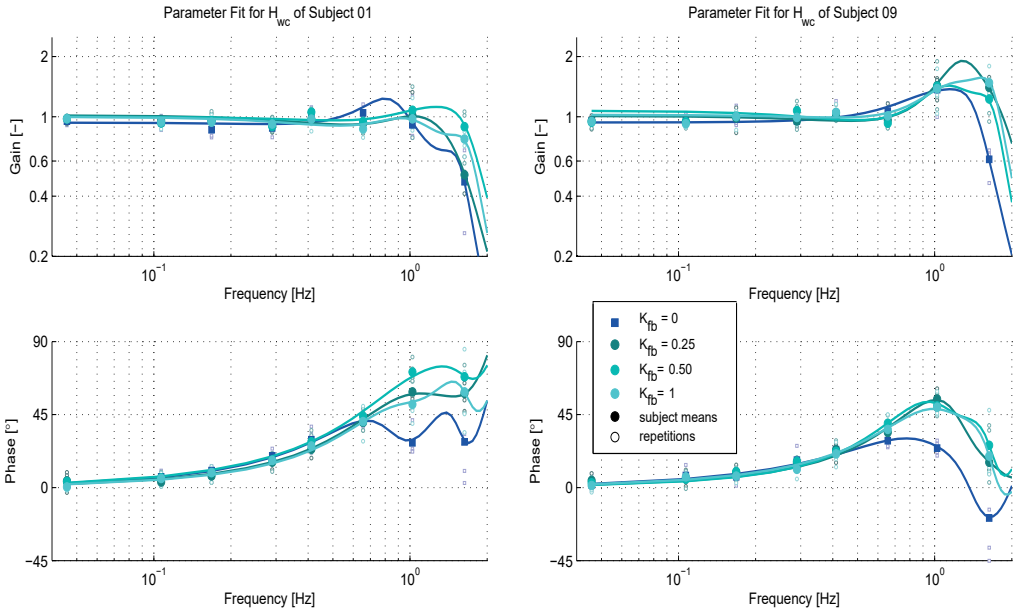

(a) Model fits for subject 1

(b) Model fits for subject 9

Figure 4.11: Model fits for subject 1 and 9. Circles and squares represent the identified FRFs, which are an average of four repetitions. The lines represent the fitted models. Both subjects show a higher phase lead at high frequencies for conditions with feedback, compared to conditions without. Such phase lead corresponds to decreases in τ_v.

For $H_{o,PI}$, damping factor ζ_{PI} is not affected by haptic feedback and the values of 0.06-0.35 [-] are in line with previous work (e.g. 0.1-0.3 [-] for Drop et al. (2013), and 0.18-0.67 [-] for van der El et al. (2016)). Similarly, with natural frequencies ω_{PI} of 1.4-2.1 Hz, the cutoff frequency of $H_{o,PI}$ is in line with typical values for the open-loop filtering behavior of the neuromuscular system, which is often lumped as a second-order filter with a cutoff frequency around 2 Hz (Damveld et al., 2009; Pick and Cole, 2008). Haptic feedback does affect the natural frequency: it increases with about 8% for conditions with feedback compared to no haptic feedback. These changes can be attributed to changes in the neuromuscular system, whose settings and contribution cannot be identified in this study, but would require mechanical disturbances and EMG measurements (e.g. Damveld et al. (2009)).

The lag systems $H_{o,f}$ and $H_{o,e}$ both incorporate an equalization term which can be interpreted as filters on the inputs of the operator's open-loop ($H_{o,f}H_{o,e}$) and feedback error ($H_{o,e}$) response. Interestingly, neither of these filters is affected by haptic feedback gain K_{fb}. This suggests that operators do not change the bandwidth over which they attempt to control the slave system depending on feedback conditions. The absolute values of the gains (K_f and K_e) and time constants (T_{If} and T_{Ie}) are difficult to interpret and compare to previous work as they are heavily affected by, among others, the chosen controlled dynamics, reference trajectory and visualization. Firstly, K_f >1 which means that operators emphasize feedforward over

feedback control. This was also found for the gain dynamics in van der El et al. (2016). Also, T_{If} is comparable to the values found in van der El et al. (2016). Furthermore, from a stability perspective, gain and control bandwidth (given by filter cutoff frequency $1/T_I$) have an inverse relation: when the gain increases, the cutoff frequency should decrease.

The data shows that the open-loop gain $K_f K_e$ is indeed generally two times larger than the feedback gain K_e, while the corresponding cutoff frequency is lower (~0.22 Hz versus ~0.27 Hz for open-loop response $H_{o,f}H_{o,e}$ and feedback error response $H_{o,e}$, respectively). In the minority of cases where this does not hold, subjects apparently prioritize performance and sacrifice stability.

Besides an equalization term, $H_{o,f}$ and $H_{o,e}$ incorporate a future viewpoint, located τ_f s ahead and an effective time delay τ_v, respectively. The mean value of 0.087 s for τ_v for the conditions without feedback ($K_{fb} = 0$), is slightly below the typical value of this parameter, which ranges between 0.1-0.2 s for zero order compensatory or pursuit tasks (e.g. McRuer and Rex (1967); van der El et al. (2016)). 0.1 s is considered a lower boundary for the human's central nervous system to react, by first processing visual information and subsequently acting through our neuromuscular system. However, the two seconds of trajectory preview are likely to cause operators to anticipate as opposed to react, leading to time delays below 0.1 s. Operators respond to an error ahead in time, instead of a momentaneous error. Indeed, one cannot compensate for momentaneous errors due to inherent physical limitations. In contrast, such anticipation could not have appeared in previous studies on pursuit tasks, as these studies make use of an (additional) unpredictable perturbation signal to identify the feedback loop (Drop et al., 2013; van der El et al., 2016).

Interestingly, haptic feedback decreases the effective time delay τ_v even further, namely by about a factor 3 to ~0.026-0.032 s, compared to no haptic feedback. Haptic feedback allows operators to not solely control towards a visual reference, but to also apply (haptic) feedback control towards the remote slave. By exploiting their neuromuscular viscoelastic and reflexive capabilities, operators can compensate for errors in the dynamic estimates of the controlled system (i.e., internal models (Ito, 2005; Passot and Arleo, 2010)). Such neuromuscular response is much faster than visual or vestibular cues responses. This means that the inclusion of haptic feedback may directly reduce the time to respond to an error, thus reducing effective time delay τ_v by 0.06 s on average and max. 0.03-0.21 s for a single subject, for conditions with feedback compared to no feedback.

Operators use preview to generate phase lead to compensate for their own and slave system time delays (van der El et al., 2017), by positioning their future viewpoint τ_f s ahead on the previewed target. Therefore, when their own response delays (i.e., τ_v) decrease due to, for example, haptic feedback, operators will use less preview. Indeed, both τ_v and τ_f decreases for all haptic feedback conditions, compared to no haptic feedback. This relation is characterized by the difference between future viewpoint and effective time delay (i.e., τ_f-τ_v), which is constant and resides between 0.42-0.45 s for all conditions.

In summary, the cybernetic model indicates that the observed control benefit of haptic feedback (in terms of reduced tracking error and increased phase lead), is caused by reductions

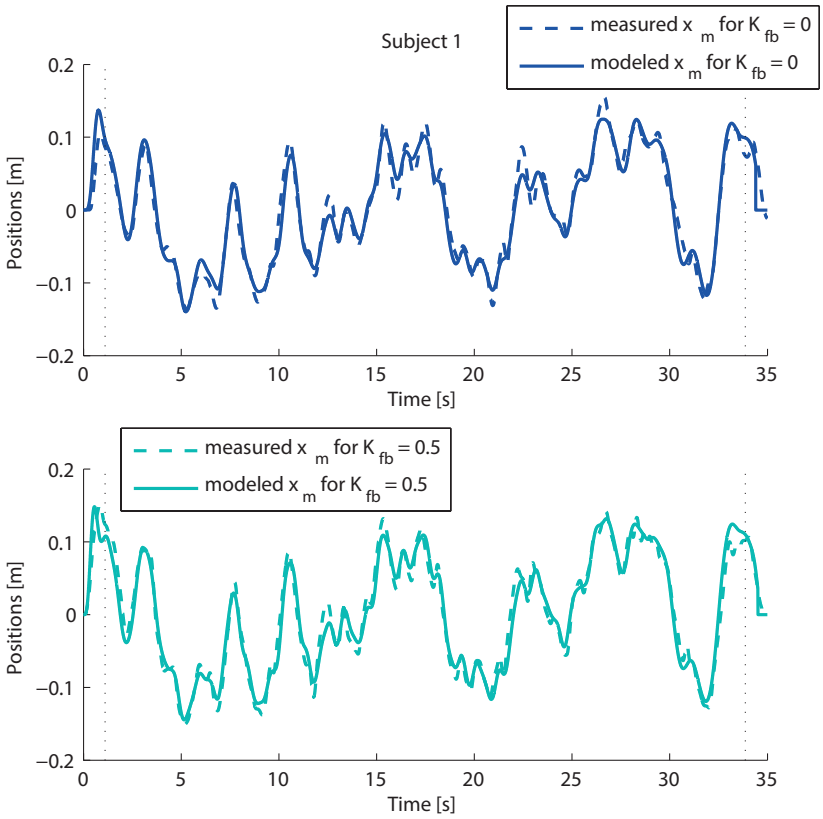

Figure 4.12: Measured (dashed line) and modeled (solid line) operator control input of a single repetition of two conditions for subject 1. Their high similarity illustrate the VAFs of typically >90%.

in effective time delay τ_v and a preview τ_f. Changes in these parameters suggest that haptic feedback allows operators to exploit their fast neuromuscular system to compensate for internal model errors which cannot be compensated with their relatively slow visual feedback only.

The estimated model accurately represented the data (i.e., high VAF of typically >90%). Also, coherences of >0.8 indicate that the use of quasi-linear computational models was not substantially complicated during the experiment by large amounts of noise, non-linearities or time variance (i.e., small remnant r). The repeatability and reproducibility was high for most parameters, with standard deviations of typically 10-20% of the mean (see table 4.2). Gain K_e and time constant T_{Ie}, and to a lesser extent K_f and T_{If}, show an increased variability as gains and time constants mutually affect each others sensitivity: for low gains, the time constant loses sensitivity and vice versa, for high time constants, the gain loses sensitivity.

Although the cybernetic model does not explicitly account for haptic feedback, the model allows to study the meta or high-level control adaptations caused by haptic feedback. Haptic

feedback is an implicit yet inherent part of the transfer function from a visual input to a physical control output, as described by the model. The present model can be supplemented or extended with neuromuscular control models (e.g. van der Helm et al. (2002)), if it is desired to expose underlying low-level neuromuscular control control adaptations. Also, the adaptation with respect to the model of van der El et al. (2016), to omit one of the two future viewpoints as inputs to the operator, seems justified. The single-input model is well capable of describing the FRFs for each subject for all conditions, with sufficient sensitivity in the frequency as well as the time domain.

Specifically, the cybernetic model showed sensitivity to describe free-space tasks (e.g. tool movement, pick-and-place, visual inspection and metrology tasks) with slave systems that have substantial dynamics (e.g. cranes and robot arms with and without loads) in for example maintenance activities in nuclear (e.g. Boessenkool et al. (2014)) or sub-sea (e.g. Kuiper et al. (2013)) environments. The model can describe and predict human control behavior for such tasks, but also for tasks that involve control of vehicles such as cars (e.g. curve negotiation) or aircraft (e.g. pitch and roll angle control (McRuer and Rex, 1967)); the abstract task - preview tracking of a reference trajectory - is a conceptual representation of a broad variety of control tasks.

Moreover, the cybernetic model can be used as a basis to formalize augmented haptic support design, by serving as the underlying control structure to generate guidance forces in, for example, haptic shared control (Abbink et al., 2011; O'Malley et al., 2006). While shared control can substantially improve task execution as shown in the automotive domain (e.g. lane changing (Abbink and Mulder, 2010; Pick and Cole, 2008)), and in teleoperation (e.g. obstacle avoidance (Alaimo et al., 2011; Janabi-Sharifi and Hassanzadeh, 2011), path guidance (Boessenkool et al., 2014)), its benefits decrease due to conflicts between individual human operators and intelligent system (de Jonge et al., 2016). The cybernetic model can be used to individualize support trajectories, reducing discomfort and increasing performance.

Hence, in order to fully benefit from the prediction capabilities of (cybernetic) models, and to allow for a priori design of haptic interfaces and haptic support systems, it is required to further develop these computational models for tasks where contact with the environment is made and multiple degrees of freedom, and to verify its applicability in other application domains.

4.5. CONCLUSION

A human factors study was conducted during which subjects used a 1 DoF haptic master device to control a slave system (with either *fast* or *slow* dynamics) in a pursuit task with preview. Subjects received four different levels of haptic feedback from the slave dynamics: full haptic feedback, no haptic feedback and scaled haptic feedback (25% or 50%). For the experimental conditions studied it can be concluded that:

- When controlling *fast* dynamic systems, task execution is only marginally affected by

manipulating haptic feedback levels; haptic feedback has no effect on task performance, but improves control effort.

- For *slow* dynamic systems, full haptic feedback substantially improves task execution (in terms of mean tracking error, number of reversals) compared to no haptic feedback, but at the cost of substantially increased operating forces at the master device.
- Interestingly, scaled haptic feedback (25% or 50%) yields identical performance benefits as full haptic feedback, but with a beneficial decrease in physical control effort.

In order to understand underlying operator control behavior for the slow slave, frequency-response functions were estimated on which a linear cybernetic control model incorporating both feedforward and feedback was fit. The estimated model accurately captured individual operator control behavior in both time and frequency domain (i.e., high VAF), and yielded repeatable and reproducible results. This analysis led to the following conclusions:

- Any of the tested haptic feedback levels enable operators to generate more phase lead compared to no feedback, allowing improved compensation for the lag of the *slow* slave system.
- Haptic feedback enables operators to substantially reduce their effective time delay and, consequently, the amount of preview used, compared to no haptic feedback.

This indicates that the availability of haptic feedback allows operators to adapt their feedback and feedforward responses, such that slow slave systems can be controlled more accurately in free-space, with a higher bandwidth. The parameterized cybernetic model can be used to describe and predict human-in-the-loop telemanipulated control of slave systems (e.g., cranes, robot arms), as well as form a basis to formalize augmented haptic support design, such as haptic shared control or haptic guidance.

REFERENCES

(2012). The role of haptic feedback when manipulating nonrigid objects. *Journal of neurophysiology*, 107(1):433–41.

Abbink, D. A. (2006). *Neuromuscular Analysis of Haptic Gas Pedal Feedback during Car Following*. PhD thesis, Department of Biomechanical Engineering, Delft University of Technology, Delft, The Netherlands.

Abbink, D. A. et al. (2011). Measuring neuromuscular control dynamics during car following with continuous haptic feedback. *IEEE Transactions on Systems, Man, and Cybernetics - Part B: Cybernetics*, 41.

Abbink, D. A. and Mulder, M. (2010). Motivation for a neuromuscular basis for haptic shared control. In *Symposion on Analysis, Design and Evalution of Human-Machine Systems*, volume 33.

Alaimo, S., Pollini, L., Bresciani, J., and Bülthoff, H. (2011). Evaluation of direct and indirect haptic aiding in an obstacle avoidance task for tele-operated systems. In *Proceedings of the 18th IFAC World Congress*, volume 33, page 6472–6477.

Boessenkool, H., Thomas, J., Heemskerk, C., de Baar, M., Steinbuch, M., and Abbink, D. (2014). Task analysis of human-in-the-loop tele-operated maintenance: What can be learned from jet? *Fusion Engineering and Design*, 89(9-10):2283–2288.

Bolopion, A. and Regnier, S. (2013). A review of haptic feedback teleoperation systems for micromanipulation and microassembly. *IEEE Transactions on Automation Science and Engineering*, 10(3).

Damveld, H., Abbink, D., Mulder, M., Mulder, M., van Paassen, M., van der Helm, F., and Hosman, R. (2009). Measuring the contribution of the neuromuscular system during a pitch control task. In *Proceedings of the AIAA Modeling and Simulation Technologies Conference*.

De Gersem, G., van Brussel, H., and Tendick, F. (2005). Reliable and enhanced stiffness perception in soft-tissue telemanipulation. *The International Journal of Robotics Research*, 25(10).

de Jonge, A. W., Wildenbeest, J. G. W., Boessenkool, H., and Abbink, D. A. (2016). The effect of trial-by-trial adaptation on conflicts in haptic shared control for free-air teleoperation tasks. *IEEE Transactions on Haptics*, 9(1):111–120.

Draper, J. V. et al. (1986). Effects of force reflection on servomanipulator task performance. In *Proceedings of the International Topical Meeting on Remote Systems and Robots in Hostile Environments*.

Drop, F. M., Pool, D. M., Damveld, H. J., van Paassen, M. M., and Mulder, M. (2013). Identification of the feedforward component in manual control with predictable target signals. *IEEE Transactions on Cybernetics*, 43(6):1936–1949.

Dudragne, J. et al. (1989). A generalized bilateral control applied to master slave manipulators. In *Proceedings of the 20th ISIR*.

Hannaford, B., Wood, L., McAffee, D. A., and Zak, H. (1991). Performance evaluation of a six-axis generalized force-reflecting teleoperator. *IEEE Transactions on Systems, Man and Cybernetics*, 21(3).

Hanneton, S., Berthoz, A., Droulez, J., and Slotine, J. (1997). Does the brain use sliding variables for the control of movements? *Biological Cybernetics*, 77.

Huang, F., Gillespie, R., and Kuo, A. (2004). Haptic feedback improves manual excitation of a sprung mass. In *12th International Symposium on Haptic Interfaces for Virtual Environment and Teleoperator Systems*.

Ito, M. (2005). Bases and implications of learning in the cerebellum–adaptive control and internal model mechanism. *Progress in brain research*, 148:95–109.

Janabi-Sharifi, F. and Hassanzadeh, I. (2011). Experimental Analysis of Mobile-Robot Teleoperation via Shared Impedance Control. *IEEE Transactions on Systems, Man and Cybernetics-Part B: Systems and Humans*, 41(2):591–606.

Kim, W. S., Tendick, F., Ellis, S. R., and Stark, L. W. (1987). A comparison of position and rate control for telemanipulations with consideration of manipulator system dynamics. *IEEE Journal on Robotics and Automation*, 3(5).

Krendel, E. S. and McRuer, D. T. (1960). A servomechanisms approach to skill development. *Journal of the Franklin Institute*, 269(1):24—-42.

Kuiper, R. J., Frumau, J. C. L., van der Helm, F. C. T., and Abbink, D. A. (2013). Haptic support for bi-manual control of a suspended grab for deep-sea excavation. In *IEEE International Conference on Systems, Man, and Cybernetics, Manchester*.

Lawrence, D. A. (1993). Stability and transparency in bilateral teleoperation. *Proceedings of the 31st Conference on Position and Control*.

Linde, R. v. d., Lammertse, P., Frederiksen, E., and B (2002). The hapticmaster, a new high-performance haptic interface. In *Proceedings of EuroHaptics*.

MacDonald, W. A. and Hoffmann, E. R. (1980). Review of relationship between steering wheel reversal rate and driving task demand. *Human Factors*, 22.

Massimino, M. J. and Sheridan, T. B. (1994). Teleoperator performance with varying force and visual feedback. *Human Factors: The Journal of the Human Factors and Ergonomics Society*, 36(145).

McRuer, D. T. and Rex, H. R. (1967). A review of quasi-linear pilot models. *IEEE Transactions on Human Factors in Electronics*, 8(3).

O'Malley, M. K., Gupta, A., Gen, M., and Li, Y. (2006). Shared Control in Haptic Systems for Performance Enhancement and Training. *Journal of Dynamic Systems, Measurement, and Control*, 128(1):75.

Passot, J.-b. and Arleo, A. (2010). A new coupling scheme of cerebellar internal models: Online and offline adaptation in procedural tasks. In *From Animals to Animats 11*, pages pp 435–446.

Pick, A. J. and Cole, D. J. (2008). A mathematical model of driver steering control including neuromuscular dynamics. *Journal of Dynamic Systems, Measurement, and Control*, 130(3).

Shadmehr, R. and Mussa-ivaldi, F. A. (1994). Adaptive representation of dynamics during learning of a motor task. *The Journal of Neuroscience*, 14(5).

Uzawa, J., Pekny, S., Marko, M., Haswell, C., Shadmehr, R., and Mostofsky, S. (2012). Motor learning relies on integrated sensory inputs on adhd, but over-selectively on proprioception in autism spectrum conditions. *Autism Research*, 5(2):124–136.

van der El, K., Pool, D. M., , van Paassen, M. R. M., and Mulder, M. (2017). Effects of preview on human control behavior in tracking tasks with various controlled elements. *IEEE Transactions on Cybernetics*, online preprint.

van der El, K., Pool, D. M., Damveld, H. J., van Paassen, M. R. M., and Mulder, M. (2016). An empirical human controller model for preview tracking tasks. *IEEE Transactions on Cybernetics*, (11):2609–2621.

van der Helm, F. C., Schouten, A. C., de Vlugt, E., and Brouwn, G. (2002). Identification of intrinsic and reflexive components of human arm dynamics during postural control. *Journal of Neuroscience Methods*, 119(1):1–14.

Vitense, H. (2003). Multimodal feedback: An assessment of performance and mental workload. *Ergonomics*, 46:68–87.

Wasicko, R. J., McRuer, D. T., and Magdaleno, R. E. (1966). Human pilot dynamic response in single-loop systems with compensatory and pursuit displays. Technical report, Air Force Flight Dynamics Laboratory, Wright-Patterson Air Force Base, OH, USA.

Wildenbeest, J., Kuiper, R., van der Helm, F., and Abbink, D. (2014). Position control for slow dynamic systems: Haptic feedback makes system constraints tangible. In *2014 IEEE International Conference on Systems, Man, and Cybernetics October 5-8, 2014, San Diego, CA, USA*, pages 3990–3995.

Wildenbeest, J. G. W., Abbink, D. A., Heemskerk, C. J. M., van der Helm, F. C. T., and Boessenkool, H. (2013a). The impact of haptic feedback quality on the performance of teleoperated assembly tasks. *IEEE Transactions on Haptics*, 6(2).

Wildenbeest, J. G. W., Abbink, D. A., and Schorsch, J. F. (2013b). Haptic transparency increases the generalizability of motor learning during telemanipulation. In *World Haptics Conference (WHC), 2013*.

Yokokohji, Y. and Yoshikawa, T. (1994). Bilateral control of mater-slave manipulators for ideal kinesthetic coupling-formulation and experiment. *IEEE Transactions on Robotics and Automation: a Publication of the IEEE Robotics and Automation Society*, 10(5):605–620.

5

Design of Natural Force Feedback for Rate Control

Roel J. Kuiper & Jeroen G.W. Wildenbeest, Frans C.T. van der Helm and David A. Abbink

to be submitted to IEEE Transactions on Haptics, 2019

Rate control is a common control method for sub-sea machinery. But because the joystick input position is not directly matching the output position, the measured interaction force of the controlled system with its environment cannot be directly reflected to the human operator. This chapter compares two approaches for offering natural feedback in rate control, a force-based feedback and stiffness feedback method. Force-based feedback reflects the derivative of measured interaction forces to the operator, where stiffness feedback maps this measured force as an added virtual stiffness on the input device. The effectiveness of both methods is compared to a baseline static virtual stiffness, not containing environmental feedback.

The design of both approaches for offering natural feedback, force-based and stiffness feedback is given in section 5.2, as well as the baseline static stiffness design. In section 5.3 are the experimental methods given of a human factors experiment for comparing both methods when conducting abstract tasks. Three fundamental abstract task types are used in this experiment, covering most remote controlled subtasks: free-space, contact transition and force level tasks. The experimental results for comparing both feedback methods for task performance and control effort are given in section 5.4. It is concluded that offering stiffness feedback is most beneficial over all three subtasks combined.

R.J. Kuiper & J.G.W. Wildenbeest, F.C.T. van der Helm and D.A. Abbink; Exploring Haptic Feedback Designs for Rate Controlled Systems; to be submitted to IEEE Transactions on Haptics in 2019

ABSTRACT

In rate control, the position of the operators input device commands a desired velocity for the controlled machine. This type of control is the industry standard for operators controlling heavy machines over large workspaces. The operator usually only has visual feedback and feels no haptic feedback concerning the machine dynamics, or its interaction forces with the environment. Where haptic information potentially makes task execution more intuitive and easier to control, especially with complex machine dynamics. This study explores four design options for providing an operator with haptic feedback on the input device, 1) a basic spring stiffness to convey manipulator position, 2) the basic spring with an additional deadband force around zero, 3) an approach from literature to feedback the derivative of the machine's measured interaction forces, and 4) a novel method to feedback the interaction forces by manipulating the stiffness of the input device. Subjects (n=12) used a haptic manipulator to control a virtual slow dynamic system with rate control, performing three generic subtasks: goal-directed movements, minimizing impact force during contact transitions, and controlling the level of slave force when in contact with a visco-elastic environment. The results show improvements for offering an advanced static spring to the basic spring during goal-directed movements, but equal results for reflecting environment feedback compared to the advanced spring. For reflecting environment forces as additional stiffness, improvements were found when conducting force level tasks. We conclude that the novel stiffness feedback provides operators most advantages in task performance and control effort over the entire range of task types.

5.1. INTRODUCTION

TELEOPERATION of large heavy machines such as excavators or cranes, is often performed using rate control; where the position of the operators input device (e.g. joystick) commands the desired velocity remote machine (hereafter called slave) (Sepehri et al., 1994; Sheridan, 1989; Sheridan et al., 1978). Rate control allows the slave's movement to be commanded over a large (theoretically infinite) workspace, as opposed to the position control encountered in bilateral telemanipulation (Elton et al., 2013; Kim et al., 1987). Typically, in rate controlled large heavy machines, visual feedback of task-related information is available on screens. The control device is typically passive, with a static centring stiffness (Lawrence et al., 1997; Sepehri et al., 1994). Therefore the operator feels no feedback on the control device concerning the machine dynamics, or its interaction forces with the environment (e.g. soil or attached loads). Such important information can then only be perceived by ambient cues (sounds and vibrations).

This paper focuses on feedback of the interaction forces during rate control, with the aim to contribute to improvements in task execution for rate controlled large heavy machines (Ostoja-Starzewski and Skibniewski, 1989). Previous work on force feedback in position controlled slow dynamic systems has shown understanding and predicting the dynamic behaviour. This has led to improvements in task execution and control effort for slow dynamic systems during free space tasks (Wildenbeest et al., 2014). The goal of this paper is to experimentally evaluate different haptic feedback designs to facilitate operators during rate control of heavy slaves. Literature describes two methods to translate interaction forces between slave and environment

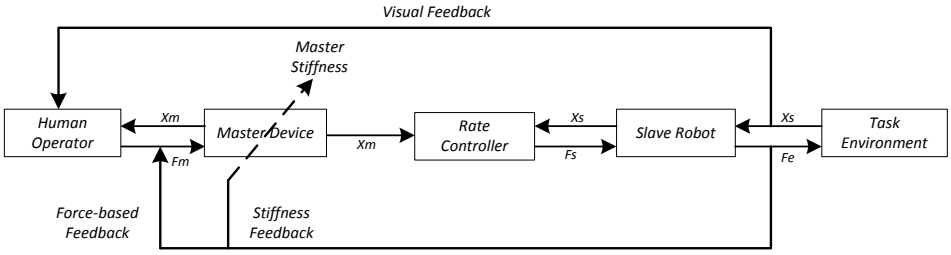

Figure 5.1: Schematic representation of a human controlling a rate controlled remote machine with two methods of haptic feedback visualized, adapted from Salcudean [9]. Note that the rate controller block is modified to be able to separately visualize the environment interaction force Fe directly. Fe is either directly fed back as a force (or its derivative) on the master device or as an adapting factor of the master stiffness.

to a master device held by the operator: force-based feedback and stiffness-based feedback (Lawrence et al., 1997; Parker et al., 1993; Salcudean et al., 1998, 2000). Both types of feedback methods are illustrated in figure 5.1.

Two main information channels (position error and interaction forces) can be reflected with haptics when the four-channel structure in position control is used (based on the work of Yokokohji and Yoshikawa (1994) and Hannaford (1989)). The same approach is used for rate control by Salcudean et al. (Salcudean et al., 2000; Zhu and Salcudean, 1995) by reflecting the velocity error and the measured environment forces to the human operator. The velocity error informs the operator about the dynamics of the controlled machine, by reflecting the difference on the acquired velocity to the commanded velocity. This informs the state of the vehicle of (de)accelerations. Reflecting the dynamic information seems most informative when operating slow dynamic vehicles in free-space tasks (Wildenbeest et al., 2014). Reflecting the measured environment forces informs the operator of the interaction of the vehicle with the environment.

The theoretical design of haptic feedback during rate control has been extensively investigated by Salcudean et al. (Lawrence et al., 1997; Parker et al., 1993; Salcudean et al., 1998, 2000; Zhu and Salcudean, 1995). One of the things they suggested is that the derivative of the measured force should be reflected instead of the force itself. Reflecting forces in a rate controlled task shows promising results for velocity and force tracking in theory (Salcudean et al., 2000; Zhu and Salcudean, 1995). This concept solves the potential problems of direct force feedback that lead to possible instabilities because the feedback drives the input device out of its neutral point of zero input. The practical applicability of reflecting these derivative forces has been questioned, because it results in no longer a natural feel of the occurring contact forces (Lawrence et al., 1997; Parker et al., 1993).

Another way of overcoming this problem was suggested by Parker et al. (1993). He proposed stiffness feedback to indicate a clear neutral point and maintain stability also for zero inputs. Similar effects for stiffness feedback compared to direct force feedback has been researched for car driving applications by Abbink and Mulder (2009), to maintain stability for a haptic guidance systems using shared control (Mulder et al., 2012). Stiffness feedback remains the

general centring stiffness around the central neutral point clearly informed to the human operator, therefore stability is easily maintained as well. Mobasser and Hashtrudi-Zaad (2008) investigated the stability when reflecting forces in rate control and compared this for various methods. They found for moderate time delay problems that reflecting an estimated environment impedance as a form of stiffness feedback to improve transparency while remaining robust stability. However to maintain stability under time delay, Park et al. (2011) used velocity error to reflect forces to the operator. They found also when colliding with objects that robust stability was guaranteed with variable time-delays by means of an energy-bounding algorithm. Combining velocity error feedback with environment forces incorporated as stiffness feedback seems promising to overcome instability by maintaining the general centring stiffness.

Besides the importance of the method of reflecting haptic information to the operator, another important question is what information type (e.g. velocity error and/or measured environment forces) is relevant to the operator? To study this question, a useful classification for tele-operated task execution is the division in three main task types: free-space, contact transition and force level tasks, based on Wildenbeest et al. (2013). Rate con-trolled operations are most often conducted in free-space tasks and typically controls large heavy machines with a slow dynamic system response. Therefore, controlling these machines might benefit most from a reflected velocity, informing its dynamic response. However, when making contact in a contact transition task, informing the environment interaction forces might indicate the impact more clearly. And controlling a specific force level onto the environment during a force level task could also benefit from information about the environment forces.

The objective of this study is to understand the extent to which different feedback paradigms affect task execution in rate control. It seems most beneficial for stability and satisfactory to remain a clear neutral point of zero input (Parker et al., 1993). Therefore, it is hypothesized that offering stiffness feedback is most useful of either the velocity error or environment forces. It is also hypothesized that when offering only haptic feedback of the state of the input device (i.e. static spring), a clear neutral point of zero input has to be noticeable when using rate control.

In this study, a human factors experiment is conducted to evaluate the different feedback designs. In section 5.2 the four designs are described: two static springs, force-based feedback and stiffness feedback. The methods are described in section 5.3 and the results for each task type are described separately in section 5.4. The discussion and conclusion can be found in section 5.5 and 5.6 respectively.

5.2. HAPTIC FEEDBACK DESIGN

Usually, during rate control the only forces an operator feels on the control interface are due to the passive dynamics (mainly a static spring). No task-related feedback of the controlled machine is given, such as its achieved velocity or encountered environment force. This section details four different approaches to design haptic feedback on the control interface; two static spring designs, force-based and stiffness feedback. This section also includes the tuning of each approach for subsequent human-in-the-loop experiments as described in section 5.3.

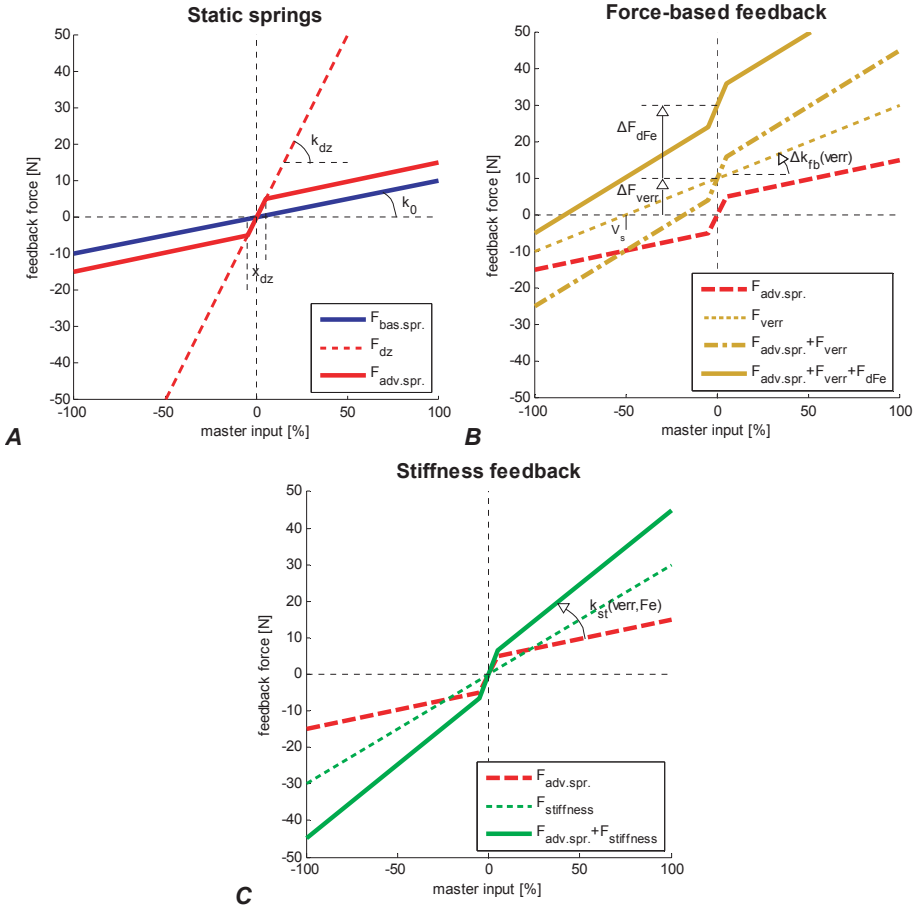

Figure 5.2: The static relation between master force Fm and master input x_m for the four haptic feedback design methods (the thick solid lines) and relevant design components (dotted and dashed lines). A) Two static spring designs with a basic spring ($F_{bas.spr.}$) and advanced spring with clear zero indication ($F_{adv.spr.}$). B) Force feedback designs based on literature, including the baseline spring ($F_{adv.spr}$), with added velocity error ($F_{adv.spr.} + F_{verr}$) and derivative of environment ($F_{adv.spr.} + F_{verr} + F_{dFe}$). C) Stiffness feedback design including the baseline spring ($F_{adv.spr.}$), with added stiffness ($F_{adv.spr.} + F_{stiffness}$).

5.2.1. TWO STATIC SPRING DESIGNS

In rate control the input device position corresponds to a commanded slave velocity. Hence, it is helpful to have a centring stiffness to help indicate the difference between a zero-velocity command, accelerating or decelerating. A basic static spring can increase the knowledge of the commanded velocity, due to the absolute position information from the spring force (Mugge et al., 2009). Implementation of such spring force is common in rate control because of its simplicity and not requiring any additional sensory feedback.

In figure 5.2 A the blue thick solid line indicates the most basic spring, as typically implemented in academic research (e.g. Lawrence et al. (1997); Mobasser and Hashtrudi-Zaad (2008); Parker et al. (1993); Salcudean et al. (2000)). The basic spring merely consists of a stiffness gain k_{spr} on the input position xm, as given in Eq. (5.1). In the block diagram as shown in figure 5.3, this static spring is depicted with H_{spr} which effectively creates the impedance of the master dynamics H_{master}. The stiffness gain k_{spr} is tuned to 40 N/m to result in approximately 8 N of force at maximal input, therefore enabling to augment other forces (as clearly seen in figure 5.10 at item II). The damping gain b_{spr} is set to 6 Ns/m, to achieve a closed loop damping ratio of 0.3.

$$F_{bas,spr} = k_{spr} \cdot x_m + b_{spr} \cdot \dot{x}_m \tag{5.1}$$

Industry practice typically incorporates an out-of-zero switch in the joystick mechanism, to ensure zero input at a certain deadband (e.g. Gessmann GmbH industrial joystick mechanism Schulein and Ehrensperger (2012)). This also gives a much better indication of the zero position at an overall low spring stiffness. This nonlinear spring characteristic was implemented by overlaying a much higher stiffness within a small deadband, as given in Eq. (5.2). The deadband position x_{db} of 4 mm, 1% of maximal stroke, contained a stiffness k_{db} tuned to 1500 N/m to result in 3 N of constant force outside the deadband.

$$\begin{aligned} F_{adv,spr} &= k_{spr} \cdot max(|x_m| - x_{db}, 0) \cdot sign(x_m) + k_{db} \cdot min(|x_m|, x_{db}) + b_{spr} \cdot \dot{x}_m \\ b_{adv,spr} &= \begin{cases} b_{db}, & |x_m| < x_{db} \\ b_{spr}, & |x_m| \geq x_{db} \end{cases} \end{aligned} \tag{5.2}$$

This advanced spring gives a clear zero velocity indication inside the deadband for a complete stop of the slave velocity. In figure 5.2 A the red thick line indicates the advanced spring with deadband force indication. The thin red dashed line indicates the increases stiffness k_{db} which is limited to the deadband position x_{db}. The damping $b_{adv.spr.}$ is kept equal to the basic spring for outside of the deadband and within set to 37 Ns/m to maintain an equal damping ratio of 0.3.

5.2.2. FORCE-BASED FEEDBACK DESIGN

Information of the state of the slave can also be reflected to the operator. These states include the velocity error (between commanded and realized slave velocity), and the measured interaction force between slave and environment (e.g., mud, rock and tools).

The velocity error v_{err} is defined as the difference in the commanded velocity (based on the master position xm) and the realized system velocity v_s Eq.(5.3). Because the slave operates at a larger workspace then the master device is capable of, a scaling factor G_{scale} of 0.2 is implemented. The block diagram in figure 5.3 shows that the velocity error not only can be reflected to the operator, but also is used to control the slave $H_{control}$. Therefore the scaling factor G_{scale} also determines the commanded desired slave velocity based on the master position x_m in figure 5.3.

$$v_{err} = v_s - \frac{x_m}{G_{scale}} \tag{5.3}$$

The feedback force of the velocity error is comparable to the controlled slave force F_C as shown in figure 5.3, therefore includes the controller gains K_P and K_D, based on (Salcudean et al., 2000). This force is reduced with a force feedback gain $G_{fb,verr}$ of 0.1 to keep the forces tangible to the operator, as shown in Eq.(5.4). This velocity error feedback force is shown in figure 5.2 B as the thin brown dashed line, which essentially creates a spring stiffness around the acquired velocity v_s of the slave.

$$F_{err} = G_{fb,v_{err}} \cdot \left(K_P \cdot v_{err} + K_D \cdot \frac{\partial v_{err}}{\partial t} \right) \tag{5.4}$$

The measured contact environment force F_{env} is fed back to the operator as a derivative in time, for a transparent four channel system (Salcudean et al., 2000). This is implemented with gain $G_{fb,\dot{F}e}$ of 0.05 on top of the scaling gain G_{scale}, as shown in Eq.(5.5), for which the environment force F_{env} is filtered with a 50 Hz lowpass second order Butterworth filter.

$$F_{dFe} = G_{fb,\dot{F}e} \cdot \left(F_{env} \cdot \frac{\partial v_{err}}{\partial t} \right) \tag{5.5}$$

The total force feedback based on literature using the complete four channel approach is a combination of the static spring $F_{adv,spr.}$ of Eq.(5.2), the velocity error $F_{v_{err}}$. and the environment force $F_{\dot{F}e}$ as shown in Eq.(5.6). The summation of feedback for these two different information channels is also depicted in figure 5.3 with the two parallel blocks for force-based feedback.

$$F_{force,lit} = F_{adv.spr.} + F_{v_{err}} + F_{\dot{F}e} \tag{5.6}$$

The thick brown dash-dotted line in figure 5.2 B shows that when adding the velocity error force $F_{v_{err}}$ to the static spring force $F_{adv.spr.}$, the neutral point shifts from the acquired velocity v_s of the slave towards zero. The addition of the environment force derivative may cause substantial oscillations in the neutral point after impact due to the nature of this signal. This results in loss of a clear zero point of commanded slave velocity.

5.2.3. STIFFNESS FEEDBACK DESIGN

The fourth haptic feedback design is based on the work of Parker et al. (1993), whom also applied stiffness feedback instead of force-based feedback to maintain stability in hard environments.

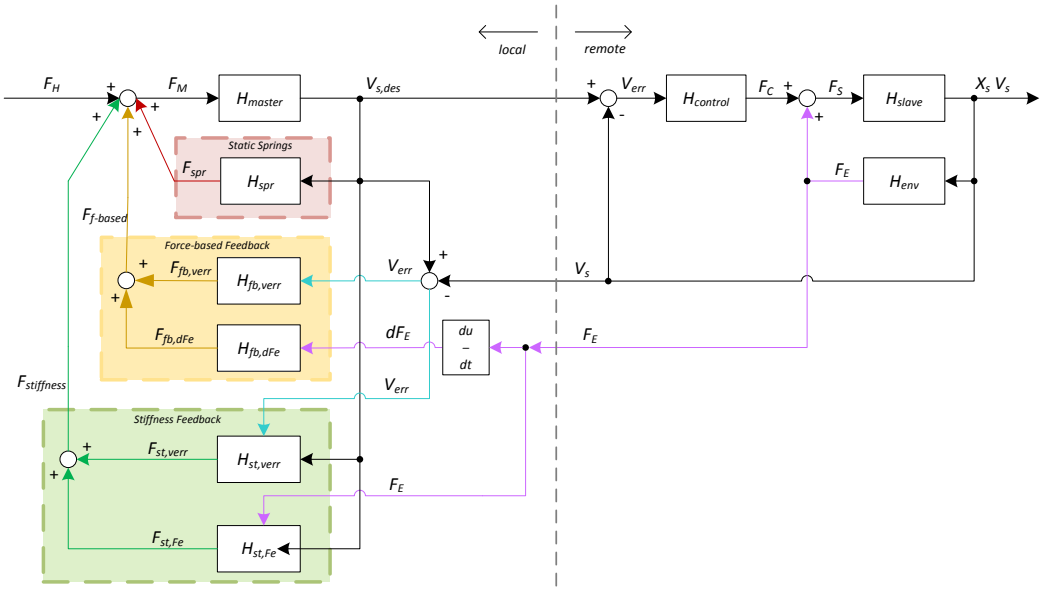

Figure 5.3: Block diagram demonstrating the three haptic feedback design types, static springs (red), force-based feedback (yellow) and stiffness feedback (green). The block diagram consists of a local master device from which a human force is converted into an input position, and scaled to a desired slave velocity. From this a closed loop controller actuates the remote slave device with a controller force, which again interacts with a remote environment. Both the achieved slave velocity and interaction forces are fed back to the lower two feedback designs types.

However in this study the additional stiffness gain is based on both the velocity error $k_{st,v_{err}}$ and the environment force $k_{st,Fe}$, as shown in Eq.(5.7).

$$F_{stiffness} = \left(k_{st,v_{err}}\{x_m, v_s\} + k_{st,Fe}\{F_{env}\}\right) \cdot x_m \tag{5.7}$$

The stiffness gain $k_{st,v_{err}}$ is a function of the absolute velocity error as stated in Eq.(5.8), with a gain $G_{st,v_{err}}$ of 0.2.

$$k_{st,v_{err}} = G_{st,v_{err}} \cdot \left| v_s - \frac{x_m}{G_{scale}} \right| \tag{5.8}$$

The stiffness gain $k_{st,Fe}$ is a function of the absolute measured scaled environment force with a gain $G_{st,Fe}$ of 0.7, as stated in Eq.(5.9).

$$k_{st,Fe} = G_{st,Fe} \cdot |F_{env} \cdot G_{scale}| \tag{5.9}$$

The stiffness force $F_{stiffness}$ of Eq.(5.7) is based on the input position x_m and is a linear stiffness around zero as shown with the thin green dashed line in figure 5.2 C. The total stiffness feedback design is a combination (shown in Eq.(5.10)) of both the static spring of Eq.(5.2) and the additional stiffness force of Eq.(5.7), shown in figure 5.2 C with the thick solid green line.

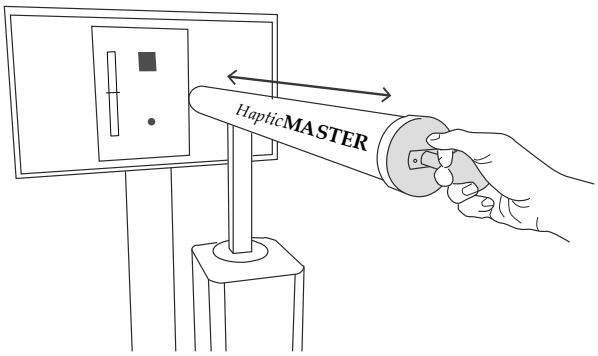

Figure 5.4: Human subject holding master input device *Haptic*MASTER of Moog Inc. while executing a single degree of task under rate control.

$$F_{stiffn,des} = F_{adv.spr.} + F_{stiffness} \tag{5.10}$$

The stiffness force of Eq.(5.7) consists of two parts (velocity error and environment force), depicted in the block diagram in figure 5.3 with the two parallel blocks for stiffness feedback. However the environment force $F_{st,Fe}$ only gives feedback when in contact with an environment. And when in contact the slave velocity would be near zero, thus the feedback would not inform clearly on the system dynamics. Therefore the feedback is designed to switch off the velocity error feedback when making contact, essentially switching between environment forces and velocity error feedback.

5.3. EXPERIMENTAL METHODS

5.3.1. SUBJECTS

Twelve subjects, 10 male and 2 female, with an average age of 27.8 years and 5.5 year standard deviation, volunteered for the experiment. None of the subjects had previous experience with teleoperation and were naive about the experiment. All subjects gave their written informed consent prior to the experiment. The setup and experiments were approved by the local ethics committee of the Delft University of Technology.

5.3.2. APPARATUS

The experiments were performed on the *Haptic*MASTER (FCS Moog Inc.) as shown in figure 5.4, on which the four feedback designs were implemented. The *Haptic*MASTER is 3 DoF, but was constrained to only allow movement along the forward/backward-axis of the device, which was aligned with the sagittal plane of the subject (fig. 5.4). The admittance-controlled *Haptic*MASTER has a position resolution of $12e^{-3}$mm, a stiffness of 10 kN/m, force sensitivity of 10 mN and frequency response of 25 Hz (Linde and Lammertse, 2003). The virtual inertia

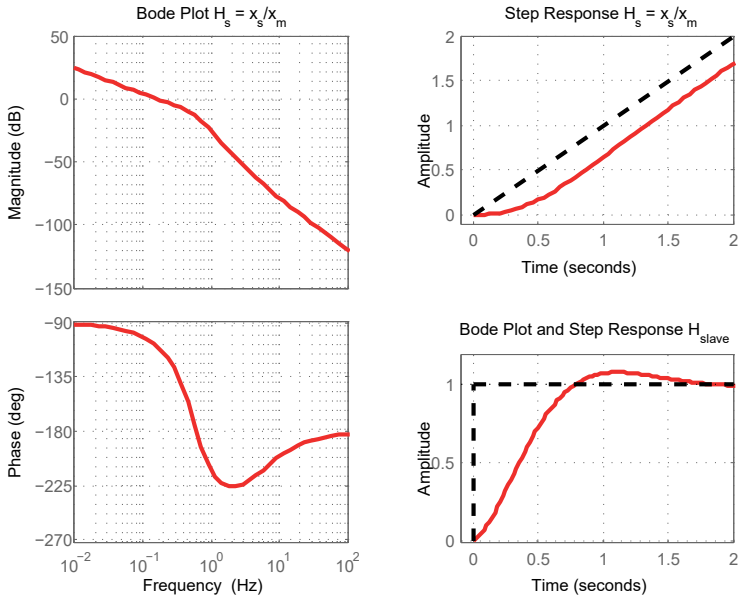

Figure 5.5: Bode plot and step response of the slave system (open-loop). The Bodeplot on the left is showing the cut-off frequency of approx. 0.57 Hz of a first order system with second order dynamics. This is also shown in the right for the step response shown for slave position and the derivative to a step input on the master position.

and damping of the master device were respectively set at J_m of 2.5 kg and B_m of 5 Ns/m. The manipulator was controlled with a VxWorks RT operating system running at 2048 Hz.

The slave system, designed in Matlab Simulink, was simulated on an additional real- time controller by Bachmann GmbH. The virtual slave was implemented according to Eq. (5.11), with an inertia J_s of 200 kg and global damping B_s of 800 Ns/m. A two port position error controller was tuned with a maximally achievable stable parameters of gains K_P of 2000 and K_D of 70, similarly to Wildenbeest et al. (2014). With a scaling factor G_{scale} of 0.2, the transfer function H_s of the rate controlled virtual slave in Eq.(5.11) has a cut-off frequency of approximately 0.57 Hz as indicated with 5.5 with frequency and time response plots. This system response is similar to large heavy machines such as excavators or cranes.

$$H_s = \frac{x_s}{x_m} = \frac{1}{G_{scale}} \cdot \frac{K_D \cdot s + K_P}{J_s \cdot s^3 + (K_D + B_s) \cdot s^2 + K_P \cdot s} \tag{5.11}$$

The simulated controller design of the virtual slave runs at 1000 Hz and logs position and force at equal frequency. The visualization on the display was updated at a rate of 25 Hz.

5.3.3. EXPERIMENT DESIGN

While controlling the virtual slave subjects were offered with each of the four feedback designs from section 5.2, static springs, force-based and stiffness feedback. These designs were tested

Table 5.1: Description of Experimental Conditions per Sub-Task

	Free Space Task	**Contact Transition Task**	**Force Level Task**
1. Bas. Spr.	Basic static spring	-	-
2. F-based	Advanced static spring with deadband indication	Advanced static spring with deadband indication	Advanced static spring with deadband indication
3. F-based	Advanced static spring with velocity error as force-based feedback	Adv. static spring with vel. error and derivative of environment force as force-based feedback	Adv. static spring with vel. error and derivative of environment force as force-based feedback
4. Stiffness	Advanced static spring with velocity error as stiffness feedback	Adv. static spring with vel. feedback in free-space and environment force when in contact as stiffness feedback	Adv. static spring with environment force as stiffness feedback

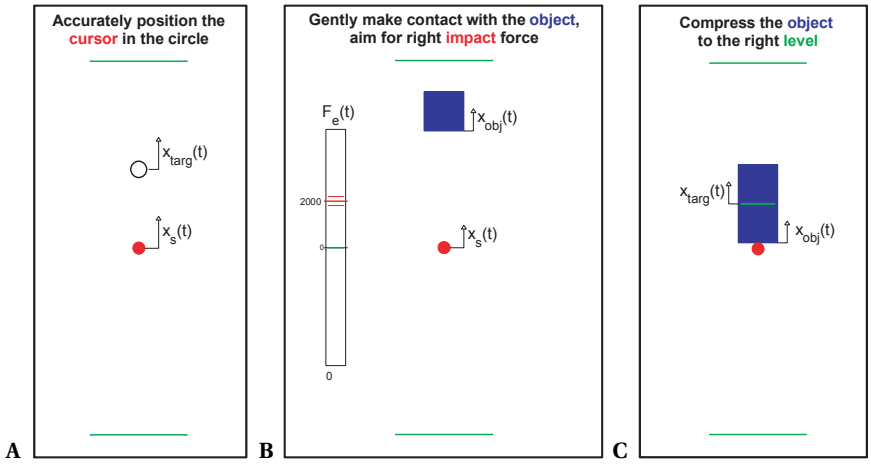

Figure 5.6: Visualizations of the three subtasks. A) Free-Space task, the red dot indicates the slave position and the black circle the target position. B) Contact Transition task, the blue block represents the object and the three small red lines in the rectangle on the left the required target impact force. C) Force Level task, the blue block represents the object that needs to be compressed up to the thin green line.

in three general task types, free-space, contact transition and force level. In figure 5.6 the visualization of each task type is given and in table 5.1 above are the corresponding condition explanations. The content of each experimental condition depends on the conducted task (e.g. in free-space there is no measured environment force).

The *Free-Space task* (FS) consisted of four experimental conditions: 1) baseline condition of a simple spring, 2) industry practice of an advanced spring with clear zero velocity indication, 3) velocity error as force-based feedback and 4) as stiffness feedback. The target to reach varied in free-space step size of 20% and 30% of screen size in both directions for unpredictability of task execution to the subjects. Only the small step size was used for analysing task execution to emphasize on the final positioning and reduce noise during the travelled distance, where the target size is 1.25% of the smaller step size.

The *Contact Transition task* (CT) consisted of three experimental conditions: 2) industry practice of an advanced spring, 3) velocity error as force-based feedback plus the derivative of the measured environment force, and 4) both velocity error and environment force as stiffness feedback. The margin to the objects to make contact with varied in free space distance of 19% and 28% of screen size in both directions. Only the largest margin was used for analysing task execution to emphasize on the achieved impact force. The object consisted of a stiff spring-damper properties of respectively 100 kN/m and 2 kNs/m, combined with the slave damping and inertia resulting in a second order system with a 3.6 Hz natural frequency and damping ratio of 0.32.

The *Force Level task* (FL) also consisted of three experimental conditions: 2) industry practice of an advanced spring with clear zero velocity indication, 3) velocity error as force-based feedback plus the derivative of the measured environment force and 4) environment force as a stiffness. The object had to be compressed to half its size as indicated with the green thin line (which consisted of 10% of the screen size). The stiffness of the blocks that had to be compressed varied accordingly to the target interaction force levels of 2750 N and 1833 N for equal compression distance. Only the largest force level was used for analysing task execution. For the feedback to the operator the interaction force was scaled using the designs as described in section 5.2, for an equivalent direct force feedback as example this scaling would be approximately 1% of this force to the operator.

During the experiment, each experimental condition was tested using eight repetitions of either of the three task types to be completed. These eight repetition consisted of two variations for each task types, applied in two directions. The order of the three or four experimental conditions and the order of the three subtasks were both counterbalanced using a Balanced Latin Square Design (BLSD) (Steel et al., 1986). Variations with each task type and direction were also counterbalanced using a BLSD.

5.3.4. PROCEDURE

Each subject was asked to stand in front of the input device, *Haptic*MASTER, and hold the black knob with one hand as depicted in figure 5.4. The display behind the input device showed either of the three subtasks as shown in figure 5.6, indicating the free-space, contact transition

or force level task. The subjects were asked to conduct the task as fast as possible and each prior task execution time was shown to the subject. For the free-space task subjects had to hold the operated red dot within the black target circle for one second until the next target appeared. The contact-transition task was instructed and trained to aim for the target impact force as indicated and was constant throughout the experiment. The force level task was instructed to compress the blue rectangular block with the red controlled dot up to the green indicated target line. When subjects completed each repetition of either of the subtasks a short beep was given auditory to indicate the completion of the repetition.

Prior to each experimental condition, the subjects were presented with a training sequence also consisting of eight repetitions of the subtask to be conducted. Also, prior to each subtask the subjects were presented with a familiarization task, which consisted of the baseline condition for that particular subtask (basic or advanced spring). The familiarization trial also consisted of the eight repetitions, but was repeated until consistent task execution of under 10 seconds was achieved.

5.3.5. MEASURED VARIABLES AND METRICS

Task performance is measured with *settling time* and *overshoot* for both the free-space (FS) and force level (FL) task. Settling time is the time elapsed from the start of the step input until the operator stayed within the target. Overshoot of the target is defined as the percentage of distance the target was exceeded outside of the boundaries. For the contact transition (CT) task the *time-to-contact* and *impact error* were used as performance metrics. The time it took before making contact is the time the operator had actively control over the task. After making contact the time of the task was defined by a fixed impact measurement time of 200 ms. The impact force is relevant for what the operator did during contact, which had a target interaction impact force of 1000 N and the error between what was maximally realized, is defined as impact error.

For all three subtasks *steering reversals* and *master force* are used as objective metrics for control effort. Steering reversals is defined as the amount of zero crossings of the operator force input, using a second order Butterworth filter with a 5 Hz cutoff frequency, a deadband threshold of 25 mN and a minimum of 250 mN between each reversal was required to filter out unintentional noise on the signal, similar to Boessenkool et al. (2013) and Kuiper et al. (2016). Physical effort was calculated as the mean of the amount of force applied to the input device.

For subjective measures the Van der Laan questionnaire was used to capture the *usefulness* and *satisfying* score of the feedback design for all three subtasks (van der Laan et al., 1997). The usefulness consisted of 5 components: useful, good, effective, assisting and raising alertness. The satisfying consisted of four components: pleasant, nice, likeable and desirable. Subjects rated the usefulness and satisfying components on a five point scale from -2 to +2. Usefulness and satisfying scores were calculated by averaging respective components.

5.3.6. DATA ANALYSIS

For each subject and form of support system, the metrics are computed per trial and averaged subsequently over the four repetitions. Per metric, the means are compared between the forms

of support using a repeated measures analysis of variance (RM-ANOVA). A Greenhouse-Geisser correction was applied when sphericity was violated. For significant main effects ($p<0.05$), post-hoc comparisons with Bonferroni correction for multiple comparisons was applied.

5.4. RESULTS

The results of all metrics as explained in section 5.3.5 are given for the task type free-space, contact transition and force level in tables 5.2, 5.3, 5.4 respectively. For clarity, the results presented in figures 5.7, 5.8, 5.9 only include the results of the two most relevant performance metrics, an objective effort metric and subjective metrics. The data tables include the detailed result and statistical results for each metric in each task type.

5.4.1. FREE-SPACE TASK

In the free-space task subjects had to perform the task as fast as possible. This resulted in a tradeoff for performance of speed and accuracy of reaching the target. In figure 5.7.A are therefore the results shown of the overshoot and settling time in a two dimensional graph, where overshoot is a metric of accuracy and settling time of the speed tradeoff. Results show a significant difference in settling time (p=.005, F=8.2) and post-hoc comparisons show a reduced settling time when offering an advanced static spring with clear zero velocity indication

Table 5.2: Results of Free Space Task

	T settling [s]	Overshoot [%]	Reversals [-]	F master [N]	Usefulness [-]	Satisfying [-]
1. Basic Spring [1]	7.86 (6.46, 9.25)	4.06 (1.76, 6.35)	15.75 (13.35, 18.15)	1.81 (1.62, 2.00)	-0.38 (-0.80, 0.04)	-0.63 (-1.25, 0.00)
2. Adv. Spring [1]	5.45 (5.05, 5.86)	2.87 (1.25, 4.48)	14.81 (13.61, 16.01)	4.26 (4.05, 4.46)	0.55 (0.10, 1.00)	1.06 (0.70, 1.43)
3. F-based Feedback [1]	6.13 (5.58, 6.67)	3.64 (2.40, 4.87)	21.48 (18.77, 24.19)	6.53 (5.96, 7.11)	0.35 (-0.04, 0.74)	0.13 (-0.29, 0.54)
4. Stiffness Feedback [1]	6.15 (5.75, 6.56)	1.88 (1.23, 2.53)	19.92 (17.50, 22.34)	6.17 (5.14, 7.20)	0.62 (0.35, 0.89)	0.29 (-0.15, 0.74)
Statistics [2]	p=.005 (F=8.2)	p=.191 (F=1.7)	p<.001 (F=9.4)	p<.001 (F=67)	p=.001 (F=7.5)	p<.001 (F=8.8)
Post-hoc [3]	1 to 2, p=.028	-	1 to 3, p=.014 2 to 3, p=.003 2 to 4, p=.017	all, p<.01 except 2 to 4, p=.024 3 to 4, p>.1	1 to 2, p=.039 1 to 4, p=.003	1 to 2, p=.005 2 to 3, p=.033

Main mean results of all evaluation metrics for performance, control effort and subjective measures, accompanied with their statistical results for free-space tasks.

[1] Group mean (95% Confidence Interval).

[2] Statistics are shown with a p and F value for a Repeated Measures ANOVA with Greenhouse-Geisser corrections when sphericity was violated.

[3] Post-hoc comparisons were applied using Bonferroni compensation.

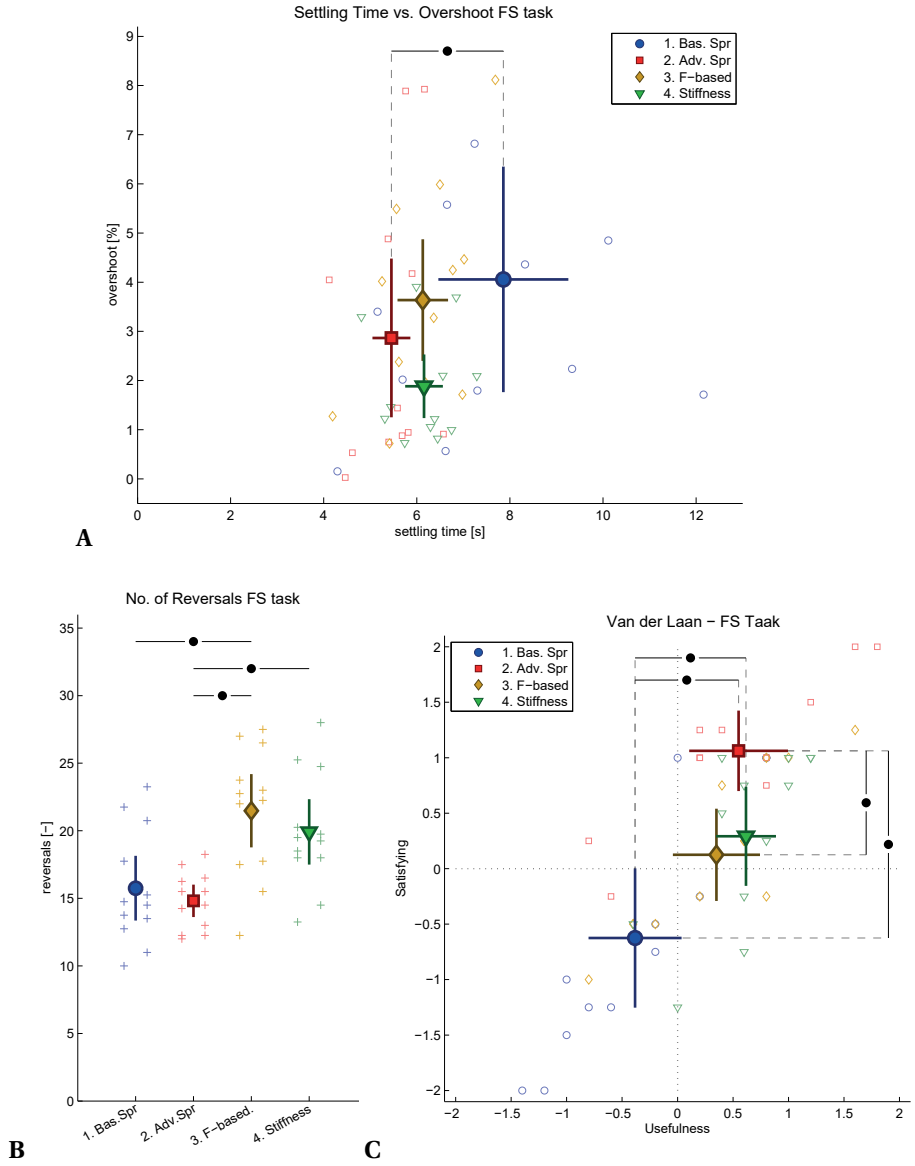

Figure 5.7: Results of **free-space task** for all four conditions applied. A) settling time (x-axis) versus overshoot (y-axis). B) number of steering reversals. C) subjective Van der Laan measure. All results are shown of the group mean (thick filled marker) and their 95% confidence interval (thick error bars), combined with individual subject means (thin markers). The horizontal bars indicate a significant difference over the factor environment or support, where "•" denote the significance level of p<0.05.

compared to a basic spring (31% mean reduction, p=.028). No difference in overshoot was found as also given in table 5.2.

Control effort obviously increased for physical effort by the measured master force when offering more feedback (p<.001, F=67). Interestingly, mental effort increased when operators received feedback of the state of the slave, as shown in 5.7.B with a difference in steering reversals (p<.001, F=9.4). This can be seen by the increased steering reversals when offering force-based feedback compared to the baseline static spring (36% mean increase, p=.014) or advanced spring (45% mean increase, p=.003). And this can also be seen with an increase for stiffness feedback to the basic spring (35% mean increase, p=.017).

Subjective measures show a clear increase in satisfying (p=.005) and usefulness (p=.039) of the advanced spring compared to the basic spring. Usefulness also increased when offering stiffness feedback compared to the basic spring (p=.003).

5.4.2. CONTACT TRANSITION TASK

In the contact transition task subjects had to make contact with the object with a given impact force as fast as possible. This gives a tradeoff in time to complete and accuracy of achieving the impact force. In 5.8.A this is shown for the time to contact and impact error results, in a two dimensional graph but with no statistical significant difference.

Control effort however reduces when offering force-based feedback compared to both the advanced static spring and stiffness feedback (mean reduction of 38% and 28% respectively, both p<.001) as can be seen in 5.8.B. Physical effort also increases when offering force-based or

Table 5.3: Results of Contact Transition Task

	T contact [s]	Impact err. [N]	Reversals [-]	F master [N]	Usefulness [-]	Satisfying [-]
2. Adv. [1] Spring	5.50 (5.10, 5.91)	142.8 (-53.7,339.3)	16.85 (14.8, 18.9)	6.20 (5.93, 6.47)	0.07 (-0.27, 0.41)	0.33 (-0.08, 0.74)
3. F-based [1] Feedback	5.41 (5.06, 5.77)	448.4 (233.2,663.6)	10.52 (9.4, 11.7)	8.88 (8.18, 9.57)	0.22 (-0.19, 0.63)	-1.25 (-1.53, -0.97)
4. Stiffness [1] Feedback	5.73 (5.41, 6.06)	288.0 (147.8,428.2)	14.67 (13.1, 16.3)	9.81 (8.63, 10.98)	0.67 (0.22, 1.11)	0.00 (-0.59, 0.59)
Statistics [2]	p=.210 (F=1.7)	p=.118 (F=2.7)	p<.001 (F=20)	p<.001 (F=29)	p=.091 (F=2.7)	p<.001 (F=16)
Post-hoc [3]	-	-	2 to 3, p<.001 3 to 4, p<.001	2 to 3, p<.001 2 to 4, p<.001	-	2 to 3, p<.001 3 to 4, p=.003

Main mean results of all evaluation metrics for performance, control effort and subjective measures, accompanied with their statistical results for free-space tasks.

[1] Group mean (95% Confidence Interval).

[2] Statistics are shown with a p and F value for a Repeated Measures ANOVA with Greenhouse-Geisser corrections when sphericity was violated.

[3] Post-hoc comparisons were applied using Bonferroni compensation.

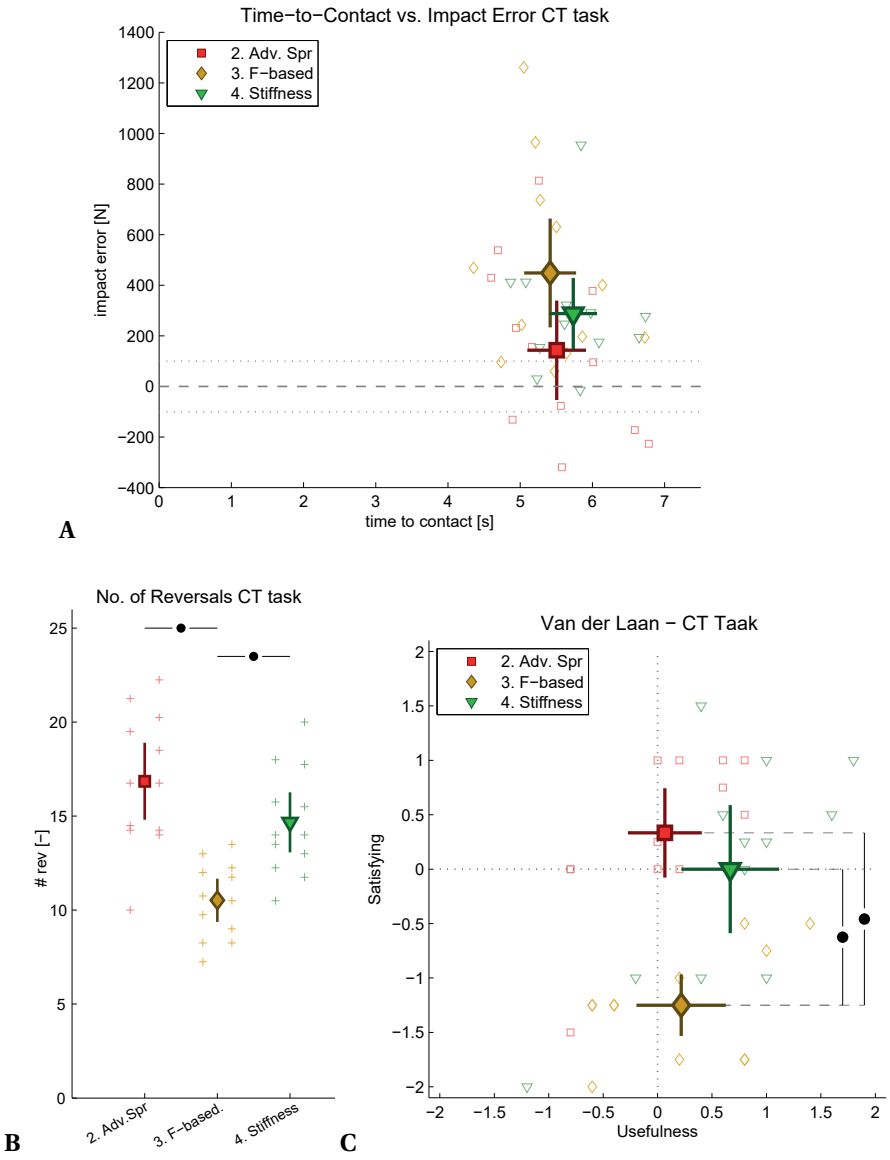

Figure 5.8: Results of **contact transition task** for all three conditions applied. A) time to contact (x-axis) versus impact error (y-axis), with the dashed lines representing the given impact force range indication. B) number of steering reversals. C) subjective Van der Laan measure. General figure representations of metrics are described in the caption of figure 5.7

stiffness feedback (p<.001).

Subjective measures however show a clear reduction of satisfying for when offering force-based feedback to the static spring and stiffness feedback (p<.001 and p=.003 respectively) as can be seen in 5.8.C.

5.4.3. FORCE LEVEL TASK

In the force level task subjects had to compress the object to a specific point and therefore corresponding force level. This resulted in a tradeoff between speed and accuracy which can be seen in settling time and overshoot respectively as can be seen in 5.9.A. Results show a large reduction of overshoot when offering stiffness feedback compared to an advanced static spring (77%, p=.038). However this comes with an increased settling time for stiffness feedback compared to the static spring (10%, p=.017).

Control effort reduces when offering information regarding the state of the slave, both force-based and stiffness feedback have reduced reversals compared to the advanced static spring (both 37%, p<.01).

Subjective measures show a clear difference in both satisfying and usefulness of the static spring compared to offering force-based and stiffness feedback. Both force-based and stiffness feedback have a reduced satisfying score (p=.029 and p=.007 respectively).

Table 5.4: Results of Force Level Task

	T settling [s]	Overshoot [%]	Reversals [-]	F master [N]	Usefulness [-]	Satisfying [-]
2. Adv. Spring [1]	4.70 (4.36, 5.03)	3.09 (1.68, 4.50)	18.85 (16.32, 21.39)	5.37 (5.08, 5.65)	0.10 (-0.36, 0.65)	0.96 (0.71, 1.21)
3. F-based Feedback [1]	4.96 (4.64, 5.27)	3.05 (1.39, 4.71)	11.94 (10.77, 13.10)	19.42 (18.44, 20.41)	0.63 (0.34, 0.93)	0.10 (-0.38, 0.58)
4. Stiffness Feedback [1]	5.19 (4.79, 5.58)	0.72 (0.29, 1.14)	11.81 (10.23, 13.40)	17.10 (16.44, 17.75)	0.78 (0.47, 1.10)	0.02 (-0.45, 0.49)
Statistics [2]	p=.018 (F=4.9)	p=.010 (F=5.7)	p<.001 (F=16)	p<.001 (F=532)	p=.028 (F=4.2)	p=.002 (F=8.2)
Post-hoc [3]	2 to 4, p=.017	2 to 4, p=.038 3 to 4, p=.083	2 to 3, p=.009 2 to 4, p=.001	all, p<.001 except 3 to 4, p=.004	2 to 4, p=.105 -	2 to 3, p=.029 2 to 4, p=.007

Main mean results of all evaluation metrics for performance, control effort and subjective measures, accompanied with their statistical results for free-space tasks.
[1] Group mean (95% Confidence Interval).
[2] Statistics are shown with a p and F value for a Repeated Measures ANOVA with Greenhouse-Geisser corrections when sphericity was violated.
[3] Post-hoc comparisons were applied using Bonferroni compensation.

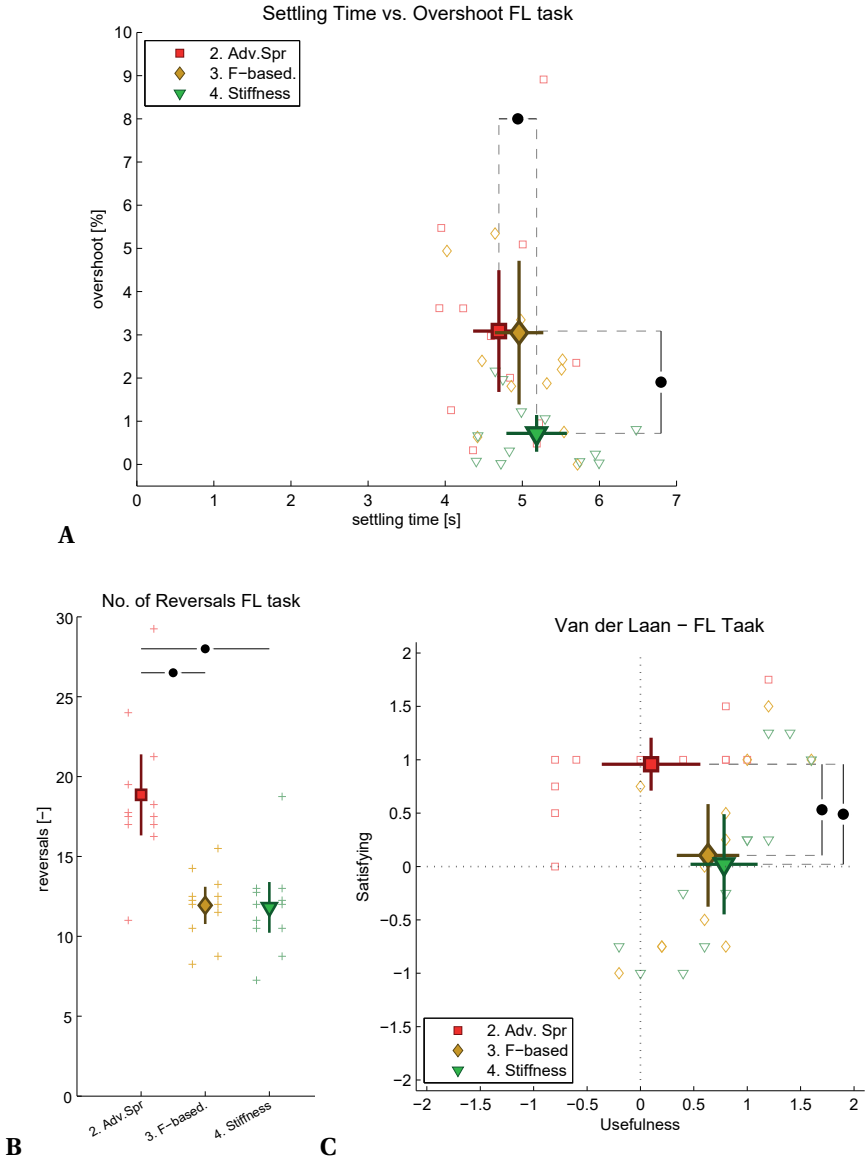

Figure 5.9: Results of **force level task** for all three conditions applied. A) settling time (x-axis) versus overshoot (y-axis). B) number of steering reversals. C) subjective Van der Laan measure. General figure representations of metrics are described in the caption of figure 5.7

5.5. DISCUSSION

The tested control interface designs substantially affected the execution of rate controlled tasks. The analysis focused on analysing the impact of different interface designs for three generic subtask types: free-space, contact transition and force level tasks.

The free-space task was most challenging to execute with the basic spring (lowest reported usefulness and satisfaction), which evoked large inter-subject variability. The advanced spring (with clear zero velocity indication) improved rate control compared to the basic spring, both in terms of settling time and in reported usefulness and satisfaction. Interestingly, in research static springs are typically only implemented as a basic spring (e.g. Lawrence et al. (1997); Mobasser and Hashtrudi-Zaad (2008); Parker et al. (1993); Salcudean et al. (2000)) and not as an advanced spring as usually implemented in industry (e.g. Gessmann GmbH Schulein and Ehrensperger (2012)). This research shows that implementing this simple nonlinear spring characteristic into a static spring already shows clear improvements for task execution.

The two designs that feedback information regarding the state of the slave (i.e. force-based and stiffness feedback conditions) entailed a higher number of steering reversals. This increased control effort could suggests a higher mental load, due to the additional information offered to the operator. The participants rated both the force-based and stiffness feedback conditions as more useful than the basic spring, although force-based feed-back was reported to be less satisfying. In terms of objective metrics, stiffness feedback seemed to result in similar small settling times and lower overshoot as the advanced spring but did not differ significantly to the basic spring. No difference in performance was found between the force-based and the other three designs. This corresponds to results found in simulation by Zhu and Salcudean (1995), who showed accurate tracking results during free motion and improved transparency when offering force-based feedback. Salcudean et al. (2000) also found accurate tracking results with experimental data up to 8 Hz when offering force-based feedback.

Both force-based and stiffness feedback did not yield in substantial benefits compared to the advanced spring, for the additionally required sensors and controllers to enable this type of state feedback. Concluding, for pure free-space tasks an advanced spring would be the best choice.

The contact transition task was most frustrating to control when force-based feedback was offered and was rated with lower satisfaction scores, although it did not result in larger errors. This may be due to oscillatory forces at impact resulting in instabilities and user discomfort. These oscillations are a result of feeding back the derivative of force, an effect that is not mentioned in the simulation studies of Salcudean et al. (2000). The oscillating effect occurs in human-in-the-loop contact transitions during force-derivative feedback, this is shown for a typical subject in 5.10.A in box I. A similar effect is seen when offering only the derivative component as for the all components combined. In the top sub figure of 5.10.A it can be seen that equal task execution was performed when offering each individual component of force-based feedback (velocity error and derivative environment force feedback). The derivative of the environment force shows a strong oscillating effect for approximately 500 ms. The number of steering reversals was reduced for the force-based feedback, possibly indicating subjects

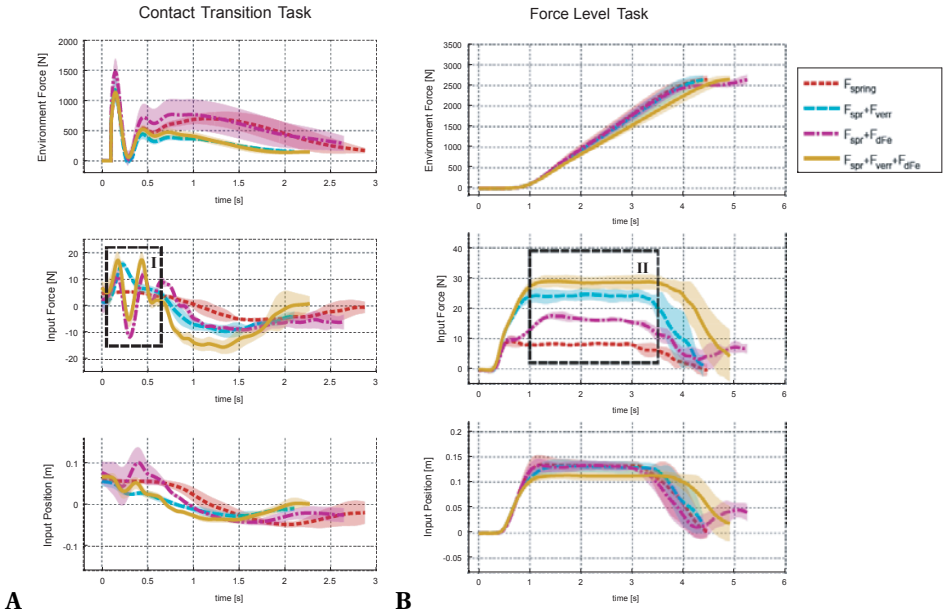

Figure 5.10: Time trace results of each component of force-based feedback, obtained from a typical subject for A) in contact task. B) force level task. Force-based feedback (solid brown lines) consist of a static spring component (red short-dotted lines), combined with velocity error feedback (cyan long-dotted lines), or combined with the derivative environment force (magenta dashed-dotted lines).

were hesitant of the oscillating feedback when making contact.

Similar oscillating results during force-based feedback were found by Salcudean et al. (2000). They showed force tracking performance for a single operator while interacting with a flexible and rigid environment. During initial contact with both environment types, their results show similar oscillating forces. Parker et al. (1993) demonstrated that stiffness feedback avoided such oscillations during contact transitions due to the inherently stabilizing factor of finite restoring force of stiffness feedback.

In the force level task a significantly lower overshoot and increased settling time was found during stiffness feedback compared to the advanced static spring. The beneficial decrease in overshoot (77% reduction in means) is substantial compared to the relatively small increase of settling time (10% increase in means). 5.9.A illustrates this trade-off of a relatively large reduced overshoot, which comes with an increased settling time. Both interface designs that feedback information about the physical interaction with the environment (force-based and stiffness feedback) have the lowest workload in terms of number of reversals and rating of usefulness and satisfaction.

Similar control inputs are given for the varying individual feedback components as illustrated in the lowest sub figure of 5.10.B, resulting in similar force-level task executions as shown in the top sub figure. Box II in 5.10.B shows that the velocity error component of force-based

feedback results in substantial additional static stiffness during in-contact, even though using similar control inputs when offered individual feedback components. When combined feedback is given, the velocity error dominates the feedback signal and does not add important information to the operator during this task execution. During stiffness feedback the velocity error component is switched off when environment contact forces are detected, therefore not having this issue. And because stiffness feedback is based on the absolute contact interaction force and not its derivative, the feedback remains increasing for increasing contact forces.

Salcudean et al. (2000) found comparable experimental results for force tracking up to 8 Hz. During static inputs the derivative of interaction forces becomes constant when in-contact. This is proven mathematically as perfect transparency by Hashtrudi-Zaad (Hashtrudi-Zaad and Salcudean, 2002; Mobasser and Hashtrudi-Zaad, 2008), based on the perfect transparency control law of Lawrence (1993) for position control. To increase the awareness of the environment interaction forces Hashtrudi-Zaad and Salcudean (2002) suggests to reflect the contact force itself instead of the derivative, which might lead to an unnatural feel (Mobasser and Hashtrudi-Zaad, 2008; Parker et al., 1993). Offering stiffness feedback as proposed by Parker et al. (1993), avoids this problem, which our human-in-the-loop study confirms.

In our study subjects performed rate control during abstracted (sub)tasks, which allows detailed evaluation of task performance, but complicates generalization of the findings to real-world tasks. The relatively small benefits of offering feedback of the state of the slave found in this study are expected to be more substantial in more realistic tasks, such as controlling a remote subsea vehicle or operating container cranes. Based on this study, it is recommended to offer the stiffness feedback design from this study when rate-controlled task consist of all three tested subtasks. When information regarding the state of the slave is not present or costly to obtain, an advanced static spring with clear zero indication as used in this study is recommended.

5.6. CONCLUSION

A human factors experiment was conducted to determine the efficacy of four different haptic interface designs for rate control: two passive designs based on springs (standard and advanced) and two designs reflecting physical interaction in the remote environment (based on velocity error or on measured environment forces). The four designs were tested during rate control of a slow virtual slave for three abstract subtasks: free-space (FS), contact transition (CT) and force level (FL) tasks. For the experimental conditions studied, the following is concluded:

- Compared to a basic spring, the advanced spring design with clear zero velocity indication improves task performance (i.e. overshoot) and is rated as more useful and satisfying (FS task).
- Feedback of velocity error either as force-based or additional stiffness does not improve task performance and increases control effort (FS task).
- Feedback of the derivative of the environment force requires less control effort, but is

also rated less satisfying as a support (CT task).

- Reflecting the environment force as additional stiffness, improves task performance (i.e. over-shoot) and costs less control effort (i.e. steering reversals) (FL task).

These results indicate that passive spring designs are sufficient for rate-controlled tasks where free-space sub-tasks dominate. Feeding back information about the physical interaction is beneficial for in-contact tasks and force level tasks, where stiffness feedback results in benefits over feedback back the derivative of the environment interaction force.

REFERENCES

Abbink, D. A. and Mulder, M. (2009). Exploring the Dimensions of Haptic Feedback Support in Manual Control. *J. Comput. Inf. Sci. Eng. Spec. Haptics Ed.*, 9(March):1–9.

Boessenkool, H., Abbink, D. A., Heemskerk, C. J. M., Van Der Helm, F. C. T., and Wildenbeest, J. G. W. (2013). A task-specific analysis of the benefit of haptic shared control during telemanipulation. *IEEE Trans. Haptics*, 6(1):2–12.

Elton, M., Winck, R., and Book, W. (2013). Command Feedback for Position Control of Hydraulic Machines. *ASME/BATH 2013 Symp. Fluid Power Motion Control*.

Hannaford, B. (1989). A design framework for teleoperators with kinesthetic feedback. *IEEE Trans. Robot. Autom.*, 5(4):426–434.

Hashtrudi-Zaad, K. and Salcudean, S. E. (2002). Transparency in Time_Delayed Systems and the Effect of Local Force Feedback for Transparent Teleoperation. *IEEE Trans. Robot. Autom.*, 18(1):108–114.

Kim, W. S., Tendick, F., and Stark, L. W. (1987). Visual Enhancements in Pick-and-Place Tasks: Human Operators Controlling a Simulated Cylindrical Manipulator. *J. Robot. Autom.*, 3(5):418–425.

Kuiper, R. J., Heck, D. J. F., Kuling, I. A., and Abbink, D. A. (2016). Evaluation of Haptic and Visual Cues for Repulsive or Attractive Guidance in Nonholonomic Steering Tasks. *IEEE Trans. Human-Machine Interfaces*.

Lawrence, D. A. (1993). Stability and Transparency in Bilateral Teleoperation. *IEEE Trans. Robot. Autom.*, 9(5):624–637.

Lawrence, P., Salcudean, S., and Sepehri, N. (1997). Coordinated and force-feedback control of hydraulic excavators. In *Exp. Robot. IV*, pages 181–194.

Linde, R. V. D. and Lammertse, P. (2003). HapticMaster – a generic force controlled robot for human interaction. *Ind. Robot An Int. J.*, 30(6):515–524.

Mobasser, F. and Hashtrudi-Zaad, K. (2008). Transparent Rate Mode Bilateral Teleoperation Control. *Int. J. Rob. Res.*, 27(1):57–72.

Mugge, W., Schuurmans, J., Schouten, A. C., and van der Helm, F. C. (2009). Sensory Weighting of Force and Position Feedback in Human Motor Control Tasks. *J. Neurosci.*, 29(17):5476–5482.

Mulder, M., Abbink, D. a., and Boer, E. R. (2012). Sharing Control With Haptics: Seamless Driver Support From Manual to Automatic Control. *Hum. Factors J. Hum. Factors Ergon. Soc.*

Ostoja-Starzewski, M. and Skibniewski, M. (1989). A master-slave manipulator for excavation and construction tasks. *Rob. Auton. Syst.*, 4(4):333–337.

Park, S., Seo, C., Kim, J.-P., and Ryu, J. (2011). Robustly stable rate-mode bilateral teleoperation using an energy-bounding approach. *Mechatronics*, 21(1):176–184.

Parker, N., Salcudean, S., and Lawrence, P. (1993). Application of force feedback to heavy duty hydraulic machines. *[1993] Proc. IEEE Int. Conf. Robot. Autom.*, pages 375–381.

Salcudean, S., Tafazoli, S., Hashtrudi-Zaad, K., Lawrence, P., and Reboulet, C. (1998). Evaluation of impedance and teleoperation control of a hydraulic mini-excavator. *Exp. Robot. V.*

Salcudean, S. E., Zhu, M., Zhu, W.-H., and Hashtrudi-Zaad, K. (2000). Transparent Bilateral Teleoperation under Position and Rate Control. *Int. J. Rob. Res.*, 19(12):1185–1202.

Schulein, G. and Ehrensperger, A. (2012). Multi-axle manual control unit.

Sepehri, N., Lawrence, P. D., Sassani, F., and Frenette, R. (1994). Resolved-Mode Teleoperated Control of Heavy-Duty Hydraulic Machines. *J. Dyn. Syst. Meas. Control*, 116(2):232.

Sheridan, T. (1989). Telerobotics. *Automatica*, 25(4):487–507.

Sheridan, T. B., Verplank, W. L., and Brooks, T. L. (1978). Human/computer control of undersea teleoperators. Technical report, Tokyo.

Steel, R. G. D., Torrie, J. H., and Dickey, D. (1986). *Principles and procedures of statistics: A biometrical approach*.

van der Laan, J., Heino, A., and de Waard, D. (1997). A simple procedure for the assessment of acceptence of advanced transport telematics. *Transp. Res. Part C Emerg. Technol.*, 5(1):1–10.

Wildenbeest, J. G., Kuiper, R. J., van der Helm, F. C., and Abbink, D. A. (2014). Position control for slow dynamic systems: Haptic feedback makes system constraints tangible. *2014 IEEE Int. Conf. Syst. Man, Cybern.*, pages 3990–3995.

Wildenbeest, J. G. W., Abbink, D. A., Heemskerk, C. J. M., Van Der Helm, F. C. T., and Boessenkool, H. (2013). The impact of haptic feedback quality on the performance of teleoperated assembly tasks. *IEEE Trans. Haptics*, 6(2):242–252.

Yokokohji, Y. and Yoshikawa, T. (1994). Bilateral Control of Master-Slave Manipulators for Ideal Kinesthetic Coupling - Formulation and Experiment. *IEEE Trans. Robot. Autom.*, 10(5):605–620.

Zhu, M. and Salcudean, S. E. (1995). Achieving Transparency for Teleoperator Systems under Position and Rate Control. *IEEE Int. Con. Intell. Robot.*, pages 1–6.

6

Natural Force Feedback for Rate Controlled Excavators

Roel J. Kuiper, Henri Boessenkool, Jan C.L. Frumau and David A. Abbink

to be submitted in the Journal of Mechanical Sciences, 2019

Natural force feedback by means of stiffness reflection showed improvements in task execution for abstract task types (free space movements, contact transitions and force level) in chapter 5. It is unclear how this would affect a realistic task such as controlling a backhoe excavator, which combines three subtask types; moving in water, making contact with the seabed and cutting through sand. This chapter describes the development of a realistic haptic excavator simulator, including a force reflecting joystick that allows for rapid design and evaluation of haptic feedback prototypes.

The contents of this chapter describes the development of a haptic excavator simulator and a proof-of-principle evaluation of the complete system. In section 6.2 is the design and fabrication of a novel actuated 3 DOF joystick given, enabling high fidelity force reflection. An excavator consists of 4 DOF (slew, boom, stick and bucket), which typically is controlled using a double 2 DOF joystick for each hand of the operator. The development of a backhoe excavator simulation environment is described in section 6.3, consisting of a physical model combined with a visualization of the machine. Section 6.4 describes an initial design and implementation of a haptic feedback algorithm for reflecting environment interaction forces between a backhoe excavator and the soil. Finally section 6.5 gives a proof-of-principle by means of a human factors case study controlling the excavator simulator with haptic feedback, simplified for only a 2 DOF control of the boom and stick angle.

R.J. Kuiper, H. Boessenkool, J.C.L. Frumau and D.A. Abbink; A Haptic Backhoe Excavator Simulator: Design of a Force Reflecting Joystick and Feedback Algorithms; to be submitted in the Journal of Mechanical Sciences in 2019

ABSTRACT

In the dredging industry, backhoe dipper excavators are frequently used on a pontoon for underwater dredging in harbors and shallow waters. These operations are controlled manually by rate control, while the operator is supported by displayed visual information based on sensors mounted on the excavator. Controlling such excavators is difficult due to the complicated multi-degree of freedom kinematics (4 DOF) and complex slow dynamic response, especially when in contact with soil because the interaction forces are not fed back. A potential approach to facilitate excavator control is through haptics: providing the operator with force feedback on the control interface. This paper describes the development of a haptic excavator simulator to allow rapid design and evaluation of haptic feedback prototypes. The main contributions of this paper are 1) the design and fabrication of a novel actuated 3 DOF joystick enabling high fidelity force reflection 2) an initial design and implementation of a haptic feedback algorithm for reflecting environment interaction forces of a backhoe excavator, and 3) proof-of-principle evaluation of the complete system. A proof of principle is given by means of a human factors case study controlling the excavator simulator simplified in 2 DOF with haptic feedback by I) making contact with the seabed, II) transitions in soil conditions and III) contact with hard boulders. In conclusion, the developed haptic excavator simulator has been successfully realized, enabling bi-lateral haptic feedback. The simulator allows for functional high-fidelity force feedback about the task-relevant force information during the executed tasks. The developed setup paves the way for human factors experiments to quantify the effect of the force feedback designs on the operator workload and performance when controlling a backhoe excavator.

6.1. INTRODUCTION

To dredge materials in harbors or shallow offshore operations, backhoe dipper excavators are often used. Typically such excavators are very large in size and mass and mounted on a pontoon, fixed with three spud poles. The bucket of these machines can reach a size of 40 m^3, about the size of a full dump truck. Materials are dredged below the water surface, using an artificial visualization based on rotation sensor values of each link (see indicative figure 6.5 for an example of the software DipMate® from Seatools (Kempkes, 2007)). Apart from displays and outside visuals, expert operators use ambient cues for control and situation awareness. They use the sound of the hydraulic oil through the valves and the engine sound to determine the system load, and for example the cabin movement and vibrations to determine the environment interaction forces (Elton and Book, 2011; Kontz and Book, 2006; Lawrence et al., 1997).

Complicating factors in excavator control include the non-intuitive multi-link kinematics (4 DOF) and the slow dynamic behavior (a full stroke of approximately 10 m can take about 20 seconds to complete at full speed) (Elton et al., 2009; Osafo-Yeboah et al., 2010). Additionally the dynamics are different for each joint, and include many nonlinearities due to for instance gravity, power limitation, valve delay and a dead-band (Elton et al., 2009; Sepehri and Lawrence, 1992). These effects all result into complex endpoint control of the bucket, resulting in a very long and costly operator training period (Elton and Book, 2011). Controlling these large machines

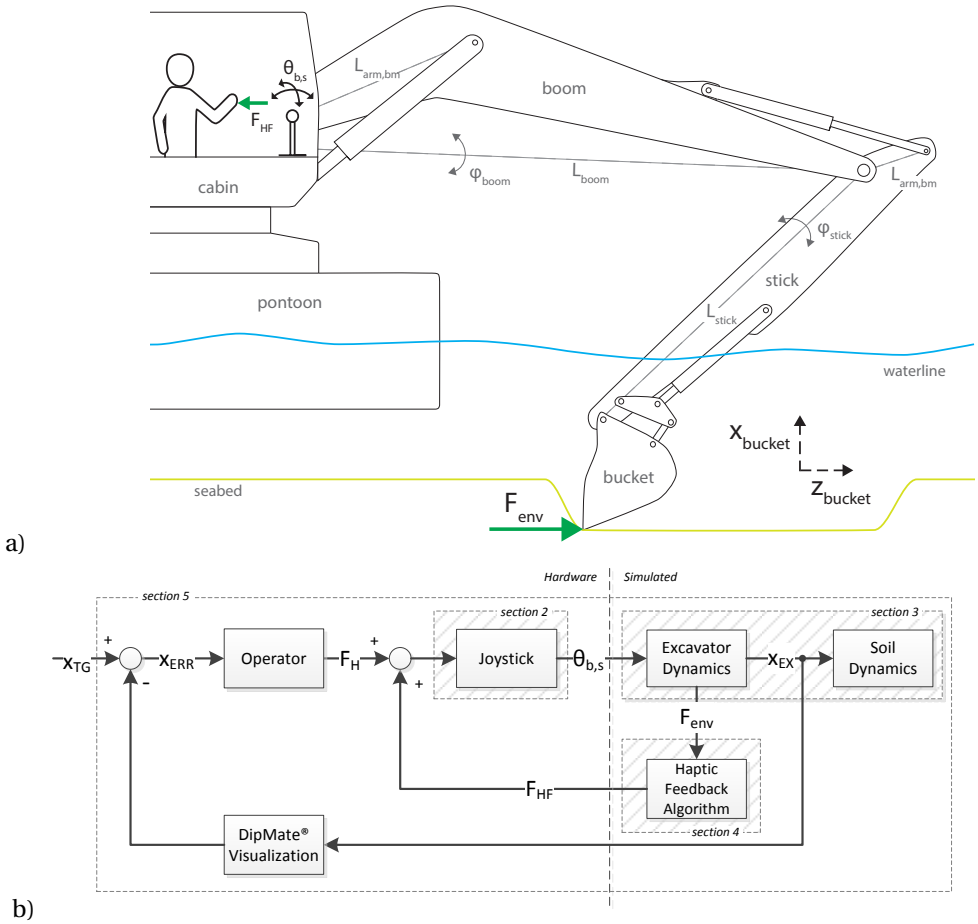

Figure 6.1: Schematic overview of an excavator with force feedback. a) indicated with the main two effective degree of freedom for translations and environment feedback force, b) schematic block diagram of required components for enabling feedback for excavators. Indicating the operator with its target x_{tg}, controlling with its force F_h combined with the haptic feedback force F_{hf} the joystick output $\theta_{b,s}$, controlling the excavators dynamic output x_{ex} and the environment interaction force F_{env} used for feedback.

using only a visual representation is challenging and requires highly trained operators with constant concentration, inattention has caused severe damage to the machine and environment (Mourik and Ouwerkerk, 2010).

An interesting approach to support crane operators is by providing them with task-relevant haptic feedback on the control joystick (Elton and Book, 2011; Osafo-Yeboah et al., 2010). By providing the operator with force feedback of the interaction forces a more novice operator should also capable of deducing this information more quickly (Draper et al., 1987; Hannaford et al., 1991; Massimino and Sheridan, 1989; Wildenbeest et al., 2013). This form of haptic feedback potentially can improve the operator's understanding of the machine's capabilities

(Hannaford et al., 1991; Ostoja-Starzewski and Skibniewski, 1989; Wildenbeest et al., 2014). For hydraulic excavators it is suggested to implement stiffness modulation as feedback method to maintain stability (Parker et al., 1993; Salcudean et al., 2000; Tafazoli et al., 2002). In previous work various haptic feedback methods were compared under rate control (i.e. controlling the velocity of the excavator) (Kuiper et al., 2017). Stiffness modulation was found to be most beneficial for various tasks types, such as free space movements and in-contact subtasks. It enables robust feedback, while maintaining the central neutral point clearly.

This paper describes the design of a haptic simulator for backhoe excavator operations, to enable the design and evaluation of various haptic feedback algorithms for improving the control of an excavator. An excavator is typically operated by means of two 2 DOF joysticks, controlling the hydraulic actuation and therefore indirectly the velocity of each individual joint (Elton et al., 2009; Lawrence et al., 1997; Roper et al., 1989; Winck et al., 2015). The developed hardware part of the simulator is the mechatronic design of an actuated 3-DOF joystick (see figure 6.2a). The designed joystick can render high fidelity force feedback to the operator, as well as sense position, actuation force and grip force inputs from the operator. This enables classic bi-lateral haptic feedback, as well as augmented guidance forces such as haptic shared control (Abbink et al., 2012; Abbink and Mulder, 2009; Abbott and Okamura, 2003; Mulder et al., 2012), which may be adapted based on grip force (Smisek et al., 2017). In figure 6.1a an outline is given of reflecting environment forces F_{env} to the operator, controlling the joystick input angles θ. This is schematically represented in a block diagram in figure 6.1b, also representing the main contributions of this paper. The operator has a target position x_{tg} and error x_{err} and controls the joystick with its hand F_h. From the joystick the hydraulic valves are controlled $\theta_{b,s}$, thereby controlling the velocity of the excavators output x_{ex}. Based on the excavator forces with the environment F_{env}, an haptic feedback algorithm can reflect these forces F_{hf} onto the joystick back again.

The four main contributions of this paper are marked in figure 6.1b and described in the following sections. The first main contribution is the developed Tria$R$ joystick as shown in figure 6.2a, with a parallel mechanism for three rotations, resulting in fixed based motors and therefore low inertia and high stiffness of the joystick kinematics. The joystick design includes custom integrated torque sensing on each rotation and a grip sensor in section 6.2. The second contribution is the excavator simulation environment, which includes hydraulic cylinders and environment interaction forces of soil dynamics (section 6.3). The third contribution is the haptic feedback algorithm, which can be offered to the operator based on the measured excavator cylinder pressures, by means of stiffness modulation based on previous work (Kuiper et al., 2017). This modulation includes a detailed description of the static stiffness implementation of the joystick in section 6.4. The final contribution is the evaluation of the combined closed-loop system using a human factors case study in section 6.5 for cutting through the seabed horizontally, simplified for a 2 DOF task only (boom and stick angle).

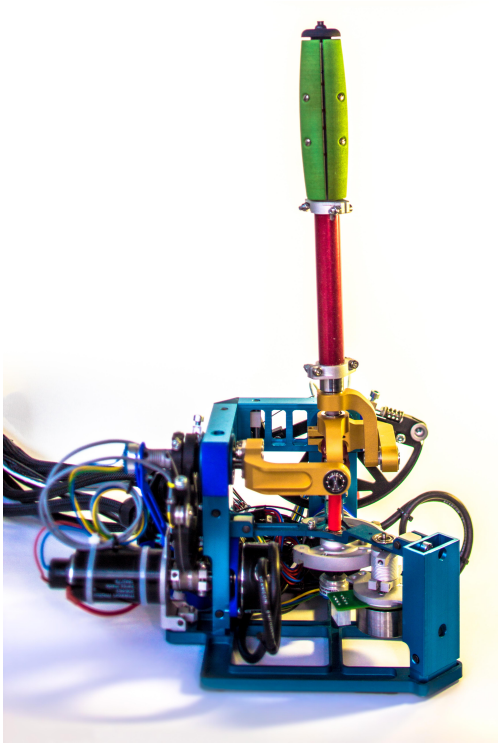

a)

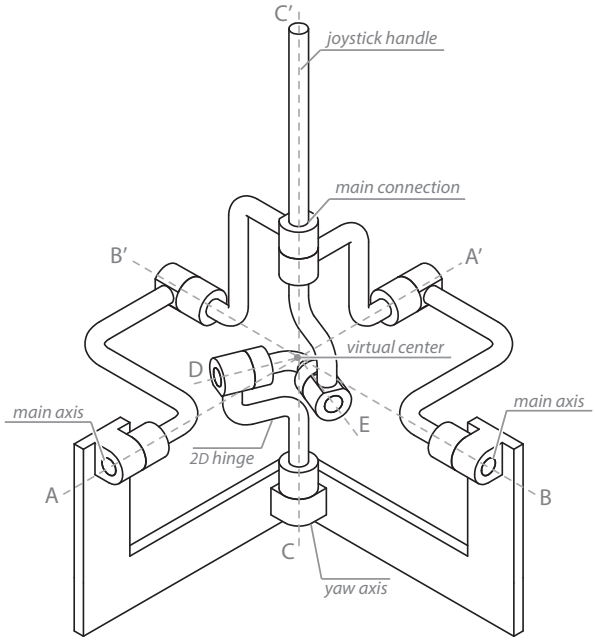

b)

Figure 6.2: Tria*R* joystick, three degrees of freedom force reflecting joystick. a) Fabricated prototype including motors and sensor on the three axis and a grip with integrated grip force sensor. b) Schematic representation of kinematics of the joystick joints, including the two main axis and yaw axis for the transmission connections and the joystick handle for the grip connection.

6.2. HAPTIC JOYSTICK DESIGN

The main novel component of the haptic excavator simulator is the developed Tria*R* joystick as shown in figure 6.2a. The joystick consists of three force reflecting rotational degrees of freedom, combined with custom integrated torque sensing for all three actuators and grip force sensing in the handle. The kinematics of the parallel mechanism with the three motors placed fixed at the base is described in section 6.2.1 and schematically indicated in figure 6.2b. The capstan transmission design combined with integrated torque sensing is described in section 6.2.2 and shown in figure 6.3a, combined with embedded grip sensing in figure 6.3b as described in section 6.2.3. Finally the developed joystick design is validated for its performance by measuring the frequency response as described in section 6.2.4 and shown in figure 6.4.

6.2.1. KINEMATIC DESIGN

The kinematic design is based on a parallel mechanism for three rotations in total, enabling complete control of the arm and hand position when rotating either of the main two axis. The parallel mechanism results in three fixed based motors for actuation of each axis, remaining in a fixed position mounted in the frame. This results in low inertia for each link, making the joystick more transparent in reflecting forces (Hoevenaars et al., 2014). The kinematic design is shown in figure 6.2b schematically for the three rotations.

The two main joystick axis are labeled with A-A' and B-B' in figure 6.2b, essentially controlling the roll and pitch angles of the joystick, and axis C-C' describes the yaw angle of the joystick. What can be noted is that all axis are intersecting in a virtual center of rotation point in the joystick. The yaw angle is required to have a two degrees of freedom hinge as well, represented with axis D and E. Without this hinge the kinematics are only described by axis A and B, comparable to the kinematics described by Rosenberg et al. (1998). But to be able to control or even fixate the yaw angle C of the joystick the additional hinge D and E needed to be added, requiring the connection from A' and B' with C' to be lifted above the center point of rotation. Therefore it is beneficial for the design in terms of overall dimensions and stiffness to have hinge D and E fairly small, but aligned with the main axis. For this purpose a Cardan joint (i.e. universal joint) was implemented, with bearings in the outer flanges to enable a small compact center part. The joint enables simple stiff control over the joint angle, but needs compensation for the transmitted torque over its rotation.

The use of a parallel mechanism typically enables a fixed based motor location (i.e. fixed to the frame and not moving its position). But this comes with the cost of a limited workspace and the occurrence of singularities at the workspace boundaries (Gosselin and Angeles, 1990; Hoevenaars et al., 2014). For this design with rotations only, the occurring singularities at the boundaries are comparable to a Gimbal lock known for Euler rotations. But the design is limited to 65 degrees of rotation each way, therefore avoiding this phenomenon.

The main challenge for this design was to create a relative compact design of the rotational joints due to the lifted contact point of axis A' and B' onto axis C', as indicated in figure 6.2b. This is the mayor difference between the design presented by Rosenberg (An and Stiles, 2002; Rosenberg et al., 1998, 2001), and enables the control of the rotation of axis C-C'. That is why

the joint of axis D and E needed to be as small as possible, while remaining the flexibility to rotate over the large workspace of 130 degrees in total.

6.2.2. CAPSTAN TRANSMISSION

The capstan transmission connects the motor axis with the main joystick axis, F, G and H in figure 6.2b. The capstan transmission is a cable wounded over two different radii creating a rigid rotational connection with a gear ratio. In figure 6.3a is a simplified partial exploded view shown of one of the two main axis A and B of figure 6.2b. The transmission consists of two main parts, the larger capstan disk rotating with the main axis of 130 degrees in total, and the smaller drum connected to the motor axis.

The main joystick axis is connected to axis F-F' of the capstan transmission at F' as denoted. This axis is connected with a bearing to the main capstan disk for translational support, but not transmitting any torques. The force sensor connects to the rectangular end of axis F, transmitting the joystick torque with is lever arm as a force to axis G-G', fixed on the larger capstan disk. On top of the capstan disk are two cable connection points mounted, transferring the torque of the disk to a cable force. One side of the cable connection points has a compression spring included, ensuring pretension in the cable. The tensioner is designed such that the compression spring is fully compressed to block length, disabling any additional dynamics to the transmission. The cable is connected to the capstan drum on axis H-H' after wounded at least three times extra over the drum for friction.

The motor axis is fixed to the drum and can therefore power the joystick axis up to axis F-F'. The designed gear ratio is the relative diameter of the disk of 140 mm compared to the drum groove diameter of 19.6 mm. Both diameters are increased by the wire thickness of 0.9 mm to a gear ratio of 140.9/20.5 = 6.873, resulting in 2.48 motor rotations for the full 130 deg joystick rotation.

The force sensor is transmitting the torque between axis F and G. Due to the bearing in the central disk, the force sensor is only transferring torque. The total system is designed for a load case of 100 N at the center of the grip handle, with a safety factor for mechanical failure. The design load would result in a torque of 25.5 Nm for an effective joystick lever arm of 255 mm. This would therefore require a motor torque of 3700 mNm to generate this peak force, the currently mounted motor RE40 is only limited to 2560 mNm stall torque. The integrated force sensor would deflect for the designed load 0.75 mm in total at axis G relative to axis F in tangential direction.

6.2.3. GRIP SENSOR

The grip base at the end of the joystick handle is the interface for the operator to hold the joystick, as shown in green in figure 6.2a. The amount of grip force the operator applies to the handle can be a measure of the task difficulty experienced by the operator due to an increased arm admittance (Nakamura et al., 2011). Furthermore the grip force can therefore be integrated in active guidance systems to shift the level of control authority of the human operator and decrease the guidance strength (Abbink et al., 2012; Smisek et al., 2017)

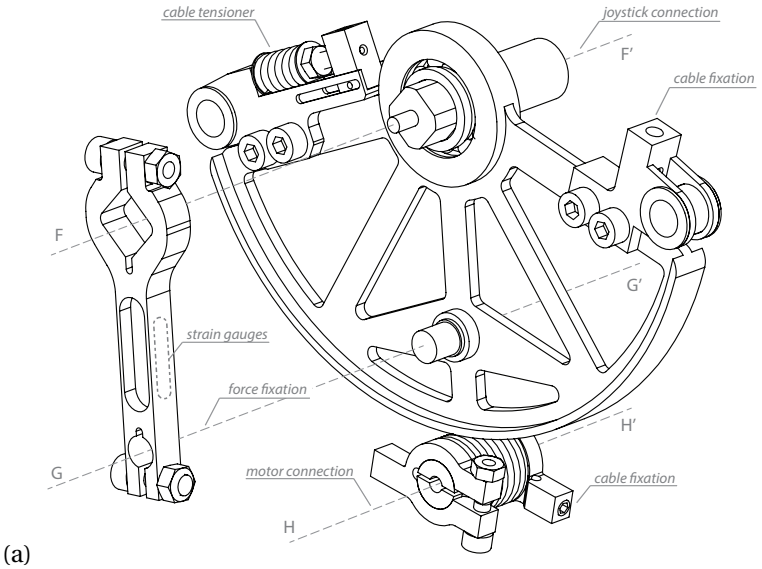

(a)

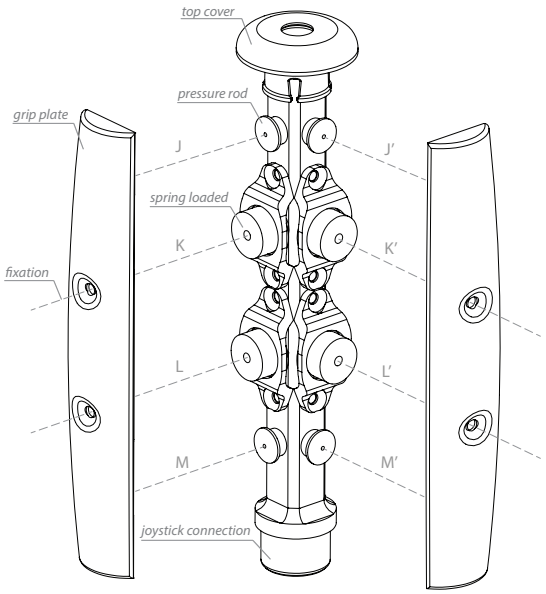

(b)

Figure 6.3: Partial exploded view of, a) Capstan transmission with integrated torque sensor between axis F-F' and G-G', transmitting the torque and hold the strain gauges on both sides for force sensing. b) Grip base with integrated force sensor, with on axis J-J' and M-M' are the eight force sensors mounted and the axis K-K' and L-L' hold the spring alignment placeholders.

The grip base consists of four grip plates on which the operator can exert a certain grip force. This is schematically shown in a partial exploded view in figure 6.3b of the handle with two of the grip plates. The grip plates are connected to axis K-K' and L-L', which are moving spring loaded cylinders pushing the plates outwards. The cylinders are made from POM and act as linear bearings in the aluminum center. The small rods on axis J-J' and M-M' are rigidly connected to the aluminum base and make contact with the plates at these axis locations. The grip plates have thin flexible force sensors mounted Tekscan FlexiForce A301 with a maximal force range of 111N each, making contact with these rods. The force sensors are implemented with a minimum force threshold of 9.8 N due to the mounted springs, which could be lowered to approximately 3 N in future modifications by a reduced spring stiffness. In total 8 pressure sensors therefore measure the grip force exerted on the four grip plates. Opposite grip plates define the grip force in each direction with two sensors per plate to average the off center exerted force. The total grip force is therefore limited up to a maximum of 45 kg. The sensors are measured using a voltage divider, giving an exponential correlation to the applied force of $F_{grip} = \exp\left[(c_1 - V_{meas})/c_2\right] \cdot c_3$, with constants c using $\{4.5, 3.0, 50\}$. The measured force has a resolution limited by the D/A converter of 16-bits resulting in 8.2 mN force at full load per sensor, but dominated by the hysteresis of 0.94 N measured for a grip plate consisting of two sensors.

6.2.4. PERFORMANCE RESULTS

The closed-loop dynamics of the TriaR are evaluated by means of a Frequency Response Function (FRF), obtained using a multi-sinus force disturbance. The disturbance contains power at 30 logarithmically distributed frequencies ranging from 0.5 to 30 Hz with a total amplitude of about 5 degrees (Wildenbeest et al., 2014). The disturbance signal was 35 s long, with a fade-in and fade-out of the signal only 32.7 s of the signal was used for identification, exactly matching 16 times the lowest disturbance frequency (Mugge et al., 2007).

The results are shown in figure 6.4 for all three axes of the TriaR joystick. The disturbance was tracked using a PD-controller with gains (180 P, 70 D) tuned up to its maximum with basic filtering on the encoder input signal (14-bits resolution) for the controller. The calculated frequency response is the measured joystick position divided over the disturbance, with a signal to noise ratio of at least 40 for the applied disturbance frequency points. It shows a tracking performance up to 10 Hz for the two main axes A and B (roll and pitch axis). The vertical axis has lower performance results up to 6 Hz due to a small actuator. Still the position tracking performance is sufficient to track a typical human response up to 2 to 3 Hz maximal (up to 7 Hz for skilled professionals like fighter pilots) (Wildenbeest et al., 2018). Therefore high quality feedback can be offered for the human operating inputs (e.g. stiffness feedback) and for higher frequencies this is most likely required to be open-loop feedback perturbations. The mechanical design is designed for force capabilities up to 100 N at the handle, but for now electrically limited up to 25 N at end point resulting in an endpoint deflection of 0.35 mm.

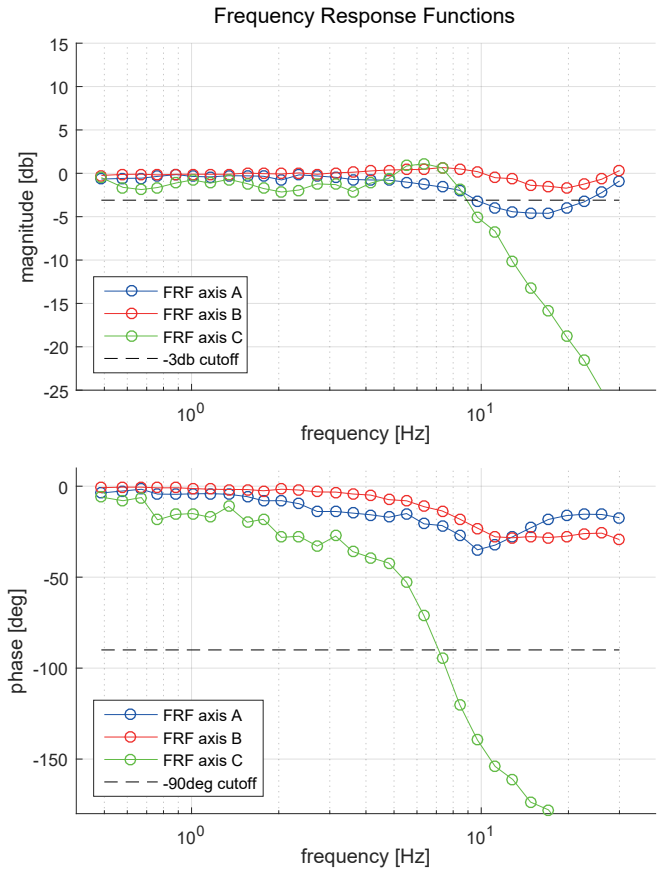

Figure 6.4: Frequency Response Functions (FRF) of all three axis, indicating the performance of the force reflecting joystick. The response is the measured position over the disturbance.

6.3. EXCAVATOR SIMULATION ENVIRONMENT

A backhoe excavator simulator was developed in order to test the effect of haptic feedback on controlling such a machine type. The simulator consists of a physical model combined with a visualization of the machine as depicted in figure 6.5. This enables the coupling of the described developed joystick in section 6.2 to control an excavator.

The simulators physical modeling consists of the kinematics and dynamics of the machine, powered by hydraulic actuators as described in section 6.3.1. The mayor simulation model parameters are listed appendix table 6.1. The complexity of the simulation arises when making contact with the seabed. A novel soil interaction model is developed to reflect various forces of the environment onto the excavator as described in section 6.3.2. The visualization to enable the operator to control the simulated excavator, is a commercial product DipMate® by Seatools bv. This shows a 3D visualization of the excavator from a bird-eye perspective and a top and

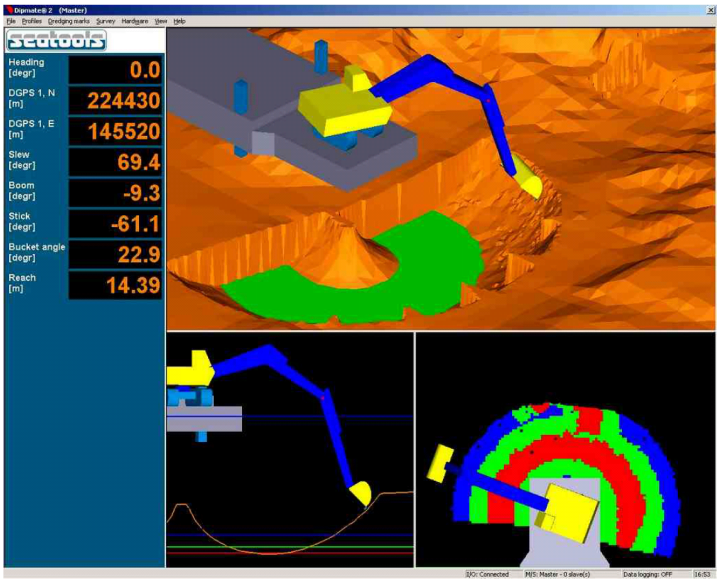

Figure 6.5: Seatools DipMate® backhoe dipper visualization software tool, adapted from Kempkes (2007). Human machine interface used for human-factors experiment, visualizing the position of each joint connected to the real-time dynamic simulation of a backhoe excavator.

projected side view as described by Kempkes (2007).

6.3.1. EXCAVATOR DYNAMICS AND HYDRAULICS

A backhoe excavator fixed on a pontoon consists of four degrees of freedom: rotation of the cabin around the vertical axis called slew and the three rotations in the 2D plane as shown in figure 6.1a) rotating the boom, stick and bucket. The two main axis to control the excavator in the 2D plane to conduct the excavation task are executed with the boom and stick. Rotating the bucket is to maintain a certain cutting angle throughout the process and to close the bucket when finished.

Each rotational joint links have a second order dynamics and are actuated by hydraulic cylinder forces. The links are modeled with a lumped mass model (6.1) and have water resistance by drag, gravity and actuation by hydraulic cylinders acted on this model. Both the stick and boom have two parallel cylinders mounted powering these links. The calculated rotational acceleration $\ddot{\theta}_{link}$ in (6.1) is integrated twice to reach a new joint angle using a Runge-Kutta ODE4 fixed step numerical solver in Matlab Simulink. The effective link arm for the cylinder actuation force is varied with the rotation of the joint, which is calculated by the angle γ between the cylinder and the link. The inertia is calculated for the link as the rotational inertia of the link mass m_{link} and the attached mass m_{add} (e.g. for the stick the bucket is attached as a point

mass at a given length form the stick's rotation).

$$\ddot{\theta}_{link} = \frac{F_{cyl} \cdot L_{arm} \cdot \left(cos(\frac{\pi}{2} - \gamma)\right)}{\frac{1}{3} \cdot m_{link} \cdot L_{link}^2 + m_{add} \cdot L_{add}^2} \tag{6.1}$$

The cylinder actuation force is calculated based on (6.2), using the cylinder piston side pressure p_{pist} and rod side pressure p_{rod} with corresponding surface areas based on the diameters d_{pist} and d_{rod}. Additionally the cylinder force is corrected for a stick-slip phenomena of 5% of the pressure as static friction in the seals.

$$F_{cyl} = p_{pist} \cdot \tfrac{\pi}{4} \cdot d_{pist}^2 - p_{rod} \cdot \tfrac{\pi}{4} \cdot \left(d_{pist}^2 - d_{rod}^2\right) \tag{6.2}$$

The cylinder pressure is controlled by hydraulic valves controlling the oil flow q_{valve} to the cylinder by an Orifice opening (6.3). The pressure difference Δp over the valve is either the difference between the pump pressure p_{pump} of 300 bar and the piston side pressure p_{pist}, or the rod side pressure p_{rod} of the cylinder. The flow through the valve controlling the cylinder is defined by the varying opening area $A_{valve,i}$, a function of the control input $\theta_{control,i}$, where i stands for either the boom of stick joint.

$$q_{valve,i} = C_d \cdot A_{valve,i}\{\theta_{control,i}\} \cdot \sqrt{\frac{2 \cdot \Delta p}{\rho_{oil}}} \tag{6.3}$$

The measured input control value is normalized to the maximum set boundary of θ_{max} of 40 degrees. This normalization factor is applied to the gain G_{valve} which correspondents to the maximal valve area, defined using (6.3) to reach a maximal flow of 550 l/min and 450 l/min for the boom and stick respectively for a maximal pressure difference over the valve.

$$A_{valve,i} = \frac{\theta_{control,i}}{\theta_{max}} \cdot G_{valve} \tag{6.4}$$

The cylinder pressures in (6.5) and (6.6) are based on the bulk modulus B_s of 1.2 GPa, the compressibility of the oil, combined with the static volume V_{pipes} and the moving cylinder stroke L_{cyl}.

$$\begin{aligned} p_{pist} &= B_s \cdot \frac{\int q_{valve,i}(t)dt - V_0(t)}{V_0(t)} \\ &\text{with,} \\ V_0(t) &= L_{cyl}(t) \cdot A_{pist} + V_{pipes} \end{aligned} \tag{6.5}$$

The cylinder pressure of the rod side in (6.6) is almost equal to the piston side, only in reversed direction for the moving cylinder compared to the maximal stroke L_{stroke}.

$$\begin{aligned} p_{rod} &= B_s \cdot \frac{\int q_{valve,i}(t)dt - V_0(t)}{V_0(t)} \\ &\text{with,} \\ V_0 &= \left(L_{stroke} - L_{cyl}(t)\right) \cdot A_{rod} + V_{pipes} \end{aligned} \tag{6.6}$$

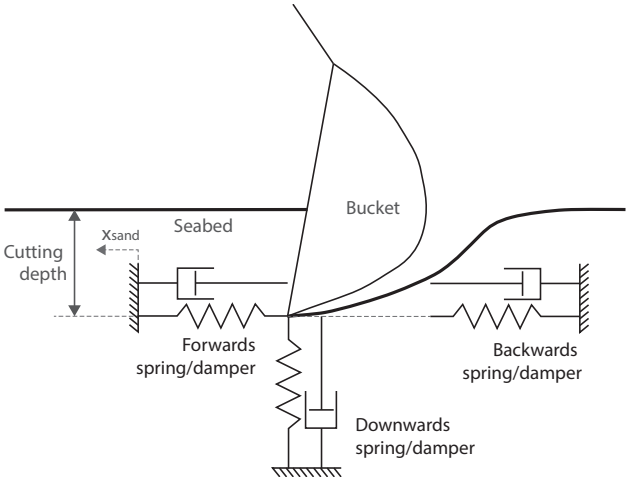

Figure 6.6: Soil interaction model including spring/damper interactions. The forward cutting force is modeled as a spring/damper which moves along (x_{sand}) with the bucket position when the maximal cutting force is exceeded for the particular cutting depth. The downward spring supports the bucket and the backwards spring restricts backwards motion of the bucket.

The hydraulic flow in (6.3) is created by opening the valve area in (6.4), creating the cylinder pressures of (6.5) and (6.6). However external forces also influence this pressure, such as drag resistance in the water, gravity and interaction with the environment.

6.3.2. SOIL INTERACTION

The soil interaction is modeled based on a realistic maximal soil resisting model adapted from Kuiper et al. (2016), originating from the sand cutting model of Miedema and Zijsling (2012) developed for modeling a macroscopic failure mechanism. The resisting force is modeled on the excavator by means of a spring stiffness, as indicated with the forward spring/damper in figure 6.6. The spring is compressed up to the force level that the soil maximally can resist for that particular cutting depth. When the force level is exceeded the spring force is kept constant and the initial spring position (x_{sand}) is pushed forward, indicating the removal of the seabed.

The maximal soil resisting force F_{soil} is calculated with the simplified model in (6.7), based on the varying soil cohesive stress c and cutting depth h_i. Furthermore static parameters are included in the calculation of the bucket width w, internal soil friction angle ϕ, cutting angle α and external friction angle δ between the bucket and the soil.

$$F_{soil} = \frac{2 \cdot c \cdot h_i \cdot w \cdot cos(\phi) \cdot sin(\alpha + \delta)}{1 + cos(\alpha + \delta + \phi)} \tag{6.7}$$

The cohesive stress c is based on the sand unconfined compressive strength σ_{UCS} and the internal friction angle ϕ, as shown below in (6.8).

$$c = \frac{\sigma_{UCS} \cdot [1 - sin(\phi)]}{2 \cdot cos(\phi)} \tag{6.8}$$

The cutting force the that is applied on the excavator is either based on the spring force $F_{env.spr}$ or on the soil resisting force F_{soil} when the spring is fully compressed, as shown below in (6.9).

$$F_{cut} = min\left(F_{soil}\,,\, F_{env.spr}\right) \tag{6.9}$$

When the spring force is limited by the maximal soil resisting force as described in (6.9), the spring position $x_{env.spr}$ (x_{sand} in fig 6.6) is shifted simultaneously with the bucket position x_{bucket} combined with the spring deflection $u_{env.spr}$ at that instance. In (6.10) this horizontal cutting spring force is shown with the spring stiffness $K_{env,spr}$ of 5.0 kN/mm and spring damping $B_{env.spr}$ of 10 kNs/mm , resulting in a spring deflection of 20 mm for a cutting force of 10 ton at a cutting depth of about 1 m.

$$\begin{aligned} F_{env.spr} &= K_{env.spr} \cdot u_{env.spr} + B_{env.spr} \cdot \dot{u}_{env.spr} \\ &\text{with,} \\ u_{env.spr} &= x_{bucket} - x_{env.spr} \end{aligned} \tag{6.10}$$

The detailed soil parameters used in the simulator are listed in the appendix table 6.2, including also the vertical and backwards resisting spring parameters as indicated in figure 6.6. The downward spring supports the bucket on the seabed, which moves downwards with the bucket at the applied cutting angle. The backwards spring restricts backwards motion of the bucket and always moves along with the bucket position.

6.4. HAPTIC FEEDBACK

Haptic feedback potentially enables the operator to be more aware of the state and capabilities of the controlled machine. This can be accomplished by two main components, awareness of the commanded inputs and knowledge of the machine's exerted force on the environment. Providing force feedback from the environment has shown to improve task performance by reduction of completion time (Hannaford et al., 1991). However force feedback from the environment is not suitable to be reflected directly when controlling the machine by rate control (Salcudean et al., 2000). In previous work a stiffness modulation was investigated and found most effective under rate control to reflect interaction forces to the operator (Kuiper et al., 2017).

Feedback of the environment interaction force can be used as a gain for the stiffness modulation feedback. The designed haptic feedback in (6.11) consists of three components, a static centering spring force $F_{spring,i}$, an excavator feedback force $F_{exe,i}$ and a boundary force $F_{boundary}$. The centering spring force depends only on the control input angle θ_i and informs the operator about the commanded input, where the index i represents either the boom or stick input. The boundary force informs about the maximum commanded inputs.

$$F_{feedback,i} = F_{spring,i} + F_{exc,i} + F_{boundary,i} \tag{6.11}$$

The centering spring force $F_{spring,i}$ is described in detail in section 6.4.1 and visualized in figure 6.7a). The feedback force $F_{exc,i}$ is described in section 6.4.2 and shown in figure 6.8a). The boundary force $F_{boundary}$ is only modeled as a basic spring with stiffness K_{bdr} of 30 Nm/rad acting beyond the boundary limitation θ_{bdr} of 40 degrees.

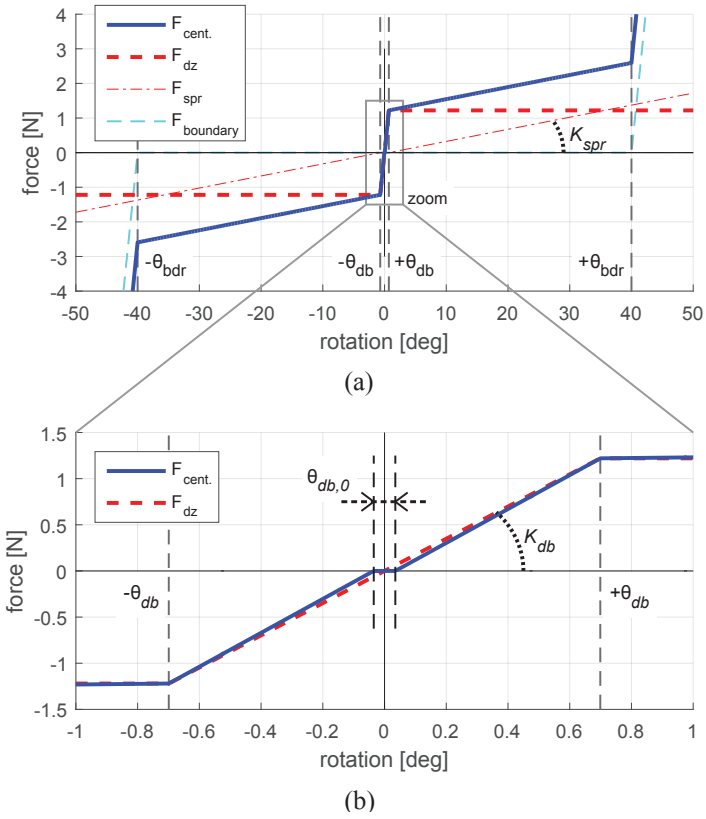

Figure 6.7: The static centering spring design $F_{cent.}$. It illustrates the combination of the individual components, including the boundary force at $\theta_{boundary}$. a) indicating the static spring stiffness components of a basic soft spring F_{spr} and the deadzone spring F_{dz}. b) the zoomed in part of centering spring around the deadband θ_{db}, indicating zero correction at $\theta_{db,0}$ to the deadband part of the centering spring

6.4.1. CENTERING SPRING FORCE

In previous work the effect of centering springs amongst others was investigated for the task execution of rate controlled machines (Kuiper et al., 2017). The work resulted in showing benefits of a centering spring with a clear distinction between a zero-velocity and acceleration or deceleration command. Therefore the centering spring force $F_{spring,i}$ described in (6.12) and shown in figure 6.7a) contains two components: a basic spring torque $T_{bas,spr,i}$ and a deadband spring torque $T_{db,spr,i}$. Both torques are converted to a force combined with the handle length L_{handle} of 150 mm, defined as the center of rotation to the center of the grip point where the force is felt by the user.

$$F_{spring,i} = \left(T_{bas,spr,i}\{\theta_i\} + T_{db,spr,i}\{\theta_i\}\right) \cdot L_{handle} \tag{6.12}$$

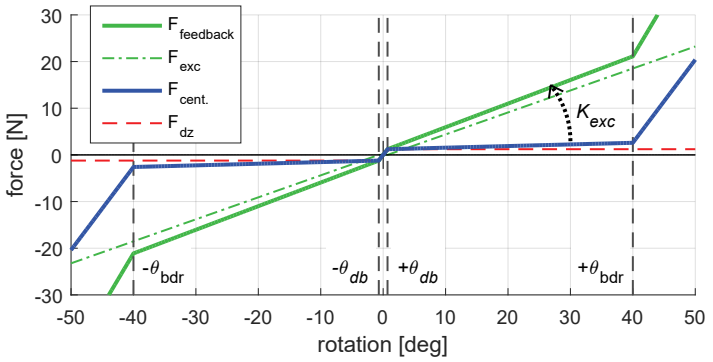

(a)

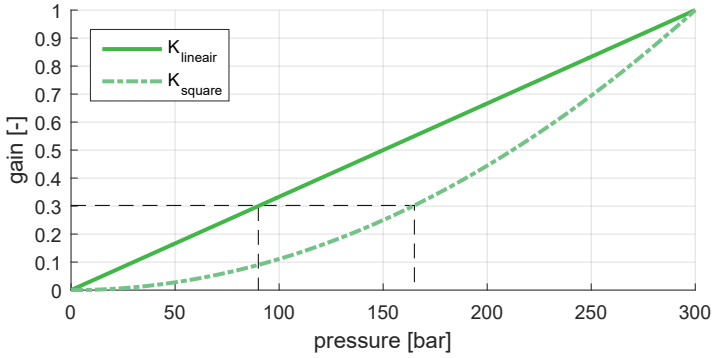

(b)

Figure 6.8: Feedback design from excavator. In a) the feedback force $F_{feedback}$. Indicating the total centering spring $F_{cent.}$ with additional stiffness K_{exc} from the feedback forming F_{exc} at maximal feedback. In b) the effect of the quadratic relationship is given between measured pressure and the feedback stiffness, highlighting feedback of measured pressures over 50% of the maximal pressure.

The centering spring force is split into two components, the basic spring force in (6.13) and the deadband force in (6.14). The basic spring in (6.13) is slightly complex formulated, but essentially acts only outside the deadband as a linear spring-damper. The control input θ_i stands for both the control inputs of the boom and the stick denoted with index i. The spring stiffness K_{spr} and damping coefficient b_{spr} in (6.13) are tuned to 0.6 Nm/rad and 0.06 Nm.s/rad respectively. such that is a noticeable but easily to overcome force of 1.4 N at full input.

$$T_{bas,spr,i} = K_{spr} \cdot max(|\theta_i| - \theta_{db},\, 0) \cdot sign(\theta_i) + B_{spr} \cdot \dot{\theta}_i$$

with,

$$B_{spr} = \begin{cases} 0, & |\theta_i| < \theta_{db} \\ b_{spr}, & |\theta_i| \geq \theta_{db} \end{cases} \tag{6.13}$$

The deadband spring torque $T_{db,spr,i}$ in (6.14) is the high gain spring element within the deadband θ_{db} of 0.7 degrees (1 % of full rotation of $2 \cdot 70$ degrees). The spring stiffness K_{db} is tuned to 30 Nm/rad, and damping b_{db} remains 0.06 Nm.s/rad in (6.14), resulting in maximal 1.2 N for an input of 0.7 degrees or more. This enables a clear force threshold to overcome when pushing the joystick out of zero.

$$\begin{aligned} T_{db,spr,i} &= K_{db} \cdot min(|\theta_i|,\, \theta_{db}) \cdot sign(\theta_i) + B_{db} \cdot \dot{\theta}_i \\ &\text{with,} \\ B_{db} &= \begin{cases} b_{db}, & |\theta_i| < \theta_{db} \\ 0, & |\theta_i| \geq \theta_{db} \end{cases} \end{aligned} \tag{6.14}$$

An addition to the deadzone feedback torque of (6.14) is applied to increase the stability of the haptic feedback algorithm and therefore allow for larger feedback gains. This entails an additional zero range correction $\theta_{db,0} = p_{zero} \cdot \theta_{db}$ within the deadband, with p_{zero} of 5%. This addition is visualized n the zoomed in part in figure 6.7 (b).

$$\begin{aligned} &\text{for } |\theta_i| < \theta_{db}\,, \\ T_{db,spr,i} &= K_{db} \cdot max(|\theta_i| - p_{zero} \cdot \theta_{db},\, 0) \cdot sign(\theta_i) \\ &\text{with,} \\ K_{db} &= \begin{cases} 0, & |\theta_i| \leq p_{zero} \cdot \theta_{db} \\ k_{db} \cdot \frac{1}{1-p_{zero}}, & |\theta_i| > p_{zero} \cdot \theta_{db} \end{cases} \end{aligned} \tag{6.15}$$

Optionally this inner part can be changed by a so called S-curve function or a cosine function to increase the smoothness of the force fade in. However in practice this did not show any increasing stability by allowing larger feedback gains compared to the described linear method.

6.4.2. EXCAVATOR FEEDBACK FORCE

The feedback of the environment interaction forces from the excavator is based on the hydraulic pressure measured in the cylinders. The feedback method is a stiffness modulation based on previous work (Kuiper et al., 2017) for reflecting environment interaction forces for a rate controlled task. This method is comparable to the stiffness modulation for the automotive application of reflecting augmented guidance forces on a steering wheel (Abbink and Mulder, 2009; Abbott and Okamura, 2003). The feedback force $F_{exc,i}$ in (6.16) is equal for both control inputs θ_i, boom steering and stick steering input angles. The stiffness modulation is visualized in figure 6.8a) additional to the previous described centering force.

$$F_{exc,i} = K_{exc}\{p_{hydr,i}\} \cdot \theta_i \cdot L_{handle} \tag{6.16}$$

The stiffness K_{exc} in (6.16) is based on the measured hydraulic pressure $p_{hydr,i}$ of the excavator. The varying feedback stiffness K_{exc} is defined in (6.17), reflecting either the positive

or negative part of the feedback gain $G_{fb,i}$, depending on the sign of the control input θ_i.

$$K_{exc} = \begin{cases} +max\left(G_{fb,i}\ ,\ 0\right) \cdot k_{max,exc}, & \theta_i > 0 \\ -min\left(G_{fb,i}\ ,\ 0\right) \cdot k_{max,exc}, & \theta_i < 0 \end{cases} \tag{6.17}$$

The feedback gain $G_{fb,i}$ defined in (6.18) is based on the difference between the normalized piston and rod side of the hydraulic cylinder. The pressure is normalized by dividing it with the maximal hydraulic pressure p_{max} of 300 bar. This normalized pressure of both the rod and piston side is taken quadratically to amplify in-contact forces on top of the typical forces acting on the cylinders such as gravity. The maximal feedback gain $k_{max,exc}$ is tuned to 7.5 Nm/rad, resulting in a maximum feedback force of 17.5 N for a full rotational input of 40 degrees.

$$G_{fb,i} = \left[\frac{p_{pist,i}}{p_{max}}\right]^2 - \left[\frac{p_{rod,i}}{p_{max}}\right]^2 \tag{6.18}$$

The quadratic component of the normalized pressure in (6.18) enables the distinction between background noise and the relevant forces based on the measured pressures. This method is required because no direct force measurement of the interaction forces is possible on such machines due to the harsh conditions the bucket is operating in. This quadratic method reduces the additional forces of gravity, water resistance and friction and therefore focuses on reflecting the interaction forces based on the measurements. This is partly visualized in figure 6.8a) where the difference is shown for a typical noticeable value of 30 % feedback, now corresponding to more than 50 % cylinder pressure.

6.5. EXPERIMENTAL RESULTS

A proof-of-concept experiment was conducted to illustrate the capabilities of the combined contributions of this paper. The experiment incorporates the force reflecting joystick Tria*R*, the excavator simulator and visualization, combined with reflecting haptic feedback on the joystick based on the simulator measured variables of section 6.2, 6.3 and 6.4 respectively.

The experiment consists of three main events, (I) making contact, (II) transition of soil conditions and (III) contact a boulder. The measured results are shown in figure 6.9 for the excavator position and forces, and in figure 6.10 the operator control inputs and feedback forces.

6.5.1. PROCEDURE

The task procedure consisted of a participant controlling a simulated virtual backhoe excavator, visualized using the human machine interface as shown in figure 6.5. The excavator was controlled using the developed joystick Tria*R* as shown in figure 6.2, only using the two main axis controlling the boom and stick angle (bucket automated relative to vertical and fixed slew angle). The force feedback algorithm as described in section 6.4, based on the measured hydraulic cylinder pressures of the virtual excavator. During the experiment the offered feedback was demonstrated for three events of controlling a backhoe excavator, showing the capabilities

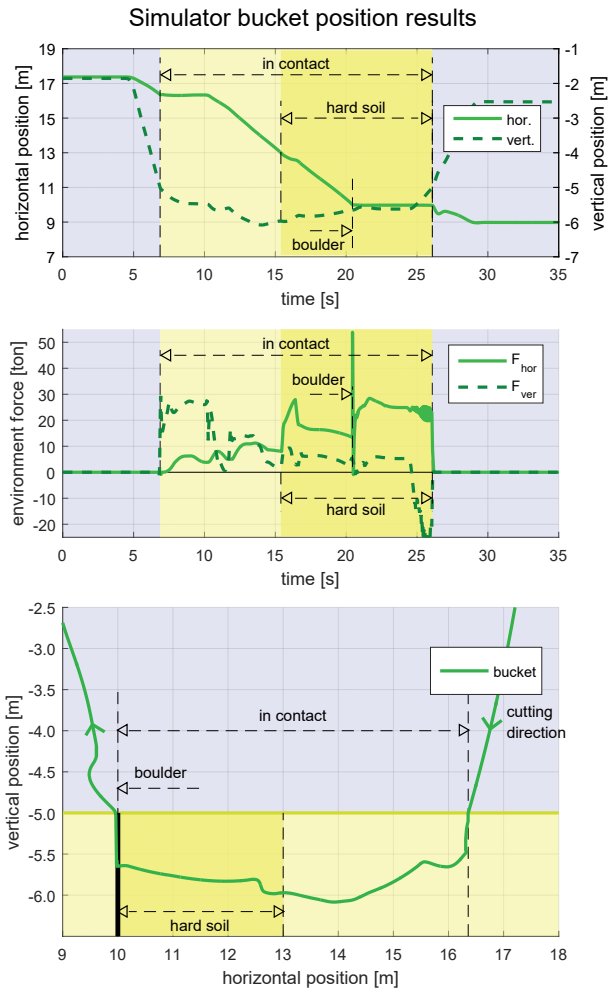

Figure 6.9: Simulation results of the human factors case study demonstrating haptic feedback for controlling an excavator. Position results of the tip of the bucket of the controlled excavator, with the horizontal and vertical component separately over time in the top figure and corresponding forces in the middle. The lower figure displays vertical position over the horizontal combined.

of the force reflecting method for these events. The results describe the closed-loop behavior of the combined system as described in figure 6.2b).

The task started with the tip of the bucket of the excavator fully submerged in the water, 3 meters above the seabed with a almost fully extended stick. From this start position the instruction was first (I) to quickly make contact with the seabed and fully cut into the soil. Then when the bucket cannot go deeper into the soil a horizontal cutting motion of the bucket teeth was conducted at full speed. Halfway the horizontal cutting motion the soil properties changed (II) into a harder layer of material, 3 times the start conditions. Finally at the end of

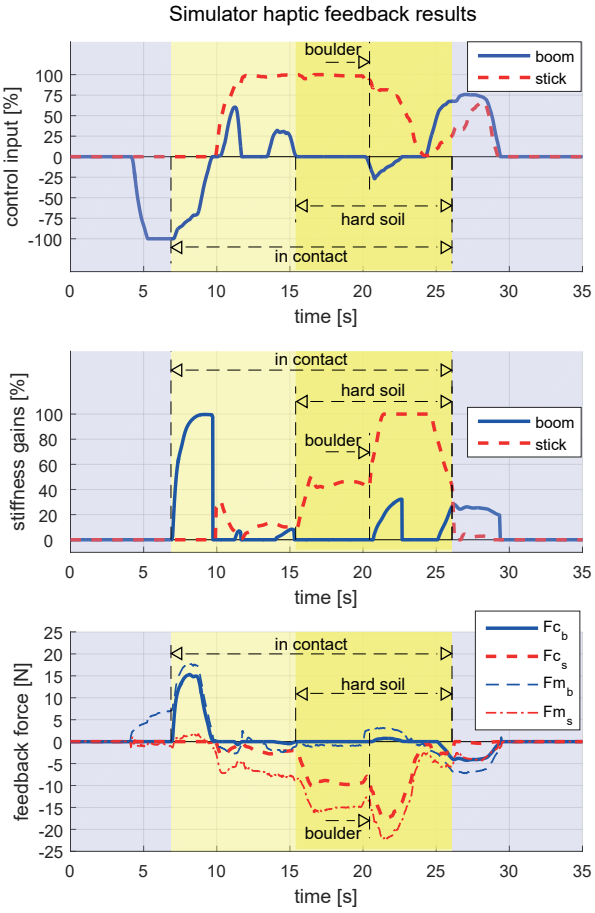

Figure 6.10: Simulation results of the human factors case study demonstrating haptic feedback for controlling an excavator. Haptic feedback results when controlling the excavator with the control input on top, stiffness modulation gain in the middle and reflected forces at the bottom including the measured forces.

the horizontal stroke a hard boulder was modeled (III), not penetrable nor moving and forcing the bucket to a full stop. After making contact the instruction was to recover from it by uplifting the bucket out of the seabed in an upward direction.

6.5.2. RESULTS

The results show the excavators bucket endpoint position in the environment in figure 6.9 along with the interaction forces. This describes the task execution in the lower figure indicating the vertical position with respect to the horizontal position. The upper part in figure 6.9 shows the same position for both horizontal as vertical with respect to time, indicating the three events and how they were executed. The middle part shows the environment interaction forces for the three main events, which are essentially reflected by the hydraulic pressure measurements to

the operator.

In figure 6.10 are the results shown for the operators input and felt feedback forces. This shows the control inputs in the top with respect to time during the three main events. In the lower part in figure 6.10 are the measured and calculated feedback forces shown, where the measured forces also include the static centering spring stiffness. The middle part shows the stiffness modulation gains over time, based on the measured hydraulic pressure for each controlled joint.

I) MAKING CONTACT WITH SEABED

In the lower part of figure 6.9 is the start of the executed task indicated with the cutting direction from right to left, first making contact with the seabed at 16.4 m horizontally. The cutting from right to left is because the excavator only cuts material towards the pontoon. The same data of the lower part figure 6.9 can be seen in the upper part for the time traces horizontally and vertically, making contact at the time interval of 7 seconds. After the interaction force has settled after impact for about 3 seconds the forward motion is initiated to start cutting through the seabed, shown in the middle part of figure 6.9.

The same effects for making contact can also be seen for the control inputs in the upper part of figure 6.10. First a downward motion is initiated and held after making contact for about 3 seconds, then about 3 seconds after making contact the stick motion is initiated. In the middle part of figure 6.10 can be seen that after making contact the stiffness modulation gain rapidly increases completely for the boom angle, similar to the interaction forces measured and reflected. Additionally the measured feedback forces show initially the static centering component before making contact with the seabed at approximately 5 seconds time interval. The feedback force at impact shows an increase from 7 N to 18 N, 2.6 times the force after impact.

II) TRANSITION IN SOIL CONDITIONS

After making contact, first soft material was removed between 16.4 m and 13 m horizontally as indicated in the lower graph of figure 6.9. It can be noted that cutting with a straight line in soft soil conditions of 100 kPa is challenging and requires constant corrections on the boom angle as can be seen in the top part of figure 6.10. After motion initiation at 10 seconds the interactions forces are about 10 tons, but hardly reflected to the operator as can be seen in 6.10. This low force reflection is due to the quadratic term in the feedback gain of Eq. (6.18), which reduces low interaction forces and emphasizes the unexpected larger interaction forces.

This emphasize is noticeable when transitioning to hard soil at about 15 s, 13 m horizontally. This increase is 3 times the soft soil condition and is reflected with approximately 45% of added stiffness gain, resulting in an addition of about 8 N of reflected environment force at full control input. The lower part in figure 6.10 shows this transition to 16 N clearly on top of the static centering force of about 8 N, an increase of 2 times the feedback.

III) CONTACT WITH HARD BOULDER

At 10 m horizontal position a hard boulder was modelled in the soil, not penetrable nor moving. Therefore it can be seen that at 20 seconds initial contact was made with the boulder. Because

of the inertia of the excavator and the spring stiffness in the hydraulics, this resulted in a spike in interaction force at impact. In the top part of figure 6.10 it can be seen that for about 2 seconds the input was maintained in a forward direction, to clearly demonstrate the feedback force. When making contact the reflected force is maximal 22 N, about 1.4 times the feedback compared to when in contact with hard soil.

At 24 seconds the forward control input is reduced and the bucket end position is uplifted by an upward boom motion. This resulted in the bucket sliding over the boulder surface until no longer in contact with the seabed at about 26 seconds. After contact has been lost the horizontal feedback gain immediately drops and only gravity resulted in some feedback.

6.6. CONCLUSIONS

An excavator simulator was developed with haptic feedback capabilities, to enable the design and evaluation of haptic feedback algorithms for improving the control of backhoe dipper dredgers. The simulator development firstly includes the design and fabrication of a high fidelity force reflecting joystick with integrated grip sensor. Secondly the simulator contains a dynamic model of a virtual backhoe excavator. Thirdly a haptic feedback algorithm was designed to reflect environment interaction forces of the endpoint of the backhoe excavator when cutting through soil. Finally the combined closed-loop system is evaluated using a human factors case study experiment.

The designed joystick is capable of reflecting forces on three rotational degrees of freedom with integrated grip sensor. With the two main axis capable of 130 degrees rotation, and the vertical axis up to 250 degrees of rotation in total. The joystick is tested capable of reflecting forces up to 10 Hz for the two main axis and 6 Hz for the vertical axis, all beyond human capabilities. The mechanical design is designed for force capabilities up to 100 N at the handle, but for now electrically limited up to 25 N at end point. The grip sensor is capable of measuring force up to 22.6 kg in four individual directions. This joystick design enables a variety of haptic feedback methods to be investigated for rate controlled machines with a large workspace and high quality force capabilities.

The case study results show that the three main simulated events were clearly noticeable in the force feedback to the operator by stiffness modulation for, I making contact, II transition of soil conditions, III making contact with a hard boulder. Making contact increased the stiffness gains rapidly, resulting in a feedback force of 11 N in 700 ms time. The transition to three time the hardness of the soil resulted in 8 N force increase and making contact with a boulder in 6 N in 800 ms. This was all conducted while maintaining stability of the closed-loop system and completing the total task execution.

This study shows that the developed simulator is cable of reflecting various types of events when controlling a backhoe excavator. The developed hardware is suitable for various types of experiments with force feedback and the designed haptic feedback algorithm showed capable of reflecting these events, although the simulator is not limited to this algorithm. Future work will consist of quantifying the beneficial effect of the force feedback for controlling an excavator. Additionally the effect of reflecting natural occurring forces will be compared to offering artificial

augmented guidance forces such as haptic shared control. It needs to be investigated if these two methods can offer incremental support to the operator without conflicting in information.

APPENDIX A: SIMULATION PARAMETERS

Table 6.1: Simulator Parameters

Variable	Symbol	Value
Boom link length	L_{bm}	12.0 m
Stick link length	L_{st}	7.0 m
Bucket link length	L_{bc}	2.3 m
Boom link mass	m_{boom}	14.1 ton
Stick link mass	m_{stick}	7.1 ton
Bucket link mass	m_{bucket}	3.9 ton
Boom piston diameter	$d_{pist,bm}$	260 mm
Boom rod diameter	$d_{rod,bm}$	80 mm
Boom cylinder stroke	$L_{stroke,bm}$	2.35 m
Stick piston diameter	$d_{pist,st}$	225 mm
Stick rod diameter	$d_{rod,st}$	80 mm
Stick cylinder stroke	$L_{stroke,st}$	1.97 m
Boom cylinder arm	$L_{arm,bm}$	4.85 m
Stick cylinder arm	$L_{arm,st}$	1.06 m
Pump pressure	p_{pump}	300 bar

Table 6.2: Soil Parameters

Variable	Symbol	Value
unconfined compressive strength	σ_{UCS}	100 kPa
internal friction angle	ϕ	30 deg
external friction angle	δ	20 deg
cutting angle	α	45 deg
target cutting depth	h_i	0.5 m
blade width	h_b	1.5 m
hard soil USC gain	G_{UCS}	3
horizontal cutting stiffness	$K_{env,spr}$	5.0 kN/mmm
horizontal damping gain	$B_{env,spr}$	10 kNs/mm
boulder stiffness	$K_{boulder}$	5.0 kN/mm
boulder damping gain	$B_{boulder}$	0.5 kNs/mm
vertical resistance stiffness	K_{vert}	0.5 kN/mm
vertical damping gain	B_{vert}	1.0 kNs/mm
backwards resistance stiffness	K_{back}	1.0 kN/mm
backwards damping gain	B_{back}	10 kNs/mm

REFERENCES

Abbink, D., Mulder, M., and Boer, E. (2012). Haptic shared control: smoothly shifting control authority? *Cogn. Technol. Work*, pages 19–28.

Abbink, D. A. and Mulder, M. (2009). Exploring the Dimensions of Haptic Feedback Support in Manual Control. *J. Comput. Inf. Sci. Eng. Spec. Haptics Ed.*, 9(March):1–9.

Abbott, J. and Okamura, A. (2003). Virtual fixture architectures for telemanipulation. *IEEE Int. Conf. Robot. Autom.*, pages 2798–2805.

An, B. and Stiles, W. (2002). Haptic Feedback Joystick. *Assignee Microsoft Corp.*, page 17.

Draper, J., Moore, W., Herndon, J., and Weil, B. (1987). Effects of Force Reflection of Servomanipulator Task Performance. *Energy*.

Elton, M. D. and Book, W. J. (2011). Comparison of human-machine interfaces designed for novices teleoperating multi-DOF hydraulic manipulators. In *IEEE Int. Symp. on Robot and Human Interactive Communication*, pages 395–400.

Elton, M. D., Enes, A. R., and Book, W. J. (2009). A virtual reality operator interface station with hydraulic hardware-in-the-loop simulation for prototyping excavator control systems. In *IEEE/ASME Int. Conf. on Advanced Intelligent Mechatronics*, pages 250–255.

Gosselin, C. and Angeles, J. (1990). Singularity Analysis of Closed-Loop Kinematic Chains. *IEEE Trans. Robot. Autom.*, 6(3):281–290.

Hannaford, B., Wood, L., McAffee, D. A., and Zak, H. (1991). Performance evaluation of a six-axis generalized force-reflecting teleoperator. *IEEE Trans. Syst. Man Cybern.*, 21(3):620–633.

Hoevenaars, A. G., Lambert, P., and Herder, J. L. (2014). Kinematic design of two elementary 3DOF Parallel Manipulators with Configurable Platforms. *Mech. Mach. Sci.*, (January 2016):315–322.

Kempkes, A. (2007). Dredging Monitoring System for marine excavators. In *Proc. West. Dredg. Assoc. (WEDA XXVIII) Tech. Conf. Dredg. Semin.*, page 10, Brazil.

Kontz, M. E. and Book, W. J. (2006). *Kinematic analysis of backhoes/excavators for closed-loop coordinated control*, volume 8. IFAC.

Kuiper, R. J., Chen, X., and Frumau, J. C. L. (2016). Reduction of Energy Consumption When Using a Grab for Deep-Sea. In *Offshore Technol. Conf. 2016*, page 13, Houston. OnePetro.

Kuiper, R. J., Wildenbeest, J. G. W., Helm, F. C. T. V. D., Abbink, D. A., and Member, S. (2017). Exploring Haptic Feedback Designs for Rate Controlled Systems. *IEEE Trans. Haptics*, submitted.

Lawrence, P., Salcudean, S., and Sepehri, N. (1997). Coordinated and force-feedback control of hydraulic excavators. In *Exp. Robot. IV*, pages 181–194.

Massimino, M. and Sheridan, T. (1989). Variable force and visual feedback effects on teleoperator man/machine performance. *Proc.of NASA Conf. Sp. Telerobotics*, pages 89–98.

Miedema, S. A. and Zijsling, D. (2012). Hyperbaric Rock Cutting. In *Proc. ASME Int. Conf. Ocean. Offshore Artic Eng.*, pages 1–14.

Mourik, R. and Ouwerkerk, R. (2010). Automated Excavator, First Experiences in Germany. In *Proc. West. Dredg. Assoc. (WEDA XXXI) Tech. Conf. Dredg. Semin.*, pages 92–103.

Mugge, W., Abbink, D. A., and Frans, C. T. (2007). Reduced Power Method : how to evoke low-bandwidth behaviour while estimating full-bandwidth dynamics. 00(c).

Mulder, M., Abbink, D. a., and Boer, E. R. (2012). Sharing Control With Haptics: Seamless Driver Support From Manual to Automatic Control. *Hum. Factors J. Hum. Factors Ergon. Soc.*

Nakamura, H., Abbink, D., and Mulder, M. (2011). Is grip strength related to neuromuscular admittance during steering wheel control? In *Conf. Proc. - IEEE Int. Conf. Syst. Man Cybern.*, pages 1658–1663.

Osafo-Yeboah, B., Elton, M., Jiang, X., and Book, W. (2010). Usability Evaluation of a Coordinated Excavator Controller with Haptic Feedback. In *Industrial Eng. Research Conf.*

Ostoja-Starzewski, M. and Skibniewski, M. (1989). A master-slave manipulator for excavation and construction tasks. *Rob. Auton. Syst.*, 4(4):333–337.

Parker, N., Salcudean, S., and Lawrence, P. (1993). Application of force feedback to heavy duty hydraulic machines. *[1993] Proc. IEEE Int. Conf. Robot. Autom.*, pages 375–381.

Roper, C., Lawrence, P., and Wallersteiner, U. (1989). Resolved Control of Teleoperated Systems. In *IEEE int. Conf. Ocean.*, pages 782–784, Seattle, USA.

Rosenberg, L. B., Braun, A. C., and Levin, M. D. (1998). Method and Apparatus for Controlling Force Feedback Interface Systems Utilizing a Host Computer. *Assignee Immers. Corp.*, page 58.

Rosenberg, L. B., Braun, A. C., and Schena, B. M. (2001). Low cost force feedback peripheral with button activated feel sensation.

Salcudean, S. E., Zhu, M., Zhu, W.-H., and Hashtrudi-Zaad, K. (2000). Transparent Bilateral Teleoperation under Position and Rate Control. *Int. J. Rob. Res.*, 19(12):1185–1202.

Sepehri, N. and Lawrence, P. D. (1992). Model-based sensor-based velocity control of Teleoperated Heavy-Duty Hydraulic Machines.

Smisek, J., Mugge, W., Smeets, J. B., van Paassen, M. M., and Schiele, A. (2017). Haptic guidance on demand: A grip-force based scheduling of guidance forces. *IEEE Trans. Haptics*, (November).

Tafazoli, S., Salcudean, S. E., Hashtrudi-zaad, K., and Lawrence, P. D. (2002). Impedance Control of a Teleoperated Excavator. 10(3):355–367.

Wildenbeest, J. G., Kuiper, R. J., van der Helm, F. C., and Abbink, D. A. (2014). Position control for slow dynamic systems: Haptic feedback makes system constraints tangible. *2014 IEEE Int. Conf. Syst. Man, Cybern.*, pages 3990–3995.

Wildenbeest, J. G. W., Abbink, D. A., Heemskerk, C. J. M., Helm, F. C. T., and Boessenkool, H. (2013). The Impact of Haptic Feedback Quality on the Performance of Teleoperated Assembly Tasks. *IEEE Trans. Haptics*, 6(2):242–252.

Wildenbeest, J. G. W., Kuiper, R. J., Van Der El, K., Van Der Helm, F. C. T., and Abbink, D. A. (2018). A Cybernetic Approach to Quantify the Effect of Haptic Feedback on Operator Control Behavior in Free-Space Telemanipulation.

Winck, R. C., Elton, M., and Book, W. J. (2015). A practical interface for coordinated position control of an excavator arm. *Automation in Construction*, 51(C):46–58.

PART III

EXPLORING HAPTIC GUIDANCE FEEDBACK

7

Evaluation of Haptic Shared Control Designs

Roel J. Kuiper, Dennis J.F. Heck, Irene A. Kuling, and David A. Abbink

published in IEEE Transactions on Human-Machine Systems, 2016

Augmented guidance forces can also be offered to the human operator instead of offering natural force feedback from previous chapter 3 and 4, informing of the occurring interaction forces. Guidance can be offered either as repulsive or attractive forces to the human operator, assisting in either collision prevention or as global task support. This chapter evaluates both methods by reflecting information content from the intelligent controller, either only including local environment information or global task information. These two information types are reflected either visually or haptically to the human operator while steering a virtual remote vehicle around obstacles to a specific target.

The working principle of the resulting four support designs are described in section 5.2 for the two information types (repulsive and attractive) and their two offered modalities (visual and haptic). The experimental methods of a human factors experiment for the evaluation is given in section 5.3, describing the virtual vehicle dynamics and environment. The experimental results are presented in section 5.4, including results of catch trials which incorporated errors in the support designs to test for over reliance on the support. It is concluded that it is most beneficial when global task information is available to reflect this using attractive haptic guidance.

Roel J. Kuiper, Dennis J.F. Heck, Irene A. Kuling, and David A. Abbink; Evaluation of Haptic and Visual Cues for Repulsive and Attractive Guidance in Nonholonomic Steering Tasks; IEEE Transactions on Human-Machine Systems, Vol 46, Issue 5, pp 672-683, 2016.

ABSTRACT

Remote control of vehicles is a difficult task for operators. Support systems that present additional task information may assist operators, but their usefulness is expected to depend on several factors such as 1) the nature of conveyed information, 2) what modality it is conveyed through, and 3) the task difficulty. In an exploratory experiment, these three factors were manipulated to quantify their effects on operator behavior. Subjects (n = 15) used a haptic manipulator to steer a virtual nonholonomic vehicle through abstract environments, in which obstacles needed to be avoided. Both a simple support conveying near-future predictions of the trajectory of the vehicle and a more elaborate support that continuously suggests the path to be taken were designed (factor 1). These types of information were offered either with visual or haptic cues (factor 2). These four support systems were tested in four different abstracted environments with decreasing amount of allowed variability in realized trajectories (factor 3). The results show improvements for the simple support only when this information was presented visually, but not when offered haptically. For the elaborate support, equally large improvements for both modalities were found. This suggests that the elaborate support is better: additional information is key in improving performance in nonholonomic steering tasks.

7.1. INTRODUCTION

REMOTE control, or teleoperation, is much more difficult for operators than direct manipulation due to delays and limited sensory feedback of the task (Massimino and Sheridan, 1989; Wildenbeest et al., 2013). Visual information from available cameras of the remote location is typically limited (in terms of view angle and depth perception) and makes it difficult to interpret what the actual state of the vehicle or manipulator is (Kim et al., 1987) and (Sayers et al., 1995). Vestibular feedback of the remote vehicular movements is inherently absent, unless linked to a motion-based simulator (Zaal et al., 2012). Moreover, naturally occurring auditory or haptic feedback of the vehicle interaction with the remote environment (e.g., wind gusts, currents, contact) is absent unless re-engineered (Sheridan, 1989).

An alternative to restoring natural sensory feedback is to add artificial task-related feedback. For example, limited visual feedback can be compensated for by using augmented reality such as grid lines to enhance depth perception (Kim et al., 1987). Other visual overlays (Lüttgen and Heuer, 2012; Milgram et al., 1995; Stigter et al., 2007), predictors (flight director, visual guidance for landing planes (Stigter et al., 2007)), or visual feedback can be replaced by virtual reality entirely (Sayers et al., 1995). Assistive haptic feedback can be presented as artificial guidance forces to the human operator. These guidance forces can be offered as passive guidance forces, also known as virtual fixtures, e.g., a virtual wall to support operators in a peg-in-hole task (Rosenberg, 1993). They can also be extended to more complex guidance using soft fixtures to create a virtual tunnel (Bettini and Marayong, 2004; Prada and Payandeh, 2009). For remote control of aerial vehicles in an unstructured environment, potential fields are commonly used to provide assistive haptic feedback (Diolaiti and Melchiorri, 2002; Lam et al., 2009, 2006). This method uses only nearby environment information around the vehicle without involving any task-related strategy and has been applied to subsea robotics (Sayers and Paul, 1994), needle

steering (Majewicz and Okamura, 2013), and telemanipulation (Abbott and Okamura, 2003). The required remote environment information is obtained from sensors on the vehicle.

Another, more comprehensive, approach to support operators with assistive haptic feedback is to use guidance toward an optimal steering input based on a suggested path. The feedback forces, based on a predicted vehicle position, act as a haptic prediction to the suggested path. This concept essentially acts as a second controller and is known as haptic shared control (Abbink et al., 2012; Steele and Gillespie, 2001). It has been applied to car driving (Abbink et al., 2012; Abbink and Mulder, 2009; Griffiths and Gillespie, 2005; Steele and Gillespie, 2001), subsea robotics (Kuiper et al., 2013), teleoperated surgery (Marayong and Okamura, 2004), and nuclear maintenance (Boessenkool et al., 2013).

Haptic guidance based on potential fields or haptic shared control has either been compared for a one-degree-of-freedom (DOF) steering task (Forsyth and MacLean, 2006), or solely combined for path planning and haptic guidance along an adaptive path (Brandt et al., 2007). In this study, both haptic guidance types are compared with each other and additionally compared to visual guidance based on similar additional information.

7.1.1. TYPE OF ADDITIONAL INFORMATION

For nonholonomic steering, task-related feedback to the user could come in the form of repulsive or attractive guidance cues. Repulsive cues relate to the likelihood of adverse events, such as collisions with nearby obstacles, whereas attractive guidance cues relate to a desired path throughout the entire environment. To calculate desired steering inputs to either avoid obstacles or follow the suggested path, detailed knowledge of the vehicle kinematics and dynamics is required. In contrast with information to avoid obstacles, the suggested path information also conveys strategic information and requires prerequisite knowledge of the task and the environment.

Furthermore, information can be conveyed through different modalities: either visually or haptically. An advantage of using the visual modality is that the information about the position and the required action can be very detailed. On the other hand, the visual channel can be easily overloaded, and other modalities have to be considered. Presenting information through the haptic channel is typically faster, since it enables the operator to respond to the forces through fast reflexes (Abbink and Mulder, 2009; Lüttgen and Heuer, 2012; Stigter et al., 2007). To compare the types of additional information between modalities, the calculated near-future predicted trajectory can be visualized to the operator by using augmented reality, or felt as an artificial haptic potential field. The same applies to the suggested path, which can both be visualized or reflected as a haptic shared controller.

The usefulness of the support system not only depends on the design of the support, but also on the difficulty of the task. Nonholonomic steering, used for vehicles with front wheel steering, is a common but relatively complex kinematic system to control (Rankine, 1869). The input relation between the steering angle and the resulting turning radius of the vehicle is easily underestimated (Majewicz and Okamura, 2013). When the task environment requires sharp steering angles close to the minimal turning radius of the vehicle, e.g., to avoid obstacles

along the way, the operator has limited options to change the current trajectory. The support system should help the operator decide the timing and magnitude of the correct steering inputs with respect to the spatial-temporal constraints of the environment. Depending on the task difficulty, either a local trajectory prediction to avoid obstacles or a suggested path incorporating a strategy to avoid obstacles throughout the entire environment might be more beneficial.

7.1.2. EXPERIMENTAL OUTLINE

In this study, a human factor experiment is conducted to test the effect of different types of information (predicted vehicle trajectory and suggested path, *factor 1*), presented in different modalities (visually and haptically, *factor 2*), on the performance of a nonholonomic steering task in environments of varying difficulty (*factor 3*). This is accomplished by using a haptic input device and a virtual abstract vehicle driving through several virtual mazes of varying difficulty. In this experiment, we aimed to compare the most promising ways to present to the operator identical sensor information through either the visual or the haptic channel.

It takes longer for the operator to process and react upon the visual information compared to the haptic information, since in the latter case the haptic guidance only needs to be agreed on. Therefore, it is hypothesized that receiving the information haptically would result in improved performance and reduced control effort compared to receiving the additional information visually (*factor 2*). Second, it is hypothesized that there is an interaction between the type of additional information (*factor 1*) and the task difficulty based on different environments (*factor 3*). It is expected that more information is particularly useful when the task difficulty is high. This aspect could be reflected in the interaction by improved performance and reduced effort; there will only be a performance benefit when the additional information of a suggested path is presented in environments with obstructed targets and not in environments with reduced distance between obstacles.

7.2. SUPPORT DESIGN

In this study, four types of support systems were designed and evaluated, each constituting a combination of two factors. The design included either only local environment information or also global task information. Additionally, the support system was either communicated via haptic or visual cues.

During all conditions, the vehicle, obstacles, and target location were shown on the visual display and transparent feedback forces (i.e., vehicle dynamics and contact forces) were reflected on the translational direction of the input device (further described in section 7.3.2). The haptic support systems were offered as a torque on the planar rotational steering direction of the input device. As a result, the reflected torques are decoupled from the natural forces and assist the operator in steering the vehicle. The following sections describe the different forms of haptic and visual support systems in more detail.

7.2.1. REPULSIVE HAPTIC GUIDANCE AROUND OBSTACLES

Repulsive haptic guidance is defined as a haptic potential field around the obstacles to assist the subjects in avoiding contact, similar to (Lam et al., 2009). Haptic guidance torques are generated based on a predicted position of the slave after a translation of L_p with the current orientation input of the master device. When the predicted slave position is within the detection distance d_p of the obstacle [see figure 7.1A], a virtual repulsive force is applied on a distance L_p from the current slave position. This virtual force is proportional, with gain k_p, to the penetration depth $d_p - d_s$. Furthermore, the repulsive forces are only reflected to the subjects when the slave tends to move toward an obstacle. This is done by activating the repulsive fields only when the obstacle is within an angle α of the orientation of the slave. Finally, in order to make a fair comparison with the application of attractive guidance, an attractor is designed around the target area. Apart from a negative stiffness gain k_s, the design of the attractor is similar to the design of the repulsive haptic guidance. For each obstacle i, the resulting repulsive guidance torque is implemented as,

$$\tau_{HR,i} = \begin{cases} k_p \cdot L_p \cdot (d_p - d_{si}), & \text{if } d_{si} \leq d_p \text{ and } |\theta_i| \leq \alpha \\ 0, & \text{else} \end{cases} \tag{7.1}$$

The guidance torque presented to the subjects is the sum of the guidance torques $\tau_{HR,i}$ for all obstacles, i.e.,

$$\tau_{HR} = \sum_{i=1}^{n} \tau_{HR,i} \tag{7.2}$$

with $n = 5$ the number of obstacles and attractors. The parameters were tuned to provide an informative repulsive torque that can be overruled by the subjects. The obtained values are $L_p = d_s = 10mm$, $\alpha = 90^o$, and $k_p = 6N/m$ for the repulsors and $k_p = -6N/m$ for the attractor of the target.

7.2.2. ATTRACTIVE HAPTIC GUIDANCE TO A SUGGESTED PATH

Attractive haptic guidance torques guide the operator toward a predefined suggested path from the starting position to the target location, similar to Abbink and Mulder (2009). The designed suggested paths avoid all obstacles with a minimal distance, equal to the distance d_p used for repulsive feedback (see Section 7.2.1), and consist of radii equal or larger than the minimal turning radius of the vehicle. The blue dashed line in figure 7.1C shows an example of such a suggested path through an environment. Comparable with the repulsive guidance, torques are computed from a virtual guidance force acting on an arm L_p from the current slave position. This virtual guidance force is proportional, with gain k, to the horizontal distance d between the suggested path and a predicted position of the slave [see figure 7.1B]. The sign of the virtual guidance force is related to the relative horizontal position of the suggested path with respect to the predicted slave position and results in a guidance torque towards the suggested path. The predicted position of the slave is updated online and obtained by computing the slave position after a translation of L_p with the current orientation input of the master device. By rotating

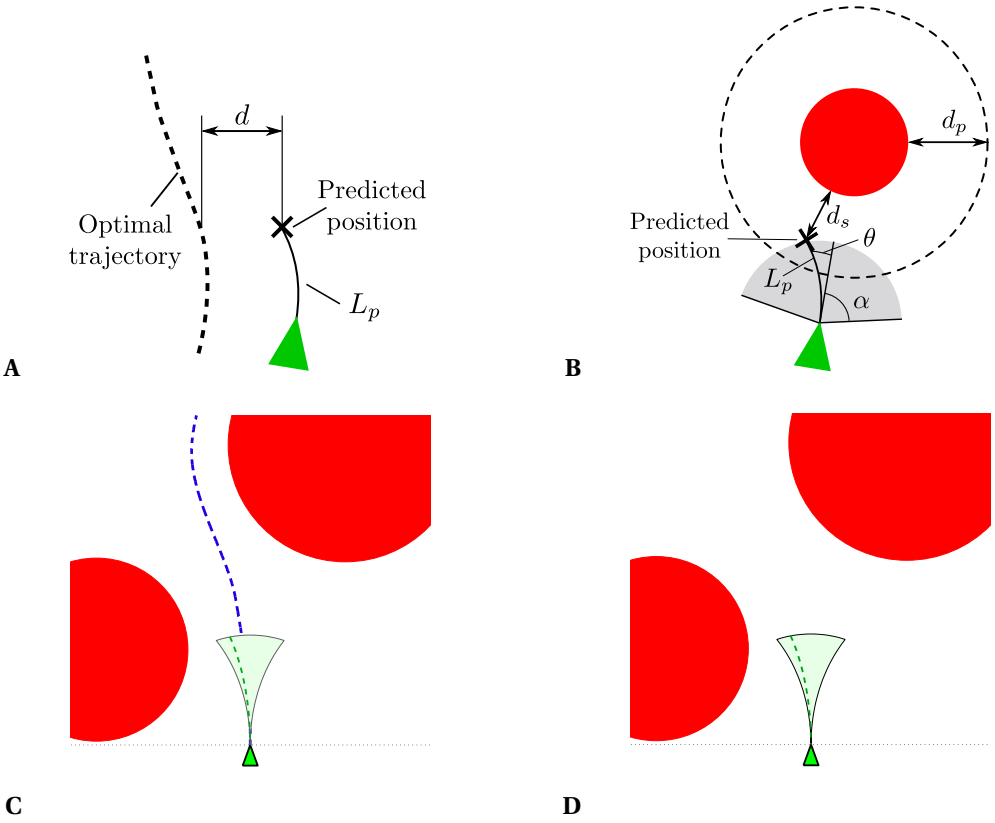

Figure 7.1: Representation of the underlying information required to generate the haptic support, in their simple realizations and their more elaborate realizations, and how this was displayed for their visual equivalent. (A) Repulsive haptic guidance (HR) around an obstacle, based on the predicted slave position. (B) Attractive haptic guidance (HA) to a suggested path also based on the predicted slave position. (C) Example of repulsive visual guidance (VR) displaying the predicted slave position visually in green. (D) Example of attractive visual guidance (VA), displaying the entire suggested path in blue throughout the environment in combination with the predicted slave position.

the master device, the predicted position of the slave is affected, resulting in a change in the distance d. As a result, the subjects feel a torsional stiffness on the master device. The attractive guidance torque is implemented as

$$\tau_{HA} = k \cdot L_p \cdot d \tag{7.3}$$

The distance L_p and stiffness k were tuned to provide an informative assistive torque that can be overruled by the subjects. The obtained values are $L_p = 0.01m$ and $k = 5N/m$.

7.2.3. VISUAL EQUIVALENT SUPPORT SYSTEM

The haptic guidance is either based on information of the suggested path (attractive guidance) or information to prevent collisions with the obstacles (repulsive guidance). In order to investigate

if the transmitted type of additional information or the reflection via the haptic channel results in improved performance for this task, this information is also visually represented. In the visual equivalent of the repulsive haptic guidance, subjects received visual information regarding the predicted slave position. The predicted slave position is indicated by a green dashed line starting from the front of the slave [see figure 7.1C]. This line informs the subjects where the slave will be when the master is translated $L_p = 1cm$ with the current orientation. The green area reflects the range of possible slave steering angles, taking into account the maximum steering radius. In the visual version of the attractive guidance, subjects additionally received information regarding the suggested path, indicated with a blue dashed line from start to target. Both the predicted slave position and the suggested path are visualized, as shown in figure 7.1D.

7.3. EXPERIMENTAL METHODS

7.3.1. SUBJECTS

Fifteen subjects, ten males and five females, with an average age of 26.7 years and 3.8 year standard deviation, volunteered for the experiment. All subjects had no experience with tele-operation and were naive about the experiment. All subjects gave their written informed consent prior to the experiment. The setup and experiments were approved by the local ethics committee of the Delft University of Technology.

7.3.2. APPARATUS

The experiments were performed using a three DOF planar parallel master device (as depicted in figure 7.2) (Christiansson, 2007) and a virtual slave, running on a Mathworks xPC Target real-time operating system at 1 kHz with an estimated time delay between master and slave of 1.5 ms.

Subjects were holding a knob at the center of rotational input of the master device and controlling the horizontal translation and rotation. The forward translation of the master device was coupled to the radial translation of the virtual slave. To make the coupling to the slave tangible, a translational damping field of 50 Ns/m was applied. The rotation of the master device was coupled to the steering of the virtual slave. The lateral translation of the master device was constrained with a stiffness of 400 N/m and not used for controlling the virtual slave.

The dynamics of the slave are represented by a planar second order bicycle model of two DOFs (orientation and radial translation) (Rankine, 1869). The virtual vehicle has a theoretical wheelbase of 0.05 m, with maximum steering angle of the front axle of 60^o. It is represented as a dimensionless point, based on the rear wheel position represented by a green triangle as shown in figure 7.1. The orientation of the vehicle is only affected when both the steering angle and forward or backward translation of the vehicle are controlled. Both forward and backward motion are allowed for master and slave, such that reversing of the slave is enabled. When reversing, the bicycle model is used with negative translational vehicle velocity such that the direction of steering is reversed. The translation of the slave is restricted when it collides with

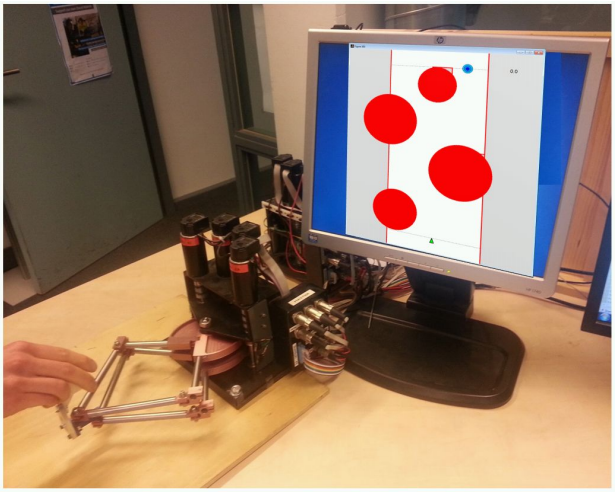

Figure 7.2: Experimental setup showing an operator holding the planar haptic master device and the display showing the virtual slave and environment.

an obstacle. Subjects must reverse the slave direction in order to continue the trial.

7.3.3. VIRTUAL ENVIRONMENT

The four virtual environments in which the slave operates measure 5 by 10 cm, as shown in figure 7.3. The slave starts at the horizontal line at x = 0 m and the target is located on a horizontal line at x = 0.1 m. The location of the target area on this horizontal line is indicated by three coincided circles (of 1-, 2-, and 3-cm diameter) of different shades of blue. The obstacles are indicated by the red circles and a green triangle represents the slave. The whole virtual environment including all obstacles and the target was always shown visually to the subjects.

Two factors of spatio-temporal constraints were varied in the experiment, namely the space between obstacles and the difficulty of reaching the target by partly blocking the approach. The distance between the edge of the first and second obstacles (d_1) was varied between 9 and 15 mm, the distance between the second and third obstacle (d_2) was varied between 10 and 15 mm, and the horizontal distance between the last object and the target (d_{tg}) ranged between 5 and -1 mm. The four different environments, shown in figure 7.3, are defined as follows.

EE Easy to avoid obstacles ($d_1 = 15$, $d_2 = 15$)
and Easy to reach the target location ($d_{tg} = 5$).

DoEt Difficult to avoid Obstacles ($d_1 = 9, d_2 = 10$),
but Easy to reach the Target location ($d_{tg} = 5$).

EoDt Easy to avoid Obstacles ($d_1 = 15, d_2 = 15$),
but Difficult to reach the Target location ($d_{tg} = -1$).

DD Difficult to avoid obstacles ($d_1 = 9, d_2 = 10$)
and Difficult to reach the target location ($d_{tg} = -1$).

7.3.4. EXPERIMENT DESIGN

During the experiments, the following five experimental conditions were presented in separate blocks to assist the subjects in completing the task. The colors used in the figures of section 7.4 are stated between the parentheses.

NO NO haptic or visual guidance. This condition forms the benchmark (blue);

VR Visual Repulsive information about the predicted slave position (red);

VA Visual Attractive information about both the predicted slave position and suggested path (orange);

HR Haptic Repulsive guidance, resulting from the predicted slave position and the objects (dark green);

HA Haptic Attractive guidance resulting from the predicted slave position and the suggested path (light green).

During the experiments, each block consisted of eight trials with one of the five experimental conditions listed above (no support or one of the four support systems). In these eight trials, the four different environments were presented twice, once as shown in figure 7.3 and once a version mirrored about the vertical axis. Environmental information regarding the objects and target is visually shown during all experimental conditions, as described in the previous section. For all experimental conditions, an additional catch-trial of the difficult environment (*DD*) was used at the end of each block to investigate the dependency of the subjects on the support system. Therefore in total, each subject was presented with 45 trials.

The order of the five experimental conditions and the order of the presented environments within one condition block were both counterbalanced using a balanced Latin square design (Steel et al., 1986).

7.3.5. PROCEDURE

Each subject was asked to take place in front of a planar three- DOF parallel master device, as depicted in figure 7.2. The display behind the master device showed several red circular obstacles in the virtual environment. Contact of the virtual slave with these obstacles had to be avoided. The subjects were asked to move the slave as close as possible to the center of the target, but over the finish line, and as fast as possible, but without colliding with any of the obstacles. When the subject crossed the target line, the trial ended. Throughout the entire trial, the traveled trajectory of the slave was shown with a thin green line.

Prior to each experimental condition, the subjects were presented with several trials in a training environment to learn to operate the system and get familiar with the applied form

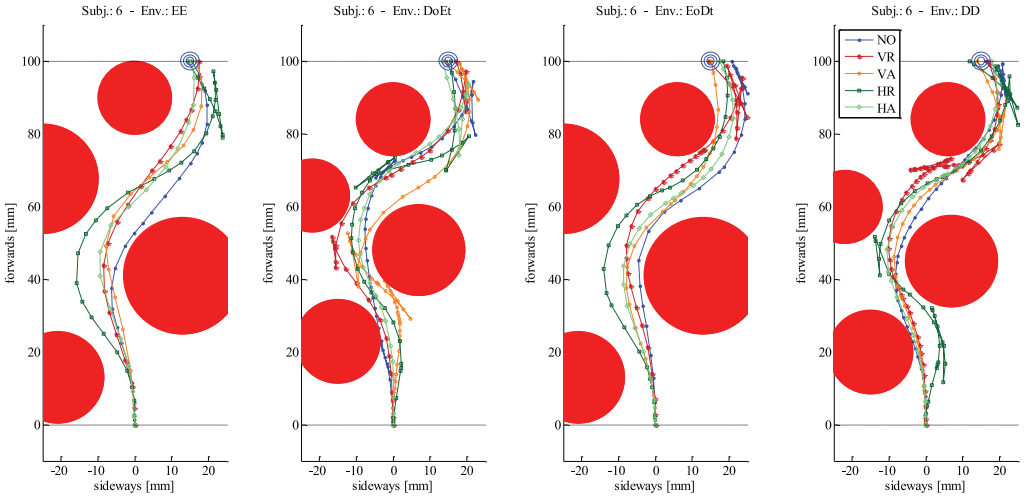

Figure 7.3: Raw position data of subject no. 6 in each of the four environments for all five experimental conditions with a single repetition. The solid colored lines represent the taken slave trajectory for that particular condition. Markers represent a 300-ms time interval. (a) Environment with easy obstacle avoidance and easy target reaching (EE). (b) Environment with difficult obstacle avoidance and easy target reaching (DoEt). (c) Environment with easy obstacle avoidance and difficult target reaching (EoDt). (d) Environment with difficult obstacle avoidance and difficult target reaching (DD).

7

of support system. All subjects were trained up to a minimal required level of performance, consisting of three sequential successful training trials in two different training environments, having no obstacle collisions or slave retractions, and a completion time of under ten seconds for each trial. The two training environments consisted of either a single obstacle for familiarization or two obstacles for strategic training of a correct task execution.

7.3.6. MEASURED VARIABLES AND METRICS

Analyzing different support systems can be done on many different aspects and metrics. To get an overview of different effects of the environment and form of support, a wide variety of metrics is selected. These metrics are roughly categorized in two groups, namely in general performance and safety metrics, and in effort metrics.

GENERAL PERFORMANCE AND SAFETY METRICS

The general performance metrics are task- and goal-related measures on how well the task was executed. The safety metrics reflect measures on the risks taken during the executed tasks. Four different metrics are considered for performance (task completion time, targeting accuracy, number of slave retractions, and mean duration of retractions) and three for safety (number of collisions, minimum time to obstacle collision, and distance to obstacles) to compare the five experimental conditions in four environments.

Task completion time: The time it took the subject to complete the task, from the starting line to the horizontal target line.

Targeting accuracy: The horizontal distance between the tip of the slave and the center of the target location when the slave crosses the horizontal target line. The targeting error reflects the accuracy at the end of each trial.

Number of slave retractions: The amount of times the slave transversal direction (back and forward) was changed, i.e., the number of sign changes of the transversal velocity of the slave. This indicates the number of wrong trajectories taken during a trial and is therefore a measure of performance of the correctness of the taken trajectory. The number of retractions were calculated using a 10 Hz Butterworth filter and a deadband threshold of 1.0 mm/s on the transversal velocity of the slave. A typical slave retraction is shown in figure 7.3(a) in the top right close to the target for the HR condition (dark green dotted line).

Total duration of retractions: The total time it took for all slave retractions during a single trial.

Number of collisions: The total number of collisions with obstacles, based on the tip of the slave and the edges of the obstacles.

Minimum time to obstacle collision: The minimum time until colliding with an obstacle, considering the current vehicle state (i.e., velocity and orientation) and the current control inputs at the master device. This metric was calculated similarly to the trigonometric computation of time to lane crossing of (van Winsum et al., 2000), calculated for each measured frame and for each obstacle, to obtain the minimum of all four obstacles over an entire trial. Note that if there is any collision with an obstacle in a trial, this metric equals zero.

Distance to obstacles: The absolute distance to the different obstacles, regardless of the direction of motion, master orientation or velocity, is measured during the trial. This metric is defined as the minimum value of the absolute distance to the obstacles. A collision results in a zero distance.

EFFORT METRICS

The effort metrics are based on objective and subjective measures to reflect the control effort of the operator during the tasks. Two objective (master and slave reversals) and four subjective metrics (TLX, comfort, effort, and preference rating) are selected to compare five experimental conditions in four environments.

Reversals master: As used in (Boessenkool et al., 2013), the number of steering corrections was used as a measure for control effort because it requires a conscious decision to change the sign of steering direction. This measure is defined as the number of steering reversals on the master input, i.e. the number of sign changes of the rotational velocity of the master, using a 10 Hz Butterworth filter. A 1.0^o threshold was used as deadband on the filtered signal to filter out unintentional oscillations of the subjects.

Reversals slave: The reversals of the slave were computed in a similar way as the reversals of the master. The slave only rotates when the subjects combine a change in rotation of the master device with a translation. Therefore, the reversals of the slave represent a more long-term change in steering angle, while the reversals of the master also show the more short-term changes of the steering and repositioning of the master device to make steering easier. A slave rotational reversal differs from a slave retraction because it represents the change of heading, not the back and forward transversal direction change.

Subjective measures: The NASA Task Load Index (NASA-TLX)was used to measure workload (Hart and Staveland, 1988). Furthermore, the subjects were asked to rank the five experimental conditions for comfort, effort, and preference.

7.3.7. DATA ANALYSIS

For each subject, form of support system, and environment, the metrics are computed per trial and averaged over two repetitions. Per metric, the means are compared between the forms of support and environment, and possible interactions with a 4 × 5 (environment × support) repeated measures analysis of variance (RM-ANOVA). A Greenhouse–Geisser correction was applied when sphericity was violated. For significant main effects ($p < 0.05$), post hoc comparisons with Bonferroni correction for multiple comparisons were done to get more insight to the origins of the effects.

7

7.4. RESULTS

7.4.1. POSITION DATA

The raw position data of a representative subject are shown in figure 7.3 for each of the four environments, including all five conditions with two repetitions in every environment. The data show smooth curvatures for the easy environment (EE) with different types of curves between the obstacles, clearly showing the available freedom for different strategies to reach the target. The same occurs at the first part of the environment EoDt, but the lines converge and more retractions can be seen near the end. For the DoEt and DD environments, retractions are visible throughout the whole environment.

It can also be seen in figure 7.3 that the HR condition (dark green) shows a different trajectory compared to the other conditions, resulting for the difficult environment (DD) in collisions in the beginning of the trial. It is a clear indication of the drawback of this local feedback, which does not include information regarding the next obstacle.

7.4.2. PERFORMANCE AND SAFETY RESULTS

The results on all task performance metrics, as explained in section 7.3.6, are described here. The analyses are done on all environments and all support systems. For clarity, the results presented in figure 7.4 only show the results of the two most different environments EE and DD. Furthermore, the text only describes the main findings, but all statistical details of all RM

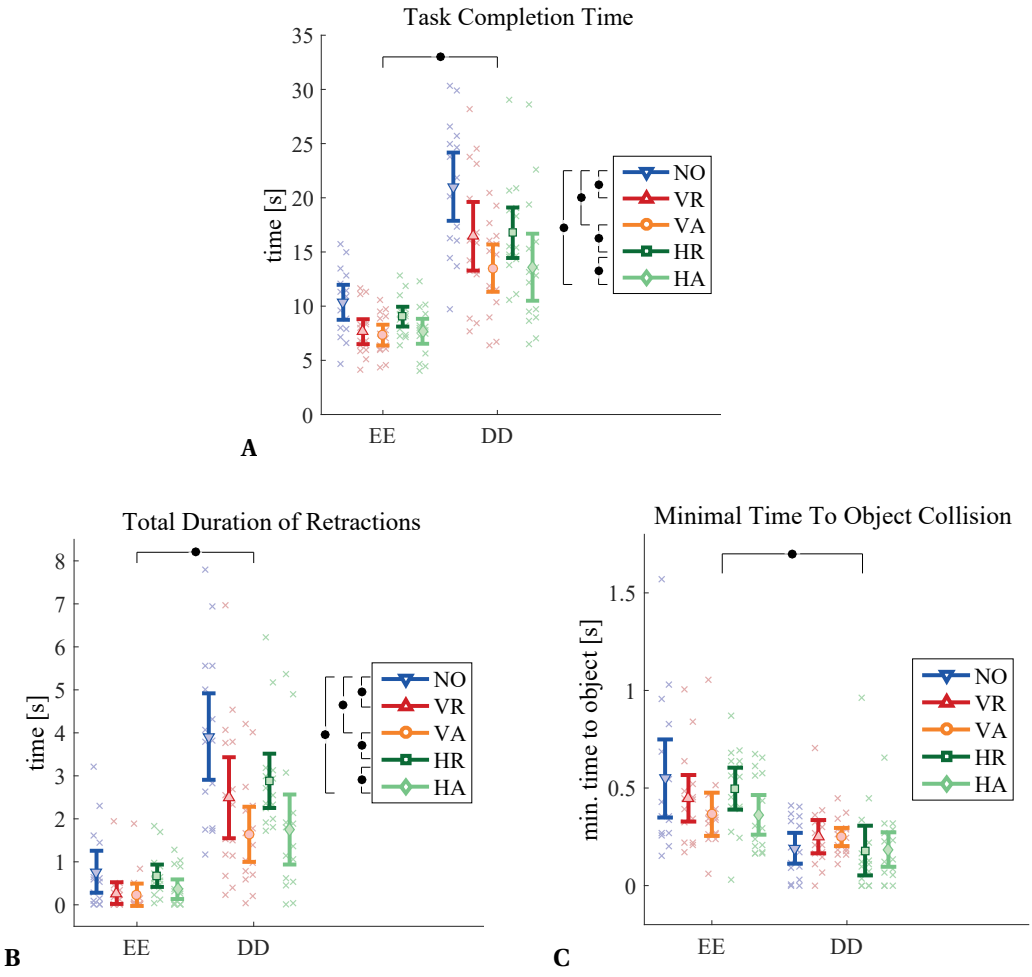

Figure 7.4: Performance and safety results of each experimental condition, for clarity only shown in the two most different environments EE and DD. A) Task completion time results. B) Number of slave retractions results. C) Minimal time to object collision results. The dots and x's represent the average individual result of two trials per subject (N = 15), the circles represent the group mean, and the error bars the 95% confidence interval of the mean. The horizontal and vertical bars indicate a significant difference over the factor environment or support, where "•" denote the significance of $p < 0.05$.

Table 7.1: Statistical Results of Performance and Safety Metrics

Metric	RM ANOVA			Post-hoc comp.	
	Env.	*Support*	*Inter.*	*Environment*	*Support*
Task completion time	$F_{1.8, 24.9} = 72.5$, $p < 0.001$	$F_{4, 56} = 15.7$, $p < 0.001$	$F_{5.1, 71.7} = 2.1$, $p = 0.07$	All comparisons $p < 0.001$ except DoEt and DD $p = 0.15$	No and VR, VA, HA $p = 0.010$, $p < 0.001$ and $p < 0.001$ respectively. HR and VA, HA $p = 0.002$, $p = 0.003$ respectively.
Target accuracy	$F_{3, 42} = 2.8$, $p = 0.054$	$F_{4, 56} = 6.8$, $p < 0.001$	$F_{5.3, 74.2} = 2.6$, $p = 0.027$	-	No and VA $p = 0.043$ HR and VA $p = 0.004$ No and VR, VR and HR, VA and HA, all $p = 0.08$
No. slave retractions	$F_{1.9, 26.3} = 52.4$, $p < 0.001$	$F_{2.1, 29.9} = 8.8$, $p = 0.001$	$F_{12, 168} = 1.5$, $p = 0.12$	All comparisons $p < 0.001$ except for DoEt and DD $p = 0.62$	No and VA, HA $p = 0.018$, $p = 0.062$ respectively HR and VR, VA, HA $p = 0.001$, $p < 0.001$, and $p<0.008$ resp.
Total duration of retractions	$F_{1.9, 27.2} = 51.5$, $p < 0.001$	$F_{2.3, 32.2} = 10.8$, $p < 0.001$	$F_{5.1, 71.6} = 2.2$, $p = 0.065$	EE and DoEt, EoDt and DD all $p < 0.001$, EoDt and DoEt, and DD, all $p < 0.001$	No and VR, VA, HA $p = 0.024$, $p < 0.001$, $p = 0.004$ resp. HR and VA, HA $p < 0.001$, $p = 0.032$ respectively
Min. time to obstacle coll.	$F_{3, 42} = 30.6$, $p < 0.001$	$F_{4, 56} = 1.9$, $p = 0.13$	$F_{4.9, 68.3} = 1.8$, $p = 0.13$	EE and DoEt, EoDt and DD all $p < 0.001$ DoEt and EoDt $p = 0.005$	-
No. of collisions	$F_{1.9, 27.7} = 15.5$, $p < 0.001$	$F_{2.2, 30.8} = 3.8$, $p = 0.029$	$F_{2.4, 33.5} = 0.8$, $p = 0.47$	EE and DoEt, EE and DD, $p < 0.001$, $p = 0.006$ resp. EoDt and DD, EoDt and DoEt, $p = 0.006$, $p = 0.001$ respectively	No and VA $p = 0.043$
Distance to obstacles	$F_{3, 42} = 472$, $p < 0.001$	$F_{3, 56} = 2.0$, $p = 0.11$	$F_{12, 168} = 2.0$, $p = 0.030$	All comparisons $p < 0.001$ except EE and EoDt $p = 0.03$ and DoEt and DD $p = 1.0$	-

Using a two-way repeated measures ANOVA on environment and support, and the interaction between the two. The post hoc analysis shows the differences per condition or environment type if RM ANOVA showed differences.

ANOVA's can be found in table 7.1. The specific differences between the results in the NO support and the other experimental conditions for all environments can be seen in table 7.3.

Task Completion Time: The mean completion time over all subjects, trials, and conditions was 12.8 s. The completion times in the NO condition are significantly larger (statistical details can be found in table 7.1) than in VR, VA, and HA, and the HR condition took significantly longer than VA and HA [see figure 7.4A]. This suggests that additional information about both the vehicle kinematics and the suggested path decrease task completion time. Moreover, a significant influence of the environment is observed; both a more narrow environment and a more difficult to reach target influence the completion time significantly. However, the narrow environments had the most effect, as can be seen in table 7.3.

Targeting Accuracy: The type of environment did not had a significant effect on the target accuracy. The support system did have a significant effect and there was a significant interaction between the environment and support (see table 7.1). Post hoc comparisons on support show that the errors in the x-directions are ($p < 0.05$, or have a tendency ($p = 0.08$) to be) smaller in the visual conditions compared with the NO and HR condition. The substantial difference is very low (ranging for the mean NO condition from 1.5 to 2.2 mm; see table 7.3), compared with the target size of 3 mm (see section 7.3.3).

Number of Slave Retractions: Both the environment and support had a significant effect on the number of slave retractions (see table 7.1). There are less retractions for the visual conditions and the HA, and more for the NO and the HR conditions, which suggests that more additional information leads to less slave retractions. The number of slave retractions is significantly lower for environments EE and EoDt compared with the other environments (see table 7.1). This shows that the number of slave retractions increases with both the narrowness of the environment and the difficulty to reach the target. The combination of the two does not increase the amount of slave retractions further.

Total Duration of Retractions: A significant effect for both the environment and support was found for the total duration of retractions (see table 7.1). Both visual supports and HA have significant less duration of the retractions than the NO condition [see figure 7.4B]. The duration of retractions in the easy environment (EE) was significantly shorter than in all other environments, followed by those in the EoDt, indicating that increasing task difficulty results in longer retractions.

Number of Obstacle Collision: The number of obstacle collisions depends strongly on the narrowness of the environment and thereby the difficulty to avoid the obstacles. Environments with large distances between obstacles (EE and EoDt) had significantly less obstacle collisions compared to narrow environments (DoEt and DD) (see table 7.1).

Minimum Time to Obstacle Collision: For the minimum time to obstacle collision, only a significant effect for the environment was found (see table 7.1). In the easy environment (EE), the time to obstacle collision was larger than in all other environments [see figure 7.4C].

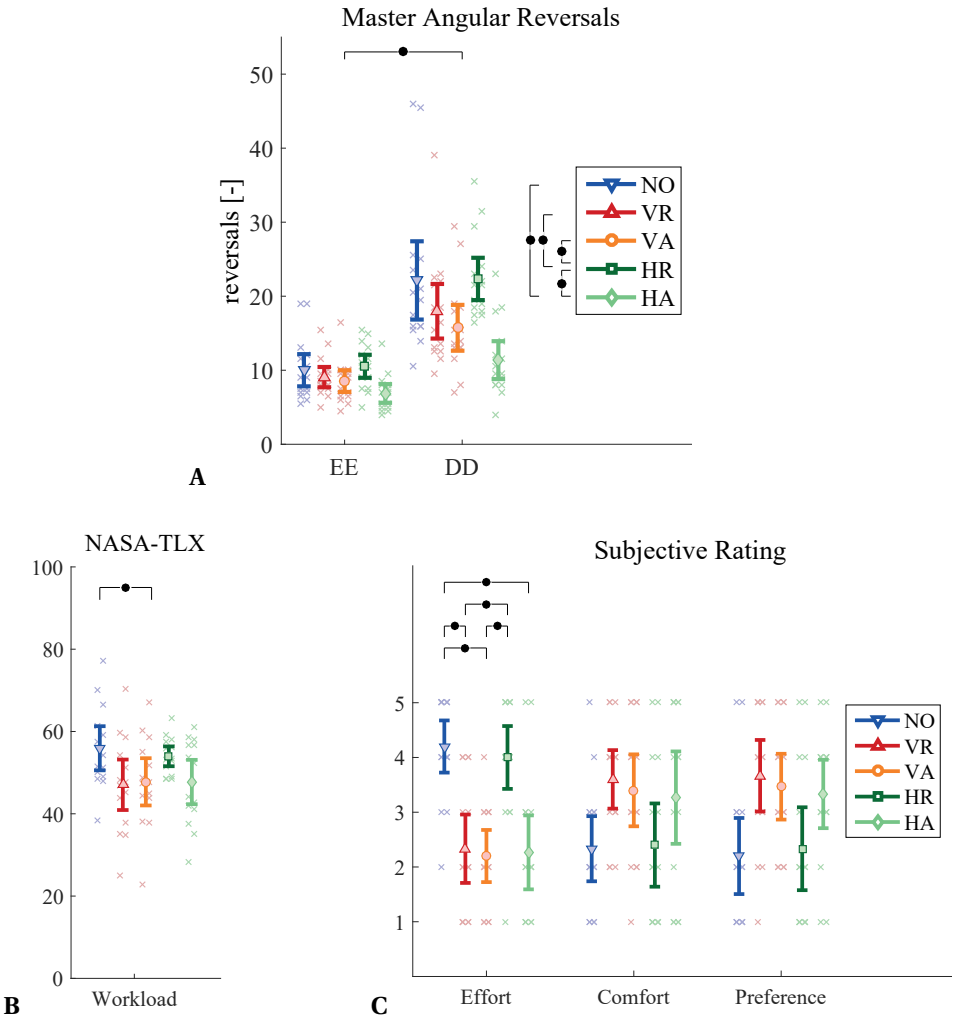

Figure 7.5: Effort results of each experimental condition, for clarity only shown in the two most different environments EE and DD. A) Number of master reversal results. B) NASA TLX workload results. C) Subjective ratings of each experimental condition over all environments. General figure representations of metrics are described in the caption of figure 7.4.

Distance to Obstacles: The distance to obstacles depends significantly on the environment. Larger distances between the obstacles result in larger distances between the slave and the obstacles (see table 7.1).

Table 7.2: Statistical Results of Control Effort Metrics

Metric	RM ANOVA			Post-hoc comp.	
	Env.	*Support*	*Inter.*	*Environment*	*Support*
No. of master reversals	$F_{2.2, 31.3} = 48.5$, $p < 0.001$	$F_{4, 56} = 13.6$, $p < 0.001$	$F_{3.9, 55.1} = 2.0$, $p = 0.11$	All comparisons $p < 0.001$ except DoEt and DD $p = 1.0$	NO and HA $p = 0.006$ HR and VR, VA, HA $p = 0.021$, $p < 0.001$, $p < 0.001$ resp.
No. of slave reversals	$F_{3, 42} = 53.4$, $p < 0.001$	$F_{2.0, 27.5} = 9.9$, $p = 0.001$	$F_{3.9, 54.5} = 2.1$, $p = 0.09$	All comparisons $p < 0.001$ except DoEt and DD $p = 1.0$	NO and VR, VA, HA $p = 0.044$, $p < 0.001$, $p = 0.050$, resp. HR and VR, VA, HA $p = 0.001$, $p < 0.001$ and $p = 0.039$ resp.
NASA-TLX	-	$F_{4, 52} = 4.7$, $p = 0.003$	-	-	No and VA, HA, $p = 0.043$, $p = 0.07$ respectively
Effort rating	-	$F_{4, 56} = 9.6$, $p < 0.001$	-	-	No and VR, VA, HA $p = 0.002$, $p = 0.004$, $p = 0.011$ resp. HR and VR, VA, $p = 0.046$, $p = 0.003$ respectively
Comfort rating	-	$F_{4, 56} = 2.3$, $p = 0.073$	-	-	-
Preference rating	-	$F_{4, 56} = 3.2$, $p = 0.020$	-	-	no differences found

Using a two-way repeated measures ANOVA on environment and support, and the interaction between the two. The post hoc analysis shows the differences per condition or environment type if RM ANOVA showed differences.

7.4.3. EFFORT RESULTS

The results for the safety and effort metrics (see section 7.3.6) are described here. Again for clarity, figure 7.5 only presents the results of environments EE and DD. All specific differences can be seen in table 7.3. Statistical details of all RM ANOVAs can be found in table 7.2.

Slave and Master Angular Reversals: Angular reversals, relating to steering corrections, are analyzed for both the master and the slave. For the slave, there are more reversals in the NO and HR conditions compared to the other conditions, while for the reversals of the master a benefit of HA over the visual conditions can be seen [see table 7.3 and figure 7.5A]. HA has less master reversals than in the NO condition, while the amount of master reversals in the visual conditions do not significantly differ from the NO condition.

Both the master and slave reversals were significantly lower for EE and EoDt compared to the other environments. This shows that the number of reversals increases with both the narrowness of the environment and the difficulty to reach to target. The combination of the two does not increase the amount of master reversals further. This is in line with the obtained results for the number of slave retractions.

NASA-TLX and Subjective Ratings: In all subjective measures, a clear trend is observed in favor of additional information, except when offered HR support. The workload measured with the NASA-TLX [see figure 7.5B], and effort ranking [see figure 7.5C], is higher for the NO and HR conditions, while they score lower on Comfort and Preference.

7.4.4. CATCH TRIALS

The results of the catch trials at the end of each condition in the difficult environment DD are shown in 7.6. The normal conditions are depicted in color and the catch trials in gray. The normal conditions are similar as shown before and consist of individual means of two repetitions, whereas the catch trials had only one repetition per condition. The results show no difference between the trials of each condition in the normal situation and the catch trials. Only for the HA condition is an increasing trend observed for the catch trial for completion time, retractions, and collisions due to several extreme values.

7.5. DISCUSSION

7.5.1. IMPACT OF TWO SUPPORT DESIGNS ON TASK EXECUTION

Most performance and control effort metrics show significant differences for the two support systems (*factor 1*) for the hypothesized effect that feedback of the predicted vehicle kinematics and the suggested path information is helpful in difficult environments. For example, task completion time significantly improves for all support systems (except for repulsive haptic guidance) compared to pure manual control. Similar results for reduction of task completion times were reported by Boessenkool et al. (2013) for haptic guidance along a suggested path. Although not tested extensively, the relative improvements suggest a very consistent pattern

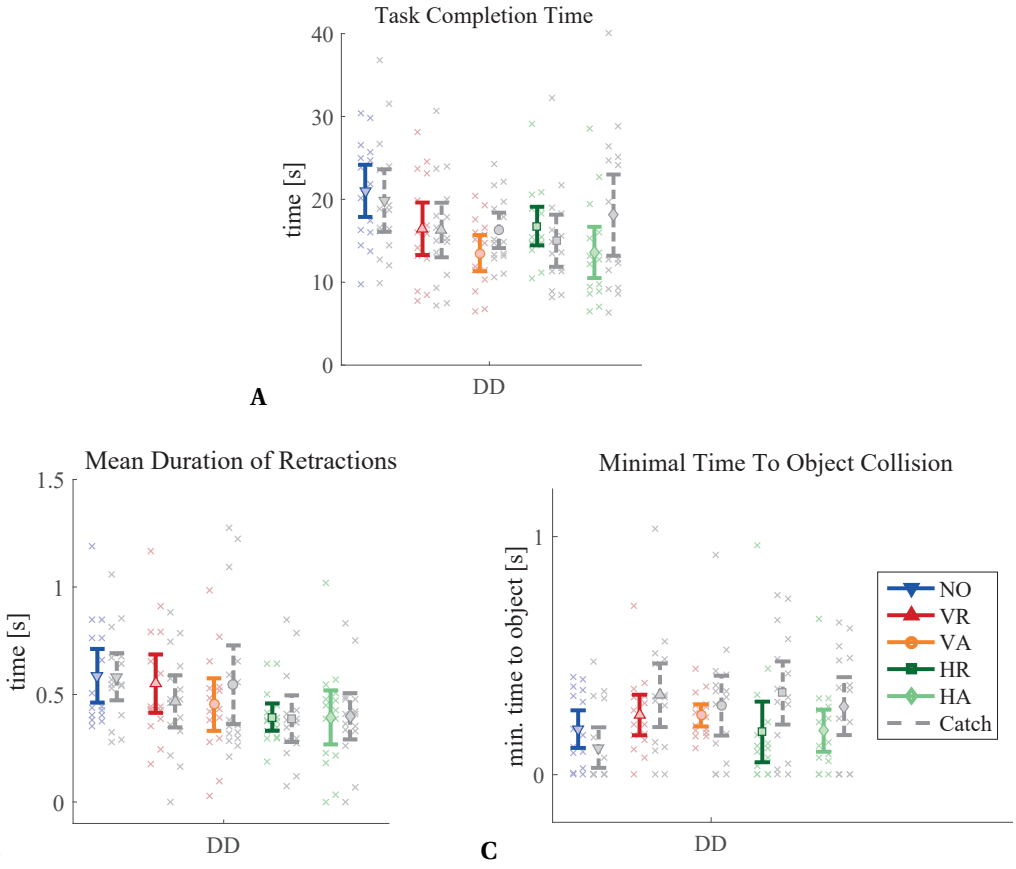

Figure 7.6: Catch trial (CT) results of each experimental condition in the most difficult environment. The catch trials are shown in gray and the normal trials as previously reported in the represented colors. General figure representations are described in the caption of figure 7.4.

Table 7.3: Percentage of improvement per subject for all experimental results for all environment types

Support		Metric								
Env.	*Sup.*	*Task Compl. time*	*Target accuracy*	*Duration of retractions*	*No. slave retract.*	*Min time obst. coll.**	*No. of collisions*	*Dist. to obstacles**	*No. master reversals*	*No. slave reversals*
EE	NO	10.4(3.2)s	1.5(0.6)mm	1.0(0.8)s	1.8(1.9)-	0.5(0.4)s	0.5(0.1)-	6.0(1.0)mm	10.0(4.3)-	5.0(3.9)-
	VR	23(20)%	42(47)%	58(78) %	12(155)%	20(86)%	100(0)%	8(18)%	1(33)%	8(59)%
	VA	27(15)%	3(74)%	76(47)%	44(89)%	-17(44)%	90(28)%	2(17)%	6(34)%	17(47)%
	HR	8 20)%	-27(86)%	18(49)%	-92(134)%	27(95)%	87(35)%	8(22)%	-17(47)%	-20(57)%
	HA	24(13)%	7(60)%	59(63)%	35(77)%	-20(38)%	87(52)%	3(20)%	26(26)%	3(42)%
DoEt	NO	17.4(4.9)s	1.5(0.5)mm	2.5(1.0)s	5.6(3.1)-	0.2(0.2)s	1.3(0.9)-	2.5(0.8)mm	19.3(7.8)-	9.8(3.1)-
	VR	23(20)%	42(47)%	12(97)%	6(110)%	86(146)%	18(111)%	19(61)%	1(68)%	17(71)%
	VA	17(35)%	15(53)%	18(81)%	-1(96)%	7(73)%	72(55)%	35(57)%	8(56)%	6(56)%
	HR	0(45)%	23(38)%	-26(98)%	-67(118)%	-26(96)%	5(165)%	26(55)%	-27(67)%	-39(87)%
	HA	20(22)%	-51(106)%	6(76)%	2(56)%	0(72)%	41(61)%	22(25)%	21(45)%	-2(45)%
EoDt	NO	14.5(4.1)s	2.2(1.8)mm	1.6(0.6)s	3.9(2.3)-	0.4(0.2)s	0.5(0.1)-	5.5(0.8)mm	13.8(5.4)-	7.6(2.6)-
	VR	20(25)%	0(101)%	35(66)%	17(106)%	-15(43)%	70(59)%	1(17)%	0(49)%	22(48)%
	VA	28(21)%	16(101)%	67(36)%	49(60)%	-16(37)%	87(52)%	4(18)%	15(30)%	37(27)%
	HR	9 (26)%	-27(164)%	-11(61)%	-14(74)%	-15(78)%	47(92)%	-1(20)%	-15(33)%	-7(44)%
	HA	35(15)%	14(68)%	60(43)%	41(49)%	-4(53)%	40(130)%	10(18)%	34(31)%	34(40)%
DD	NO	21.0 (6.2)s	1.7(0.7)mm	3.9(2.0)s	7.6(4.9)-	0.2(0.1)-	1.2(1.8)-	2.5(0.8)mm	22.1(10.4)-	12.7(6.2)-
	VR	22(19)%	22(49)%	38(36)%	22(55)%	40(87)%	47(61)%	37(145)%	13(27)%	31(33)%
	VA	34(16)%	35(46)%	58(23)%	42(48)%	51(95)%	25(104)%	31(82)%	22(30)%	36(30)%
	HR	15(27)%	-46(116)%	10(46)%	-34(75)%	-37(63)%	36(81)%	35(45)%	-14(45)%	-19(45)%
	HA	34 (24)%	-19(81)%	52(44)%	37(53)%	3(105)%	10(107)%	44(155)%	41(33)%	37(36)%

Displaying for the NO condition the mean results and standard deviation of the mean within brackets. The conditions with support are displayed as percentage of improvement per subject in each environment compared to the NO condition of that environment and the standard deviation of the mean in percentage within brackets.
*Improvements for these particular metrics are defined positive as increase compared to the NO condition, where other metrics are defined positive for a decrease.

for all environments over all metrics. For the task completion time, the averaged relative improvements were 20%, 27%, 8%, and 28% for VR, VA, HR, and HA, respectively. This suggests that for all environments there is consistently more improvement when additional information of the suggested path is given compared to only the predicted vehicle trajectory.

7.5.2. IMPACT OF TWO MODALITIES ON TASK EXECUTION

When the path information is reflected haptically, no difference in performance is found compared to visual support (*factor 2*). This is in contrast to what Stigter et al. (2007) reported, where improvements for haptics over visual support for a flight director for more accurate path following reduced the control effort. Wildenbeest et al. (2014) also reported that haptic feedback makes the system dynamics more tangible. For the conducted experiment, the visual operator load was low, therefore enabling the subjects to process the visual cues equally to the haptic cues. In real applications, the visual operator load is typically much higher due to multiple secondary tasks, resulting in larger benefits for haptic cues.

Control effort metrics in this experiment (in terms of master angular reversals) seem to improve the most when suggested path information is given haptically. This is similar to the findings of Griffiths and Gillespie (2005), who reported an increase in secondary task performance (thus reduced mental workload) during car steering with haptic assistance including suggested path information. Mulder et al. (2012) also found for reduced reversal rates when applying guidance forces including a suggested path for car driving. Boessenkool et al. (2013) found similar results for a teleoperation task, in addition to similar TLX results.

In this experiment, only additional haptic cues applied in the form of repulsive haptic guidance resulted in no significant improvements compared to the baseline without support (in terms of task completion time, slave retractions, master angular reversals). Therefore, it seems that the repulsive haptic guidance was not supportive for the given tasks. This result differs from the artificial force field implementation of Lam et al. (2006), who reported that the ability of collision avoidance for varying artificial force fields results in improved task performance. The method for obstacle avoidance of Khatib (1986) for full automation of a robotic arm also shows positive results for a time-varying artificial force field around obstacles. The raw time traces shown in figure 7.3 indicate a degrading effect of the repulsive haptic guidance, since it always steers away from obstacles, even when the limited vehicle steering angle requires cutting corners at several points. Providing this information only visually possibly enabled the subjects to extrapolate this information to longer predictions and, therefore, correct the steering input in time.

7.5.3. IMPACT OF FOUR ENVIRONMENTS ON TASK EXECUTION

The experimental results showed improvements (in terms of task completion time, number of retractions, number of collisions, and master angular reversal rate) in all four environments of varying spatio-temporal constraints (*factor 3*). The results suggest that the largest improvements were found when more critical constraints (for obstacle avoidance and target reachability) were present in the environment. This indicates that support systems are more effective when the

task becomes more difficult.

The designed environments strongly influenced the task execution behavior of the subjects. The experimental results show significant differences (for all performance and objective control effort metrics) for the environments of varying spatio-temporal constraints. Therefore, the absolute metric results show differences for most environment variations. This difference is also visible in the relative improvements in task completion time (see table 7.3) compared with manual control. For example, most relative metrics show a 5–10% improvement in the difficult environment. Moreover, the absolute averaged completion time doubles in the difficult environment (21.0 s) compared to the easy environment (10.4 s). Since the relative improvements remain approximately equal, this still means that the absolute effect of the support systems is doubled. The difficult environments took longer to complete due to their increased difficulty, such that all the support systems are effective in improving the performance.

No difference was found for the hypothesized effect that task criticality influences the required type of additional information. No specific support system improves the task more in a specific environment than others. In general, it seems that all support systems are more effective in more difficult environments.

7.5.4. LIMITATIONS, CROSS-CHECKS, AND RECOMMENDATIONS

Unfortunately, due to the large amount of comparisons, our data were not sufficient to reveal subtle interactions between type of additional information and difficulty of the environment. The effect of support systems could, therefore, only be shown for all four environments as a whole.

Furthermore, the user interface used in this study limits the generalizability of the results. The user interface was used to create a challenging but easy to understand task, which would require the operator to rely on the given feedback to improve its performance. Therefore, this demonstrates clearly the difference between the methods, but not so much the size of the effect when applied at for instance car driving. The experimental order was counterbalanced and appropriate training was given prior to the experiment to all subjects. Nonetheless, learning effects were analyzed using a linear learning curve estimation for each subject, and the obtained parameters were averaged for all subjects. All learning rates were relatively small and had large variation. For example, task completion time had a mean reduction of 18% (SD = 21%) over time (or trials), yet was based on inaccurate fits, $R2 < 0.15$. The number of angular reversals had a reduction of 14% (SD = 33%) with $R2 < 0.13$.

No evidence was found that any of the support systems resulted in overreliance or after effects (de Winter and Dodou, 2011): figure 7.6 illustrates that the catch trials (implemented at the end of each experimental condition block) showed no significant difference compared with regular trials.

Based on this study, it is recommended to offer both local environment information and global task information to the user either haptically or visually. This study shows when both types of information are offered with a support system (predicted vehicle dynamics combined with suggested path information), more improvements for conducting the task are found,

provided that the user is not overloaded with information. Future work of operator modeling could explain the found effect of this human factors study. However, if not all of the information is available, even offering only the predicted vehicle dynamics visually substantially improves conducting the task. The latter could be used when only nearby environment information is available for steering a remote controlled vehicle.

7.6. CONCLUSION

In the context of steering a nonholonomic vehicle, a human factor experiment was conducted to determine the efficacy of four support system designs. The designs were based on different types of reflected information (predicted vehicle trajectory with or without suggested path) and through what modality this is conveyed (haptically or visually). For the experimental conditions studied, the following is concluded.

- The support system designs that included both predicted vehicle trajectory and suggested path information improved task performance. No difference was found regarding the haptically or visually reflected information content.
- Solely reflecting information of the predicted vehicle trajectory resulted in no improvements when offered haptically, but resulted in improved task performance and reduced control effort when offered visually.
- Environments having more critical spatio-temporal constraints resulted in larger benefits (performance, safety, and effort) for all four support systems. No evidence was found that task criticality influenced the required type of additional information.
- Additionally, catch trials did not provide evidence for overreliance of any support system.

These results indicate that offering additional information improves performance in a nonholomic steering task, especially when task criticality is high. When both types of information regarding the task are available (predicted vehicle trajectory with or without suggested path), it seems to be beneficial to reflect them both to the operator. The choice for presenting the additional information visually or haptically is not determined by this study and should be done in correspondence with the task and workload of the application it is used in.

REFERENCES

Abbink, D., Mulder, M., and Boer, E. (2012). Haptic shared control: smoothly shifting control authority? *Cognition, Technology & Work*, pages 19–28.

Abbink, D. A. and Mulder, M. (2009). Exploring the Dimensions of Haptic Feedback Support in Manual Control. *Journal of Computing and Information Science in Engineering, Special Haptics Edition*, 9(March):1–9.

Abbott, J. and Okamura, A. (2003). Virtual fixture architectures for telemanipulation. *IEEE Int. Conf. on Robotics and Automation*, pages 2798–2805.

Bettini, A. and Marayong, P. (2004). Vision-assisted control for manipulation using virtual fixtures. *Robotics, IEEE Transactions on*, 20(6):953–966.

Boessenkool, H., Abbink, D. A., Heemskerk, C. J. M., van der Helm, F. C. T., and Wildenbeest, J. G. W. (2013). A task-specific analysis of the benefit of haptic shared control during telemanipulation. *IEEE transactions on haptics*, 6(1):2–12.

Brandt, T., Sattel, T., and Bohm, M. (2007). Combining haptic human-machine interaction with predictive path planning for lane-keeping and collision avoidance systems. *2007 IEEE Intelligent Vehicles Symposium*, pages 582–587.

Christiansson, A. V. (2007). *Hard Master , Soft Slave Haptic Teleoperation*. PhD thesis, Delft, University of Technology.

de Winter, J. and Dodou, D. (2011). Preparing drivers for dangerous situations: A critical reflection on continuous shared control. *2011 IEEE International Conference on Systems, Man, and Cybernetics*, pages 1050–1056.

Diolaiti, N. and Melchiorri, C. (2002). Tele-Operation of a Mobile Robot Through Haptic Feedback. (November):17–18.

Forsyth, B. a. C. and MacLean, K. E. (2006). Predictive haptic guidance: intelligent user assistance for the control of dynamic tasks. *IEEE transactions on visualization and computer graphics*, 12(1):103–113.

Griffiths, P. and Gillespie, R. B. (2005). Sharing Control Between Human and Automation Using Haptic Interface : Primary and Secondary Task Performance Benefits. *Human Factors*, 47(3):574–590.

Hart, S. G. and Staveland, L. E. (1988). Development of NASA-TLX (Task Load Index): Results of Empirical and Theoretical Research. *Human Mental Workload*, pages 239–250.

Khatib, O. (1986). Real-Time Obstacle Avoidance for Manipulators and Mobile Robots. *The International Journal of Robotics Research*, 5(1):90–98.

Kim, W. S., Tendick, F., Ellis, S. R., and Stark, L. W. (1987). A Comparison of Position and Rate Control for Telemanipulations with Consideration of Manipulator System Dynamics. *IEEE Journal of Robotics and Automation*, (5):426–436.

Kuiper, R. J., Frumau, J. C. L., Van Der Helm, F. C. T., and Abbink, D. A. (2013). Haptic Support for Bi-manual Control of a Suspended Grab for Deep-Sea Excavation. *2013 IEEE Int. Con. on Systems, Man, and Cybernetics*, pages 1822–1827.

Lam, T., Boschloo, H., Mulder, M., and van Paassen, M. (2009). Artificial Force Field for Haptic Feedback in UAV Teleoperation. *IEEE Transactions on Systems, Man, and Cybernetics - Part A: Systems and Humans*, 39(6):1316–1330.

Lam, T. M., Mulder, M., and Paassen, M. M. (2006). Haptic Feedback for UAV Tele-operation - Force offset and spring load modification. In *Proc. of IEEE Int. Conf. on Systems, Man, and Cybernetics*, pages 1618–1623.

Lüttgen, J. and Heuer, H. (2012). Robotic guidance benefits the learning of dynamic, but not of spatial movement characteristics. *Experimental brain research*, 222(1-2):1–9.

Majewicz, A. and Okamura, A. M. (2013). Cartesian and Joint Space Teleoperation for Nonholonomic Steerable Needles. pages 395–400.

Marayong, P. and Okamura, A. (2004). Speed-accuracy characteristics of human-machine cooperative manipulation using virtual fixtures with variable admittance. *Human Factors*.

Massimino, M. and Sheridan, T. (1989). Variable force and visual feedback effects on teleoperator man/machine performance. *Proc.of the NASA Conf. on Space Telerobotics*, pages 89–98.

Milgram, P., Rastogi, A., and Grodski, J. J. (1995). Telerobotic Control Using Augmented Reality.

Mulder, M., Abbink, D. A., and Boer, E. R. (2012). Sharing Control With Haptics Seamless Driver Support From Manual to Automatic Control. *Human Factors: The Journal of the Human Factors and Ergonomics Society*, 54(5):786–798.

Prada, R. and Payandeh, S. (2009). On study of design and implementation of virtual fixtures. *Virtual reality*, pages 117–129.

Rankine, W. (1869). On the dynamical principles of the motion of velocipedes. *The Engineer*, 28:pp. 79,129,153,175.

Rosenberg, L. (1993). Virtual fixtures: Perceptual tools for telerobotic manipulation. *IEEE Virtual Reality Int. Symposium*, pages 76–82.

Sayers, C., Lai, a., and Paul, R. (1995). Visual imagery for subsea teleprogramming. *Proceedings of 1995 IEEE International Conference on Robotics and Automation*, 2:1567–1572.

Sayers, C. P. and Paul, R. P. (1994). An operator interface for teleprogramming employing synthetic fixtures. *Presence (Cambridge, Mass.)*, 3(4):309–20.

Sheridan, T. (1989). Telerobotics. *Automatica*, 25(4):487–507.

Steel, R. G. D., Torrie, J. H., and Dickey, D. (1986). *Principles and procedures of statistics: A biometrical approach*.

Steele, M. and Gillespie, R. B. (2001). Shared control between human and machine: Using a haptic steering wheel to aid in land vehicle guidance. *Proceedings of the Human Factors and Ergonomics Society 45th Annual Meeting*, pages 1671–1675.

Stigter, S. D., Mulder, M., and Van Paassen, M. M. (2007). Design and Evaluation of a Haptic Flight Director. *Journal of Guidance, Control, and Dynamics*, 30(1):35–46.

van Winsum, W., Brookhuis, K. A., and de Waard, D. (2000). A comparison of different ways to approximate time-to-line crossing (TLC) during car driving. *Accident Analysis and Prevention*, 32(1):47–56.

Wildenbeest, J. G., Kuiper, R. J., van der Helm, F. C., and Abbink, D. A. (2014). Position control for slow dynamic systems: Haptic feedback makes system constraints tangible. *2014 IEEE International Conference on Systems, Man, and Cybernetics (SMC)*, pages 3990–3995.

Wildenbeest, J. G. W., Abbink, D. A., Heemskerk, C. J. M., Van Der Helm, F. C. T., and Boessenkool, H. (2013). The impact of haptic feedback quality on the performance of teleoperated assembly tasks. *IEEE Transactions on Haptics*, 6(2):242–252.

Zaal, P. M. T., Nieuwenhuizen, F. M., van Paassen, M. M., and Mulder, M. (2012). Modeling Human Control of Self-Motion Direction With Optic Flow and Vestibular Motion. *IEEE transactions on systems, man, and cybernetics. Part B, Cybernetics : a publication of the IEEE Systems, Man, and Cybernetics Society*, 43(2):544–556.

8

HAPTIC SHARED CONTROL FOR DEEP-SEA MINING

Roel J. Kuiper & Irene A. Kulling, Kang Wang, Frank Hoeckx and David A. Abbink

to be submitted to IEEE Transactions on Haptics, 2019

Future applications such as deep-sea mining are promising but also challenging tasks to achieve. Even though such application does not exists at the moment, remotely controlled devices are currently under development and will be challenging to control. Due to the unpredictable environments in such an application full automation will be difficult to achieve, but offering guidance force could be a promising solution for such a task. The augmented guidance forces as evaluated in the previous chapter 7 could benefit the human operator in normal operation and remain in control in unforeseen situations. Therefore this chapter investigates if offering guidance forces will benefit the best from both, automation and manual control.

Offering guidance forces by using haptic shared control is compared to supervisory control (full automation with take-over capabilities) and manual control. This is tested while driving a track-driven deep-sea mining crawler over a seabed while avoiding unexpected obstacles. The designed simulator of the crawler and environment, as well as experimental methods and procedures of this experiment, are described in section 8.2 and the four results in section 8.3 for task performance and obstacle avoidance.

R.J. Kuiper & I.A. Kulling, K. Wang, F. Hoeckx and D.A. Abbink; Haptic Shared Control for Deepsea Mining; to be submitted to IEEE Transactions on Haptics, 2019.

ABSTRACT

Deep-sea mining is currently being investigated as a possibility to harvest valuable materials from mineral-rich areas located in water depths up to 2000 meters. One promising mining method is to employ a large crawler on the seabed, remotely controlled by an operator on the supporting vessel. Controlling such a vehicle is expected to be difficult due to the unpredictable seabed environment and limited feedback from locally mounted sensors, complicating both the implementation of reliable automation and manually controlled task execution. The foreseen limited capabilities of automation solutions required the need for a human operator, commonly leaving the operator in a supervisory role and manual control when intervention is needed. An alternative approach is to use haptic shared control, which has shown to be beneficial in vehicle control tasks (automotive, UAVs), yielding improved performance but mitigating traditional human-automation interaction issues such as skill degradation, reduced situation awareness and over-reliance. This study compares supervisory control and haptic shared control to manual control, for operating a teleoperated virtual subsea crawler. A simulator was constructed, including a bi-manual control interface capable of rendering haptic feedback, two virtual displays showing primary and secondary task-related information, a mathematical model simulating the dynamics of the slow vehicle, and unpredictable soil properties of the seabed. In a human factors experiment, subjects (n=18) controlled the simulated crawler along a trajectory, where unpredictably presented automation errors required the operator to respond. During normal steering and track keeping, both haptic shared control and supervisory control improved subjects' performance compared to manual control (reduction of lateral error). In unexpected events, such as obstacle avoidance and slip recovery, manual control and haptic shared control resulted in the best performance (reduction of task completion time for both conditions). The benefits of haptic shared control over supervisory control only become apparent when the operator unexpectedly needs to resume control. Since haptic shared control has the benefits of both manual and supervisory control it is a promising method to apply in slow-dynamic applications, such as deep-sea mining.

8.1. INTRODUCTION

RESEARCH on deep-sea mining has been stimulated in recent years due to depletion of on-land mineral resources and the detection of promising amounts of mineral deposits in deep-sea (Tivey, 2007). However, deep-sea operations pose an extremely harsh working environment because of the extreme hydrostatic pressure, deprivation of natural lighting and rough seabed bathymetry caused by tectonic activities. Typically these operations are well prepared with detailed pre-survey scans of the bathymetry and various samples to determine the soil properties of the environment (Whitcomb, 2000). This enables visual support and semi-automation with generated waypoints, although remaining unpredictable due to volcanic activity, water current and unknown inhomogeneous seabed properties (Bloois and Frumau, 2009).

Given the limited capabilities of sensing and mapping, moving the crawler over the seabed floor is expected to be challenging for a human operator, and very difficult to reliably automate.

A common approach is to automate as much as possible, and leave the human operator as a supervisory controller, ready to take back manual control when required (Sheridan et al., 1978). In supervisory control, the slave system could execute autonomously under certain phases, controlled by a local automatic controller. The operator continuously receives a variety of information concerning the working status of the slave system, and only intervenes in the control loop in case of special needs or an emergency. Most of the time, supervisory control relies on automation, which is well known to reduce workload (Sheridan, 1992). However, the situation in which the limits of automation are reached and the human operator needs to be involved in the direct control loop again, is reported to cause disadvantages for supervisory control (e.g. due to inattention, skill degradation and overreliance) (Bainbridge, 1983; Parasuraman, 1997; Sheridan, 2002). Moreover, since the slave system under water is relatively slow, operator's vigilance towards unexpected events under supervisory control is highly questionable due to complacency and reduced system awareness (Endsley and Kiris, 1995). A system under manual control will not suffer from such negative effects of human-automation interaction, but will be prone to human errors and require continuous attention and control activity (Sheridan, 1992).

An alternative solution for human-automation interaction is to share the control between human and automation instead of alternating control (Abbink and Mulder, 2009; Griffin et al., 2003; Sheridan et al., 1978). Instead of using the automation system's control signals directly as inputs to the crawler, these could be converted to assistive forces based on haptic algorithms. Active force feedback is given on the control interface to guide the operator, where the force is calculated by combining the dynamics of the haptic interface with optimal control inputs. Haptic shared control has been proven to yield performance improvement compared to manual control and control effort relief in various applications like car driving (Abbink et al., 2011; Griffiths and Gillespie, 2004; Mars et al., 2014; Mulder et al., 2012) and telemanipulation (Boessenkool et al., 2013; Kuiper et al., 2016; Lam et al., 2009).

However, not much is known yet about how the performance with shared control relates to the performance with supervisory control. Flemisch et al. (2008) showed preliminary results of performance comparisons in a car steering task between levels of automation, from manual to supervisory control with two shared control conditions in between. Their results suggest that the benefits of both manual control and supervisory control are reflected in the shared control conditions and offer the best of both worlds. Petermeijer et al. (2015) investigated the effect of increasing level of authority of haptic shared control on the performance and effort of the operator. Improved performance was found for increasing higher levels of authority (e.g. higher force levels) compared to manual control.

To what extent are these findings generalizable to steering a large subsea crawler? There are two main differences between steering a car and a subsea crawler. First, subsea crawler dynamics are substantially slower than vehicle dynamics in terms of longitudinal and rotational response to control inputs. Therefore, the operator needs to predict the system's outcome with a self-built internal model of the causal relation between the control input and slow-changing system output (F. A. Muckler and R. W. Obermayer, 1964). Second, the heading angle of the subsea crawler is adjusted by the relative speed difference between two speed inputs. Most

studies on shared control in assisting car driving constrain the vehicle to a constant speed such that the human only had to concentrate on the single degree of freedom steering itself (Flemisch et al., 2008; Griffiths and Gillespie, 2004; Mulder and Abbink, 2011). For a subsea crawler where skid steering is used, the speed of the vehicle is coupled with its heading angle. Therefore the effect of guidance needs to be investigated by the cooperation between two control inputs, influencing both the steering and lateral speed combined.

In this study, two human-automation interaction solutions (haptic shared control and supervisory control) are compared against the baseline of manually controlled crawler operation. Additionally to the primary maneuvering task, a secondary visual judgment task is investigated to increase the realism of controlling a complex subsea vehicle, comparable to Flemisch et al. (2008) for automotive applications. In a normal steering task, most benefits for the supervisory control are expected, since no human intelligence is needed. To make the task more realistic and challenging unexpected events occur during the task: obstacles and vehicle slip. To overcome problems due to these unexpected events different levels of alertness and task skills are required (e.g. obstacles are visible in the environment, while vehicle slip should be noticed by the different behavior of the vehicle). It is hypothesized that shared control would have the best of both manual control and supervisory control, reflected in efficient steering through the environment, but also efficient problem solving when unexpected events occur.

8.2. METHODS

8.2.1. SUBJECTS

Eighteen subjects, of which 12 male and 6 female, volunteered for the experiment (aged 24.9 years on average, 3.2 years standard deviation). None of the subjects had previous experience of operating a crawler, and all were naive about the experiment. All subjects gave their written informed consent prior to the experiment. The setup and experiment were approved by the local ethics committee of the Delft University of Technology.

8.2.2. APPARATUS

The human factors experiment was performed on the experimental setup Gemini as shown in figure 8.1. It consists of two identical handles with each a single degree of rotation, sensed by a 10 bit encoder connected with a cable capstan transmission with a gear ratio of 10. Each handle was 15 cm from rotation point to center of the handle grabbed by the operator. The handles were actuated with a Maxon RE30 motor, limited to 188 mNm of motor torque, resulting into maximal 12.5 N of force on the handle. Both handles were controlled by a single industrial real-time controller of Bachmann GmbH, updating at 333 Hz. The controller's sample time was chosen such to accommodate both the hardware control and the simulator of the virtual crawler on the real-time controller.

VIRTUAL CRAWLER

Currently no crawler is operating in deep-sea, however prototypes have been build and used as a basis for this study (Lipton, 2008; Yu et al., 2009). The virtual crawler was designed in

Figure 8.1: Overview of the developed experimental setup Gemini, consisting of two 1 DOF control input handles with force feedback capability. Behind the input handles two displays show the 3D modeled virtual environment (left screen), and the control panel with relevant information about the crawler (e.g. track speeds, water current and vehicle status), as well as a display for a secondary task.

Matlab Simulink with a submerged weight of 16 tons, 6 meters long and 8.2 meters wide. The crawler was driven by two tracks along the sides of the vehicle as can be seen in figure 8.1 and schematically represented in figure 8.2. The crawler was operated by skid steering (i.e. controlling the speed of both tracks individually) enabling the vehicle to rotate around its axis and simply combine speed control with steering. The seabed was modeled as ductile clay with a cohesion c of 10 kPa (based on (Wong, 2009)) with maximum speed of 1.0 m/s forward and 0.5 m/s backwards. The track-soil interaction was physically modeled and therefore slip of a track could be realized when locally the clay cohesion would drop.

The track-soil interaction is based on the work of Wong (Wong, 2009) and is shown in its simplified form in Eq. (8.1) with the parameters as given in table 8.1 and control gain G_c. The actual traction force used for the virtual crawler model calculates the traction force for 11 traction pads individually for both tracks separately.

$$F_{trac} = G_c \cdot \left(c + \frac{W \cdot tan(\delta)}{2 \cdot b \cdot L} \right) \cdot b \cdot L \tag{8.1}$$

The control gain G_c is given in Eq. (8.2) as an exponential function of the commanded

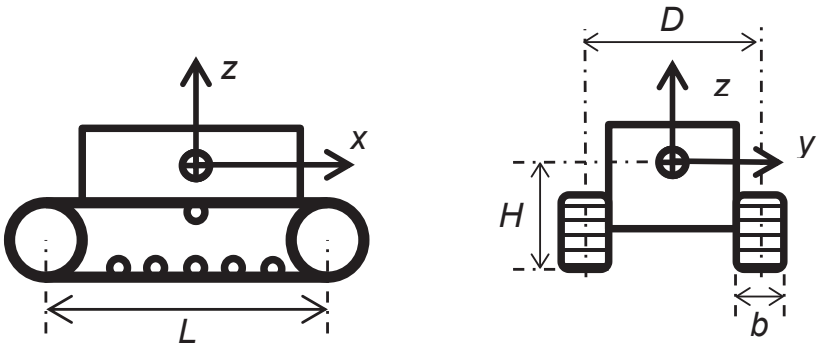

Figure 8.2: Schematic representation of the virtual crawler dimensions in sideview on the left and front view on the right subfigure.

steering input θ_{steer}, which is expressed in the exponential coefficient s.

$$\begin{aligned} G_c &= sgn(s) \cdot \left(1 - e^{-|s|/K}\right) \\ s &= \frac{\theta_{steer} - \dot{x}_{crawler}}{\theta_{steer}} \cdot \frac{L}{2} \end{aligned} \tag{8.2}$$

The actuating traction force is subtracted by the hydrodynamic resistance force F_{hydro} and the soil resisting force F_{resist}, consisting of a compaction force, a bulldozing resistance force and a grouser resistance force. The combined traction force and resiting force of both tracks results in a longitudinal velocity as given in Eq. (8.3). The difference between both components of the tracks results in a rotational velocity of the crawler vehicle.

$$\begin{aligned} \dot{x}_{crawler} &= \int \frac{\sum F_{trac} - F_{hydro} - \sum F_{resist}}{M} \, dt \\ \dot{\Psi}_{crawler} &= \int \frac{(\Delta F_{trac} - \Delta F_{resist}) \cdot D/2}{I_{zz}} \, dt \end{aligned} \tag{8.3}$$

Figure 8.3 shows the dynamic response of the virtual crawler given for both a step response on forward velocity and steering. After 1 second full throttle is simulated with both handles forward, shown with the black thick dotted line and the red thick solid line in the top sub-figure shows a rate limitation of about 300 ms. At 3 seconds the left handle remains fully forward and the right handle is fully reversed, creating a rotation of the vehicle. Because reversing has half the maximal speed than forward, a longitudinal forward command of 0.25 m/s remains with maximal differential (mean angle) of both handles. First the forward longitudinal velocity is reduced due to the dynamics. After approximately 3.8 seconds the longitudinal velocity is reduced and 0.2 seconds later the rotational acceleration and friction make the vehicle finally turn with 17 degrees per second.

AUTOMATIC CONTROLLER

The vehicle can be controlled fully automatically in normal operations. During supervisory conditions this controller was switched on and off by two buttons on top of the handles as

Table 8.1: Virtual Crawler Parameters

Variable	Symbol	Value
Track length	L	6 m
Track width	b	0.6 m
Thread width	D	3.5m
CoG height	H	1.5 m
Machine mass	M	30 t
Submerged mass	W	16 t
Projected area	A	15 m2
Rotational inertia	I_{zz}	80 t/m2
Soil cohesion	c	10 kPa
Soil friction angle	δ	6 deg
Shear deformation	K	0.015 m

shown in figure 8.1. When both buttons pressed for over 1.0 s the controller was switched on, and when both pressed for over 100 ms the controller was turned off again to enable a swift take over by the operator. During manual control conditions this controller was switched off, and the button functionality disabled. During haptic shared control conditions this automatic controller provided the optimal control angle for offering haptic assistance as further explained in section 8.2.3.

The automatic controller calculates steering inputs for both control handles θ_{opt}, including both the forward velocity v_{fwd} of 1.0 m/s and the calculated required vehicle steering angle ϕ_{opt} as given in Eq. (8.4).

$$\begin{aligned} \theta_{opt,L} &= v_{fwd} - \phi_{opt} \\ \theta_{opt,R} &= v_{fwd} + \phi_{opt} \end{aligned} \tag{8.4}$$

The required vehicle steering angle is calculated with three components, using a heading error controller ϕ_{head}, a lateral error controller ϕ_{lat} and a lateral lookahead error controller $\phi_{lat,la}$ as shown in Eq. (8.5).

$$\phi_{opt} = \phi_{head} + \phi_{lat} + \phi_{lat,la} \tag{8.5}$$

The control input ϕ_{head} based on heading error e_{head}, with vehicle heading $\Psi_{crawler}$ and path heading Ψ_{path} is shown in Eq. (8.6). A PD controller is used on the error with the gains $G_{P,head}$ of 3 and $G_{D,head}$ of 0.5.

$$\begin{aligned} e_{head} &= \Psi_{path} - \Psi_{crawler} \\ \phi_{head} &= G_{P,head} \cdot e_{head} + G_{D,head} \cdot \dot{e}_{head} \end{aligned} \tag{8.6}$$

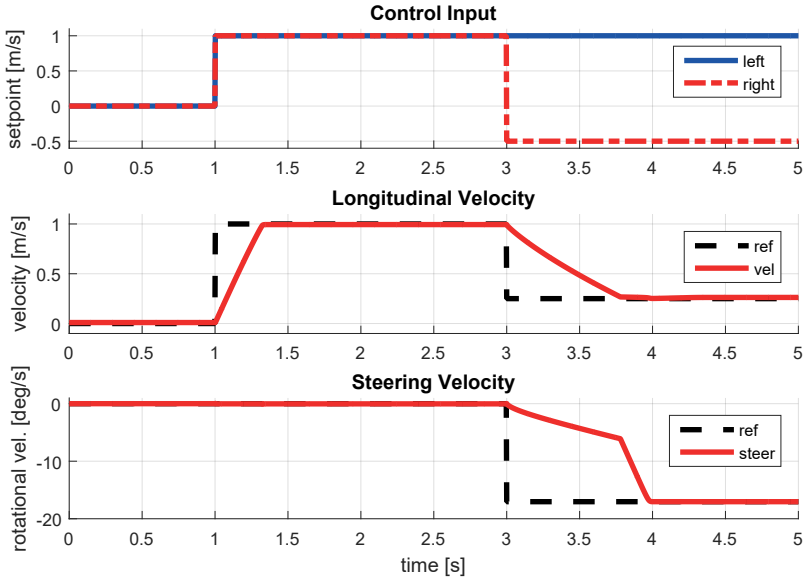

Figure 8.3: Dynamic response of virtual crawler on steering inputs. The top subfigure shows the generated commanded input velocities to both tracks. The middle subfigure indicates the commanded (black dotted line) and realized (thick red line) longitudinal velocity of the crawler. The lower subfigure indicates the rotational velocity (yaw rate) of the crawler.

The control input based on the lateral error is given in Eq. (8.7) for the difference between the closed path location x_{path} and current crawler location $x_{crawler}$. the control input is calculated with a simple proportional gain $G_{P,lat}$ of 0.1, because the latter look-ahead controller effectively acts as damping.

$$\phi_{lat} = G_{P,lat} \cdot \left(x_{path} - x_{crawler}\right) \tag{8.7}$$

In Eq. (8.8) is the lateral error taken of a future road point $x_{path,la}$ for a linear extrapolated vehicle position $x_{crawler,la}$ based on the current vehicle states, $T_{lookahead}$ of 3 seconds ahead. This controller also incorporates a simple proportional gain only $G_{P,lat,la}$ of 1.0, effectively damping the control inputs.

$$\begin{aligned} x_{crawler,la} &= x_{crawler} + T_{lookahead} \cdot \dot{x}_{crawler} \\ \phi_{lat,la} &= G_{P,lat,la} \cdot \left(x_{path,la} - x_{crawler,la}\right) \end{aligned} \tag{8.8}$$

This three folded controller is a standard control method for automotive domains and enables strong inputs based on the heading, which essentially acts faster than the lateral error. The latter is required for removing drift of the vehicle over the track, but causes instabilities because you cannot remove the current error. Therefore the look-ahead error nicely dampens the control actions, but causes cutting corners when tuned too high or looking too far forward.

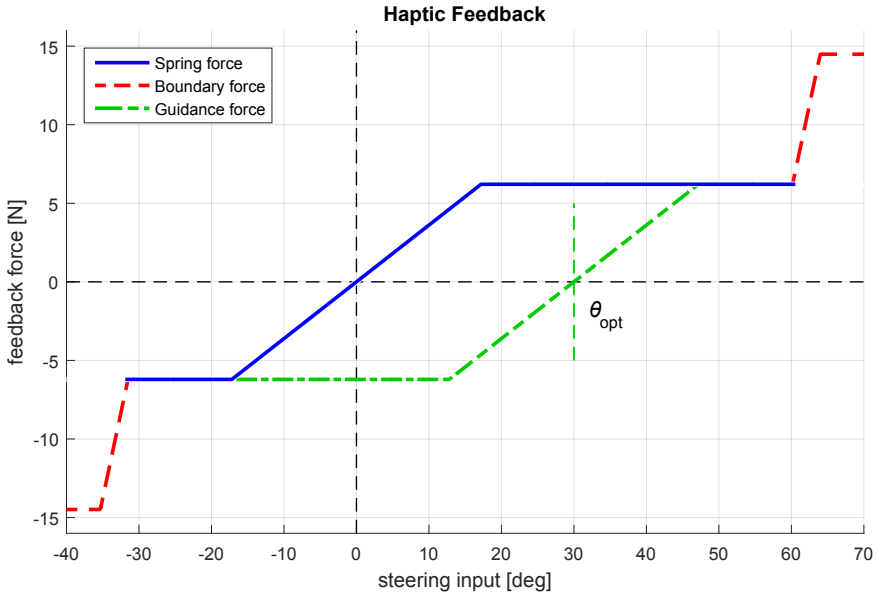

Figure 8.4: Haptic feedback design of the static spring force in manual control (blue), boundary forces (red) and guidance forces (green) with an exemplary optimal control angle of 30 degrees.

8.2.3. SUPPORT DESIGN

The operator is supported in controlling the crawler by means of force feedback on the control handles. A virtual static spring is implemented on both handles during manual control, with a restoring force to zero input. The spring force is also used for offering guidance by means of haptic shared control (Abbink et al., 2011) as described in section 8.2.3, implemented with a calculated steering angle $\theta_{opt,L/R}$ for zero spring force. Additionally the operator is offered with virtual boundaries, modeled as static springs as described in sections 8.2.3. The combination of the static spring and boundaries on the control input, is visualized in figure 8.4.

HAPTIC GUIDANCE

Guidance feedback is given by offering the calculated optimal control inputs from the automatic controller of section 8.2.2 as force feedback by means of haptic shared control. Force feedback is given by using the same spring as used in manual control conditions, but now shifting the neutral point of the spring. Force feedback is given on the difference $\Delta\theta_{HSC}$ between user control inputs θ_{steer} and optimal control inputs $\theta_{opt,L/R}$. The guidance force F_{HSC} as given in Eq. (8.9) uses a spring stiffness and damping gain K_{HSC} of 1200 N/deg and D_{HSC} of 50 N.s/deg respectively. Where $\theta_{opt,L/R}$ is either the left or right calculated optimal angle from the automatic controller from Eq. (8.4).

$$\begin{aligned} \Delta\theta_{HSC} &= \theta_{steer} - \theta_{opt,L/R} \\ F_{HSC} &= K_{HSC} \cdot \Delta\theta_{HSC} + D_{HSC} \cdot \Delta\dot{\theta}_{HSC} \end{aligned} \tag{8.9}$$

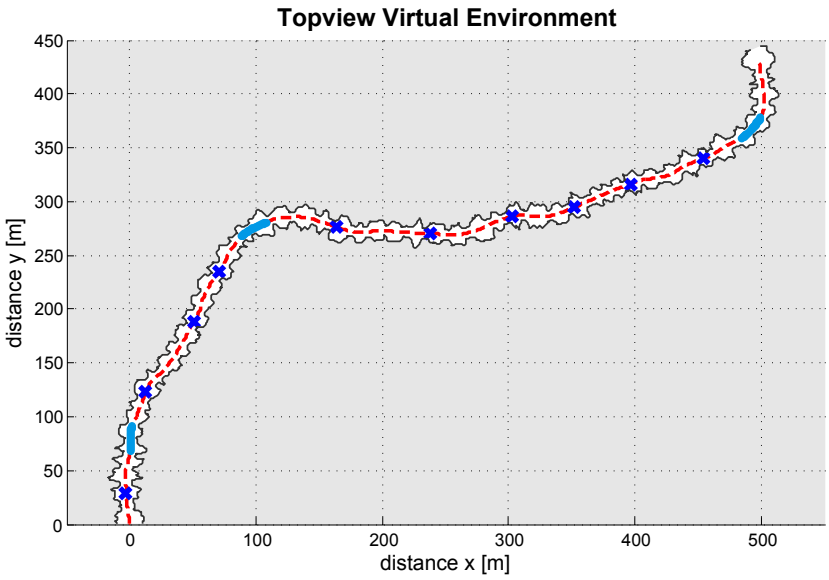

Figure 8.5: Topview of entire track and environment. Black solid lines indicate valley boundary and red dotted line the advised centre of the path. The blue x-marks indicate centre of obstacles on track and light blue thick lines the location of slip conditions.

The guidance feedback force was limited to 6.2 N on the handle, representing approximately 15 degrees of spring compression (i.e. difference of input), as indicated in figure 8.4. The green guidance dash-dotted force line replaced the solid blue static spring force during guidance conditions with changing neutral point θ_{opt}.

8

VIRTUAL BOUNDARY

On top of the static spring support, a virtual boundary is implemented to inform maximum throttle back and forwards. This boundary is implemented as a stiff spring damper as described in Eq. (8.10). The boundary limit $\theta_{boundary}$ is set to 60 degrees forward and 30 degrees backwards, corresponding to 1 m/s forward and 0.5 m/s backwards. The virtual wall is modeled with a stiffness gain K of 7000 N/deg and damper D of 500 N.s/deg. The boundary force is limited to 14.5 N, representing approximately 5 degrees of boundary spring compression as indicated in figure 8.4.

$$\begin{aligned} \Delta\theta_{bdr} &= \theta_{steer} - \theta_{boundary} \\ F_{boundary} &= K_{bdr} \cdot \Delta\theta_{bdr} + D_{bdr} \cdot \frac{\Delta\theta_{bdr}}{\delta_{bdr}} \cdot \Delta\dot{\theta}_{bdr} \end{aligned} \tag{8.10}$$

The wall deflection $\Delta\theta_{bdr}$ is limited to compression only, but has an offset for the damping D of 3 degrees prior to the stiffness K. Furthermore is damping gain D scaled with a ratio of spring deflection over scaling factor δ_{bdr} of 10 degrees and the ratio limited to 1.0. This all enables a

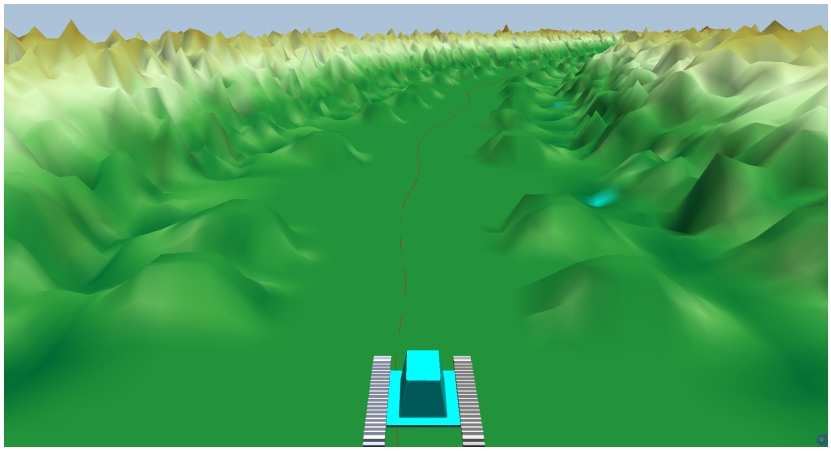

Figure 8.6: Visual representation of the crawler driving in the virtual environment with the advised path indicated.

smooth transition when making contact with the wall and remains stability for relatively large gains.

8.2.4. VIRTUAL ENVIRONMENT

Subjects were instructed to drive the crawler through a virtual environment during the experiment. The environment consisted of a curved valley of various width. The entire virtual environment is shown in topview in figure 8.5, indicating the valley boundaries and obstacle and slip locations along the path. The virtual representation of the environment is shown in figure 8.6 from the top of the crawler on a moving frame relative to the crawlers position and orientation. The figure illustrates the viewpoint for the operator and the varying width of the valley to drive over, including the suggested path (red dotted line). In figure 8.1 is the setup shown including the virtual representation of the vehicle to the operator on the left screen. On the right screen is the crawler's control panel shown, as also illustrated in figure 8.7. The control panel shows critical information to the operator regarding the vehicle's state (throttle, speeds, position and angle) and a secondary task to complete of counting dots.

OBSTACLE AVOIDANCE

Obstacles had to be avoided while driving the crawler along the suggested path through the valley. These obstacles were ditches in the terrain in the center of the valley. In figure 8.5 all 10 obstacles are shown, represented with blue x-marks distributed along the track. The obstacles were placed just after a narrow in the valley so the subject was forced to enter the obstacle from the centerline. Obstacles were visually shown as a small ditch, appearing 7 seconds before reaching the obstacle's position and had 1.2 times the vehicle's width along each side available for passing. When collided with the obstacle, the vehicle had to be reversed in direction in order to pass the object. Therefore when the object appeared and was detected by the operator, it had to steer to one side to go around the obstacle. The later the operator responded, the more

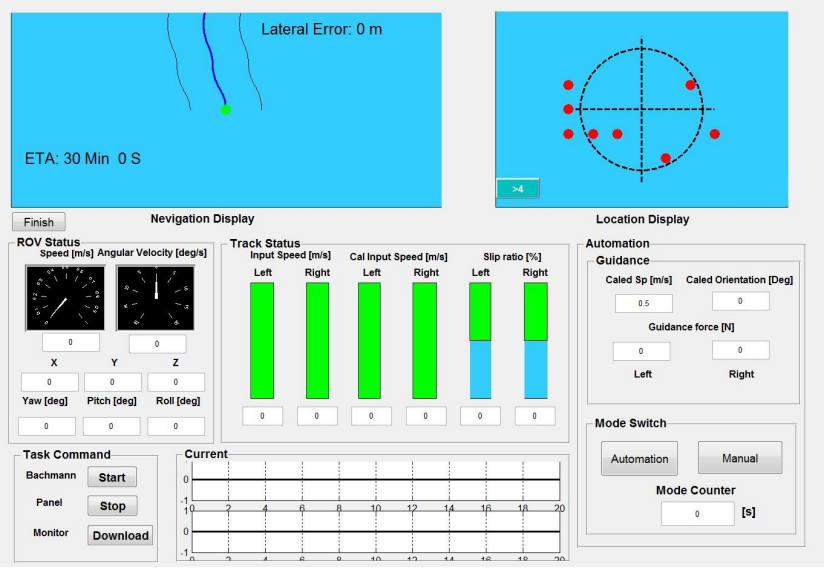

Figure 8.7: Control panel of crawler with vehicle parameters, task overview and secondary task

sharply the vehicle had to be steered around the obstacle and taking more time to do so.

SLIP CONDITIONS

Along the entire path are three slip conditions defined as indicated in figure 8.5, shown with light blue thick lines. During these slip event either the left or right track was slipping and therefore losing partial traction (30% less), resulting in slowly rotation of the vehicle for straight forward control inputs. This slip event was not visually shown to the operator, only the resulting effect of rotation of the vehicle. The slip conditions therefore shows the attention and understanding of the operator to unexpected events, resulting in a mismatch of the commanded input and reaction of the vehicle.

8.2.5. PROCEDURE

Each subject was asked to sit in front of the input device, and hold both handles as shown in figure 8.1. The display behind the input devices showed both the virtual representation of the vehicle and the environment on the left screen, as well as control parameters and the secondary task on the right screen. The subjects were asked to operate the vehicle to drive over the terrain and follow the suggested path through the valley. This path had to be followed as fast as possible while remaining on top of the suggested path.

During the control of the vehicle the subjects were presented with either manual control, haptic shared control, or supervisory control. All three experimental conditions were offered to the subjects in various order, counterbalanced using a Balanced Latin Square Design (Steel et al., 1986). For each experimental condition the subject was driving the entire length of the

path with the obstacle and slip conditions as shown in figure 8.5. During both manual control and supervisory control the feedback on the control device was a static centering spring with boundary forces for the limits of the control device. In supervisory control the control mode could be switch by pushing both buttons on top of the control inputs as shown in figure 8.1. By pushing both buttons for at least 1.0 second the automatic controller would take over, to go back to manual control both buttons had to be pushed for 100 milliseconds. In automatic control mode the inputs from the automatic controller were directly executed as described in section 8.2.2. During haptic shared control condition these control inputs were offered by means of guidance forces as described in section 8.2.3.

While controlling the vehicle, a secondary task had to be performed to count the amount of red dots in a circle. When exceeding 4 dots, any button on the control handles had to be pressed. The secondary task had an update rate of 8 seconds, 3 seconds indicating the dots and time to answer. After 3 seconds the button on the screen indicated in color if the correct answer was given for 2 seconds in combination with short a beep tone. After displaying the correctness of the answer during the remaining 3 seconds the indicator was reset, while the red dots remained present before showing the next set. The latter required clear attention to detect a new set of dots to appear and answer to be given to the next count.

Prior to the task, subjects were trained in manual control for 25 % of the path length to get familiar with the vehicle dynamics and task execution. This training was continued with 10 % of the path for both supervisory control and haptic shared control conditions to get familiar with the experimental conditions.

8.2.6. MEASURED VARIABLES AND METRICS

The data is split into three parts, normal operation, obstacle avoidance and slip events. The driven path for normal operation is measured 2 meters from the start, 15 meters before or after an obstacle and starting 6 meters after a slip event. Therefore this excluded all kinds of after affects or reactions to an event and is therefore regarded as normal operation. The obstacle avoidance is measured from the moment of showing the obstacle (7 seconds before reaching) up to passing the obstacle sideways. The slip event was measured during the period of a slipping track.

Task performance is measured for normal operation by measuring the *total task completion time* and the root mean squared (RMS) of the *lateral error* towards the suggested path. Performance during obstacle avoidance is measured by the *time passing* obstacles (the time between appearance and passing sideways) and the number of times was driven *backwards*. For slip conditions performance was measured by the *slip time*, the time it took to overcome slip and the lateral *RMS error*.

Control effort is measured for all three subtasks by the number of *steering reversals* on the control input. This is defined as the amount of zero crossings of the operator force input. Using a second order Butterworth filter with a 5 Hz cutoff frequency, a deadband threshold of 0.005 rad and a minimum of 0.05 rad between each reversal was required to filter out unintentional noise on the signal, similar to (Boessenkool et al., 2013; Kuiper et al., 2016). Physical effort was

measured by the operator *input force*, calculated as the mean of the amount of force applied on both input devices. The number of wrong answers of the *secondary task* was calculated as a form of mental effort spend on the primary task.

8.2.7. DATA ANALYSIS

For each subject and form of support, the metrics are computed per path section for normal driving, obstacle avoidance and slip conditions, and averaged subsequently over the number of repetitions. Per metric, the means are compared between the form of support using a repeated measures analysis of variance (RM-ANOVA). Greenhouse-Geisser corrections were applied when sphericity was violated. For significant main effects ($p<0.05$), post-hoc comparisons with Holm-Bonferroni correction for multiple comparisons was applied.

8.3. RESULTS

The results, as described in section 8.2.6, are presented for normal operation, obstacle avoidance and slip events in table 8.2, 8.3 and 8.4 respectively. For clarity, the results presented in figure 8.8, 8.9 and 8.10 only include a selection of the metrics. The tables include the complete detailed results and statistics for all metrics.

Table 8.2: Results of All Evaluation Metrics during Normal Operation

	Task Time [min]	RMS Error [m]	Steering Revs. [-]	Input Force [N]	Second. Task [%]
1. Manual Control [1]	16.0 (15.7, 16.3)	0.334 (0.28, 0.39)	24.3 (19.3, 29.2)	9.03 (8.12, 9.94)	19.0 (14.6, 23.4)
2. Haptic Shared Control [1]	16.3 (16.0, 16.3)	0.206 (0.145,0.268)	19.8 (12.9, 26.7)	4.50 (3.29, 5.70)	19.06 (13.8, 24.3)
3. Supervisory Control [1]	16.8 (16.4, 17.2)	0.080 (0.050,0.111)	6.52 (6.11, 6.94)	3.74 (2.62, 4.86)	18.5 (12.3, 24.7)
Statistics[2]	p<.001 ($F_{1.4,24} = 19.87$)	p<.001 ($F_{2.0,34} = 50.93$)	p<.001 ($F_{1.4,23} = 26.67$)	p<.001 ($F_{2.0,34} = 33.94$)	p=0.97 ($F_{2.0,34} = 0.030$)
Post-hoc[3]	1 to 2, p=.009 1 to 3, p<.001 2 to 3, p=.008	1 to 2, p=.001 1 to 3, p<.001 2 to 3, p<.001	1 to 2, p=.023 1 to 3, p<.001 2 to 3, p=.002	1 to 2, p<.001 1 to 3, p<.001	-

Main mean results of all evaluation metrics for performance, control effort and subjective measures, accompanied with their statistical results during normal operation.
[1] Group mean (95% Confidence Interval).
[2] Statistics are shown with a p and F value for a Repeated Measures ANOVA with Greenhouse-Geisser corrections when sphericity was violated.
[3] Post-hoc comparisons were applied using Holm-Bonferroni compensation.

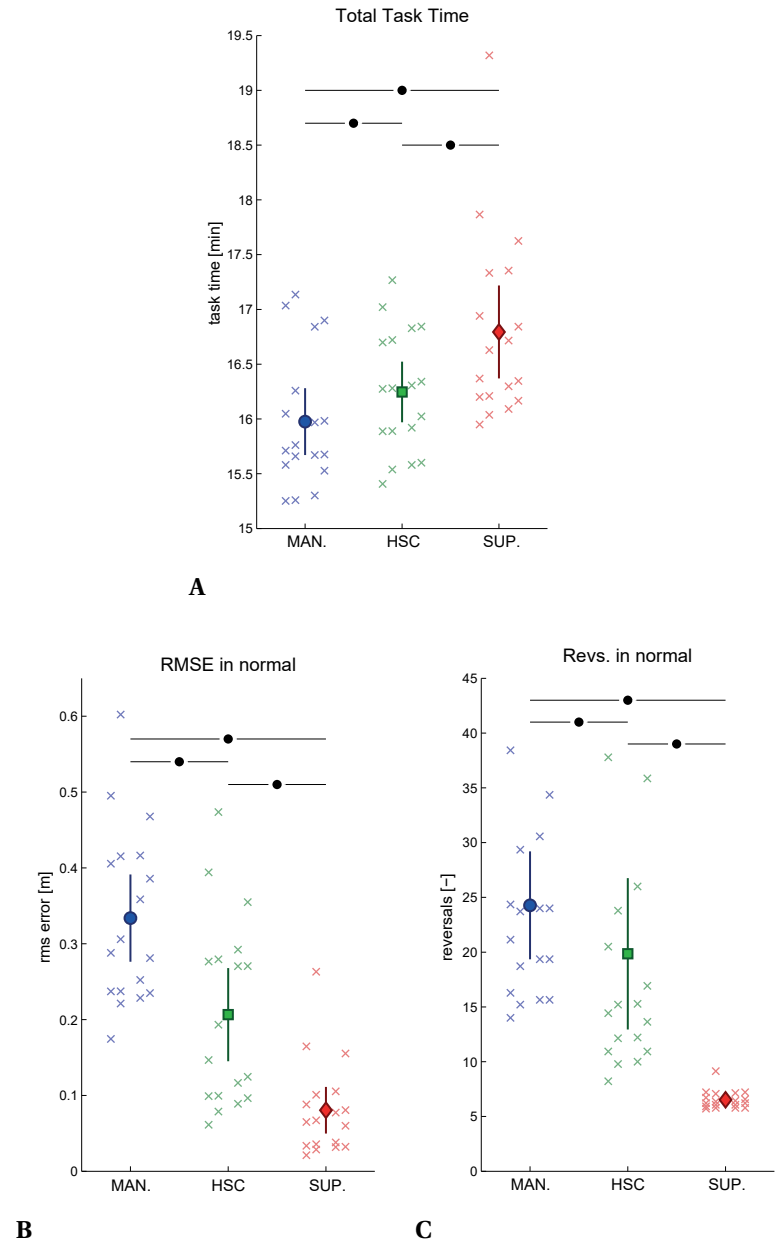

Figure 8.8: Results during normal operation. A) Total task completion time. B) RMS of lateral error. C) Steering reversals. In all figures the group mean (thick filled marker) and the 95% confidence interval (thick error bars) is shown. Individual subject means are shown as well (thin markers). The horizontal bars indicate a significant difference over the factors environment or support, where "•" denotes the significance level of p<.05.

8.3.1. NORMAL OPERATION

During normal operation, subjects had to steer the subsea crawler over a suggested path as accurate and as fast as possible. In figure 8.8A the total task completion time is shown, which predominantly reflects the time of normal operation. The RM-ANOVA shows a significant difference in *task completion time* (p<.001, F=19.9). Post-hoc comparisons show a reduced completion time for manual control compared to both haptic shared control (1.7% mean reduction, p=.009) and supervisory control (5.1% mean reduction, p<.001), and increased completion time for supervisory control compared to haptic shared control (3.4% mean increase, p=.008). The RM-ANOVA on the *root mean square lateral error* shows a significant main effect (p<.001, F=50.9) as shown in figure 8.8B. Post-hoc comparisons show an increased lateral error for manual control compared to both haptic shared control (38% mean reduction, p=.001) and supervisory control (76% mean reduction, p<.001), supervisory control shows further reduction compared to haptic shared control (61% mean reduction, p<.001).

For control effort, significant differences in *steering reversals* are found in normal operation (p<.001, F=26.7), as shown in figure 8.8C. Post-hoc comparisons show less reversals for haptic shared control compared to manual control (18% mean reduction, p=.023), supervisory control shows less reversals compared to both manual control (73% mean reduction, p<.001) and haptic shared control (67% mean reduction, p=.002). Note that for supervisory control the steering reversals are almost exclusively the required track keeping reversals of the automatic controller, which explains the small variance between subjects. The mean operator's *input*

Table 8.3: Results of All Evaluation Metrics during Obstacle Avoidance

	Time Passing [s]	Backwards [-]	Steering Revs. [-]	Input Force [N]	Second. Task [%]
1. Manual Control [1]	12.49 (11.92, 13.05)	0.333 (-0.149, 0.816)	9.77 (8.42, 11.13)	9.01 (8.17, 9.85)	30.23 (23.27, 37.19)
2. Haptic Shared Control [1]	12.55 (11.99, 13.12)	0.333 (-0.178, 0.845)	11.28 (9.61, 12.96)	6.53 (5.68, 7.38)	29.90 (21.82, 37.98)
3. Supervisory Control [1]	14.35 (13.69, 15.02)	0.833 (-0.150, 1.817)	11.66 (10.06, 13.26)	6.73 (6.04, 7.42)	23.05 (16.19, 29.92)
Statistics[2]	p<.001 ($F_{2.0,34}$ = 22.9)	p=.33 ($F_{2.0,34}$ = 1.15)	p=.017 ($F_{2.0,34}$ = 4.59)	p=<.001 ($F_{2.0,34}$ = 25.7)	p=.10 ($F_{2.0,34}$ = 2.46)
Post-hoc[3]	1 to 3, p<.001 2 to 3, p<.001	-	1 to 2, p=.050 1 to 3, p=.022	1 to 2, p<.001 1 to 3, p<.001	-

Main mean results of all evaluation metrics for performance, control effort and subjective measures, accompanied with their statistical results during normal operation.
[1] Group mean (95% Confidence Interval).
[2] Statistics are shown with a p and F value for a Repeated Measures ANOVA with Greenhouse-Geisser corrections when sphericity was violated.
[3] Post-hoc comparisons were applied using Holm-Bonferroni compensation.

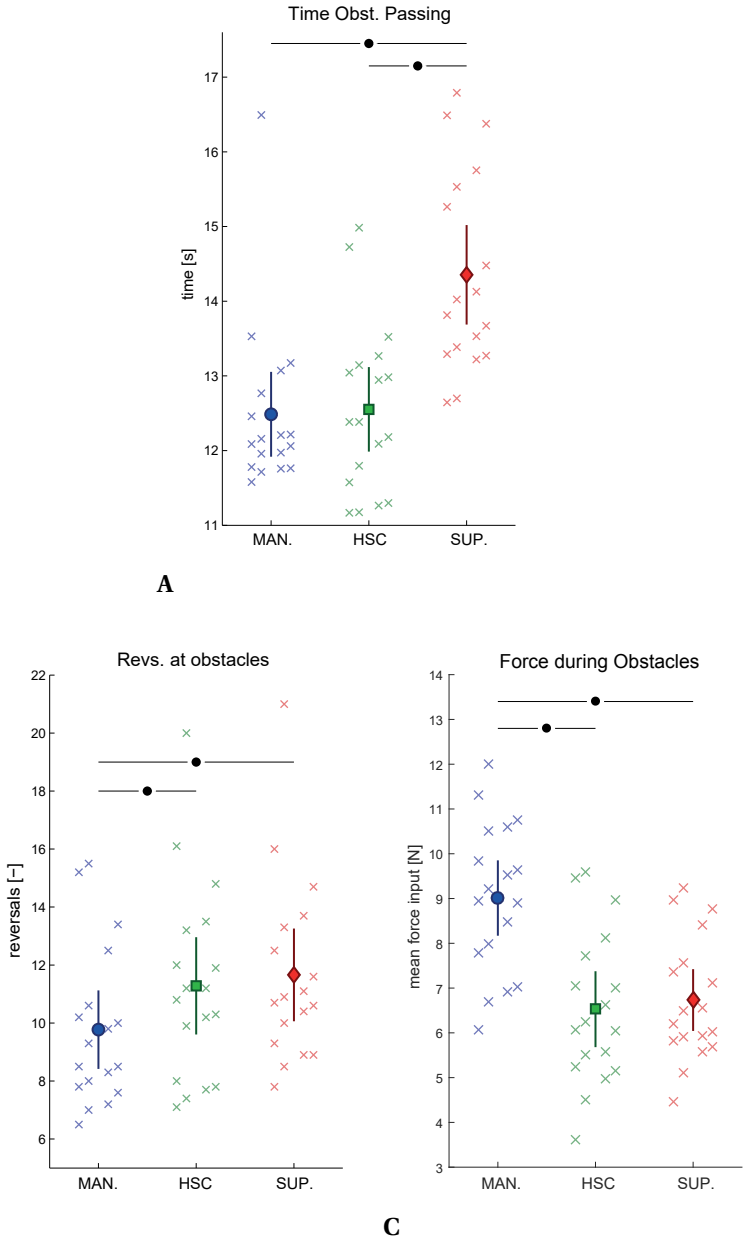

Figure 8.9: Results during obstacle avoidance. A) Average time to pass the obstacles. B) Steering reversals. C) Human mean input force. Color-coding and details as in figure 8.8.

force level during normal operation shows significant differences between the form of support (p<.001, F=33.9), as shown in table 8.2. Post-hoc comparisons show increased input force level during manual control compared to haptic shared control (50% mean increase, p<.001) and supervisory control (59% mean increase, p<.001). The amount of errors in the *secondary task* does not differ between the form of support, as shown in table 8.2. On average, 19% of the questions were answered wrong, out of an average of 87 trials during normal operation.

8.3.2. OBSTACLE AVOIDANCE

Obstacles (which had to be avoided) were placed approximately evenly spread over the total track. The time required to pass the obstacles is shown in figure 8.9A for all three forms of support. A significant main effect can be seen for the *obstacle passing time* (p<.001, F=4.6) and post-hoc comparisons shows an increased time for supervisory control compared to manual control (15% mean increase, p<.001) and to haptic shared control (14% mean increase, p<.001). The number of times the vehicle went *backwards*, note that this rarely happened, does not differ significantly between the form of support (p=.33, F=1.15).

The RM-ANOVA on the *steering reversals* shows a main effect of the form of support (p=.017, F=4.6), as shown in figure 8.9B. Post-hoc comparisons show more steering reversals in both haptic shared control (15% mean increase, p=.050) and supervisory control (19% mean increase, p=.022) compared to manual control. A significant main effect in the operator's *input force level*

Table 8.4: Results of All Evaluation Metrics during Slip Conditions

	Slip Time [min]	RMS Error [m]	Steering Revs. [-]	Input Force [N]	Second. Task [%]
1. Manual Control [1]	41.64 (41.32, 41.97)	0.327 (0.267, 0.387)	35.37 (27.88, 42.86)	9.02 (8.32, 9.72)	20.87 (16.02, 25.71)
2. Haptic Shared Control [1]	41.67 (41.51, 41.83)	0.318 (0.245, 0.391)	36.04 (29.66, 42.42)	7.22 (6.20, 8.23)	22.75 (14.71, 30.79)
3. Supervisory Control [1]	44.59 (42.65, 46.53)	0.441 (0.339, 0.542)	36.96 (29.67, 44.26)	7.31 (6.66, 7.95)	28.61 (20.33, 36.89)
Statistics[2]	p=.004 ($F_{1.06,18.0}$ = 10.9)	p=.015 ($F_{2.0,34}$ = 4.77)	p=.83 ($F_{2.0,34}$ = 0.18)	p=<.001 ($F_{2.0,34}$ = 9.87)	p=.15 ($F_{2.0,34}$ = 1.98)
Post-hoc[3]	1 to 3, p=.009 2 to 3, p=.010	1 to 3, p=.031 2 to 3, p=.054	-	1 to 2, p=.008 1 to 3, p<.001	-

Main mean results of all evaluation metrics for performance, control effort and subjective measures, accompanied with their statistical results during normal operation.
[1] Group mean (95% Confidence Interval).
[2] Statistics are shown with a p and F value for a Repeated Measures ANOVA with Greenhouse-Geisser corrections when sphericity was violated.
[3] Post-hoc comparisons were applied using Holm-Bonferroni compensation.

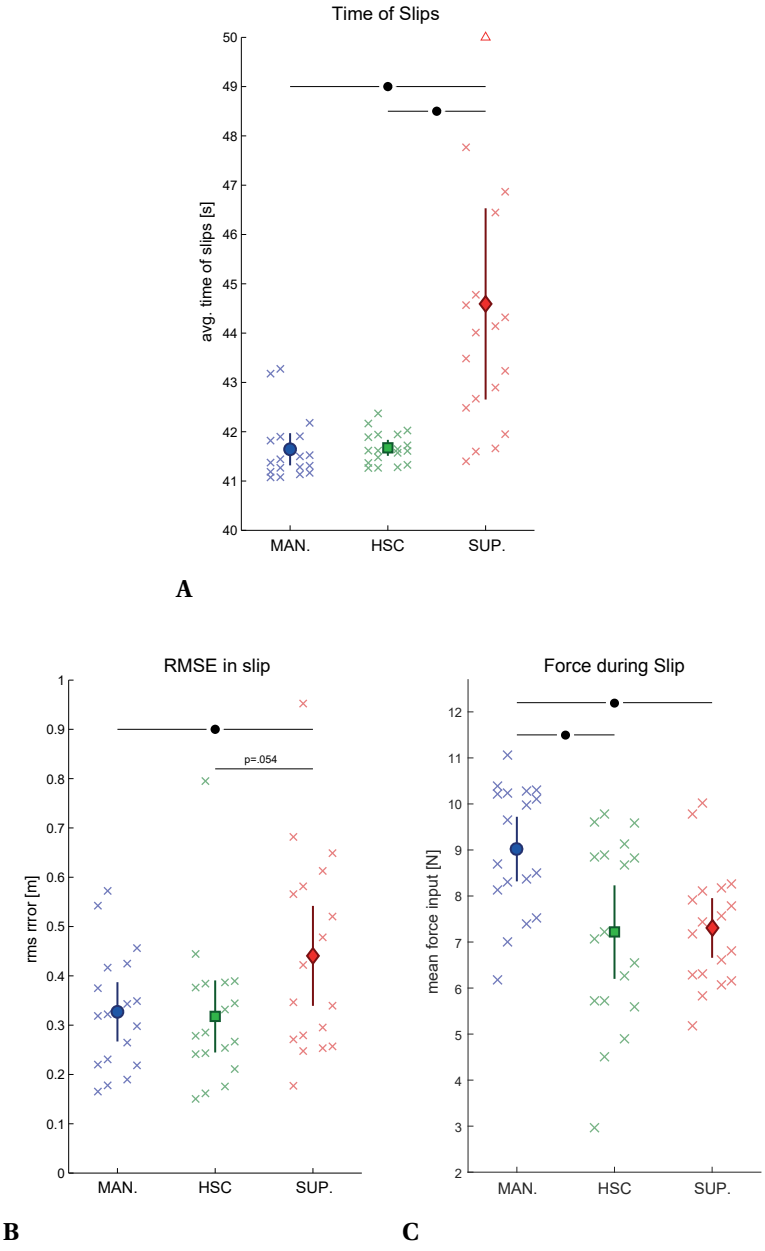

Figure 8.10: Results during slip. A) Average time to overcome slip events. B) RMS of lateral error. C) Human mean input force. Color-coding and details as in figure 8.8.

(p<.001, F=26), as shown in table 8.3 indicates differences in physical control effort. Post-hoc comparisons shows that in manual control a higher force level was used compared to both haptic shared control (28% mean increase, p<.001) and supervisory control (25% mean increase, p<.001). Subjects made on average 28% errors in the *secondary task*, out of an average of 26 trials. Again, the secondary task shows no significant difference amongst the of support (p=.46, F=.80), as shown in table 8.3.

8.3.3. SLIP CONDITIONS

The *time to overcome slip* is a performance metric for task execution in slip conditions and differs significantly between the form of support (p=.004, F=11), as shown in figure 8.10A. Post-hoc comparisons show an increase of time to overcome slip for supervisory control compared to both manual control (7.1% mean increase, p=.009) and haptic shared control (7.0% mean increase, p=.010). Also, significant differences between the form of support were found in the RM-ANOVA on the *root mean square lateral error* (p=.015, F=4.7), as shown in figure 8.10B. Similar to results on the time to overcome slip, the post-hoc comparisons show that the lateral errors increase for supervisory control compared to manual control (35% mean increase, p=.031), and have a clear tendency to be larger compared to haptic shared control (39% mean increase, p=.054) as well.

For control effort, no significant differences for *steering reversals* were found between the form of support (p=.83, F=.18), as can be seen in table 8.4. As during the obstacle avoidance, the *input force level* differs significantly between the form of support (p<.001, F=9.9), as shown in figure 8.10C. Post-hoc comparisons show that in manual control an increased force level was used compared to both haptic shared control (20% mean increase, p=.008) and supervisory control (19% mean increase, p<.001). The *secondary task* shows no significant differences (p=.11, F=2.4), as shown in table 8.4. Subjects made on average 24% errors, out of an average of 25 trials.

8.4. DISCUSSION

In this study, three levels of automation were tested in a bi-manual slow-dynamic skid steering task. The automation levels ranged from manual control to supervisory control, with shared control in between (Sheridan, 2011).

Steering through the environment and following the presented path in *normal operation* was executed significantly more accurate in supervisory control then in manual control (76% smaller lateral error) and reduced control effort (73% reduced steering reversals). The supervisory control mode was almost entirely executed automatically. The resulting evaluation metrics therefore indicate the controller performance (lateral error) and control effort (steering reversals) for the specified task and machine dynamics. Interestingly, during manual control participants reduced the task completion time slightly compared to supervisory control (5%) by cutting corners and taking more risks than the automated controller. Another part of the time difference originates from recovering from obstacles, included in the total task completion

time. In manual control subjects steered more slowly towards the suggested path, where in supervisory control subjects preferred a quick take over by the controller to reduce the control effort. The input force during manual control was almost doubled compared to haptic shared control (50%) and supervisory control (59%). The operator had to push against the static spring in manual control to achieve forward velocity, where in haptic shared control the spring equilibrium was at full throttle. Obviously during supervisory control the input force was low because the operator did not had to push the handles forward during automatic control, where some leaned into the spring slightly when holding the handles to answer the secondary task. The results for haptic shared control was for all evaluation metrics in between manual and supervisory control (38% reduced lateral error and 67% reduced steering reversals compared to manual control). This indicates that, in line with the results in literature (Griffiths and Gillespie, 2004; Marayong and Okamura, 2004), the operator did not completely conform to the guidance in the shared control condition, but did use the guidance in a beneficial way during normal operation.

When unexpected *obstacles* had to be avoided, it took participants significantly longer with supervisory control compared to manual control (15%). The suggested path did not included avoiding the obstacles and the operator had to intervene the automated controller by taking over control. Since the obstacles appeared relatively late, only 7 seconds before the vehicle would collide with it, participants had to respond fast. Because the participants had to answer a secondary task, their attention was slightly reduced in supervisory control to the main steering task. This resulted in a slightly longer response then manual control (approximately 1 to 2 seconds), which resulted in a sharper steering inputs and therefore reduced vehicle speed. As hypothesized, the performance in the supervisory control decreased, e.g. more time was needed to avoid the obstacle and get back to the path. Additionally the control effort during obstacle avoidance was also increased for the supervisory condition compared to manual control (19%). Even though during the supervisory control condition the operator was also controlling the vehicle manually for this part. Individual results show more steering corrections to compensate the late response to avoiding objects and more corrections due to sharper steering. Remarkably due to this short sharp steering the mean input force level drops due to more straight driving, although more perpendicular to the path. The results for haptic shared control for performance was approximately equal to manual control (14% reduced lateral error compared to supervisory control), but requires approximately equal increased control effort as supervisory control compared to manual control (15% increased steering reversals). Interestingly the input force was almost equally lower for both supervisory control (25%) and haptic shared control (28%) compared to manual control condition when avoiding obstacles. Where in supervisory control the task had to be executed entirely manual. During haptic shared control the automatic controller constantly had to be overwritten, however apparently still requiring less input force compared to manual control condition. This indicates that the guidance force was not tuned too strong, while remaining useful during normal operation.

In the *slip* events, the physical slip of the vehicle itself was not directly visible since only the dynamics of the vehicle changed. To overcome the vehicle slip the input on one of the handles

had to be lowered. During manual control and haptic shared control conditions, the coupling between input and steering angle was expected to be more intuitive and therefore changes would be detected earlier and easier to overcome than with supervisory control. The task performance results show indeed for supervisory control larger path deviations (35% increased lateral error) and the time needed to get back on the path (7.1% increased slip time) compared to manual control. However no statistical difference in control input (steering reversals) was found for all conditions. Interestingly the input force shows comparable effect as for obstacle avoidance, almost equally lowered for supervisory control (19%) and haptic shared control (20%) compared to manual control. The results for haptic shared control were as hypothesized equal to manual control during slip conditions. By continuously feeling the control inputs to the vehicle, changes in vehicle dynamics are more easily noticed.

The results on the *secondary task* did not show any significant effects between the different control methods for the three different subtasks. Since the error rates were substantial (20-30%) and the participants indicated their frustration about it, the secondary task was very useful in increasing the difficulty of the overall task. What is noticeable is the increasing error rate during obstacle avoidance and slip conditions compared to normal operation for all experimental conditions. The finding that the operator performs as well on the secondary task in the manual control condition as in de supervisory control condition indicates that the mental workload is not overloaded during manual steering.

Overall our results show that, as hypothesized, shared control has benefits of both manual control and supervisory control. This is reflected in efficient steering through the environment, but also efficient problem solving when unexpected events occur. An explanation for the improvement of shared control over supervisory control is suggested to be the insights of an internal model of the control system (Gibo and Abbink, 2016; Shadmehr et al., 1995). By handling the steering input in a continuous way, the operator creates an internal model of the control system. This enhances the amount of feed-forward control that one can use compared to a supervisory system in which one has to wait for the feedback to correct the input. Errors in the system between input and output, as represented by slip in this experiment, are earlier detected and easier to overcome with an active internal model of the system.

One of the main questions remaining is the tuning of the shared control. In this study, we used a relatively soft shared control, or a low level of automation (assisted according to (Flemisch et al., 2012, 2008)), since our forces were relatively low (*force level is ~6 N*). This could be seen by the large influence of the manual aspects (both benefits and limitations). For future applications the level of automation could be increased with forces up to ~20% MVC, which is still a fatigue-free level of operation (Hichert, 2017; Monod, 1985). At this level (*force level is ~40 N*), the forces can still be easily ignored or overtaken and the benefits of the automation are clearly present. Since the operator in a shared control system needs to hold the handles during the task, proprioception and motor planning will help the awareness about the situation and vehicle dynamic awareness.

This study investigated driving over a terrain with a crawler in subsea. During deep-sea mining the task will also be extended with extensive soil interaction in-contact tasks by exca-

vating the material while slowly driving. Haptic shared control can also be beneficial for these subtasks during maneuvering when full automation is not feasible in all circumstances or when human supervision is required. This study has shown the benefits over supervisory control by keeping the human in the loop, which can be extended to other slow-dynamic subtasks as well.

8.5. CONCLUSION

A human factors experiment was conducted to compare two human-automation interaction designs against manual control of a (virtual) heavy subsea crawler: supervisory control and haptic shared control. The experiment quantified how fast and accurately the crawler completed a trajectory, both during normal operation conditions and during unexpected situations where the automation failed and operator intervention was required. Two types of such situations occurred in the experiment, requiring the operator to avoid an unpredictably appearing obstacle or to stabilize control during slip conditions. For the experimental conditions studied, the following is concluded:

- During *normal operation*, haptic shared control offers benefits over manual control (the trajectory was completed 38% more accurately with 18% less control effort). However, supervisory control results during normal operation only, in more benefits compared to manual control (the trajectory was completed 76% more accurately with 73% less control effort)
- During unexpected situations of *avoiding obstacles*, haptic shared control did not suffer from reduced performance to manual control, only in control effort (the subtask was also completed in 14% less time than supervisory control and 15% more effort than manual control). Whereas supervisory control did suffer from reduced performance compared to manual control (the subtask was completed in 15% more time and 19% more control effort).
- During unexpected *slip conditions*, haptic shared control also did not suffer from reduced performance (the subtask was completed in 7% less time compared to supervisory control). Whereas supervisory control also did suffer from reduced performance compared to manual control (the subtask was completed in 7% more time and 35% less accurate).

These results indicate that haptic shared control has the benefit of both the automation and human input combined. Within the design boundaries of the automation (normal operation) haptic shared control benefits by more accurate task execution, as well as supervisory control. And when the operator needs to unexpectedly resume control (obstacle avoidance and slip conditions), haptic shared control does not suffer from lack of attention and thereby reduced task performance. Haptic shared control allows better catch of automation errors, while still gaining considerable performance benefits compared to manual control.

REFERENCES

Abbink, D. A. and Mulder, M. (2009). Exploring the Dimensions of Haptic Feedback Support in Manual Control. *J. Comput. Inf. Sci. Eng. Spec. Haptics Ed.*, 9(March):1–9.

Abbink, D. A., Mulder, M., Van Der Helm, F. C. T., Mulder, M., and Boer, E. R. (2011). Measuring neuromuscular control dynamics during car following with continuous haptic feedback. *IEEE Trans. Syst. Man, Cybern. Part B Cybern.*, 41(5):1239–1249.

Bainbridge, L. (1983). Ironies of automation. *Automatica*, 19(6):775–779.

Bloois, J. W. V. and Frumau, J. C. L. (2009). Deep Sea Mining , The New Horizon for Dredging Technology. In *Proc. Offshore Technol. Conf.*, number May, page 8.

Boessenkool, H., Abbink, D. A., Heemskerk, C. J. M., van der Helm, F. C. T., and Wildenbeest, J. G. W. (2013). A task-specific analysis of the benefit of haptic shared control during telemanipulation. *IEEE Trans. Haptics*, 6(1):2–12.

Endsley, M. R. and Kiris, E. O. (1995). The Out-of-the-Loop Performance Problem and Level of Control in Automation. *Hum. Factors J. Hum. Factors Ergon. Soc.*, 37(2):381–394.

F. A. Muckler and R. W. Obermayer (1964). Control system lags and man-machine system performance. Technical report.

Flemisch, F., Heesen, M., Hesse, T., Kelsch, J., Schieben, A., and Beller, J. (2012). Towards a dynamic balance between humans and automation : authority , ability , responsibility and control in shared and cooperative control situations. pages 3–18.

Flemisch, F. F. O., Kelsch, J., Loper, C., Schieben, A., Schindler, J., Heessen, M., and Matthias, H. (2008). Cooperative Control and Active Interfaces for Vehicle Assistance and Automation. In *FISITA World Automot. Congr.*, number 2, pages 301–310, Munich.

Gibo, T. L. and Abbink, D. A. (2016). Movement Strategy Discovery During Training via Haptic Guidance. 1412:1–12.

Griffin, W., Provancher, W., and Cutkosky, M. (2003). Feedback strategies for shared control in dexterous telemanipulation. *Int. Conf. Intell. Robot. Syst.*, 3.

Griffiths, P. and Gillespie, R. B. (2004). Shared Control Between Human and Machine: Haptic Display of Automation During Manual Control of Vehicle Heading. *Symp. Haptic Interfaces Virtual Environ. Teleoperator Syst.*, pages 358–366.

Hichert, M. (2017). *User Capacities and Operation Forces*. Phd dissertation, Delft University of Technology.

Kuiper, R. J., Heck, D. J. F., Kuling, I. A., and Abbink, D. A. (2016). Evaluation of Haptic and Visual Cues for Repulsive or Attractive Guidance in Nonholonomic Steering Tasks. *IEEE Trans. Human-Machine Interfaces*.

Lam, T., Boschloo, H., Mulder, M., and van Paassen, M. (2009). Artificial Force Field for Haptic Feedback in UAV Teleoperation. *IEEE Trans. Syst. Man, Cybern. - Part A*, 39(6):1316–1330.

Lipton, I. (2008). Mineral Resource Estimate Solwara 1 Project Bismarck Sea Papua New Guinea. Technical Report February.

Marayong, P. and Okamura, A. (2004). Speed-accuracy characteristics of human-machine cooperative manipulation using virtual fixtures with variable admittance. *J. Hum. Factors Ergon.*

Mars, F., Deroo, M., and Hoc, J. M. (2014). Analysis of human-machine cooperation when driving with different degrees of haptic shared control. *IEEE Trans. Haptics*, 7(3):324–333.

Monod, H. (1985). Contractility of muscle during prolonged static and repetitive dynamic activity. *Ergonomics*, 28(1):81–89.

Mulder, M. and Abbink, D. A. (2011). Correct and faulty driver support from shared haptic control during evasive maneuvers. *2011 IEEE Int. Conf. Syst. Man, Cybern.*, pages 1057–1062.

Mulder, M., Abbink, D. a., and Boer, E. R. (2012). Sharing Control With Haptics: Seamless Driver Support From Manual to Automatic Control. *Hum. Factors J. Hum. Factors Ergon. Soc.*

Parasuraman, R. (1997). Humans and automation: Use, misuse, disuse, abuse. *Hum. Factors J.*, 39(2):230–253.

Petermeijer, S. M., Abbink, D. A., and de Winter, J. C. F. (2015). Should Drivers Be Operating Within an Automation-Free Bandwidth? Evaluating Haptic Steering Support Systems With Different Levels of Authority. *J. Hum. Factors*, 57(1):5–20.

Shadmehr, R., Brashers-Krug, T., and Mussa-Ivaldi, F. A. (1995). Interference in Learning Internal Models of Inverse Dynamics in Humans. *Adv. Neural Inf. Process. Syst.*, 7:1117–1124.

Sheridan, T. (1992). *Telerobotics, Automation, and Human Supervisory Control*. The MIT Press, Cambridge.

Sheridan, T. (2011). Adaptive automation, level of automation, allocation authority, supervisory control, and adaptive control: Distinctions and modes of adaptation. *IEEE Trans. Syst. Man Cybern. Part A*, 41(4):662–667.

Sheridan, T. B. (2002). *Humans and Automation: System Design and Research Issues (3)*, volume 3. New York.

Sheridan, T. B., Verplank, W. L., and Brooks, T. L. (1978). Human/computer control of undersea teleoperators. Technical report, Tokyo.

Steel, R. G. D., Torrie, J. H., and Dickey, D. (1986). *Principles and procedures of statistics: A biometrical approach*. McGraw Hill Text.

Tivey, M. K. (2007). Generation of Seafloor Hydrothermal Vent Fluids and associated Mineral Deposits. *Oceanography*, 20(1):50–65.

Whitcomb, L. L. (2000). Underwater Robotics: Out of the Research Laboratory and Into the Field. pages 1–8.

Wong, J. Y. (2009). Development of high-mobility tracked vehicles for over snow operations. *J. Terramechanics*, 46(4):141–155.

Yu, D., Shaojun, L., Li, L., Yan, L., Gang, W., and Xiren, C. (2009). Virtual prototype modeling and fast dynamic simulation of the complete integrated sea trial system for deep-ocean mining. In *Proc. IEEE Conf. Comput. Model. Simul.*, pages 244–250.

9

General Discussion and Conclusions

This thesis explored haptic support solutions for operators of remote controlled sub-sea machines, with the aim to provide guidelines for future deep-sea mining operations. Remotely controlled sub-sea machines constantly interact with their environment. Excavation tasks specifically require accurate positioning over large workspaces. The continuing use of rate controlled parts of the machines is therefore inevitable. This thesis focused on two approaches to haptically support the human operator in controlling rate controlled sub-sea machines, by offering natural force feedback and haptic shared control. Both aspects were investigated for rate controlled machines and compared to feedback in position controlled tasks.

This chapter describes the main conclusions of this thesis and reflects on the limitations of this work, and the developed simulators for this research. Two potential harvesting approaches for future deep-sea mining have been compared, using a crawler and a grab. A theoretical analysis showed that a grab requires substantially reduced specific excavation energy. Controlling such heavy machinery can be improved by offering natural force feedback, increasing the situational awareness of the operator. Supporting the operator with guidance forces assists in correct control inputs, improving the task execution. Therefore it is recommended to offer both natural haptic feedback combined with haptic guidance forces, increasing both the understanding of the machine and the execution of the task.

9.1. Main Conclusions

Deep-sea mining applications are an extreme case of remotely operated subsea vehicles, excavating the seabed to gather minerals. This work has investigated the main difficulty of large water pressure in deep-sea and how to support controlling these remote large and slow responsive machines. The aim of this thesis is to investigate the design of effective haptic feedback in rate control for remotely controlled subsea vehicles, including both natural force feedback and guidance forces. In figure 9.1 this duality in approach is shown schematically resulting in stiffness modulation and haptic shared control, and describes the used terminology of this work. The main conclusions are given for the four main topics of this work, mining applications, natural and guidance feedback and constructed simulators.

- For excavating rock material in deep-sea, the effects of the hydrostatic pressure have been experimentally investigated (section 9.1.1). The results show a limited increase of apparent material properties for low strain rates, which favors excavation with a grab. Using a grab thereby reduces the specific excavation energy compared to a cutter head.
- Reflecting interaction forces of the controlled machine to the human operator as natural force feedback, has shown to improve the situational awareness and capabilities for predictive inputs (section 9.1.2). Stiffness feedback showed to be the best way to present natural haptic feedback for a rate controlled task, remaining an unchanged neutral position.
- The operator can also be supported with haptic guidance feedback to assist the operator in correct control inputs for more optimized tasks performance (section 9.1.3). Haptic shared control showed to be the best solution for guiding an operator to a suggested path, controlling subsea machinery when full automation is not feasible.
- Various simulators are designed and constructed, for abstract tasks with merely a single degree of freedom, or more realistic simulators (section 9.1.4). The constructed simulators are based on a parallel mechanism with fixed-based motors, using cable capstan transmissions for low intertia and friction without any form of backlash, capable of high fidelity haptic feedback.

The main contributions of these listed four topics are described in the following sections below in more detail based on the individual results of each chapter.

9.1.1. Conclusions on Excavation in Deep-Sea Mining

Rock behavior in deep-sea mining is subject to hyperbaric conditions which hardens the material due to the external pressure on the material (**chapter 2**). This makes the material more ductile during excavation of the material. However if the cutting force is applied slowly, the water has time to equalize over the stressed deflected zone and therefore reduce the pressure difference which is pressing on the crack to prevent it opening. Therefore excavating with slow strain rates is beneficial to reduce hardening due to dilatation effects. This proves a developed

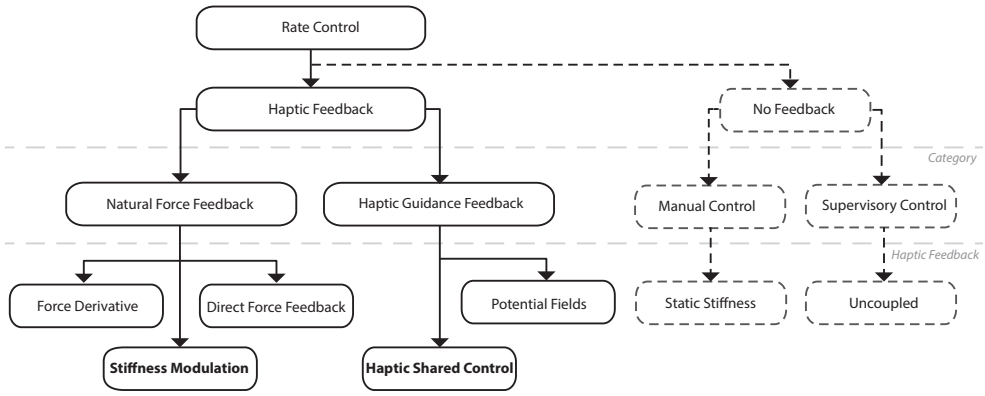

Figure 9.1: Definition of feedback type terminology for haptic feedback including natural force feedback variants leading to the choice for stiffness modulation, and haptic guidance feedback types leading to haptic shared control.

theorem based on the elastic deformation of the rock grain matrix for slow strain rates instead of crack reinforcement, an adjusted relationship of Griffith for normal and shear strength. The reduced amount of cutting force also results in less cutting energy when excavating the material with slow strain rates, such as a grab. In **chapter 2** it is deducted that the specific energy required to excavate rock material is reduced up to 20% by using a grab compared to traditional cutting with a high speed rotational cutter head, for equal production rates. Additionally only 29% of installed power is required to excavate the rock material using a grab compared to conventional excavation. This makes a grab a viable option for excavating the initial top layer of mineral rich rock or for small scaled production operations.

Based on the beneficial results for using a grab, controlling such a complex machine is investigated with the potential of haptic feedback. Excavating deep-sea rock material remotely is a challenging task to execute and requires situational awareness of the controlled machine. In **chapter 3** it is shown that increased awareness during control prevents a grab from falling over during cutting into hard rock, with a specifically developed haptic simulator. Especially when the rock material behaves not uniformly under pressure and can result into unequal movement of the clamshells and thereof tilt of the grab. Reducing the control effort for an operator controlling a grab leads to less fatigue and therefore increases the attention of the operator. Eventually this leads to a reduction of human errors, reducing production losses and damage to the system.

The other potential method for deep-sea mining is to use a large crawler driving over the seabed, with a high speed rotating drum or crown cutter head. In **chapter 8** a specifically developed haptic simulator was implemented for maneuvering a crawler through a valley, evaluated for three conditions: manual control, shared control and supervisory control. The environment was reacting unpredictable by means of varying soil conditions causing the vehicle to slip, or with obstacles buried in the seabed. Because tracked vehicles are typically operated by skid steering (i.e. controlling the speed of both tracks individually), making the vehicle

sensitive to traction on the seabed equally for both sides. Therefore the actual steering of the vehicle requires a local track speed controller, which makes the limits of the system for speed and steering variable. This requires attention of the operator on the control inputs, which is challenging in combination with very slow vehicle dynamics and long tasks to execute. It is shown that offering guidance by means of haptic shared control reduces the complexity of driving such a vehicle and lowers thereby the fatigue of the operator over time. This shows haptic shared control can be very beneficial for deep sea mining tasks.

9.1.2. Conclusions on Natural Haptic Feedback

Natural feedback showed promising for increasing the situational awareness in **chapter 3** for controlling a suspended grab in deep-sea mining in critical tasks. Results show a decreased inclination angle of the grab and improved production when offering natural haptic feedback, indicating more understanding of the machine.

This research was extended and investigated on the fundamentals of the effect of system dynamics on the effectiveness and quality of the feedback. In **chapter 4** it was investigated for a position controlled task how the systems' dynamic response affects the perception of natural force feedback. It was found that for controlling fast dynamics (~8 Hz bandwidth, faster than human arm dynamics) task execution is not affected by haptic feedback, but slow dynamics (~1.5 Hz bandwidth) was substantially improved with feedback (8% tracking error and 40% control effort). Scaling of the feedback force to the operator (25% or 50%) did not change the effectiveness of the feedback and resulted in identical performance. A linear cybernetic control model was made using frequency-response function (FRF) estimations, which incorporated both feedforward and feedback fittings in time and frequency domain, which captured individual operator control behavior. This showed that haptic feedback enabled operators to generate more phase lead and reduced their effective time delay, allowing improved compensation for the lag of the slow dynamic system.

Excavation tasks with large heavy machines often require a large workspace while maintaining accurate control, therefore typically operated with rate controlled inputs. However offering natural feedback in rate control is not equal to position control, where environment forces are directly mimicked to the operator. In rate control several methods exist such as the mathematically correct framework of reflecting the force derivative. In **chapter 5** this method was compared to a more intuitive method of offering stiffness feedback, where the measured environment force is mapped to a stiffness applied on the control input. Results show that stiffness feedback is most beneficial and improves task performance by reduction in overshoot of force level accuracy (77%) and reduction of control effort (37%). For free space tasks, offering only an advanced spring design with clear zero velocity indication also showed comparable improvements of task performance (i.e. overshoot reduction of 31%). The experiment showed reflecting the force derivative is causing oscillations and unnatural behavior during contact transitions due to the nature of the derivative. On top of that, the derivative causes difficulties for the operator to understand the absolute force level exerting on the environment. Stiffness feedback clearly indicates the absolute force level, while maintaining an unchanged neutral

position. This resulted in less overshoot and reduced control effort because of the intuitive feedback method.

Natural feedback by means of stiffness feedback was implemented for a real-world application of controlling a backhoe excavator for excavation of soil in shallow waters in **chapter 6**. The environment interaction forces are typically measured indirectly by means of hydraulic pressures in the cylinder actuators and therefore include dynamic information due to inertia, drag and gravity. A feedback method is developed to reflect the measured forces based on the cylinder pressures and offer this using a stiffness modulation to the operator. The feedback method included a quadratic method to suppress forces in normal operation and highlight the environment interaction forces in the feedback. This method resulted in clear feedback of a contact transition with the seabed while maintaining stability on the input control due to the stiffness modulation. Also varying force levels were clearly reflected by means of the quadratic force reflecting, highlighting these events. Finally with a hard object could clearly be rendered by means of stiffness manipulation. Additionally the stiffness feedback method was refined for controlling a backhoe excavator including a deadband on the control input without loosing stability.

9.1.3. CONCLUSIONS ON HAPTIC GUIDANCE FEEDBACK

Besides natural feedback, offering augmented guidance forces can assist the operator in more optimized steering inputs. In **chapter 3** this is investigated for a case study on operating a suspended grab remotely for deep-sea mining using rate control. For operating large heavy machines offering guidance can reduce the control effort. When large parts of the operation are predictable, control inputs can be partly automated by offering this through guidance forces. Results showed a reduction of control effort (14%) at normal excavation situations due to less control inputs and a reduced cognitive workload was measured (22%) in critical situations. This indicated that guidance made operation of the tasks easier, resulting in long-term benefits of reduced incorrect control and damage of the system.

Offering guidance forces can be done essentially in two ways, by means of repulsive or attractive forces. Repulsive forces, also known as potential fields, prevent colliding with objects or predefined regions. Attractive forces as in haptic shared control, have more task information embedded by guiding the operator over a suggested trajectory towards a certain target. Both methods are compared in **chapter 7** for their effectiveness and in addition compared their equivalent visual support method. The results show that both information types improve task performance (34% and 15% for attractive and repulsive respectively) and reduce effort (41% for attractive) compared to manual control. For attractive guidance more information was embedded in the guidance, leading to larger improvements for both modalities. This suggests that when enough information is available to apply attractive guidance, this method is most beneficial. Potential fields only support short term control inputs and prevent collisions, but not necessarily improve task performance by means of completion time or lateral error. Haptic shared control support the operator by continuously calculating suggested control inputs to perform the task in a optimal manner, therefore giving more constructive support rather

indicating where not to go. Additionally, catch trials showed the operator did not suffer from over-reliance of any support system.

Guidance forces were also implemented on a real-world application of controlling a tracked vehicle in a deep-sea mining application in **chapter 8**. The control of the vehicle was supported by haptic shared control, actively suggesting control inputs to drive over a suggested path. The vehicle was steered through a valley on the seabed for deep-sea mining. Offering guidance forces was compared to controlling the vehicle with supervisory control in predictable events, both improving task performance (38% and 76% reduction of lateral error respectively, compared to manual control). When unforeseen obstacles appeared or part of the vehicle slipped on the seabed, the automation failed to control the vehicle properly. In these cases the operator had to intervene and gave comparable results for haptic shared control to manual control (14% reduction of task completion time for obstacle avoidance and 7% in slip conditions, compared to supervisory control). Therefore haptic shared control showed to have the benefits of both manual and supervisory control.

9.1.4. Developed Haptic Simulators

Investigating both haptic feedback methods of natural and guidance feedback required the development of several simulators, for abstract tasks or more realistic simulators. A full overview of all the simulators with figures can be seen in appendix A: **List of Simulators** in this thesis, of which some are shown in figure 9.2. This section describes briefly the resulted developments for each simulator and their main additions to each chapters findings.

For a realistic deep-sea mining experiment investigating the potential of both natural force feedback and guidance feedback, a simulator *HapticGrab* of a suspended grab was developed in **chapter 3** as shown in figure A.4. The simulator consisted of a realistic physical model including hydraulic actuated clamshells and cylinders of the suspended grab, including a hoisting winch. The grab excavated rock material which was modeled in a simplified manner, based on the results found in **chapter 2**.

A simulator for abstract task levels was developed using the commercial apparatus *HapticMaster* of Moog Inc. as shown in figure A.5. An additional real-time controller was added simulating single degree of freedom spring-damper point mass as remote system. This was controlled by position control using the traditional four channel approach in **chapter 4**, capable of reflecting both the system dynamics in free-space tasks, as well as contact forces. This simulator was extended to include a rate controlled tasks in **chapter 5**, still using the four-channel approach. This structure was extended with the capability of stiffness modulation based on the measured forces of either the system dynamics, as well as the environment interaction forces.

A comprehensive mechanical design of the 3 DoF high fidelity force reflecting joystick *TriaR* is described in **chapter 6**, shown in detail in figure A.6. The joystick is developed based on a parallel mechanism with three rotations, having the motors mounted rigid on the frame. The fixed-based motors reduces the inertia of the links, maintaining a symmetric low inertia for the two main axis (roll and pitch). This enabled high stiffness of each link for reflecting

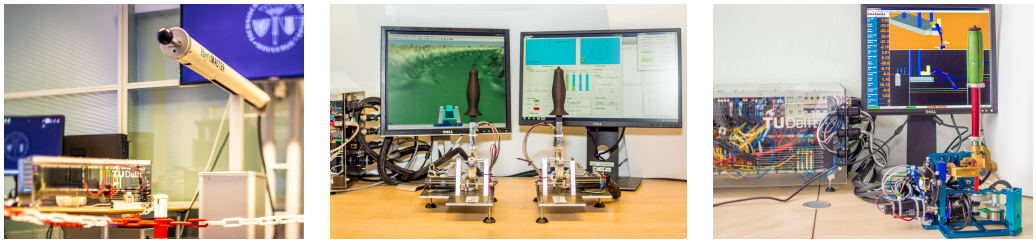

Figure 9.2: Some of the developed haptic simulators described in this thesis. The *HapticMaster* on the left was extended with a real-time controller, enabling abstract task level simulations. A realistic simulator *Gemini* in the middle for controlling a deep-sea mining crawler. The 3 DoF force reflecting joystick *TriaR* on the right, for controlling a backhoe excavator simulator.

large forces accurately. The two main axes were capable of 130 degrees of rotation, and the vertical axis up to 250 degrees of rotation in total. The joystick is tested capable of reflecting forces up to 12 Hz for the two main axis and 10 Hz for the vertical axis, all far beyond human capabilities. The mechanical design is designed for force capabilities up to 100 N at the handle, but for now electrically limited up to 25 N at end point. The setup was designed for controlling an excavator simulator as shown in figure A.7. The simulator contains a dynamic model of a backhoe excavator, including hydraulic actuators and valve control resulting in either rate or force control when in contact. A haptic feedback algorithm was designed to reflect environment interaction forces of the endpoint of the backhoe excavator when cutting through soil.

A simplified simulator for controlling a subsea vehicle (e.g. a deep-sea mining crawler) in top view was developed in **chapter 7**, using the existing setup *Munin* as shown in figure A.8. For this simulator minor hardware modifications were made to the existing developed setup of Christiansson (2007). The controller was extended with the virtual dynamics represented by a planar second order two DoF bicycle model (orientation and radial translation). The virtual slave was coupled by means of haptic feedback using the two-channel controller to the master input device, coupling the virtual dynamics. Additionally the simulator was extended with a virtual environment, displaying several obstacles to be avoided. This simulator can also be used for controlling steerable needles.

The development of a realistic simulator *Gemini* for controlling a crawler, a tracked vehicle for deep-sea mining in **chapter 8** as shown in figure A.10. The simulator was completely developed with the hardware, two single degree of freedom rotational input devices capable of force feedback. A realistic 3D visualization was created to simulate a tracked vehicle with a full physics model to drive over a deep-sea mining terrain. Currently redesigned for use of controlling maritime vessels, in particular towing, adding a rotational degree of freedom to the hardware and including the ship simulator of V-Step with a physics engine to generate the vessel motions as shown in figure A.11.

9.2. Reflections

Real-world deep-sea mining has at this moment not yet been developed, therefore remaining many uncertainties and challenges to be explored. In order to investigate the effect of haptic feedback for deep-sea mining application, simulators were used (section 9.2.1) instead of real machines. This enabled more detailed insights and flexibility in conducting experiments, which are in real-world applications not always possible. The same holds for the operator skill level, novice operators were used in order to evaluate the newly designed methods (section 9.2.2) instead of skilled operators. This enabled experiments on larger groups and made the experiment design more flexible, even up non-realistic tasks (e.g. in abstract task experiments). To analyze the effect of the developed haptic feedback method, simplified experiments were conducted in order to isolate and compare the essence and reduce noise as much as possible (section 9.2.3). Finally the implementation of haptic feedback in offshore applications with very rugged operators is debated (section 9.2.4). All of the four points above mentioned create a limitation on the conducted research as further described in the following sections below.

9.2.1. Usage of Simulators

The usage of simulators was required primarily due to lack of currently existing real-world applications for deep-sea mining. The lack of existing working machines in deep-sea also limited the level of detail that could be implemented in the simulators. Models were made based on existing similar types of machines such as used in offshore applications and preliminary work on the aspect of seabed bathymetry and soil conditions. The simulators contained scaling of the machine properties from offshore applications and soil conditions were based on theoretical models all individually validated but not as a whole. Regardless of these limitations the found results of the benefits of haptics is not so much dependent on the accuracies of these simulator models. As long as the dynamics and simulated effects are in the right order and magnitude, the found results of exploring the capabilities of offering haptics for controlling these machines still holds.

Using simulators also creates more flexibility in conducting experiments compared to real-world applications. It enables repeatability of the conducted tasks and full control over items such as noise, semi-randomization of events and the possibility to condense the experiment. The latter is sometimes a bit of a debate on how to implement to which extent. Condensation of the experiment is to reduce non-relevant parts of the executed task (e.g. for automotive application driving straight roads) and focus on parts where the effect can be measured best (e.g. curves for the automotive example). This can only be done up to a certain extent until the exaggeration becomes unrealistic. The level of condensation of the task depends on the application and the investigated effect. Where on one hand the non-relevant parts need to be removed as much to let the effect overcome the noise, but within the boundaries of the conducted task. So for the automotive example, not increase the curvature more then exists in real life and remain just enough straights to recover from each curve without effecting the next one. This also holds for the conducted experiments as executed in this work, mainly to increase the rate of events that normally occurs in a week or month simulated in about an hour.

9.2.2. OPERATOR SKILL LEVEL

The participants of the experiments were not skilled operators of real-world subsea vehicles such as ROV pilots. Typically students at the University of Technology Delft were used in the range of 20 to 25 years old, therefore novice operators with no prior experience of such machines. The novice operators had more advantage of support methods than experienced operators for the specific tasks would. However skilled operators are hard to find in real life as well and get often replaced by novice operators or sailors in offshore applications. This is also because complex machines are unique in their operation and training for that particular machine is required anyways. Therefore the trend is to go for cheaper labor costs and more initial investment in training and support methods. For now the support methods are limited to either protective measures, or fully automation of subtasks when all information is available. The use of haptic feedback with guidance forces might be beneficial in this trend of using novice operators to also boost their performance when full automation is not possible.

9.2.3. EXPERIMENT TASK COMPLEXITY

The conducted experiments consisted of rather simplified tasks to be executed by the participants. The tasks typically consisted of following a line or avoid obstacles while pursuing a fixed target. In the abstract tasks in chapter 4, 5 and 7 the tasks was kept simplified to investigate the fundamental effect of various haptic feedback methods. For these type of research the task complexity was kept low to control in detail repeatability of the outcome and reduce noise as much as possible (including human input variations). The applied tasks in chapter 6 and 8 consisted of more complexity to investigate the applicability of the haptic feedback methods in more real-world applications. However in these more complex tasks levels, the actual executed task still consisted of following a particular trajectory, although the tested events were more realistic. The main purpose of these experiments was to give the operator a more realistic experience, include effects such as boredom and quantify the effect of the support methods specifically. Increasing the realism of the task execution would also result in more realistic duration of the experiments (days or weeks instead of hours) and would most likely not directly result in more realistic results due to the increased noise level for such tasks.

9.2.4. APPLICABILITY OF HAPTICS OFFSHORE

In offshore applications typically a large surface vessel is connected to a subsea robot, remotely operated from the vessel. These are very costly operations, due to the expensive special purpose equipment used and requiring many personnel. Such operations are usually conducted 24 hours per day all year round, requiring long work shifts and creating a high pressure work environment. Working on these type of operations for weeks uninterrupted combined with large heavy machinery requires rugged operators to control these type of machines offshore. This makes the applicability of subtle haptic feedback challenging to implement in practice. The advantage of haptic feedback needs to be noticeably improving the task performance for a good acceptance in such environments. This will affect the applicability in combination with the proven technology mentality that reigns the offshore applications due to the large financial

interests. Where using haptic feedback requires new more fragile hardware interfacing to be developed, requiring extensive testing before being accepted.

However in the end the type of offshore operations are tedious to control and require constant focus and have large consequences of human errors. Combined with the unexpected environments such operations are involved, full automation remains challenging. Therefore the use of haptic feedback for such tasks could be a potential benefit, but require an extensive detailed development before being implemented in practice.

9.3. RECOMMENDATIONS

REFLECTING natural feedback on real-world applications such as backhoe excavators can potentially enhance task performance. Stiffness feedback showed promising results and is recommended for offering natural haptic feedback to an operator during a rate controlled task (section 9.3.1). The method of stiffness feedback is also recommended in combination with offering haptic guidance forces such as haptic shared control (section 9.3.2). Finally both haptic feedback types are well suited for controlling a suspended hydraulic grab, a recommended excavation method in deep-sea (section 9.3.3). The recommended topics are described in the following three sections below.

9.3.1. STIFFNESS FEEDBACK TO REFLECT NATURAL OCCURRING FORCES

Offering natural force feedback showed promising results when using stiffness feedback in rate controlled tasks. Modulating the stiffness has the benefit of remaining the neutral position of the joystick as input device. Direct force feedback changes this zero force position (e.g. hands free), creating unstable inputs of the controlled device (i.e. bouncing back when making contact). Even though the reflected forces are not directly coupled to the interaction forces in stiffness feedback, for (close to) constant inputs this is still the case. Stiffness feedback also showed promising results in **chapter 5** for in-contact tasks, enabling the operator to understand the applied force level. Although offering a static spring stiffness with a clear zero-velocity indication, already showed to be very beneficial for tasks such as in free-space. But modulating this stiffness only improves the task execution based on actuator force, including feedback of the inertia in free-space, contact transitions as well as force-level tasks. This was also shown for controlling a backhoe excavator in **chapter 6**, indicating the applicability and stability of the used method and apparatus. This demonstrated that also for realistic tasks, reflecting the actuator force as basis for stiffness modulation clearly informs the operator, while remaining stability of the controlled machine.

However the effectiveness of offering natural feedback on the task performance and control effort has not been investigated. This would require extensive research for the application of excavating the seabed and investigating the effect on various subtasks such as free space, contact transitions and force level tasks as defined in **chapter 5**. It is expected that the force level subtask of cutting through the seabed will benefit most from natural force feedback, enabling the operator to understand the maximal cutting depth can be achieved.

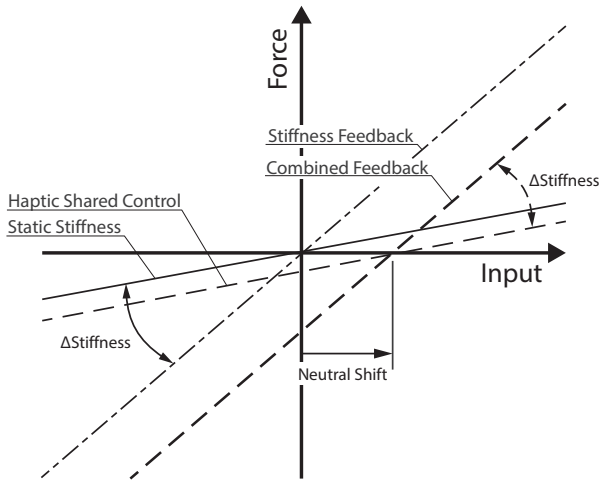

Figure 9.3: Combining natural force feedback with haptic shared control for rate controlled tasks, partly based on Abbink and Mulder (2009). Natural force feedback modulates the stiffness of the feedback, remaining an unchanged neutral position. Whereas haptic shared control shifts the neutral force point, therefore when combined not affecting each other.

9.3.2. NATURAL FORCE FEEDBACK VERSUS HAPTIC SHARED CONTROL

Offering natural feedback informs the operator of the interaction with the environment and its own dynamic limitations. Where haptic guidance feedback assists the operator in the task execution itself and cooperates with the operator based on a given goal. Thereby imperfect partial automation can be implemented assisting the operator, whom can easily intervene by continuously staying in the loop. The stiffness feedback method in **chapter 5** showed beneficial for natural feedback by leaving its neutral position unchanged. The attractive guidance method haptic shared control in **chapter 7** showed for a rate controlled system useful by manipulating this neutral position with an unchanged stiffness. In figure 9.3 this is shown schematically for a joystick rotational input with a feedback force for both stiffness feedback with an unchanged neutral position and haptic shared control, actively shifting this neutral position. The combination of both methods is therefore recommended for rate controlled tasks as also shown in figure 9.3. This can assist the operator with suggested control inputs, while also informing on the interaction forces or dynamics when the operator deviates from the suggested inputs.

It can be argued that offering haptic shared control reduces the need or effectiveness of natural force feedback. This could be the case due to the fact that the intelligent controller calculates the optimal control inputs and therefore the human operator no longer is required to have a good understanding of executed task to determine this himself. However that would be only the case when the human operator can fully rely on the intelligent controller and only has to detect unexpected events such as presented in **chapter 8**. However for situations where the correctness of the calculated control inputs by the automatic controller have to be judged, having more insight by natural feedback can be beneficial. For the latter case this has

to be investigated whether the two reflecting forces are beneficial when combined or possibly deteriorating.

9.3.3. Excavation in Deep-Sea using a Hydraulic Suspended Grab

Deep-sea mining eventually will be a most challenging task to control remotely and can benefit from haptic feedback. Excavation of deep-sea rock material is recommended by using a grab due to the slow strain rates and leaving most of the rock intact, as shown in **chapter 2**. Additionally a grab does not support on the seabed for maneuvering and therefore can work in highly unpredictable soil conditions. This makes a grab suitable for removing the initial top layer of deposits and flattening the seabed, possibly having a drum cutter removing the lower material and fine debris left by the grab.

Controlling a grab has shown benefits of haptic feedback in **chapter 3** for excavating rock materials. But haptic shared control is also recommended for maneuvering a grab over the seabed. For positioning a grab on a specific point on the seabed, over a black smoker for instance is a challenging task to execute. Haptic shared control could benefit the operator in positioning the grab at this specific location, however is bounded by the sensor accuracy for positioning in deep-sea. Offering natural haptic feedback is recommended in combination to the guidance for such a task, so the operator can feel the interaction forces for such detailed maneuvering.

9.4. Future Directions

The future will see more and more high level of automation being implemented in various types of applications. The most familiar case currently is the automotive application where vehicle control is highly automated, but still needs human supervision and corrections. The same tendency can be seen for offshore and dredging related applications with more and more subtasks being automated. Subsea vehicles typically have auto-heading and auto-position, however also subtasks such as (un)docking and controlling the density of excavated mixtures are increasingly being developed. Also for backhoe excavators the trend remains to partially automate some of the functions such as constant cutting angle or cutting depth. These semi-automated functions work under most circumstances but not all, requiring human supervision and corrections, and sometimes even direct control of the human operator.

Haptic feedback and support is expected to play an important role in facilitating direct control and human interaction with semi-automated systems. Natural haptic feedback facilitates improvement of the situational awareness for controlling these machines remotely, especially when they suffer from a slow dynamic response. Haptic guidance feedback enables also imperfect semi-automation to be implemented, by continuously keeping the human in the loop. This results in easier implementation of automated functions. Haptic shared control not only enables partial automation of the task, but also increases the understanding of the operator of the subtask automations and limitations. It remains a trade-off of liability whether haptic feedback is more beneficial or sensitive to failure. Natural haptic feedback and haptic guidance

feedback has the potential to facilitate improved control over remote subsea machines, as well as to allow a more reliable introduction of new semi-automation functions.

REFERENCES

Abbink, D. A. and Mulder, M. (2009). Exploring the Dimensions of Haptic Feedback Support in Manual Control. *J. Comput. Inf. Sci. Eng. Spec. Haptics Ed.*, 9(March):1–9.

Christiansson, A. V. (2007). *Hard Master , Soft Slave Haptic Teleoperation*. PhD thesis, Delft, University of Technology.

LIST OF SIMULATORS

This is a list of constructed simulators during this thesis, used for the human factors experiments conducted in this thesis. Several of the simulators are completely designed and build (*HapticGrab, Gemini* and *TriaR*). And several existing simulators have been modified (*HapticMaster* and *Munin*).

HAPTICGRAB

The *HapticGrab* was completely developed during the graduation project of the Master BioMechanical Engineering for investigating the effect of natural force feedback and haptic shared control while controlling a suspended remote controlled grab for deep-sea mining, as described in **chapter 3**. The setup consisted of two single DoF haptic input handles as depicted in figure A.4, and a realistic physical simulation of a grab conducting a deep-sea mining excavation task.

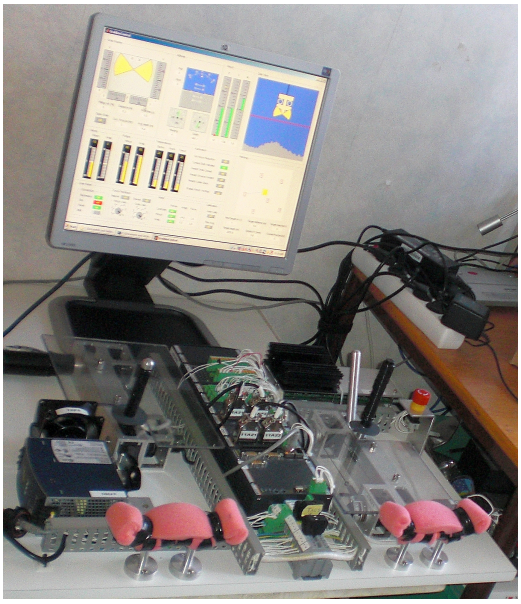

Figure A.4: Experimental setup HapticGrab, consisting of two force reflecting handles and a physical simulated grab.

HAPTICMASTER

The *HapticMaster* as shown in figure A.5, is a commercially available device, modified by adding a real-time Bachmann controller to it. This additional real-time controller enabled an open framework for controlling the endpoint force of the device and feeding back the measured position and realized force. Based on this, a four-channel controller was implemented for position control in **chapter 4**. Thereby a virtual remote (second order) system could be operated based on the input position and force, while reflecting the interaction force with the environment and the position difference between the controlled input and realized system output.

In **chapter 5** the four-channel controller was implemented for a rate controlled system, instead of position controlled. This resulted in the input position translated to velocity setpoint for the remote system and reflecting the difference between achieved and commanded velocity of the remote system.

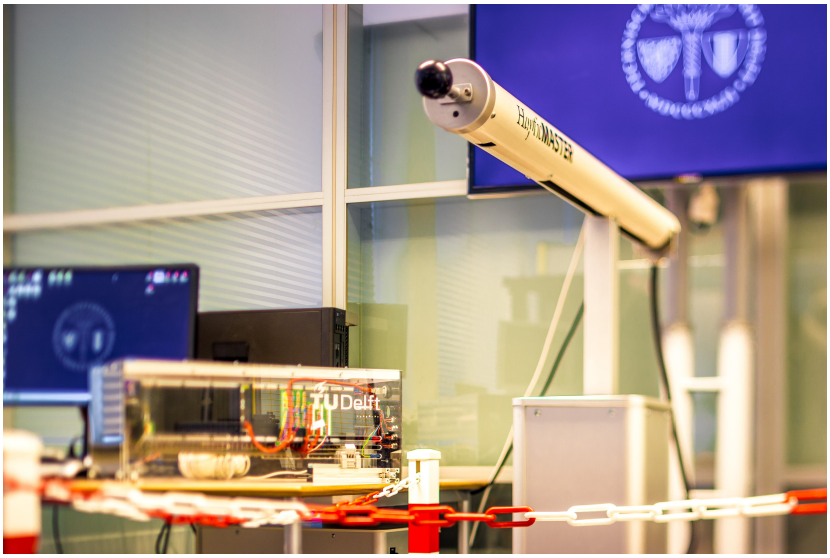

Figure A.5: HapticMASTER setup including Bachmann controller, capable of a four-channel controller for position and rate controlled tasks.

TRIAR

The *TriaR* was developed for controlling a backhoe excavator simulator by means of a force reflecting joystick, as shown in figure A.6. In **chapter 6** the design and evaluated performance of this joystick is described in detail. The design includes a parallel mechanism with three rotations, each force reflecting. The actuating motors are fixed based, meaning the motor housing is fixed to the joystick frame and not moving when another axis is rotating. This enabled low inertia and high stiffness for each link to reflect large forces accurately.

The setup includes integrated torque sensing for each rotation, custom developed. The

developed torque sensors couple the rotation to the capstan transmission, where a set of bearings fixate the axis, therefore decoupling torque from translational forces. The handle is also fitted with an integrated grip sensor, consisting of four grip plates and two sensors per plate, to capture the grip force in each direction.

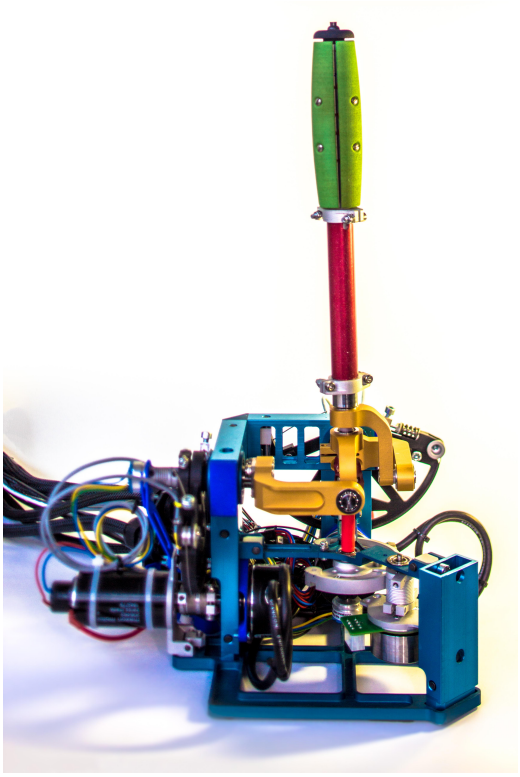

Figure A.6: TriaR 3-DOF force reflecting joystick, impedance controlled with fixed based motors for low inertia.

The developed force reflecting joystick is combined with a backhoe excavator simulator, shown in figure A.7. The simulator consists of a dynamic model of a backhoe excavator, developed in Matlab Simulink and running on a real time Bachmann controller. The simulation includes the dynamics of a multi-link system of a rotating cabin with a boom, stick and bucket attached. Each link is actuated by a simulated hydraulic cylinder, including valve dynamics and pumps. The bucket is simulated to interact with the seabed, which includes a simplified soil mechanical model to remove the material. The outcome of the simulation is represented with the visualization product DipMate of Seatools bv. All combined this enables real time digging through soil on the seabed, including force feedback of the interaction forces with the environment.

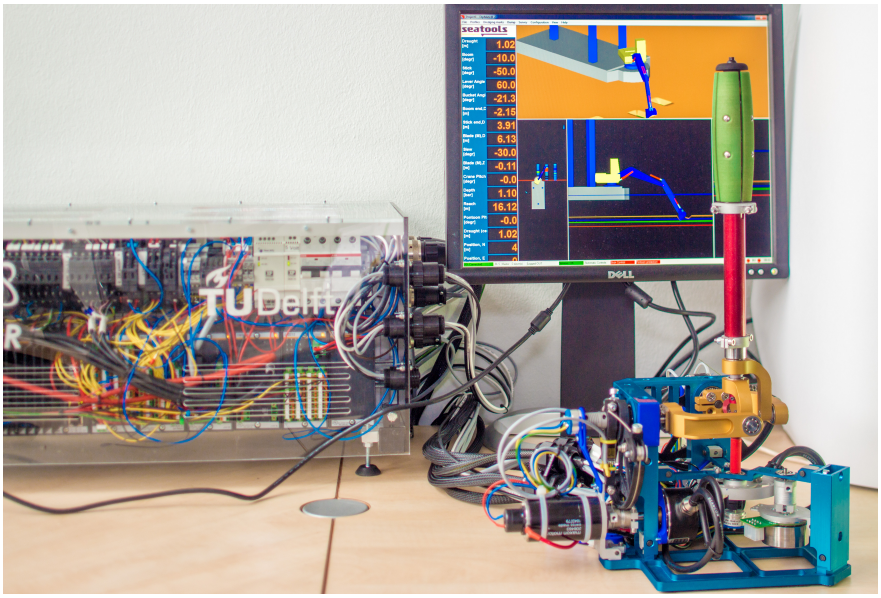

Figure A.7: TriaR backhoe excavator simulator, including a physical backhoe excavator model and connected to a 3D visualization

MUNIN

The *Munin* setup is an existing setup designed by Goran Christiansson[1], designed to demonstrate the coupling of a master slave setting. The human operator can control the planar master endpoint with two translations and one rotation. The movement is mimicked by the slave, also consisting of two translations and one rotation.

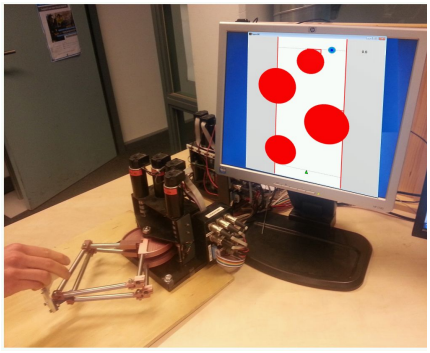

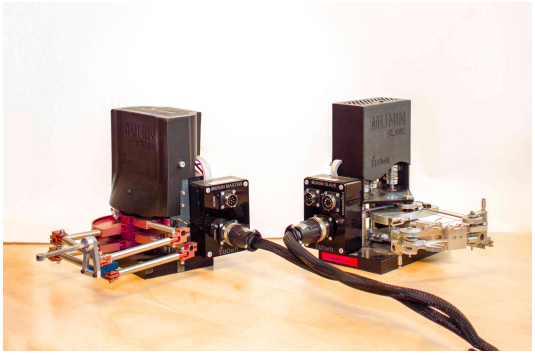

Figure A.8: Munin experimental setup of a 3D planar master, impedance controlled master-slave setup with parallel master and serial slave device.

[1] A. V. Christiansson; Hard Master, Soft Slave Haptic Teleoperation; PhD thesis Delft, University of Technology, 2007

The existing setup was modified slightly by altering the interfacing to the human operator for the human factors experiment conducted in **chapter 7**. For this experiment a simulator was developed based on a bicycle model to maneuver a remove vehicle through a virtual maze, as depicted in figure A.8. Force feedback was designed in two different ways to guide the operator through the maze, either by potential fields around the obstacles, or haptic shared control towards a suggested path between the obstacles.

GEMINI

The *Gemini* was developed initially in collaboration with the Bachelor students Leroy Boerefijn en Ward Heij to demonstrate the basic working of a single degree of master slave setup with Capstan drive. The setup enabled detailed design and testing of the capstan transmission and motor choices for haptic feedback designs. This served as a basis for the more complex TriaR joystick, which consisted of the same design principles for transmission and actuation.

The setup as illustrated in A.9 consists of two identical handles, electronically connected by a Bachmann industrial real-time controller. The handles have a single rotation, which consists of a capstan pulley and connected to a motor for generating haptic feedback. The handles also have integrated force sensing by a set of strain gauges mounted on the user end, calibrated to measure the interaction force. This enabled initially a four-channel construction, equal to what was implemented on the HapticMaster setup to couple position and force for both handles.

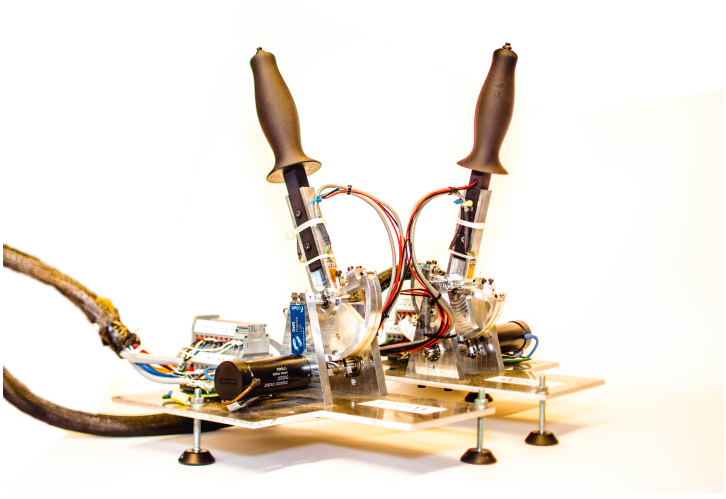

Figure A.9: Gemini Mark I haptic 1-DOF experimental setup, a pair of identical input handles impedance controlled using a capstan actuator.

In **chapter 8** both handles were used as inputs to control a virtual crawler remotely, as depicted in figure A.10. The simulator consists of a dynamic model of a track driven vehicle on the seabed, controlled by means of skid steering (manipulating the speed of each track individually). A virtual environment was constructed to drive over and sudden appearing obstacles had to be avoided. This enabled the comparison between supervisory control (full

automation with human intervention), manual control and haptic shared control (guiding the operator by means of forces).

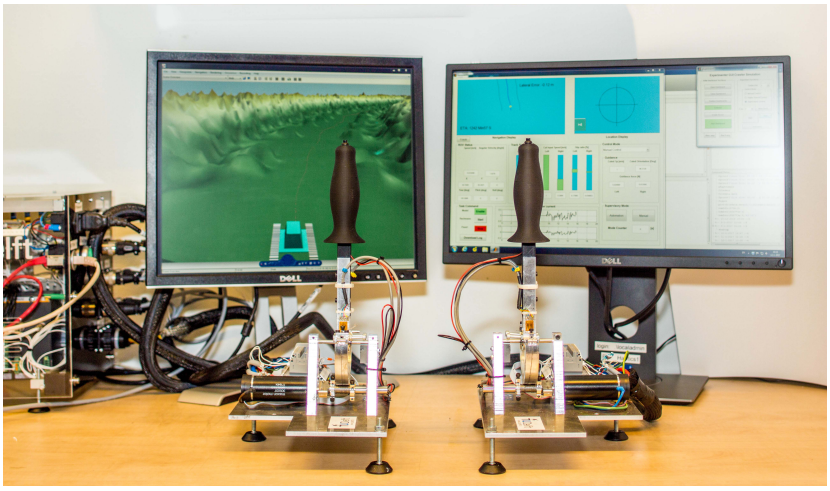

Figure A.10: Gemini Mark I crawler simulator, including a physical model of a virtual subsea crawler and seabed 3D visualized.

Recently the setup has been extended by Alfons Schure and Frank Hoeckx[2] by placing each handle on a rotating platform, as shown in figure A.11. This enables the development of a force reflecting maritime simulator with the control of two azimuth thrusters, as shown in figure A.12. The simulator consists of a tugboat simulation NAUTIS, a commercial product of VSTEP Simulation. This is connected to the Bachmann real-time controller, which is controlling the handles. The simulator was developed to investigate the potential of haptic feedback for controlling a tugboat operation. Recently this simulator is also used for improving the control of fast small navy vessels [3].

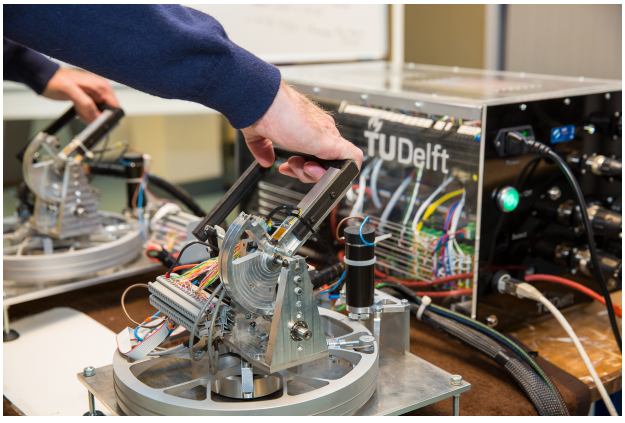

Figure A.11: Gemini Mark II haptic 2DoF setup, azimuth throttle for marine applications impedance controlled.

Figure A.12: Gemini Mark II maritime simulator, including a high-end tugboat simulation NAUTIS, using VSTEP Simulation.

[2] F. Hoeckx, A. Vrijdag, D. A. Abbink; Development of a test setup for exploring the potential of haptic feedback for maritime operations; Marine Electrical and Control Systems Safety Conference, 2016

[3] R. Kok, A. Vrijdag, A.P.. van 't Veer, D.A. Abbink; Haptic assistance to mitigate damaging vertical accelerations of small fast ships in head waves; Delft, University of Technology master thesis, 2018

List of Abbreviations

ROV	Remotely Operated Vehicle
PID	Proportional-Integral-Derivative controller
NASA	National Aeronautics and Space Administration
TLX	NASA Task Load Index
UAV	Unmanned Aerial Vehicle
HSC	Haptic Shared Control
NFF	Natural Force Feedback
DOF	Degrees Of Freedom
NMS	NeuralMuscular System
FRF	Frequency Response Function
UTS	Unconfined Tensile Strength
UTC	Unconfined Compressive strength
BTS	Brazilian Tensile Strength
ASTM	American Society for Testing and Materials

ACKNOWLEDGEMENTS

Het duurde een paar jaar, maar nu is de thesis dan ook daadwerkelijk klaar. De afgelopen zes jaar was een achtbaan met vele wendingen, die naast vele interessante wetenschappelijke kanten ook mooie en soms lastige privé situaties met zich mee bracht. Ik ben dankbaar dat ik deze mogelijkheid gehad heb, die mij door de grote vrijheid en intelectuele uitdaging een hoop geleerd heeft. Hiervoor wil ik dan ook de volgende mensen in het bijzonder voor bedanken.

Allereerst wil ik David Abbink bedanken. Jij hebt mij al met aanstekelijke enthousiastme meegetrokken vanaf mijn afstuderen, nu ruim acht jaar geleden, wat nu geleid heeft tot het afronden van een mooi boekje. Bij de vele tegenvallers en uiteraard ook mooie momenten (zoals ook op vele conferenties). Jij wist mij te stimuleren door samen te zoeken naar oplossingen en de juiste richting te geven aan het geheel. Ik zal onze vele gesprekken, diepgaande discussies, ook op persoonlijk vlak en vele mooie momenten nooit vergeten. Jij hebt mij ook goed geleerd te genieten van onderzoek, onderwijs maar ook het leven zelf.

Als tweede wil ik mijn promotor Frans van der Helm bedanken. Ook jij hebt mij al sinds mijn afstuderen begeleid met vele discussies en altijd zeer kritische vragen, die soms met veel protest toch altijd tot de mooiste ideeën en wendingen leidde. Met je ruime ervaring met human factors en inspiratie voor het bedienen van machines wist je mij altijd zeer scherp te houden op de richting van het onderzoek.

Daarnaast wil ik ook Sape Miedema en Cees van Rhee bedanken die tevens betrokken zijn vanaf mijn afstudeerwerk wat tot dit resultaat heeft geleid. Hierdoor is de mooie samenwerking en koppeling naar de offshore en bagger industrie mogelijk geweest en heb ik mij daardoor ook op dat vlak weten te verbreeden.

Uiteraard wil ik hierbij ook Seatools bedanken die dit voor mij ook sinds het afstuderen heeft mogelijk gemaakt. In het bijzonder wil ik graag Jan Frumau bedanken, je hebt altijd achter mij gestaan en de mogelijkheid en ruimte gegeven om deze uitdaging aan te gaan. Ik vond dit echt uitzonderlijk hoe ruimthartig jij hierin was en mij door deze lange periode in bent blijven steunen. Daarnaast uiteraard ook Sieds Tamsma, die met de vele discussies en koffie pauzes tot de mooiste ideeën heeft gebracht. En ook Jan Tanis, die naast het meerijden en wonen in Delft ook met het onderzoek een fijne steun was om op te kunnen leunen wanneer nodig (soms letterlijk).

Verder wil ik graag Jeroen Wildenbeest bedanken voor de vele uren samenwerking en uitgebreide discussies die we gehad hebben om nu eens eindelijk vast te stellen wat nu beter werkt, positie of snelheid (ondanks dat we aan de werkelijke vergelijking niet zijn toegekomen). Dank voor het geduld en de scherpe inzichten die we samen in dat donkere hok gehad hebben, met mijn slaap tekort. En natuurlijk wil ik ook Henri Boessenkool bedanken voor de samenwerking die we gehad hebben en de avonturen van het runnen van een lab. Dank dat je altijd klaar stond

om naast praktische hulp ook altijd mij mentaal wist te ondersteunen. And I would like to thank Jack Schorsch for the many hours we spend on contructing our hardware setups with the nice Bachmann conroller joy we had. Ik wil graag Irene Kulling bedanken voor de (wat langdurige) samenwerking die we met het schrijven van papers gehad hebben. Daarnaast wil ik ook Dennis Heck bedanken voor de samenwerking met het programmeren van een opstelling die ons beide uitdaagde. And I would like to thank Xiuhan Chen for the combined work we did, together with making the presentations for all the nice progress meetings we had.

Uiteraard wil ik ook het Delft Haptics Lab bedanken voor de leuke tijd die we gehad hebben samen, ondanks mijn gemopper of slapeloosheid en chaos. Tricia Gibo, Teun Hoevenaars, Jeroen Wildenbeest, Henri Boesenkool, Jack Schorsch en Jeroen van Oosterhout met daarbij later ook Bastiaan Petermeijer, Sarah Barendswaard, Sarvesh Kolekar en Timo Melman dank dat ik dit samen met jullie heb kunnen doen, en de vele koffie die we samen gedronken hebben. Daarbij in speciaal ook Andre van der Kraan voor de mooie vrijdag ochtenden in het lab en Frank Hoeckx voor de meeslepende maritieme toevoeging aan het verhaal. En natuurlijk hoort daar verder ook de mooie tijd met de hele H-Haptics groep bij met de lange avonden en presentaties op de jaarlijkse bijeenkomsten.

Daarnaast wil ik ook de studenten die ik begeleid heb bedanken, Vincent Honing, Kang Wang, Marjon Voskuil, Leroy&Ward Guido Hoogslag, Joost Hilte en Marco Stijnman. Maar verder natuurlijk ook Luca, Arnold, Bastiaan, Andy, Lotte, Lloyd, Frank, Erik, Martin, Jacco en Roy en nog velen die ik onderweg ben tegengekomen en daarmee ook mij hebben geholpen te komen waar ik nu ben.

Als laatste uiteraard mijn maatje en liefste Jeruëlle, met natuurlijk mijn stoere kereltjes Timo en Joah, ondanks de vele slapeloze nachten die jullie me altijd bezorgd hebben er toch doorheen hebben gesleept, zeker aan het einde met de vreugde als ik weer thuis kwam of op schoot mee aan het helpen waren. het heeft voor jullie drieen veel gekost, zeker aan het einde, maar ik had het niet zonder jullie gekund.

En tot slot dank ik God in al zijn grootheid voor de gave en inzicht die mij gegeven is.

Curriculum Vitæ

Roeland Jacobus Kuiper

29-01-1985 Born in Rotterdam, The Netherlands.

Education

1997–2003 Grammar School
Melanchthon College, Rotterdam

2003–2012 Undergraduate in Mechanical Engineering
Bachelor Mechanical Engineering (2003 – 2007)
Master Mechanical Engineering (2008 – 2012)
Master Offshore and Dredging Engineering (2007 – 2012)

2012–2017 PhD. in Mechanical Engineering
University of Technology Delft
Thesis: Haptics in Subsea
Promotor: Prof. dr. F.C.T. van der Helm

Employment

2007–2009 Msc Gusto Engineering
Mechanical Engineer (0.2 fte)

2009–2012 Seatools bv.
Mechanical Engineer (internship + 0.2fte)

2012–2017 Seatools bv.
Research & Development Engineer (0.2fte)

2017 Seatools bv.
Research & Development Engineer

List of Publications

Journal Articles

V. **R.J. Kuiper**, H. Boessenkool, J.C.L. Frumeau and D.A. Abbink, *A Haptic Backhoe Excavator Simulator: Design of a Force Reflecting Joystick and Feedback Algorithms*, to be submitted to the Journal of Mechanical Sciences, 2019.

IV. **R.J. Kuiper**, I.A. Kuling, K. Wang, and D.A. Abbink, *Haptic Shared Control Enhances Performance of Controlling a Subsea Crawler*, to be submitted to IEEE Transactions on Haptics, 2019.

III. **R.J. Kuiper** & J.G.W. Wildenbeest, F.C.T. van der Helm and D.A. Abbink, *Exploring Haptic Feedback Designs for Rate Controlled Systems*, to be submitted to IEEE Transactions on Haptics, 2019.

II. J.G.W. Wildenbeest & **R.J. Kuiper**, K. van der El, F.C.T. van der Helm and D.A. Abbink, *A Cybernetic Approach to the Effect of Haptic Feedback on Operator Control Behavior in Free-Space Telemanipulation*, to be submitted to IEEE Transactions on Haptics, 2019.

I. **R.J. Kuiper**, D.J.F. Heck, I. A. Kuling and D.A. Abbink, *Evaluation of Haptic and Visual Cues for Repulsive or Attractive Guidance in Nonholonomic Steering Tasks*, IEEE Transactions on Human-Machine Systems **46**, 672-638 (2016).

Conference Proceedings

V. **R.J. Kuiper**, X. Chen, J.C.L. Frumau and S.A. Miedema *Reduction of Energy Consumption When Using a Grab for Deep-Sea Mining Operations*, Proceedings of Offshore Technology Conference, Houston (2016).

IV. Wildenbeest, **R.J. Kuiper** F.C.T. van der Helm and D.A. Abbink, *Position control for slow dynamic systems: Haptic feedback makes system constraints tangible*, Proceedings of IEEE International Conference on Systems, Man and Cybernetics, San Diego (2014).

III. V. Honing, T.L. Gibo, **R.J. Kuiper** and D.A. Abbink *Training with haptic shared control to learn a slow dynamic system*, Proceedings of IEEE International Conference on Systems, Man and Cybernetics, San Diego (2014).

II. **R.J. Kuiper**, D.A. Abbink, F.C.T. van der Helm and J.C.L Frumau, *Haptic Support for Bi-manual Control of a Suspended Grab for Deep-Sea Excavation*, Proceedings of IEEE International Conference on Systems, Man and Cybernetics, Manchester (2013).

I. **R.J. Kuiper**, S.A. Miedema and J.C.L. Frumau *Influence of the Hyperbaric Effect on Apparent Material Strength of Fully Saturated Porous Rock for Low Strain Rates*, Proceedings of Offshore Technology Conference, Houston (2013).